Aviation Safety Council

Taipei, Taiwan

CI611 Accident Investigation

Factual Data Collection

Group Report

Structure Group

June 3, 2003

ASC-AFR-03-06-001

Intentionally Left Blank

I. Team Organization

Chairman:

David Lee / Investigator, ASC, ROC

Members:

1. Arnold Wong / Engineer, ASC, ROC
2. Kevin Pudwill / Investigator, NTSB, USA
3. TI Chang / PMI, CAA, ROC
4. David Lin / Engineer, CAA, ROC
5. Michael Marx / Consultant, CAL, ROC
6. Fred Lin / Engineer, CAL, ROC
7. William Lin / Engineer, CAL, ROC
8. Yen Lee / Engineer, CAL, ROC
9. Liang Huang Hsiang / Engineer, CAL, ROC
10. Sunny Wang / Engineer, CAL, ROC
11. Warren Steyaert / Engineer, Boeing, USA
12. Steve Chisholm / Engineer, Boeing, USA
13. Henry Missel / Engineer, Boeing, USA
14. John Thunselle / Engineer, Boeing, USA
15. Arnie Reimer/ Engineer, Boeing, USA
16. Jim Powers / Engineer, Boeing, USA
17. Kirby Johnson / Engineer, Boeing, USA
18. George Fleis/ Engineer, Boeing, USA
19. Jamie Straus / Engineer, Boeing, USA
20. Kevin Pudwill / Engineer, Boeing, USA
21. Bonnie Bakken / Engineer, Boeing, USA

22. Kelvin Dean / Engineer, Boeing, USA
23. Alex Moroseos / Engineer, Boeing, USA
24. Rod Hadley / Engineer, Boeing, USA
25. Alex Chau / Engineer, Boeing, USA
26. Terry Vallon / Engineer, Boeing, USA
27. NenitaOdesa / Investigator, FAA, USA
28. Rick Kawaguchi / Investigator, FAA, USA
29. Tammy Anderson / Investigator, FAA, USA
30. Ivan Li / Investigator, FAA, USA
31. Scott Fung/ Investigator, FAA, USA

II. History of Activities

Date	Description
05/26/02 ~ 10/19/02	● Examinations of the wreckages recovered in Makung
07/31/02 ~ 09/06/02	● Structure Items sent to CSIST for metallurgical test
11/03/02 ~ 11/25/02	● Structure Item 640 sent to BMT, Boeing, Seattle, Washington, USA for metallurgical test
12/02/02 ~ 12/19/02	● 2D reconstruction of Section 46 in TAFB Hangar
02/17/03 ~ 02/28/03	● Fwd fuselage section 41/42/44 metallurgical field examination at TAFB Hangar
03/21/03	● Right Wing Front Spar Upper Chord on item #526C3 and Left Wing Upper Internal Splice Fitting - Left Side of Body (SOB), Rear Spar on item #547C2 to Boeing BMT for metallurgical testing
03/01/03 ~ 04/14/03	● 3D Hardware Reconstruction in TAFB Hangar
03/21/03 ~ 04/10/03	● Additional Boeing BMT test

III. Factual Description

1.3 Damage to aircraft

The aircraft was completely destroyed.

1.4 Other damage

The aircraft was completely destroyed.

1.12 Wreckage and impact information

1.12.1 Introduction

Recovery positions of the wreckages from the ocean floor (red, yellow, or green zones as indicated in the Wreckage recovery group report) show that the red zone pieces (fuselage section 46/48 structure aft of the aft wheel well bulkhead at STA 1480) were separated from the rest of the airplane and that the fuselage and wing structure forward were recovered in one major debris field in the yellow zone. All four engines were recovered some distance to the south (green zone) of the major debris field.

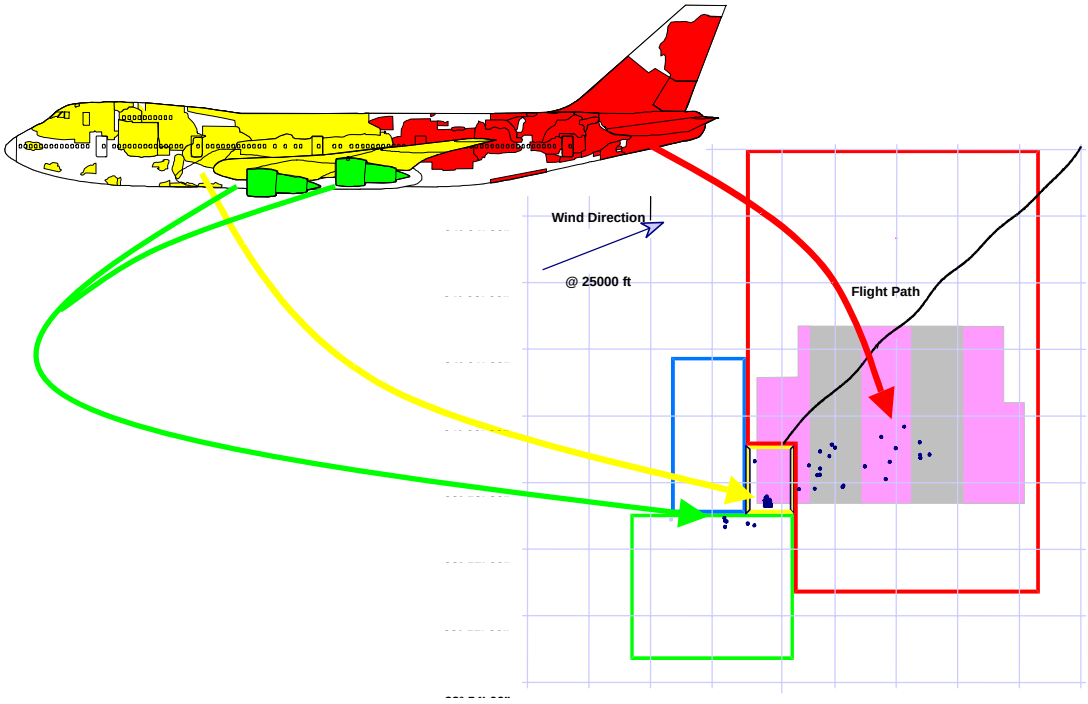

Figure 1.12-1 The majority of the wreckage was retrieved by divers within areas that were divided into four distinct zones.

1.12.2 Forward Body - Sections 41/42/44

This portion details the wreckage from sections 41/42 (the fuselage structure forward of the wing) and section 44 (fuselage structure in the vicinity of the wing and main wheel wells). The majority of the recovered portions of sections 41/42/44 were found in the main debris field in the yellow zone. All landing gear was found in main debris field except for the Right Hand Side (RHS) Body gear, which was retrieved from the green zone (possibly dragged to the green zone by fishing boat). Also retrieved from the green zone were several portions of the STA 1480 bulkhead adjacent to the RHS Body Gear support. The Wing Center Section (WCS) was also recovered in the main debris field. Many small fuselage fragments from the lower 41/42 sections were recovered but not documented and were not included in the diagrams below.

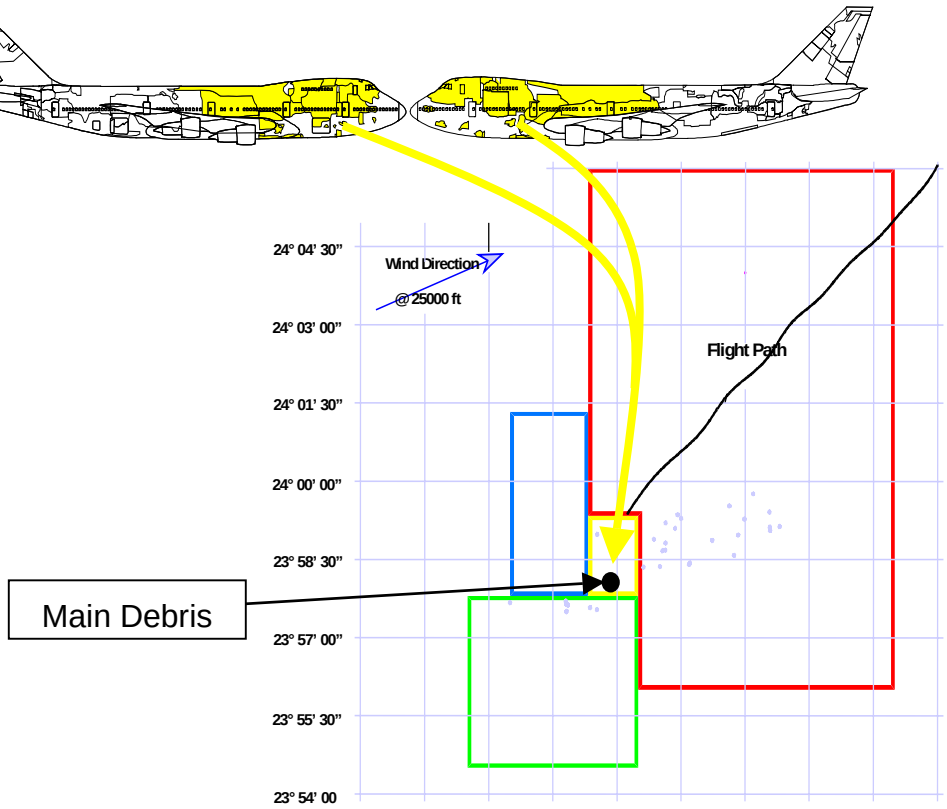

Figure 1.12-2 The majority of the recovered portions of sections 41/42/44 were found in the main debris field in the yellow zone.

(1) Sections 41/42

In sections 41 and 42, the portions of structure in the crown region were less fragmented (larger segments) than portions of structure recovered from the lower fuselage. The largest piece of structure recovered in the crown area (item 487) extended from below the main deck window belt on the Left Hand Side (LHS) to below the upper deck floor on the RHS. Most of the frame and upper deck floor beam segments were still attached. While the upper deck floor beams were fractured and the skin was folded in the crown region, the majority of the panel retained its original contour. The cockpit structure (item 545 [Figure 1.12-3(a)]) was found to be relatively intact aft to STA 500 and essentially retained its original shape. Much of the structure below these two items was found in smaller segments and with greater distortion (see items 655, 656, and 705 [[Figure 1.12-3(b)]]. Many belly segments showed general upward deformation of the skin panel between stringers and frames (see items 876 [[Figure 1.12-3(c)], 969, 973, and 1088).

Figure 1.12-3 (a) Cockpit Structure-Item 545-left photo, (b) Item 705 distorted section 42 skin- right photo

Figure 1.12-3 (c) Item 876 belly skin with upward deformation

(2) Forward Cargo Door

The upper portion of the forward cargo door was found still attached to the skin assembly above the door (Item 629). The hinge was intact and the door actuator mechanisms were attached. This portion retains normal body curvature. The condition and position of the hinge and door mechanisms indicates that the forward cargo door did not open prior to airplane breakup.

Figure 1.12-4 (a) Item 629 side view- left photo, (b) Item 629 hinge- right photo.

(3) Section 44

The section 44 upper skin structures were found relatively intact. The largest segment (item 626 [Figure 1.12-5]) extends from STA 800 in section 42 to STA 1540 in section 46 and extends nearly to the main deck on both the RHS and LHS. Prior to recovery, this item was observed to still be attached to another large item (item 625 [Figure 1.12-5]) and was separated while lifting. These segments have nearly all stringers still attached and most frames, some of which are broken into segments. A large portion of RHS structure from the STA 1350 to approximately STA 1480 was not recovered.

Figure 1.12-5 Items 625 and 626

(4) Wing

This section details recovered wreckage of the left and right wing, the wing center section and the engine support (strut) structure. All wreckage from the wing box (primary wing structure between front and rear spars) and wing center section was retrieved from within the main debris field of the yellow zone or found floating. The strut structure was recovered in either the yellow zone or still attached to the engines in the green zone. The recovery location of the three largest portions of the left and right wing (items 547, 526, and 628) placed them within 100 feet of each other on the ocean floor.

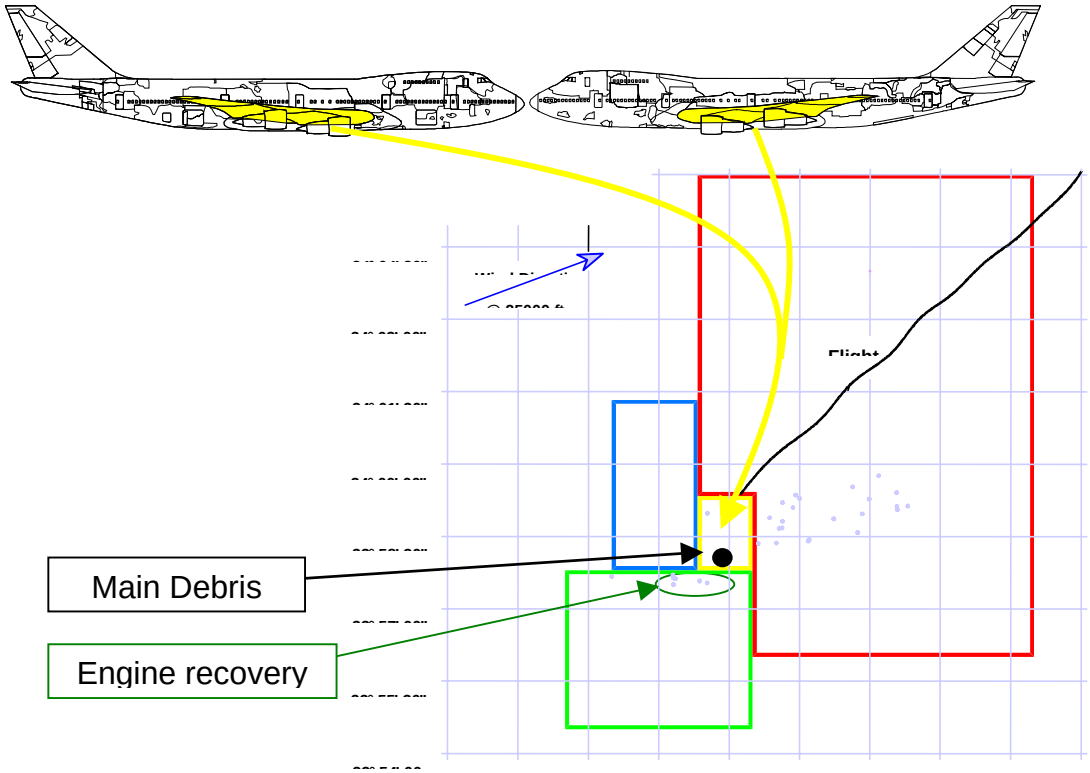

Figure 1.12-6 The wing box and wing center section were retrieved from the yellow zone. The strut structure was recovered in either the yellow zone or still attached to the engines in the green zone.

(5) Left Wing box

The major portion of the left wing box (Item 547 [Figure 1.12-7(a)]) extending from the side of body rib to WSTA 1420 (wing station 1420) was recovered as one piece. This large piece of wreckage included 94 feet of the upper and lower skin panels and the majority of the left wing front, mid and rear spars from the side of body to the outboard engine strut. Segments of the Wing Center Section (WCS) lower panel and small portions of the upper panel and span-wise beams remained attached to the left wing.

The upper and lower skin panels were essentially intact with a number of fractures and some missing skin sections. Portions of the #1 and #2 strut structure remained attached to the wing. Further documentation of the strut structure will be shown later. The side of body rib from the rear spar to the mid-spar was recovered intact (on item 547) with no noted distortion of the web. The most forward portion of the side of body rib near the front spar terminal fitting was recovered separately. Almost all of the in-spar ribs located in the outboard wing were crushed vertically. The deformations on the recovered portions of the mid-spar, from just outboard of the side of body to the end of the mid-spar at the outboard strut, were also consistent with a vertically applied compressive overload [Figure 1.12-7(b)]. The recovered portion of the front spar extended from just inboard of the #2 engine strut support location to just outboard of the #1 engine strut support location. The recovered portion of the rear spar extended from the side of body to outboard of the #1 engine strut support location.

The lower surface of the left wing (on item 547) showed areas of distinct upward deformation of the wing skin and stringers while the upper skin and stringers remained relatively straight [Figure 1.12-7(c)]. The lower panel deformations, on the inboard portion of the wing, had general upward curvature and deformations whereas the outboard portion of the lower surface, where the panel gauges are thinner, exhibited localized deformation between the stringers. This was evident not only on the outboard wing skins on item 547, but also on item 866 which is the end of the wing-box that extends outboard from item 547 [Figure 1.12-7(c)].

No evidence of soot was observed during visual examination of the wing-box interior including the interior portions of the vent stringers on the upper wing panel.

Figure 1.12-7 (a) Item 547

Figure 1.12-7 (b) Lower panel and midspar deformation on Item 547, (c) Localized deformation on outboard end of item 547

(6) Right Wing-box

The majority of the right wing-box was recovered in two major sections. Most of the upper right wing skin (Item 526 [Figure 1.12-8(a)]) was recovered as one large section that was split lengthwise along the mid-spar upper chord. This 70 foot section included the upper skin from nearly the side of body to the outboard (#4) strut and the front spar to approximately 10” to 20” forward of the rear spar along its length. Most of the upper stringers remained attached to the skin panel and the entire panel remained relatively straight. No evidence of soot deposits was found during visual examination of the interior of the wing and the interior of the vent stringers.

The lower panel of the right wing, the upper panel outboard of the outboard engine strut (outboard of item 526), the front spar between the engine strut locations and the rear spar between the side of body and the outboard engine strut were recovered as one 95 foot section (Item 628 [Figure 1.12-8(b)]).

The overall condition of the right wing was similar in nature to the condition of the left wing. The lower panel had a greater level of deformation in comparison to the upper panel. Similar to the left wing, almost all of the in-spar ribs and the mid-spar in the outboard wing were crushed in the vertical direction. In addition, the side of body rib was relatively intact from the mid-spar to the rear spar, in contrast to the recovered portions forward to the front spar. The front spar extended from just inboard of the #3 engine strut location to just outboard of the #4 engine strut location. The recovered portion of the rear spar extended from the side of body to outboard of the #4 engine strut location.

Figure 1.12-8 (a) Item 526

Figure 1.12-8 (b) Item 628I

(7) Wing Center Section

The Wing Center Section (WCS), also known as the center wing tank, is the portion of the wing that passes through the fuselage. It extends from STA 1000, which is also the junction of Fuselage Sections 42 and 44, to the rear spar at STA 1241. The WCS has a constant cross section that matches that of the outboard wing at the Side of Body. As the center part of the wing box beam, it reacts the outboard wing shear, bending, and torsion loads. It is the interface structure that reacts the loads of the fuselage onto the wing and vice versa. The keel beam attaches to the lower panel of the WCS and extends to the aft end of Section 44 at STA 1480. The Front Spar and Lower Skin are fabricated primarily from 2024 aluminum whereas the Upper Panel, Rear Spar, Mid-spar and Span-wise Beams are fabricated primarily from a combination of 7075 and 7178 aluminum alloys. Figure 1.12-9 shows the contour and components within the cross-section of the WCS.

The following Wing Center Section (WCS) detail documentation includes a

description of the following components:

- WCS Front Spar
- Span-wise Beam #3 (SWB #3)
- Span-wise Beam #2 (SWB #2)
- WCS Mid-spar
- Span-wise Beam #1 (SWB #1)
- WCS Rear Spar
- WCS Upper Panel
- WCS Lower Panel
- Left and Right Side of Body Ribs
- Keel Beam

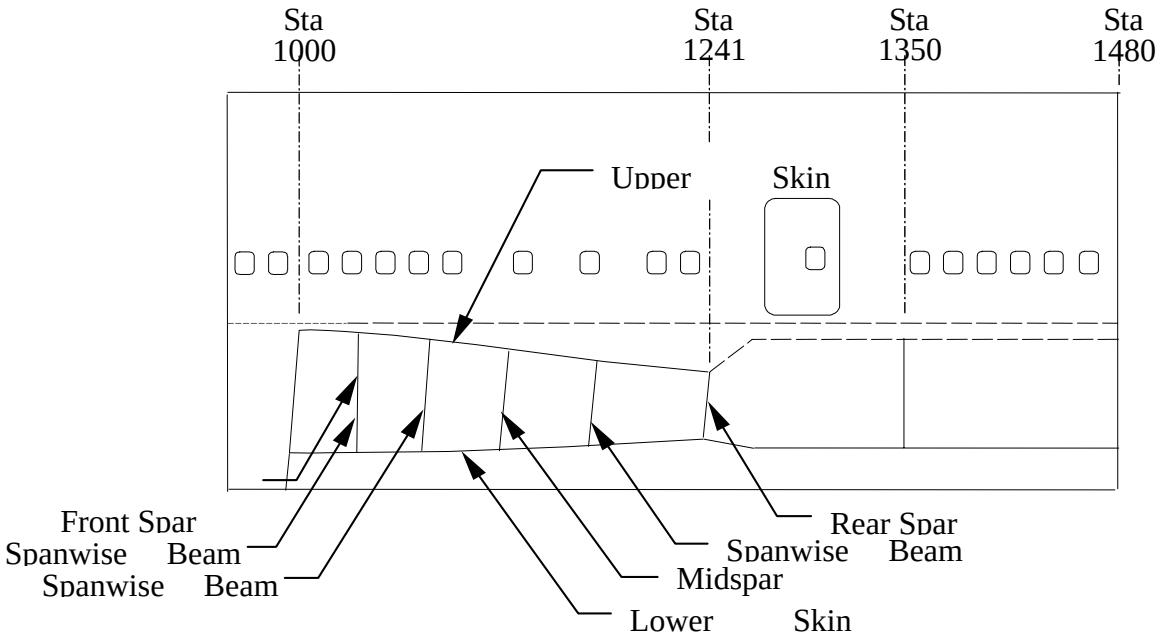

Figure 1.12-9 Wing Center Section

a. Front Spar

The recovered portion of the WCS Front Spar consists of the following 10 sections and their corresponding recovery locations:

Item 725 Lat N 23° 58’ 03.909” Long E 119° 40’ 22.464”

Item 726 Lat N 23° 58’ 11.022” Long E 119° 40’ 20.523”

Item 909 Lat N 23° 58’ 04.076” Long E 119° 40’ 21.822”

Item 2233 Lat N 23° 58’ 03.891” Long E 119° 40’ 22.584”

Item 2238 No recovery location noted

Item 2239 Lat N 23° 58’ 03.682” Long E 119° 40’ 22.750”

Item 2237 No recovery location noted

Item 546 Lat N 23° 58’ 04.380” Long E 119° 40’ 22.800”

Item 625 Lat N 23° 58’ 03.426” Long E 119° 40’ 22.323”

Item 1264 Lat N 23° 58’ 03.891” Long E 119° 40’ 22.584”

Figure 1.12-10 documents the recovered and identified portions of the Wing Center Section front spar.

All segments show similar characteristic patterns. The lower end of the stiffeners and web are curled forward in a tight radius and are separated from the lower front spar chord and lower pressure bulkhead. When the front spar item 909 is placed in proximity to the adjacent lower skin panel (See Figure 1.12-11), the stiffener and web deformations match the local upward deformation of the lower wing skin. This same pattern of front spar stiffener and web deformations are consistently repeated across the entire width of the WCS front spar (See Figure 1.12-12 and 1.12-13).

In comparison to the lower end of the stiffeners, the upper end of the stiffeners and web are mostly intact with portions of the upper chord and upper skin panel remaining attached. The aft edge of the upper skin remaining attached to Front Spar Item #726 is bent down over the entire length of the upper chord.

Item 726 has evidence of lateral front spar deformations indicated by the front spar web and stiffener free flange stabilization strap deformations.

There is no evidence of any fire or soot accumulations on either the forward or aft side of the front spar.

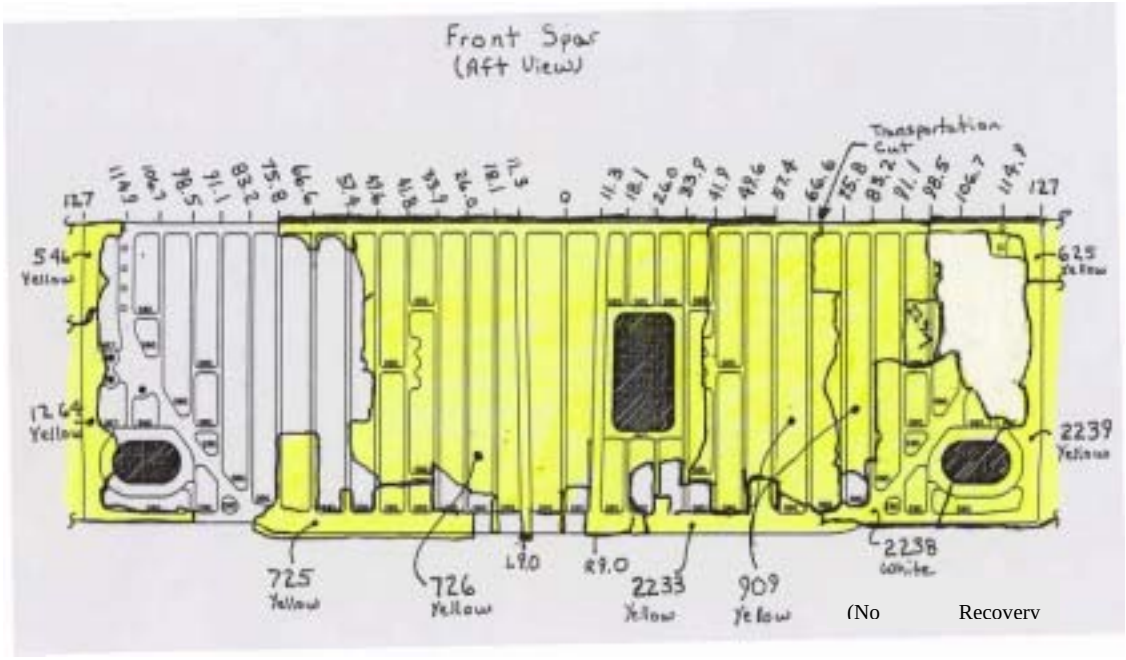

Figure 1.12-10 The recovered and identified portions of the Wing Center Section front spar

Figure 1.12-11 Front Spar Item 909 placed adjacent to Lower Skin

Figure 1.12-12 Forward side of WCS Front Spar

Figure 1.12-13 Bottom view of WCS Front Spar stiffeners

b. Span-wise Beam #3

The recovered portion of the Wing Center Section Span-wise Beam #3 consists of the following 8 sections and their corresponding recovery locations:

Item 835 Lat N 23° 58’ Long E 119° 40’ 22.750”

Item 867 Lat N 23° 58’ 04.000” Long E 119° 40’ 22.348”

Item 1250 No recovery location noted

Item 1069 No recovery location noted

Item 549 No recovery location noted

Item 2230 No recovery location noted

Item 2231 No recovery location noted

Item 2232 Lat N 23° 58’ 04.027” Long E 119° 40’ 22.348”

(Item 2232 is a piece of item 867 that was separated during reconstruction)

Figure 1.12-14 documents the recovered and identified portions of SWB #3.

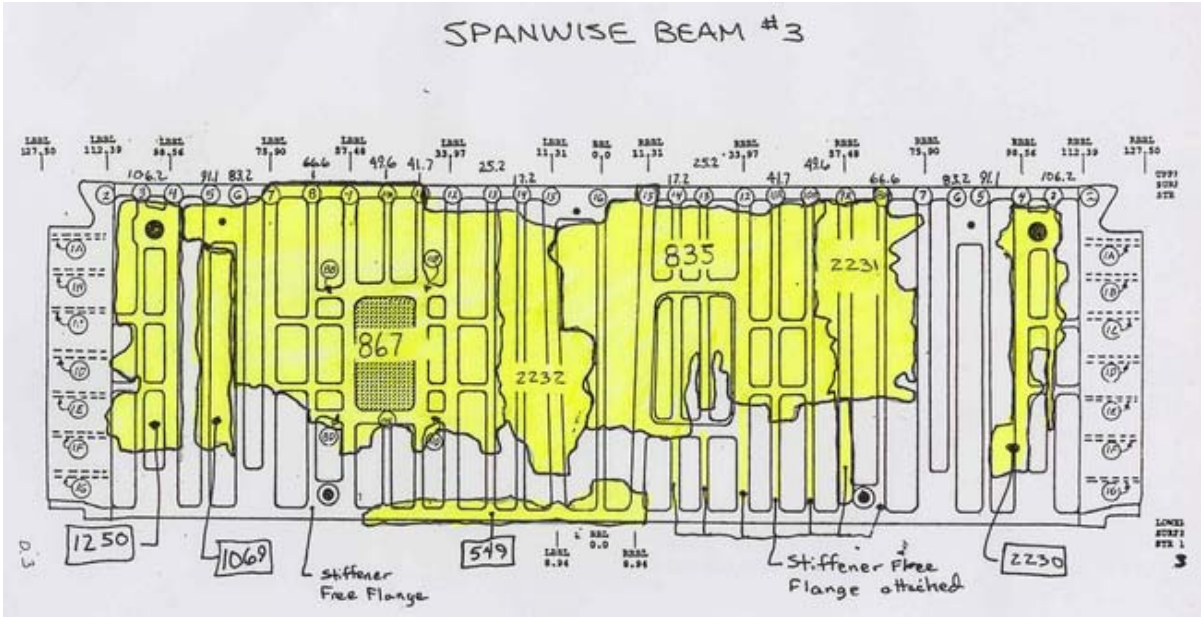

Figure 1.12-14 The recovered and identified portions of SWB #3

Nearly 75% of SWB #3 was recovered and identified. The sections that were recovered showed a consistent pattern of web and stiffener deformation and fragmentation. The upper portions of the stiffeners and web were relatively intact but the lower 25% of the web was highly fragmented and the lower end of the stiffeners free flanges were curled and bent forward (See Figure 1.12-15).

The vertical flange portion of the shear tie(s) common to the upper chord, skin and Span-wise beam stiffener remained attached to the stiffener(s). A small portion of upper chord remains attached to item 867 between LBL 41.7 to 57.5 that has portions of the fasteners common to the skin remaining above the surface of the chord.

The small portion of the lower chord attached to the lower skin panel item #549 is bent aft on the panel. The forward face of this lower chord segment has vertical witness marks extending from the lower edge of the chord to just below the lower fastener row common to the web.

There was no evidence of soot or fire damage on the recovered portions of SWB #3.

Figure 1.12-15 Aft side of SWB #3 viewed from right side

c. Span-wise Beam #2

The recovered portion of the Wing Center Section Span-wise Beam #2 consists of the following 6 sections and their corresponding recovery locations:

Item 1075 Lat N 23° 58’ 04.979” Long E 119° 40’ 22.826”

Item 1265 No recovery location noted

Item 1258 No recovery location noted

Item 2234 Lat N 23° 58’ 03.682” Long E 119° 40’ 22.750”

Item 2235 No recovery location noted

Item 2236 No recovery location noted

Item 2244 No recovery location noted

Figure 1.12-16 documents the recovered and identified portions of SWB #2.

Less than 25% of SWB #2 was recovered or identified. Two of the segments were attached to portions of the side of body rib and had significant web fragmentation and no intact vertical stiffeners. The other three segments exhibited similar fragmentation patterns to that on SWB #3. The upper portions of the stiffeners and web were relatively intact but the lower 25% of the web was highly fragmented and the lower end of the stiffeners free flanges were curled nearly 90 degrees forward (See Figure 1.12-17).

The portion of SWB #2 remaining attached to item 2236 has the inboard edge of the web bent forward and the S.O.B. rib portion is bent inboard.

The small portion of the lower chord attached to the lower skin panel item #1265 remains on the panel. The forward face of this lower chord segment has vertical witness marks extending from the lower edge of the chord to just below the lower fastener row common to the web.

There was no evidence of any soot accumulations or fire damage on the recovered portions of SWB #2.

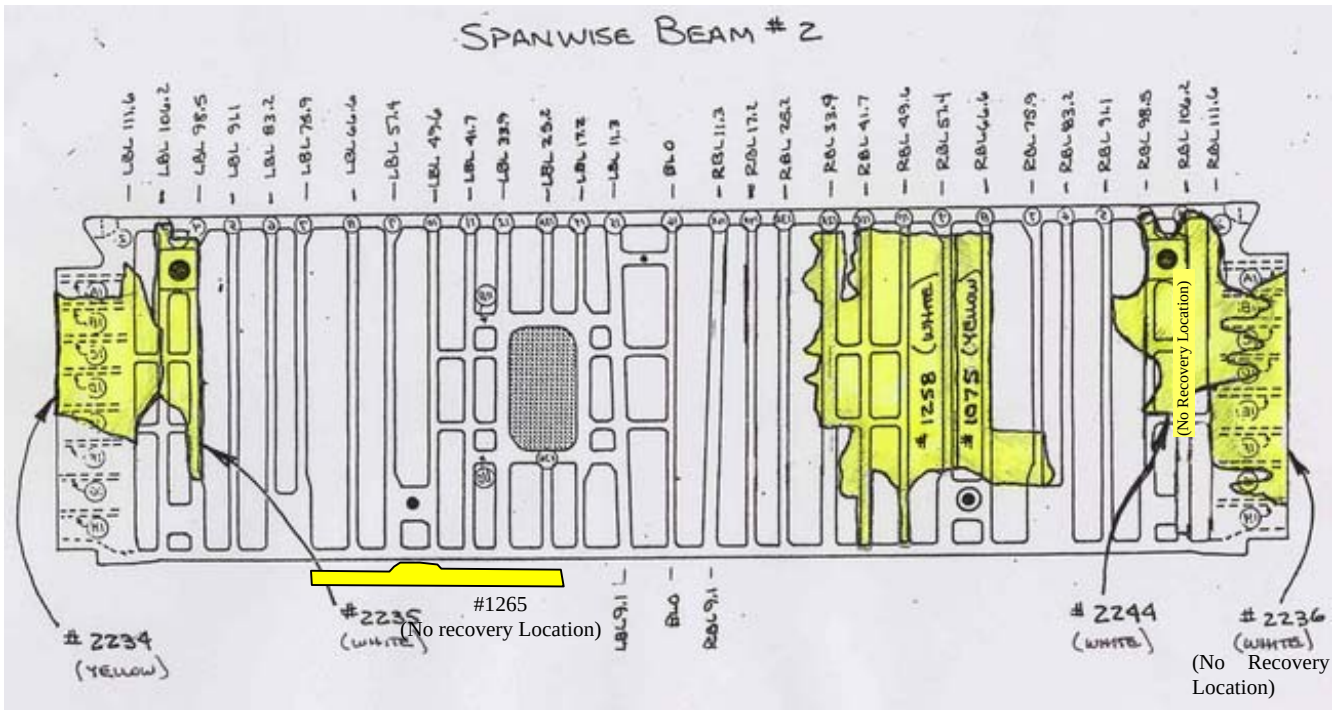

Figure 1.12-16 The recovered and identified portions of SWB #2

Figure 1.12-17 Spanwise Beam #2 Item 1258 and 1075

d. Wing Center Section Midspar

The recovered portion of the Wing Center Section Mid-spar consists of the following 8 sections and their corresponding recovery locations:

Item 546 Lat N 23° 58’ 04.380” Long E 119° 40’ 22.800”

Item 547 Lat N 23° 58’ 04.280” Long E 119° 40’ 22.910”

Item 625 Lat N 23° 58’ 03.426” Long E 119° 40’ 22.323”

Item 709 Lat N 23° 58’ 03.000” Long E 119° 40’ 22.000”

Item 908 Lat N 23° 58’ 03.682” Long E 119° 40’ 22.750”

Item 1252 Lat N 23° 58’ 04.130” Long E 119° 40’ 23.203”

Item 2229 Lat N 23° 58’ 03.682” Long E 119° 40’ 22.750”

Item 2247 No recovery location noted

Figure 1.12-18 documents the recovered and identified portions of the Midspar.

The upper chord of the Mid-spar remained attached to upper panel (Item #642) along with the floor beam tension fittings and the upper shear tie connections. The lower edge of the web and small portions of stiffeners remaining attached to the chord are bent aft over a large portion of the chord.

Most all of the stiffeners free flanges did not remain attached to the spar structure. With the exception of the spar above the keel structure (Item #1252), none of the lower 25% of the spar is recovered or identified.

The portion of the Mid-spar web that remains attached to the right wing and fuselage (item #625) is bent aft overall but the lower edge has localized bending in the forward direction.

A small portion of the BL 0 rib aft of the mid-spar remained attached to item #1252.

There was no evidence of soot or fire damage on the recovered portion of the Mid-spar.

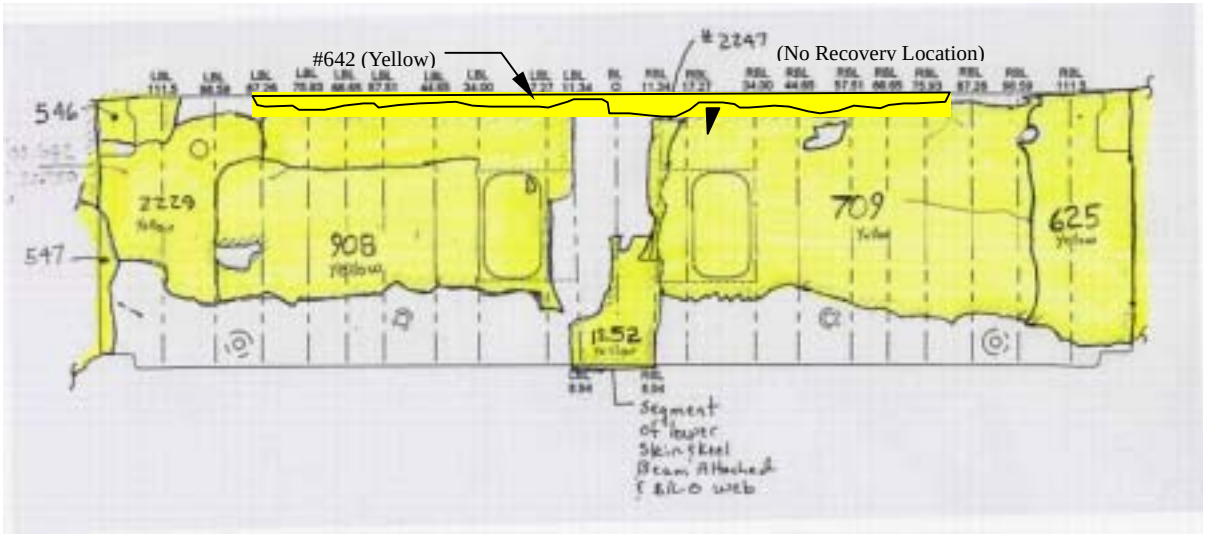

LHS **Mid Spar - View Looking Forward** **RHS**

Figure 1.12-18 The recovered and identified portions of the Midspar

Figure 1.12-19 Aft side of Midspar viewed from right side

e. Wing Center Section Span-wise Beam #1

The recovered portion of the Wing Center Section Span-wise Beam #1 consists of the following 7 sections and their corresponding recovery locations:

Item 2240 No recovery location noted

Item 2241 No recovery location noted

Item 2242 No recovery location noted

Item 2243 No recovery location noted

Item 2246 No recovery location noted

Item 1257 Lat N 23° 58’ 03.891” Long E 119° 40’ 22.584”

Item 625 Lat N 23° 58’ 03.426” Long E 119° 40’ 22.323”

Figure 1.12-20 documents the recovered and identified portions of SWB #1.

Large portions of span-wise beam #1 were not recovered or identified.

For items that were recovered, the lower edge of the parts indicated a higher degree of fragmentation than the upper edge.

The upper chord of Span-wise Beam #1 remained attached to upper panel (Item #642) along with the floor beam tension fittings and the upper shear tie connections. The lower edge of the SWB web remaining attached to the upper chord is bent aft along the length of the chord.

None of the lower chord remained attached to the skin but some of the stiffener shear ties remained attached to lower panel item #1256 and #836. For the shear ties on item #1256, the fastener holes that would have been common to the SWB stiffener web have been deformed on the lower edge of the hole or slightly off center from the lower edge of the hole.

There was no evidence of soot or fire damage on SWB #1.

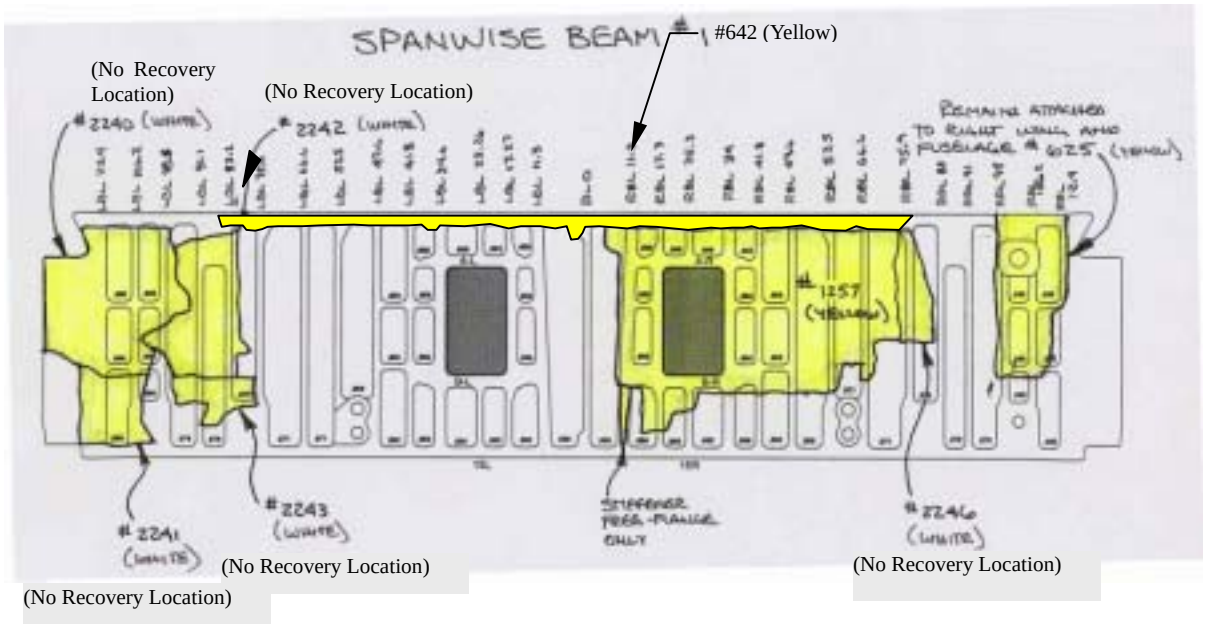

Figure 1.12-20 The recovered and identified portions of SWB #1

Figure 1.12-21 Spanwise Beam #1

f. Wing Center Section Rear Spar

The recovered portion of the Wing Center Section Rear Spar consists of the following 5 sections and their corresponding recovery locations:

Item 546 Lat N 23° 58’ 04.380” Long E 119° 40’ 22.800”

Item 625 Lat N 23° 58’ 03.426” Long E 119° 40’ 22.323”

Item 864 No recovery location noted

Item 907 Lat N 23° 58’ 04.115” Long E 119° 40’ 22.985”

Item 910 Lat N 23° 58’ 04.521” Long E 119° 40’ 22.568”

Figure 1.12-22 documents the recovered and identified portions of the Rear Spar.

The recovered portions of the web and stiffeners remained flat and the stiffeners remained attached to aft side of web. The lower edges of the recovered web segments were fractured along a straight line that at a location coincident with the upper edge of the vertical flange of the lower chord. The lower ends of the vertical stiffeners common to the WCS lower beam locations remain intact below the fractured edge of the web. The right rear spar/body bulkhead fitting remains intact on item #625 and the left fitting remains on items #546 and #547[See Figure 1.12-23(a)]. There is no obvious deformation along the fracture surface on the rear spar/body bulkhead fitting between item #546 and #547.

Item #910 was recovered as one section that ended up as two segments during transportation [See Figure 1.12-23(b)]. The center portion of this section remained attached to the keel structure aft of the spar. There is a chord fracture at LBL 21 where the two segments became separated. At this location on the outboard segment, the chord is twisted in an aft and upward direction. The upper chord on the outboard (LBL 95) end of this segment is twisted such that the skin flange is bent upward. The inboard end (RBL 11) of the upper chord on item #864 is also twisted in an upward and aft direction while the outboard end (RBL 86) is bent up with a slight rearward twist.

In the areas that the upper skin is no longer attached to the skin flange of the upper chord segments, portions of the fastener shanks remain above the surface of the skin flange of the chord where the skin would have been.

There is a localized black residue on the forward side of item #910 at approximately LBL 34. This deposit occurs only on the forward side of the web and locally on the web fracture surface. There is no evidence of this deposit on the aft side of the web in the same region. This residue does not exist on the portion of item #910 that was previously attached or on any other portion of the rear spar.

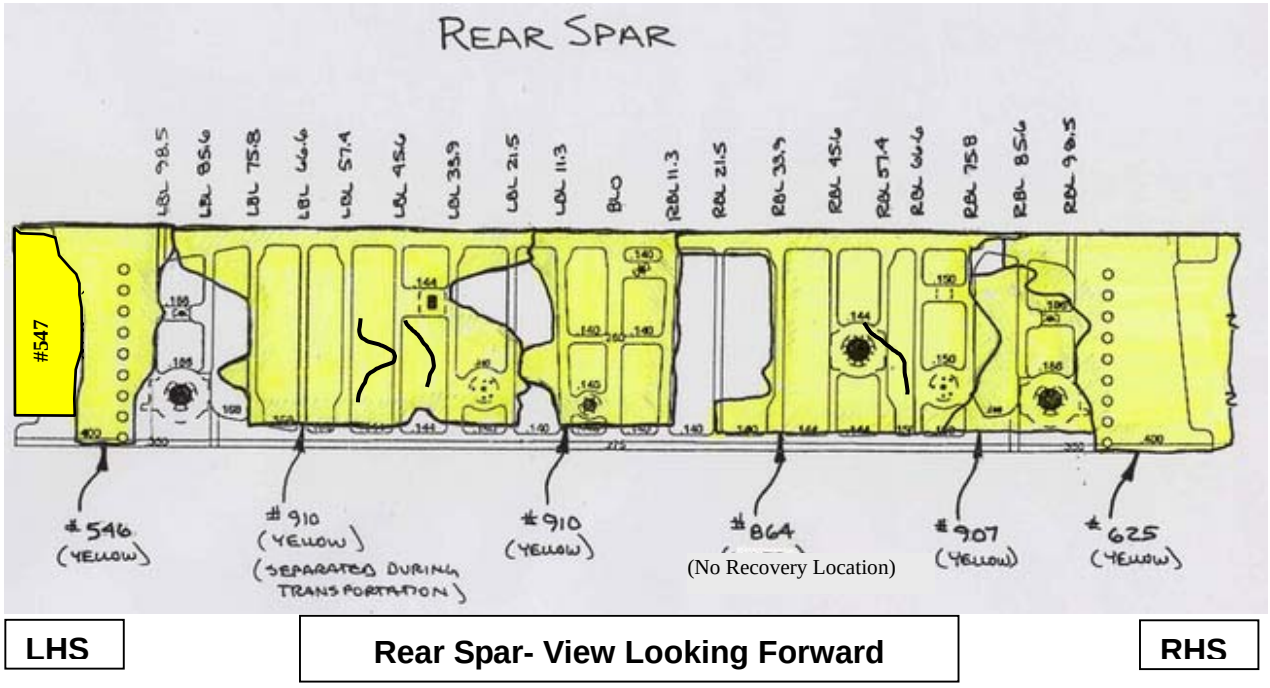

Figure 1.12-22 The recovered and identified portions of the Rear Spar

Figure 1.12-23 (a) WCS Rear Spar

Figure 1.12-23 (b) Rear Spar Item #910 as recovered with segments connected

g. Wing Center Section Upper Panel

The recovered portion of the Wing Center Section Upper Panel consists of the following 7 sections and their corresponding recovery locations:

Item 1251 Lat N 23° 58’ 04.130” Long E 119° 40’ 23.203”

Item 547 Lat N 23° 58’ 04.280” Long E 119° 40’ 22.910”

Item 910 Lat N 23° 58’ 04.521” Long E 119° 40’ 22.568”

Item 1259 No recovery location noted

Item 625 Lat N 23° 58’ 03.426” Long E 119° 40’ 22.323”

Item 2228 Lat N 23° 58’ 03.830” Long E 119° 40’ 22.480”

Item 864 No recovery location noted

Figure 1.12-24 documents the recovered and identified portions of the Upper Panel. The largest portion of the upper wing center section skin that did not remain attached to either wing was a piece that extended from the rear spar to span-wise beam 2. Unlike the lower panels, the upper panel maintained its original overall contour in both longitudinal and lateral direction (See Figure 1.12-25). This skin panel had localized skin curvature at the fracture edges on the left and right periphery.

The majority of the stringers remained attached to the upper skin. The mid-spar and span-wise beam upper chords remained attached to the upper

panel; including the floor beam tension fittings and shear ties common to the upper end of the stiffeners.

There were discolorations noted on the upper side of the panel. There were also stains that were noted on multiple segments of the upper panel. Samples were taken of the dark discolorations and the test results are contained within a separate report. There were no indications of soot or fire damage on the interior surface of the upper panel structure including vent stringers.

On item #1251, the remaining portion of the skin flange of the upper spar chord just inboard of the upper skin splice plate is bent downward. The forward edge of the skin along the forward fracture edge is also bent downward.

The right hand upper rear spar splice is intact. Note: The left hand upper skin portion of item #547 near the rear spar incurred transportation damage during wreckage recovery

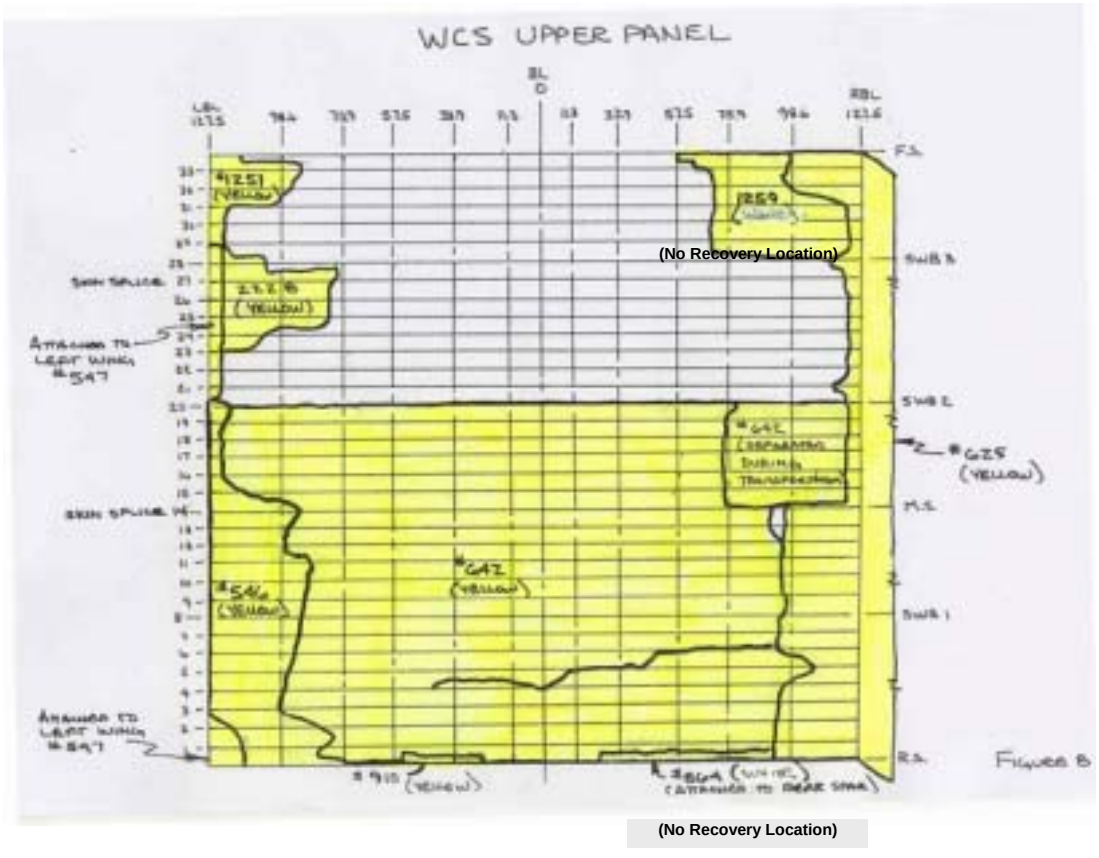

Figure 1.12-24 Documents the recovered and identified portions of the Upper Panel

Figure 1.12-25 (a) Interior surface of Upper Panel Item #642-upper photo, (b) Exterior surface of Upper Panel Item #642-lower photo

h. Wing Center Section Lower Panel

The recovered portion of the Wing Center Section Lower Panel consists of the following 13 sections and their corresponding recovery locations:

Item 547	Lat N 23° 58’ 04.283”Long	E 119° 40’ 22.902”
Item 549	No recovery location noted	
Item 606	No recovery location noted	
Item 628	Lat N 23° 58’ 04.680”Long	E 119° 40’ 22.320”
Item 725	Lat N 23° 58’ 03.909”Long	E 119° 40’ 22.464”
Item 836	Lat N 23° 58’ 03.682”Long	E 119° 40’ 22.750”
Item 837	Lat N 23° 58’ 03.682”Long	E 119° 40’ 22.750”
Item 863	Lat N 23° 58’ 04.760”Long	E 119° 40’ 21.822”
Item 1252	Lat N 23° 8’ .130”Long	E 119° 40’ 23.203”
Item 1254	No recovery location noted	
Item 1256	Lat N 23° 58’ 04.049”Long	E 119° 40’ 23.231”
Item 1265	No recovery location noted	
Item 2233	Lat N 23° 58’ 03.891”Long	E 119° 40’ 22.584”

Figure 1.12-26 documents the recovered and identified portions of the lower panel.

Two large segments of lower skin were recovered still attached to the left wing (Item #547) and right wing (Item #628) and the remainder of the panels were recovered separately (See Figure 1.12-26). There are two predominant characteristics for the recovered panel sections; 1) the lower panel segments fractured laterally into segments along the Span-wise Beam or Mid-spar locations and 2) the panels also generally exhibit upward curvature between the Span-wise Beams or Spars (See Figure 1.12-27 for a diagram of this characteristic). The exception to this curvature is on items #725, #1265 and #547 common to the keel beam attachment. At these locations, the panel retains curvature more typical of normal lower surface contour.

For the most part, the only stringers remaining attached to the panel are at the splice stringer locations and at the mid-spar (which is also a panel splice location). At SWB #1, the shear ties for the SWB stiffeners remain on the panel but the lower chord is not attached. Common to the lower panel on item #1252, a portion of the mid-spar remains attached along with the internal and external tension fittings at the keel beam. Portions of the lower chords of SWB #2 and SWB #3 remain attached to items #1265 and #549. The keel beam tension fittings at LBL 9.0 and RBL 9.0 remain attached to the lower panel at SWB #3 and at LBL 9.0 at SWB #2.

Along the aft edge of items #549, #725, #2233 and #863, there are impact witness marks on the inside of the panel at both left and right BL 33.9, BL 57.5, BL 75 and BL 98.6. The impact marks extend forward of the aft edge of the panel by approximately .5” and at some locations have torn out small segments of the skin panel. These locations are coincident with the locations of the lower internal stabilization beams within the wing center section.

The lower skin splice at the left hand rear spar/side of body (item #547) remains intact. The lower skin splice at the right hand rear spar/side of body (item #628) remains intact. The vertical flange of the spar chord at this location is missing. The lower skin and skin flange of the rear spar chord from roughly 10” outboard of the side of body splice to the fracture edge at RBL 96 is twisted such that the aft edge is down

The lower skin splice at both the right and left front spar/side of body joint (item #725 and #1254) is intact and the remnant of the vertical portion of the front spar terminal fitting is bent aft. The forward end of the vertical flange of the lower side of body rib chord is bent locally inboard.

There were uniform discolorations noted on the lower surface of the panel. Samples were taken of these discolorations and the test results are contained within a separate report. There were no indications of soot or fire on the interior panel surface.

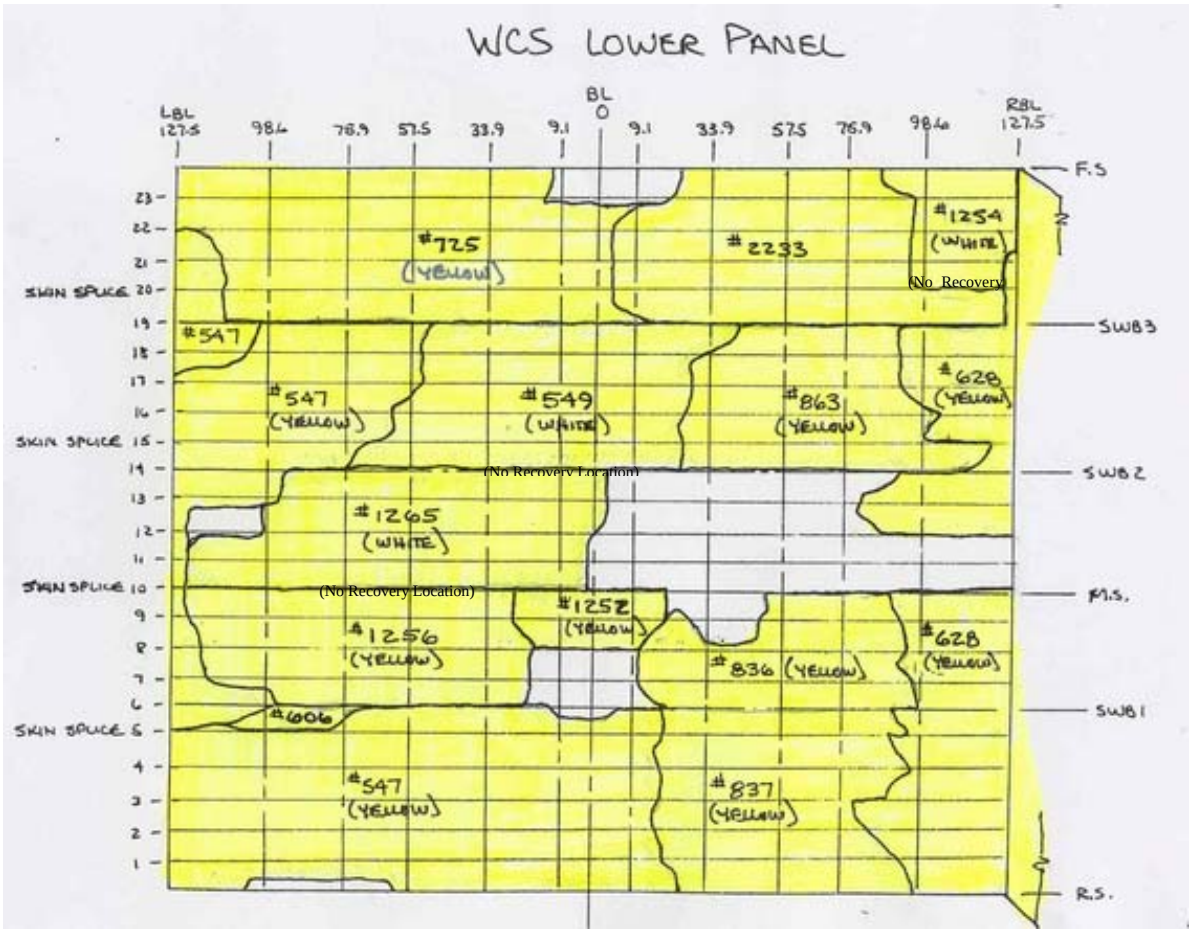

LHS

Lower Panel- View Looking Down

RHS

Figure 1.12-26 Documents the recovered and identified portions of the lower panel

Figure 1.12-27 WCS Lower Panel Reconstruction

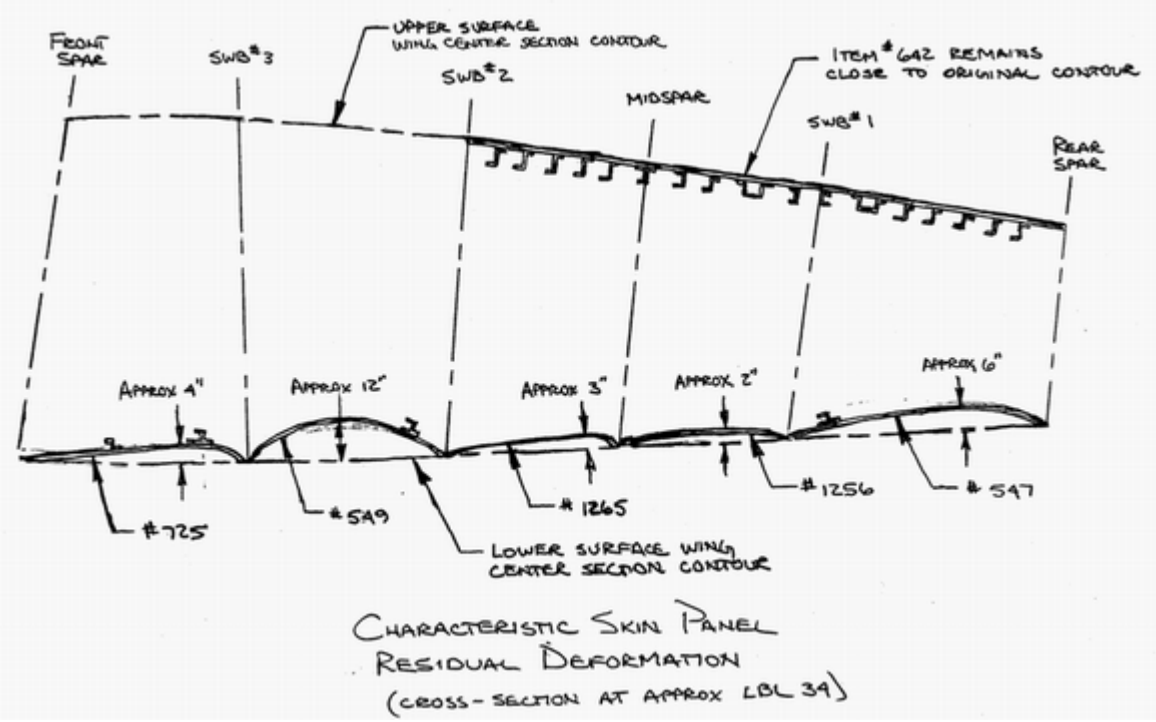

Figure 1.12-28 Characteristic Skin Panel Deformation (Cross section at approximately LBL 34)

i. Wing Side of Body Ribs

The recovered portion of the Wing Side of Body (S.O.B.) Ribs consists of the following 8 sections and their corresponding recovery locations:

(a) Left Side of Body Rib

Item 547 Lat N 23° 58’ 04.280” Long E 119° 40’ 22.910”

Item 725 Lat N 23° 58’ 03.909” Long E 119° 40’ 22.464”

Item 1264 Lat N 23° 58’ 03.891” Long E 119° 40’ 22.584”

Item 2234 Lat N 23° 58’ 03.682” Long E 119° 40’ 22.750”

(b) Right Side of Body Rib

Item 526 Lat N 23° 58’ 04.680” Long E 119° 40’ 22.320”

Item 1254 No recovery location noted

Item 2236 No recovery location noted

Item 2239 Lat N 23° 58’ 03.682” Long E 119° 40’ 22.750”

Figures 1.12-29 and 1.12-30 documents the recovered and identified portions of the left and right S.O.B. Ribs.

Both side of body ribs remained intact and flat from the rear spar to the mid-spar. Forward of the mid-spar the recovered pieces showed a higher degree of fragmentation with few stiffeners attached.

Two of the segments (item #1264 and #1019) had evidence of diagonal web buckling between the vertical stiffeners. The direction of the buckling pattern was from the lower/aft to upper/fwd direction (See Figure 1.12-31).

There was no evidence of soot or fire damage.

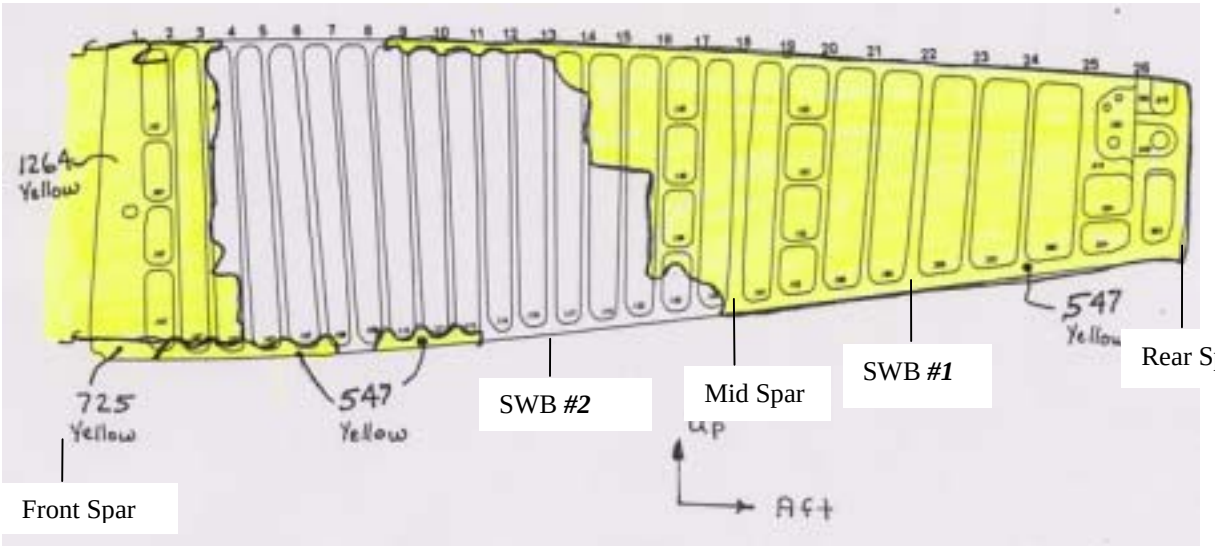

Left Side of Body Rib - View Looking Inboard

Figure 1.12-29 The recovered and identified portions of the left S.O.B. Ribs

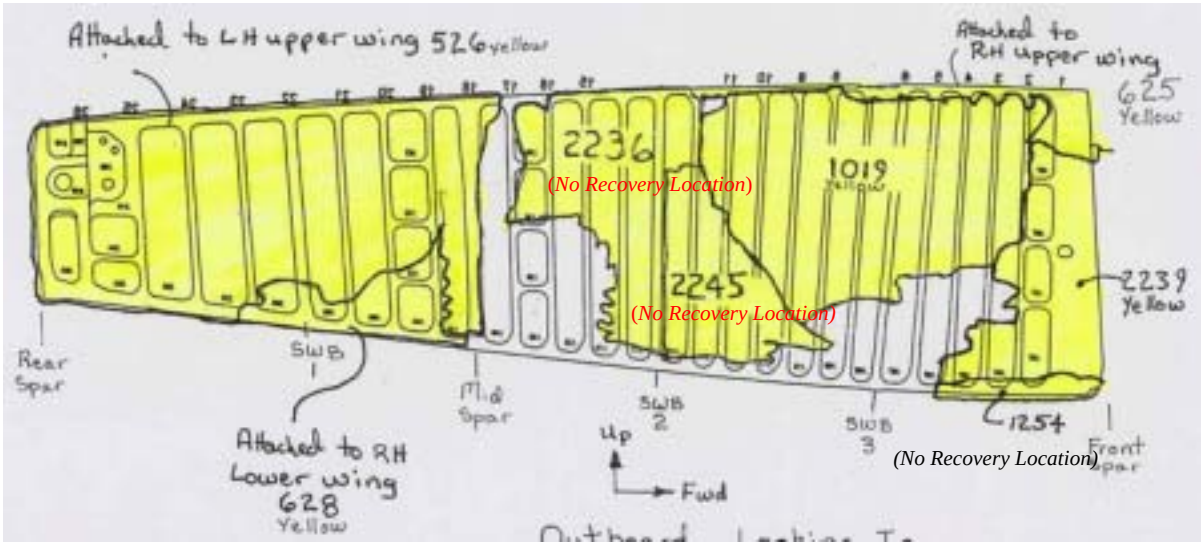

Right Side of Body Rib - View Looking Inboard

Figure 1.12-30 The recovered and identified portions of the right S.O.B. Ribs

Figure 1.12-31 (a) Left S.O.B Rib Item #1264 showing web buckling

Figure 1.12-31 (b) Left Side of Body Rib Web

j. Keel Beam

The recovered portion of the keel beam consists of the following 9 sections and their corresponding recovery locations:

Item 830 Lat N 23° 58’ 03.682” Long E 119° 40’ 22.750”

Item 831 Lat N 23° 58’ 03.682” Long E 119° 40’ 22.750”

Item 840 Lat N 23° 58’ 03.682” Long E 119° 40’ 22.750”

Item 900 Lat N 23° 58’ 04.076” Long E 119° 40’ 23.822”

Item 910 Lat N 23° 58’ 04.521” Long E 119° 40’ 22.568”

Item 969 Lat N 23° 58’ 04.796” Long E 119° 40’ 22.257”

Item 1227 Lat N 23° 58’ 04.130” Long E 119° 40’ 23.230”

Item 1252 Lat N 23° 58’ 04.130” Long E 119° 40’ 23.230”

Item 1267 No recovery location noted

Figure 1.12-32 and 1.12-33 documents the recovered and identified portions of the left and right keel beams.

The recovered portion of the right keel beam consists of the lower right keel

structure including the chords and web at RBL 9.1 from the rear spar aft to the STA1480 bulkhead. The majority of the BL 0 web aft of the rear spar was also recovered. In the region under the wing center section, only the lower keel chord and a small portion of the RBL 9.1 keel web was recovered.

The lower chord between SWB #1 and SWB #2 (item #1227) is bent overall with the center of the lower chord bent outboard relative to the ends of the part. This segment is also twisted such the aft end is twisted counterclockwise relative to the forward end when viewed looking forward. On the lower chord segment from the front spar to SWB #2 (item #1267), the fracture at the forward end adjacent to the keel beam extensions has no obvious signs of overall twisting or bending except that the last two inches of the lower chord is bent slightly upward common to the forward keel beam extension splice.

The recovered portion of the left keel beam consists of the lower right keel structure including the chords and web at LBL 9.1 from the rear spar aft to nearly the STA 1480 bulkhead. The body landing gear remained attached to the drag brace attachment on the keel just aft of the STA 1350 bulkhead. In the region of the wing center section, the lower keel structure, including portions of the upper chord, web and lower chord between the rear spar and the midspar were recovered.

On item #840(See Figure 1.12-34), there was no obvious signs of bending or twisting of the lower chord at the fracture just fwd of the STA 1350 bulkhead or on the forward end near the mid-spar. The rear spar stiffener at LBL 9 that remained attached to the keel structure is bent such that the lower end of the stiffener and the adjacent keel structure (including web and upper chord) is bent inboard relative to the lower keel chord and the stiffener portion above the upper keel chord (common to the lower WCS skin panel) is bent outboard. In the region of the upper chord from SWB#1 to the mid-spar, the upper keel beam chord skin flange is fractured at multiple locations adjacent to the fastener holes. The fracture edges at these locations are bent upward.

Only small portions of the upper chord remained attached to the lower WCS skin panel. At LBL 9.1, segments of the only the skin flange remain intermittently on the panel from S-23 to SWB#3 on item #725, SWB#3 to SWB#2 on item #549, SWB#2 to the midspar on item #1265 and from SWB#1 to S-4 on item #547. At RBL 9.1, segments of only the skin flange remain intermittently on the panel from S-23 to SWB#3 on item #2233, SWB#3 to

SWB#2 on item #549 and from SWB#1 to S-4 on item #547. Consistently, the fracture edges on these segments of upper chord are bent away from the skin and the shanks of the fasteners common to the upper chord and wing skin are still protruding out of the panel with the fastener head fractured off.

On item 910 the BL 0 web and upper chord has been separated from the horizontal pressure deck from STA 1265 and aft.

Item #969 which have the keel beam extensions forward of the front spar shows significant upward bending of the skin panel between the keel beam extensions.

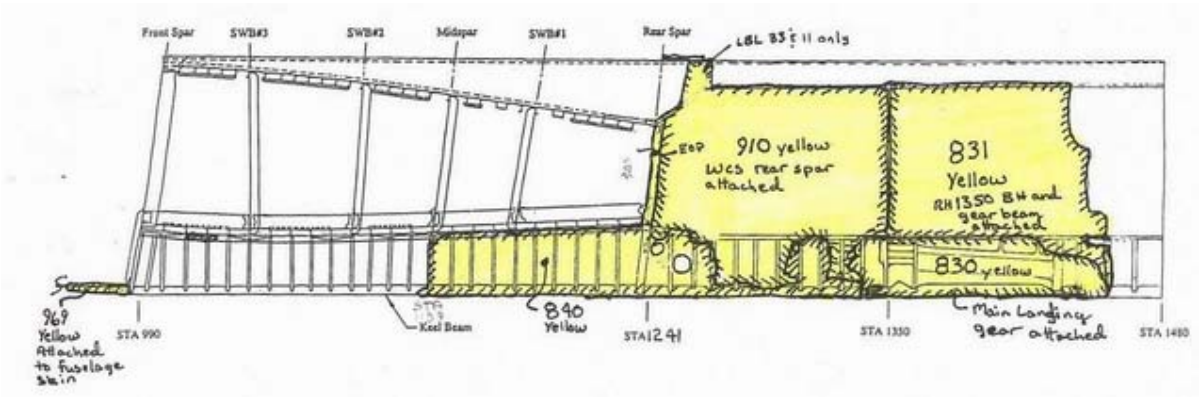

Figure 1.12-32 Left Keel Beam

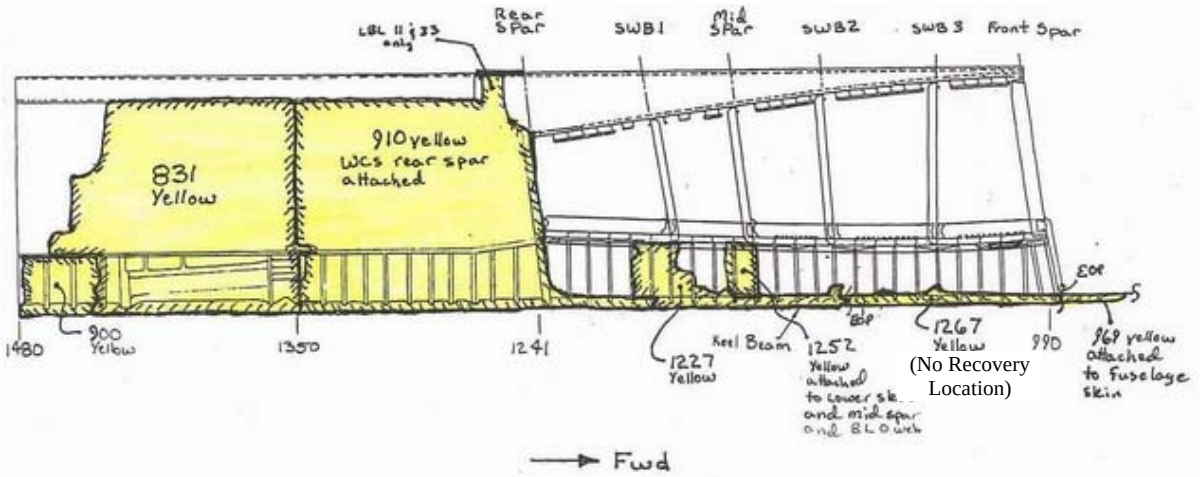

Figure 1.12-33 Right Keel Beam

Figure 1.12-34 Left Keel Beam Item #840

k. Overall Wing Center Section Observations

- Front spar, mid-spar and span-wise beams consistently had greatest level of damage occurring to the lower portion of the beam.
- The lower end of the stiffeners and webs were consistently bent forward on the front spar, SWB #3 and SWB #2.
- Lower panel showed pattern of upward deformation of the lower panel segments between span-wise beams and spars with fractures between segments also occurring at span-wise beam and mid-spar locations.
- Upper panel segments remained relatively flat in comparison to lower panel.
- All Wing Center Section tagged parts were recovered from the yellow zone.
- No visual evidence of fire damage on any recovered Wing Center Section components.

(8) Control Surfaces and High Lift Devices

With one exception, all of the wing control surfaces and high lift devices, including flaps, flap tracks, aileron, etc., (item 832, 879, 1013 as examples) were recovered from the yellow zone or were floating. The submerged items and the left and right wing were found within 275 feet of each other on the ocean floor. A portion of the inboard end of the left hand inboard mid-flap (item 2130) was recovered from trawl zone D.

Little of the wing leading or trailing edge structure remained attached to the wing-box structure on the left or right wing. The #6 leading edge variable camber flap remained attached to the left wing (item 547) and was in the stowed position. Spoiler #1 remained attached to the left wing and was in the retracted position. Spoilers #9, #10 and portions of #11 and #12 remained on the right wing (Item 628) and were in the retracted position. The #7 trailing edge flap track remained attached to the wing-box along with a portion of the flap structure. The inboard aileron was partially attached to the wing.

The flap support ball-screw mechanisms at locations #1 through #5, #7 and #8 were in the fully retracted position. The #6 ball-screw was recovered with the gimble extended by approximately 5 threads (1/8th of a degree of flap angle or 1/40th of the flap 5 detent).

1.12.3 Section 46

The majority of the section 46 structure (pressurized fuselage aft of the wing and wheel well area) was found in the red zone. The only portions found in the yellow zone were those attached to the large pieces extending from section 44 (items 626 and 659). The section 46 structure was distributed over a large area, extending more than four miles East- West（as shown in Figure 1.12-35）.

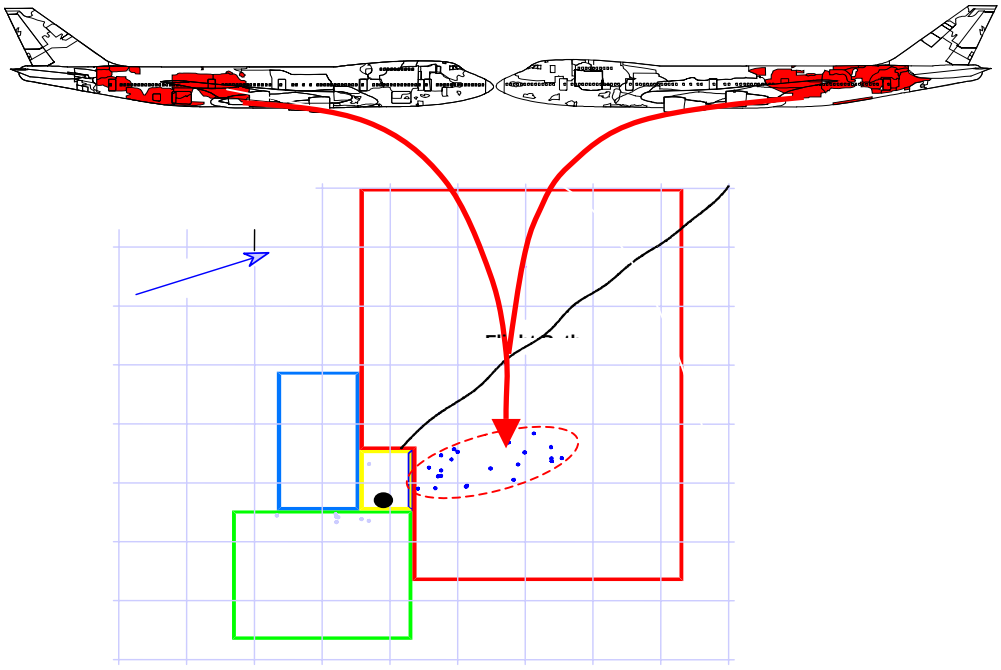

Figure 1.12-35 The section 46 structure was distributed over a large area

(1) Aft Cargo Door

The aft cargo door was retrieved in the red zone in three major segments. The upper portion of the door (item 723 [Figure 1.12-36 (a)]) was recovered with the hinge intact and the actuators in the closed position. At the time of recovery a large section of passenger floor was structurally attached to item 723. During moving and storage the structural attachment was broken and the remaining wires holding the two assemblies together were cut at the dock in Makung. The lower portion of the door (item 741 [Figure 1.12-36 (b)]), including the three forward pairs of latches, was recovered with the latches still latched and the locks engaged. Attached as part of item 741 was a sizable portion of the cargo floor structure (frames, ballmat, etc.) extending to approximately Stringer 46L (S-46L). Very little skin and stringers remained attached to the frames. The lower aft portion of the door (item 2019 [photos below]), including the aft pair of latches, was found separated from the surrounding body structure. The lower portion of the door skin was bent outboard approximately 45 degrees. The observations of the hinge, latches, and door mechanisms indicate that the aft cargo door did not open prior to airplane breakup.

The deformation common to the lower portion of item 2019(See Figure 1.12-36) indicates that this segment of the door rotated outboard about the aft latch pair. This deformation is only evident on item 2019, indicating that this aft portion of the door was still attached at the lower aft latch pair after it was separated from the forward portion of the cargo door. The fracture along the forward edge of item 2019 shows that this separation occurred due to loads transferred through the latch pair (loads from lower edge of door segment). The remaining door segments (items 723 and 741) were still intact and separated at a later time.

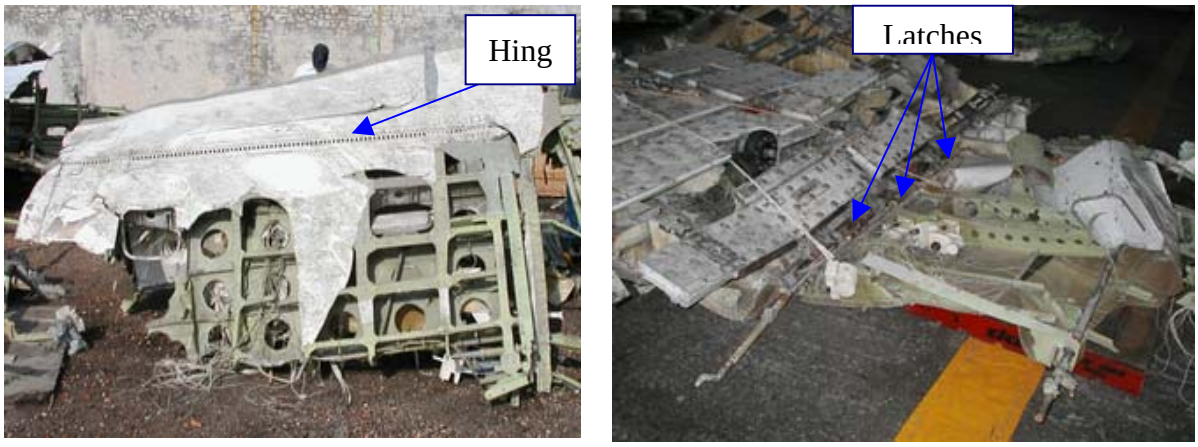

Figure 1.12-36 (a) Item 723- left photo, (b) Item 741- right photo

Figure 1.12-37 Item 2019

(2) Semi-Monocoque Structure

The recovered portions of the semi-monocoque structure (skins/frames/stringers) in Section 46（see Figure 1.12-38） were arranged in a 2D reconstruction to assist in evaluating the fractures and deformations of the panels. A field examination was conducted on the fracture faces of all parts in the reconstruction. Item 640 was found to have flat-fracture surfaces (indicative of slow growth mechanisms) on the skin adjacent to an external repair doubler. The doubler measured approximately 23 inches by 125 inches. Item 640 is discussed separately below. No slow growth mechanisms were noted on the remaining skin segments in section 46.

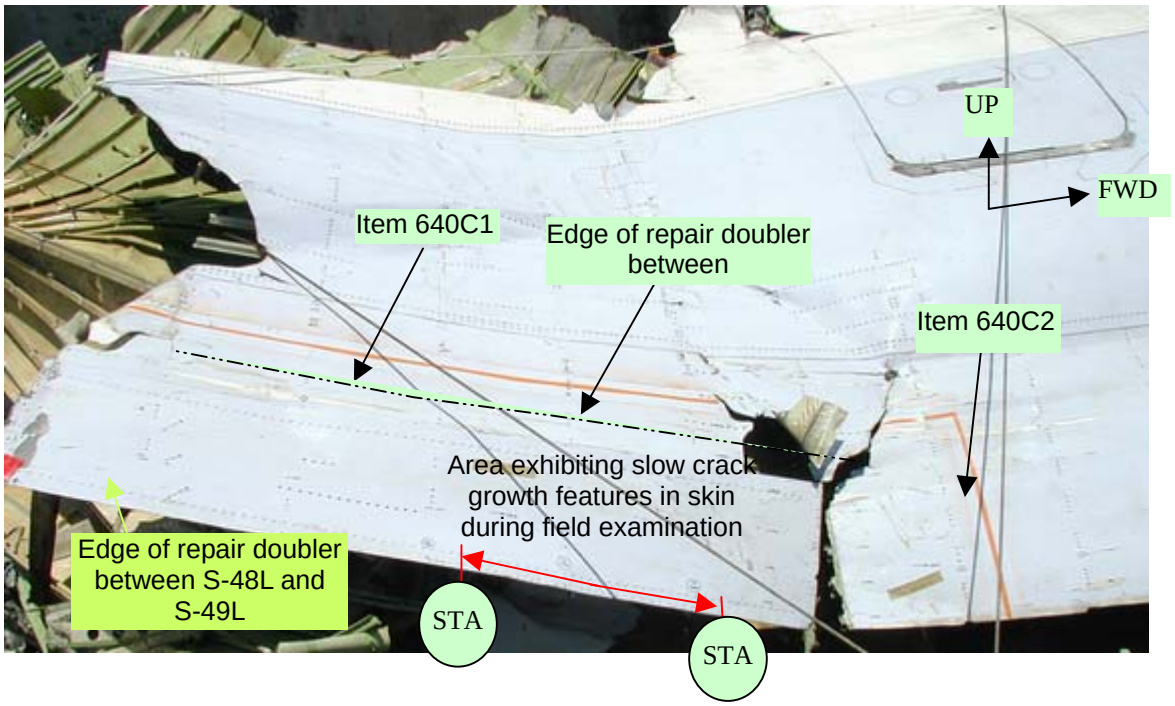

Figure 1.12-38 The recovered portions of the semi-monocoque structure (skins/frames/stringers) in Section 46

(3) Item 640

Flat fractures were observed in the skin along the edge of an external repair doubler at S-49L in the vicinity of STA 2100. The entire repair area was removed and sent for metallurgical examination. The results of this examination are the subject of reports from Chung Shan Institute of Science and Technology (CSIST) and from Boeing Materials Technology (BMT) as shown in 1.16. （See Figure1.12-39）.

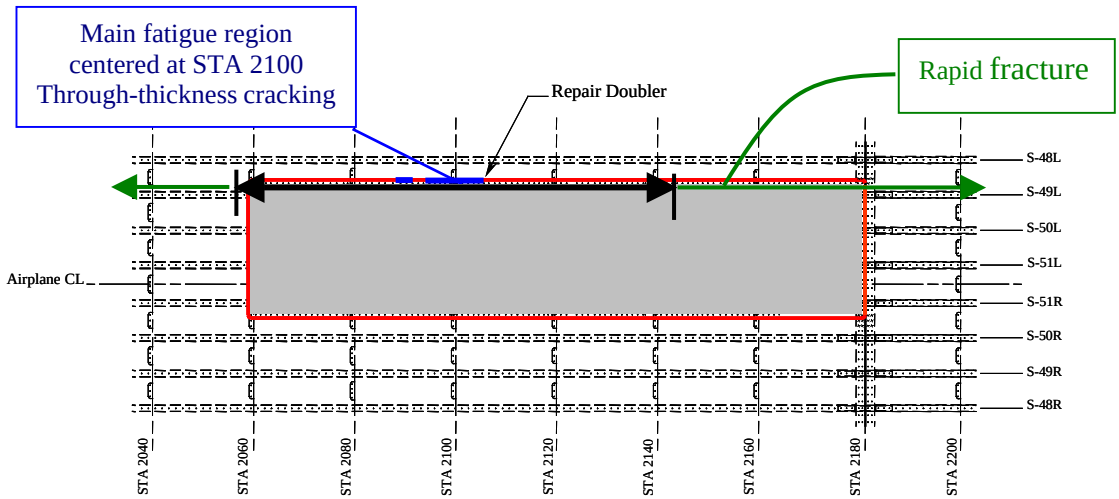

Figure 1.12-39 Flat fractures were observed in the skin along the edge of an external repair doubler at S-49L in the vicinity of STA 2100.

Also included in item 640（Figure 1.12-40） is the bulk cargo door. The segment was recovered with the door closed and latched. The lower portion of the bulk cargo door seal protruded through the space between the door and the sill.

The forward portion of item 640 includes the aft portion of the aft cargo door cutout frame. There are deformations at the lower latch fitting attachment location（Figure 1.12-40）.

Figure 1.12-40 Item 640 at lower latch attachment

(4) The direction of the fracture propagation of Section 46

The fracture directions on item 640 show the crack progressed under the belly of the airplane and then continued forward along S-50R. The crack then progressed upward at approximately STA 1900. The direction of the fracture propagation was based on hole-to-hole cracking patterns, chevron marks, and branching cracks as shown in Figure 1.12-41.

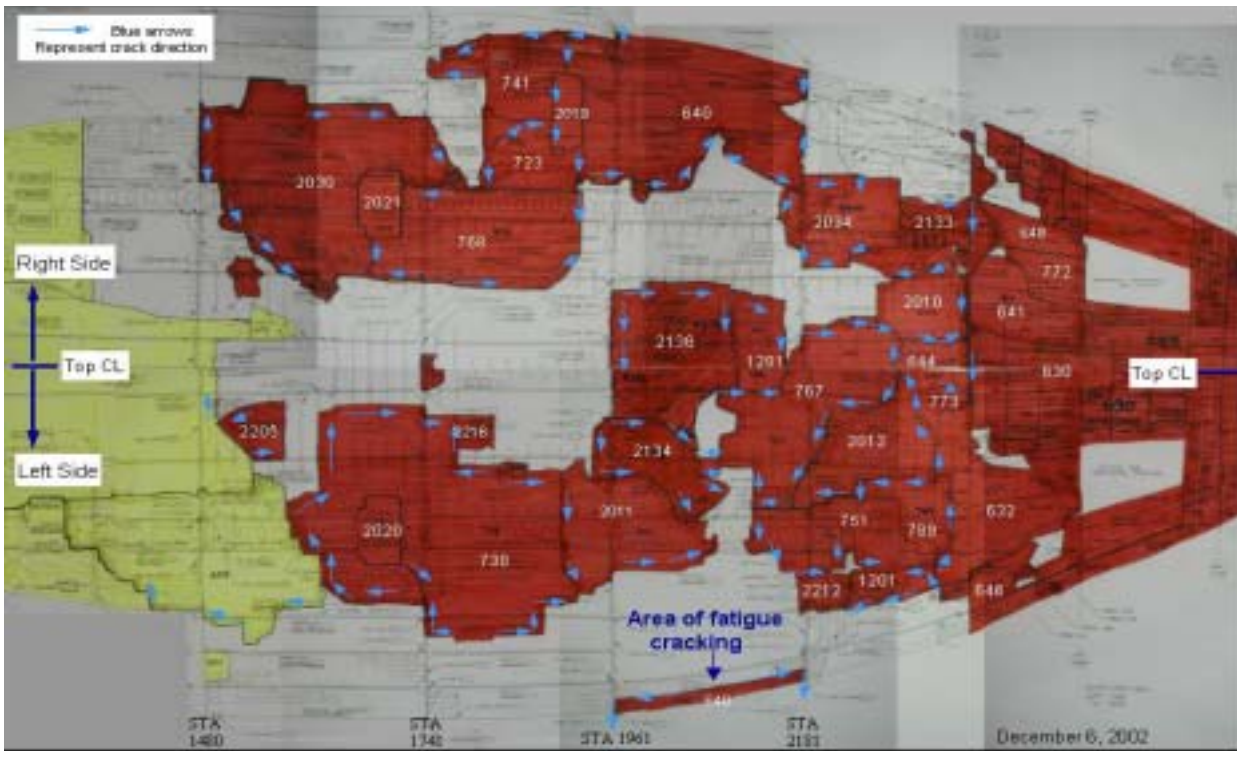

Figure 1.12-41 Arrows show the direction of the fracture propagation

1.12.4 Empennage and Section 48

The section 48 and empennage structure (the aft pressure bulkhead and all structure aft) was found in the red zone（See Figure1.12-42）. The horizontal stabilizer, the majority of the skin/stringer/bulkhead structure, and the lower third of the vertical fin were found attached and with very little damage (item 630 [photo at right]). Some fin structure, including leading edge structure and the fin cap (items 22, 23, and 960) were recovered as floating debris. A large upper portion of the fin and rudder was found separate from item 630（See Figure1.12-43）.

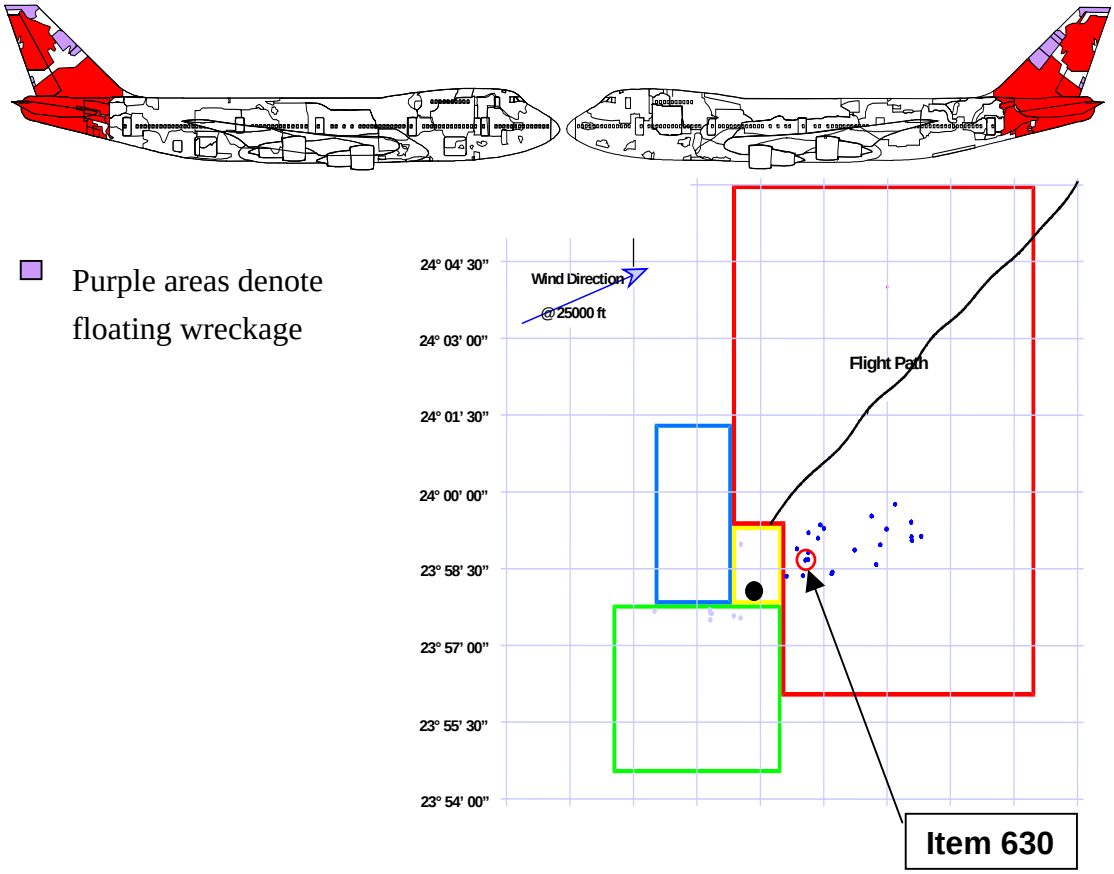

Figure 1.12-42 The section 48 and empennage structure (the aft pressure bulkhead and all structure aft) was found in the red zone.

Figure 1.12-43 Item 630

(1) Horizontal Stabilizer

Shallow dents and varying shades of blue marks were found along the leading edge of the LHS stabilizer. Laboratory examination coupons were taken for these regions for evaluation and are the subject of a separate report. There is blue paint of similar color in the forward body. However, the transfer marks [See Figure 1.12-44(a)] were confirmed to not be from aircraft exterior finishes. Samples of some interior components were also tested and no match was found.

The RHS horizontal stabilizer is considerably more damaged than the LHS. The inboard portion of the RHS leading edge is deformed upwards. At the RHS horizontal stabilizer root, the inboard 10 feet showed considerable impact damage along with upwards deformation of the compromised structure. A portion of seat support was found inside a puncture common to the lower surface of the LHS horizontal stabilizer. A small segment of fuselage stringer was also found imbedded in the RHS elevator [See Figure 1.12-44(b)]. A small fastener and shim from a stowage bin assembly were found inside a puncture common to the RHS horizontal stabilizer leading edge [See Figure 1.12-44(c)].

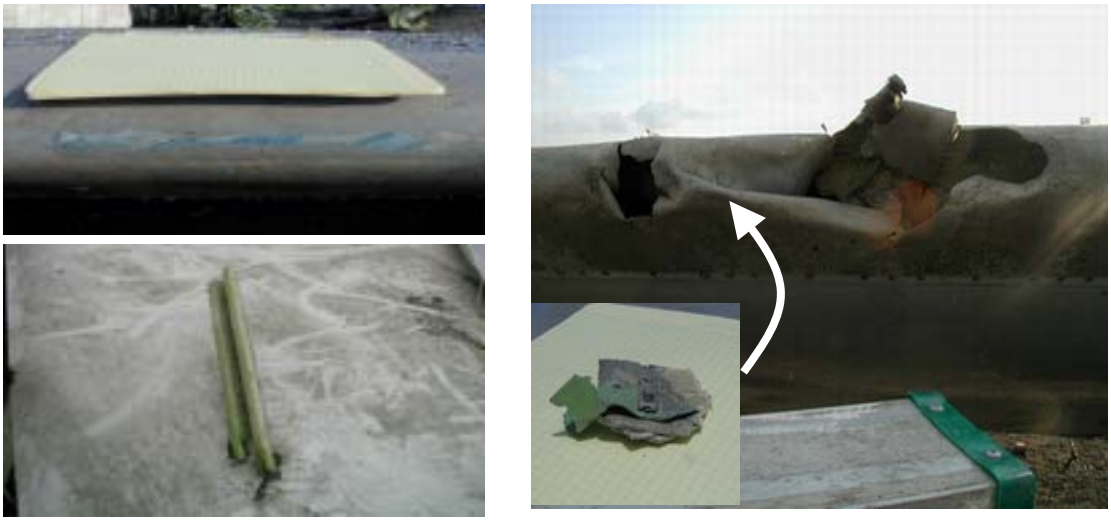

Figure 1.12-44 (a) Item 630C2 – transfer marks LHS- upper-left photo, (b) Stringer imbedded in RHS Elevator- lower-left photo, (c) Item 630C3 horizontal stabilizer with stowage bin part- right photo

(2) Vertical Fin (See Figure 1.12-45)

The majority of the upper portion of the vertical fin (item 2035) was found separate from the remaining section 48 debris, but also in the red zone. The forward edges of item 2035 were deformed to the left side indicating the leading edge portion was struck by a large object on the right side. The lower edge of this piece exhibited signs of bending and separation to the left side. At the upper forward edge of item 2035, there was significant tearing damage from fore to aft and right to left.

The middle portions of the vertical fin leading edge (items 22 [See Figure 1.12-46(a)], 23, 170, 350, and 392) were found floating. There were puncture marks evident on the RHS of these pieces. The vertical fin cap (item 960) was also found floating.

The lower portion of the vertical fin remained attached to the majority of section 48 and is now identified as item 630C1 [See Figure 1.12-46(a)] after being cut near the base to facilitate transportation. Two small stringer segments were found inside the leading edge portion of the fin adjacent to two punctures on the RHS. These stringer segments (items 630C4 and 630C5) originated from a section 46 fuselage belly panel. Item 630C4 is confirmed to be from STA 2170 at S-38R and the characteristics of item 630C5 indicate it is from STA 2170 at either S-42R or S-44R. Residue on the forward fracture face of these stringer segments indicates they entered the fin forward end first. The fractures and

adjoining skin on item 630C1 contained deformation consistent with the upper portion of the vertical fin bending to the left.

The lower portion of the fin (item 630C1), the upper portion of the fin (item 2035), and several of the floating pieces (item 22) show similar evidence of impact damage on the right side.

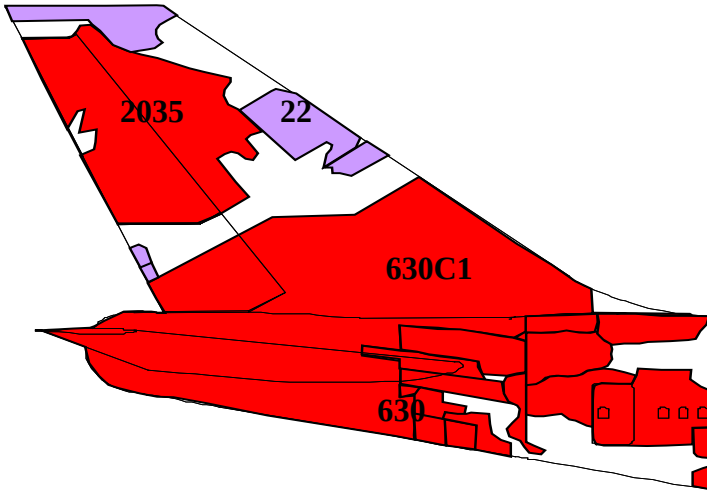

Figure 1.12-45 Vertical Fin

Figure 1.12-46 (a) Item 22- left photo, (b) Item 630C1 penetrations with 630C4 and 630C5 stringer segments placed- right photo

The entire empennage separated from section 46 forward of the aft pressure bulkhead at STA 2360. Separation of the empennage structure resulted from a combination of impact from section 46 structure and insufficient remaining section 46 structure to support the weight and loads of the empennage.

A large portion of the section 48 structure (including items 630-632, 641, 644, 646-648, 765, 766, 772, 773, 938, 939, 943, 944, and 2013) from the aft pressure bulkhead aft was found in the red zone within close proximity. The empennage impacted the water relatively intact in an attitude that appears to

be nose down and RHS horizontal stabilizer down. At the time of impact, the lower right portion of section 48 took a majority of the impact force fragmenting the skin into small pieces. The aft pressure bulkhead lower half was compressed upwards. The fuselage frames from the aft pressure bulkhead to the horizontal stabilizer jackscrew were pushed aft and fractured, predominantly on the RHS.

1.12.5 Strut Structure and Engines

All four engines were recovered in a relatively concentrated area (as shown in Figure 1.12-47. A significant portion of the engine support structure remained attached to the left and right wing (See Figure 1.12-48). All recovered fuse pins remained intact.

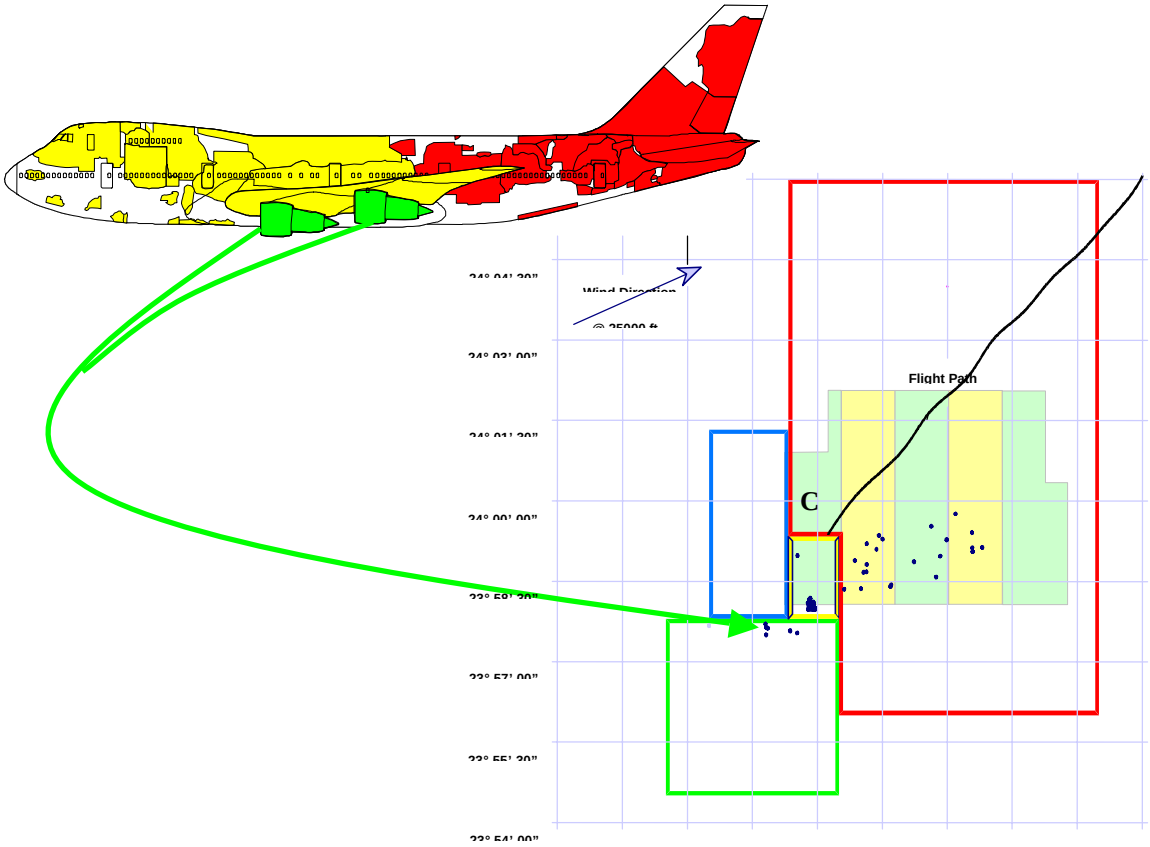

Figure 1.12-47 All four engines were recovered in a reletively concentrated area

Figure 1.12-48 View of dual side links installed by strut modification

(1) Engine #1

The strut upper link (R1) is intact and remains attached to the wing fittings. Pins on both ends are intact and a section of upper strut is attached to the strut end of the link. Under-wing and strut mid-spar fittings (R3 and R4) and fuse pins are all intact（Figure 1.12-49）. Dual side brace fittings (R7 and R8) are attached at both ends and appear normal. There is a 65” long section of mid-spar extending forward from the R3 and R4 fittings, as well as a 30” long piece of bulkhead extending below the R3, R4 fittings. The bulkhead extends across the width of the strut. The aft end of the diagonal brace (R2) had separated from its under-wing fitting. A portion of the under-wing fitting remained attached to the aft of the diagonal brace. The diagonal brace was bent outboard, such that the centerline had a pronounced curve（Figure 1.12-50）. At the forward end, the diagonal brace remained attached to the lower end of the strut aft bulkhead, but the attach fitting was bent outboard. The inboard mid-spar chord was bent downwards relative to the outboard mid-spar chord（Figure 1.12-51）. The observed deformations in the strut and attach structure were consistent with the lower portion of the strut translating outboard relative to the rest of the strut. n（Figure 1.12-52）.

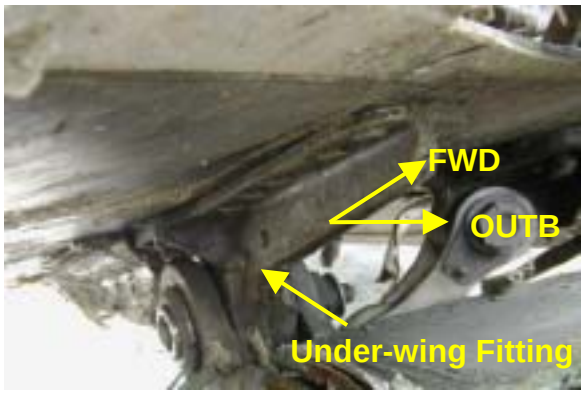

Figure 1.12-49 Under-wing and strut mid-spar fittings (R3 and R4) and fuse pins are all intact

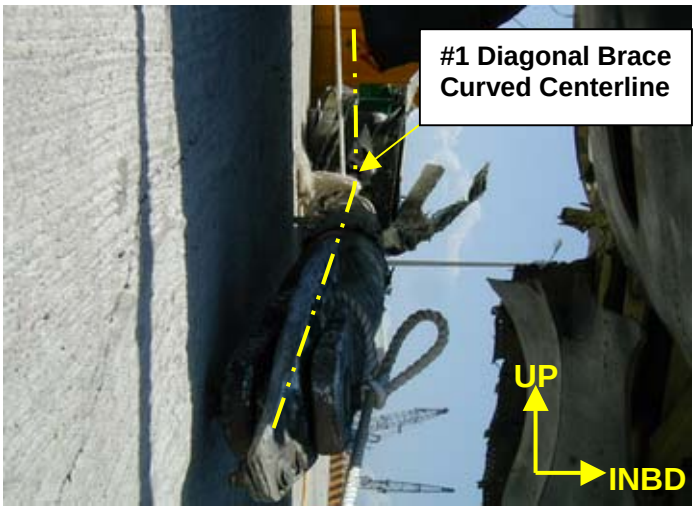

Figure 1.12-50 The diagonal brace was bent outboard, such that the centerline had a pronounced curve

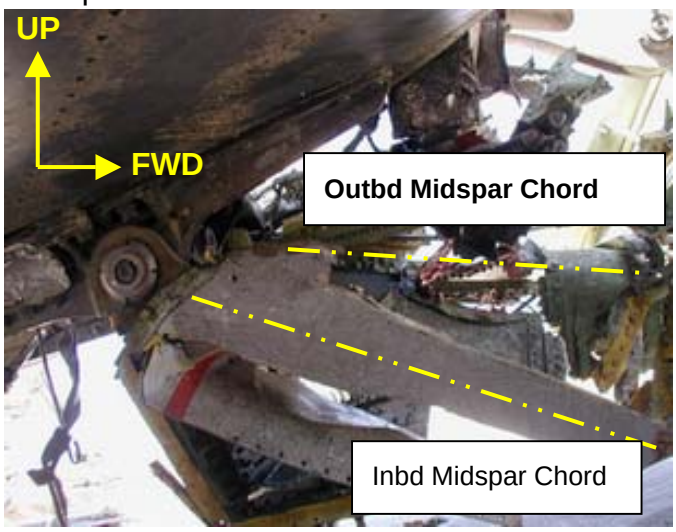

Figure 1.12-51 The inboard mid-spar chord was bent downwards relative to the outboard mid-spar chord.

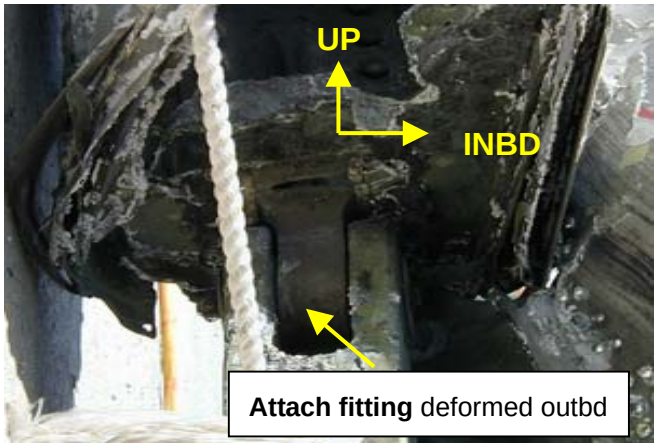

Figure 1.12-52 Deformations departing the airplane in an outboard direction.

(2) Engine #2

The strut upper link (R1) is intact and remains attached to the wing fittings. Pins on both ends are intact and a 30” section of strut is attached to the forward end of the link. Under-wing and strut mid-spar fittings (R3 and R4) and fuse pins are intact. Dual side brace fittings (R7 and R8) are attached at both ends and appear normal. There is a 72” long section of strut structure extending forward from the R3, R4 fittings, as well as a 12” long piece of bulkhead extending below R3 and R4 fittings and across the width of the strut. Another piece of the strut (about 48” long and width of strut) forward of NS 222 is attached by wires to the strut structure. The diagonal brace was recovered still attached to the under-wing fitting. The lower end of the diagonal brace was attached to lower portion of the strut aft bulkhead. The diagonal brace itself was displaced outboard nearly 90 degrees from its normal position, with severe deformation of the under-wing fitting. Some of the outboard deformation may have occurred during recovery（Figure 1.12-53）, as the diagonal brace was supporting part of the weight of the wing. During subsequent transportation, the under-wing fitting fractured completely and the diagonal brace was liberated. The upper link had rotated upward and damaged the wing mounted upper link fittings. The inboard strut mid-spar chord was bent down relative to the outboard mid-spar chord. The inboard mid-spar under-wing fitting had begun to pull away from the wing skin and a gap was visible at the forward end（Figure 1.12-54）.

The rotation of the upper link is consistent with upward motion of the strut（Figure 1.12-55）. However, the deformation of the diagonal brace, mid-spar chords, and gap between the lower wing skin and inboard under-wing mid-spar

fitting are consistent with outward motion of the strut. The two motions could not have happened simultaneously. The separation direction for the #2 engine was not conclusively determined.

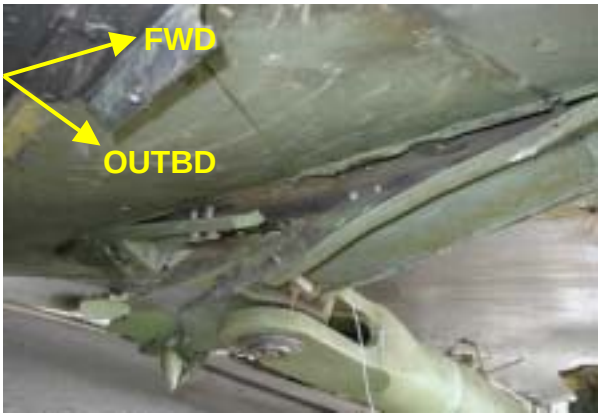

Figure 1.12-53 The diagonal brace itself was displaced outboard nearly 90 degrees

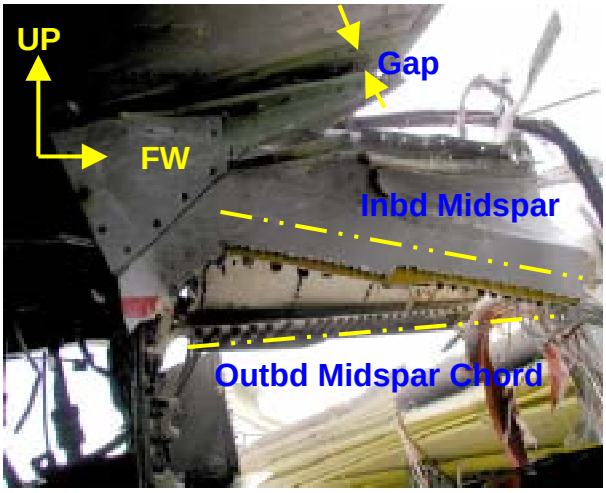

Figure 1.12-54 The inboard strut mid-spar chord was bent down relative to the outboard mid-spar chord

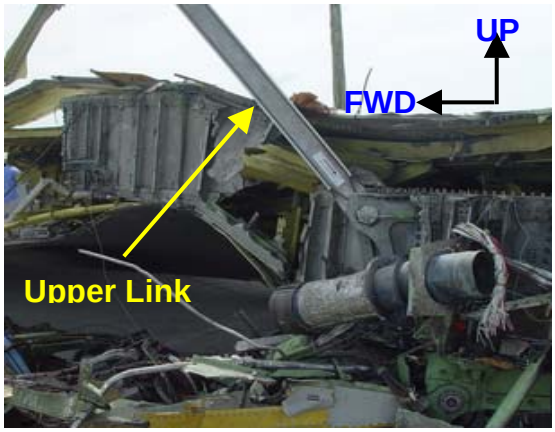

Figure 1.12-55 The rotation of the upper link is consistent with upward motion of the strut

(3) Engine #3

The strut upper link (R1) is intact and remains attached to the wing fittings （Figure 1.12-56）. Pins on both ends are intact and a 72” piece of strut beam is attached to the forward end of the link. Under-wing and strut mid-spar fittings (R3 and R4) and fuse pins are intact. Dual side brace links (R7 and R8) are attached at the top but the outboard aft link is bent aft. There is a 55” long piece of mid-spar structure extending forward from the R3 and R4 fittings, as well as a 20” long piece of bulkhead extending below R3 and R4 fittings. The bulkhead extends across the width of the strut, but has been twisted with the outboard portion pulled free from the vertical leg of the strut mid-spar fitting （Figure 1.12-57）. The diagonal brace was not recovered. The diagonal brace under-wing fitting was found fractured and the remaining portion was bent outboard（Figure 1.12-58）. The deformation of the outboard aft side link is consistent with the twisting of the aft bulkhead. The twisting of the aft bulkhead is consistent with clockwise rotation of the #3 engine (when viewed from above). The deformation of the diagonal brace under-wing fitting and the strut aft bulkhead are consistent with clockwise twisting and outward rotation of the #3 engine.

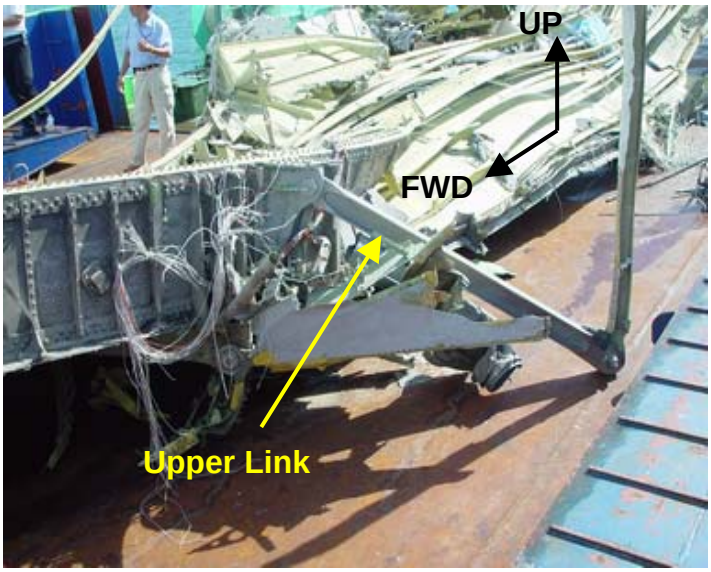

Figure 1.12-56 The strut upper link (R1) is intact and remains attached to the wing fittings

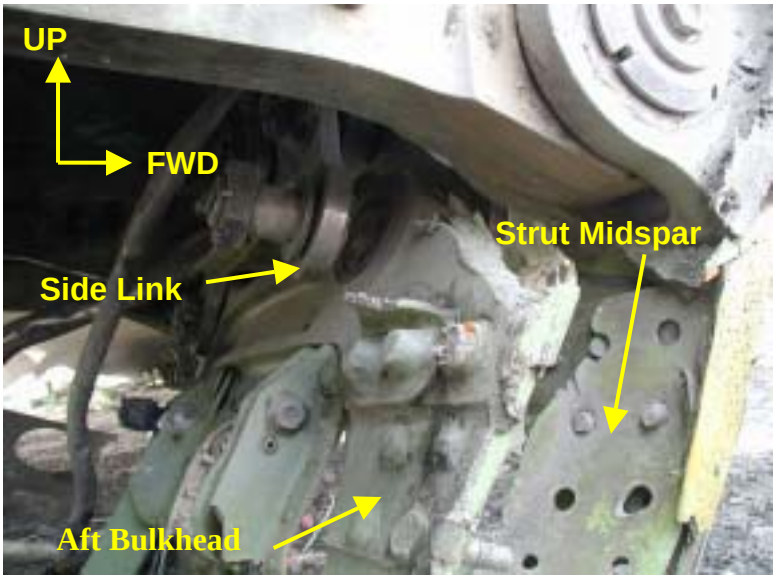

Figure 1.12-57 The bulkhead extends across the width of the strut, but has been twisted with the outboard portion pulled free from the vertical leg of the strut mid-spar fitting

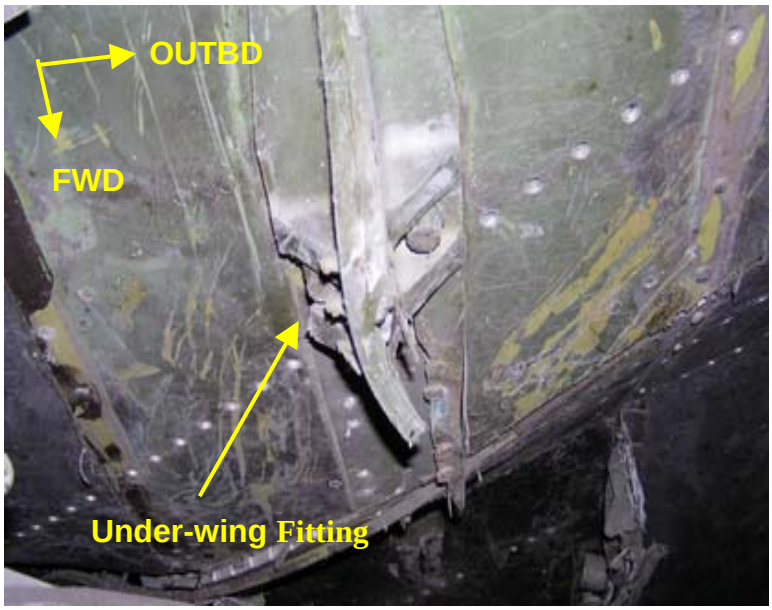

Figure 1.12-58 The diagonal brace under-wing fitting was found fractured

(4) Engine #4

The strut upper link (R1) is intact and remains attached to the wing fittings. Pins on both ends are intact and a 15” by 20” wide section of strut is attached to the forward end of the link. Under-wing and strut mid-spar fittings (R3 and R4) and fuse pins are intact. Dual side links (R7 and R8) and fittings are attached at both ends and appear normal. There is a 51” long section of strut structure extending forward from the R3, R4 fittings, as well as a 24” long piece of bulkhead extending below R3 and R4 fittings. The bulkhead extends across the width of the strut. The diagonal brace is attached to the R2 wing fitting and both appear in good condition. A small piece of strut fitting is attached to the diagonal brace forward end. The forward end of the diagonal brace is bent outboard of its normal position（Figure 1.12-59）. The outboard mid-spar chord is bent up relative to the inboard mid-spar chord（Figure 1.12-60）. The observed deformations are consistent with the #4 engine departing the airplane in an outboard direction.

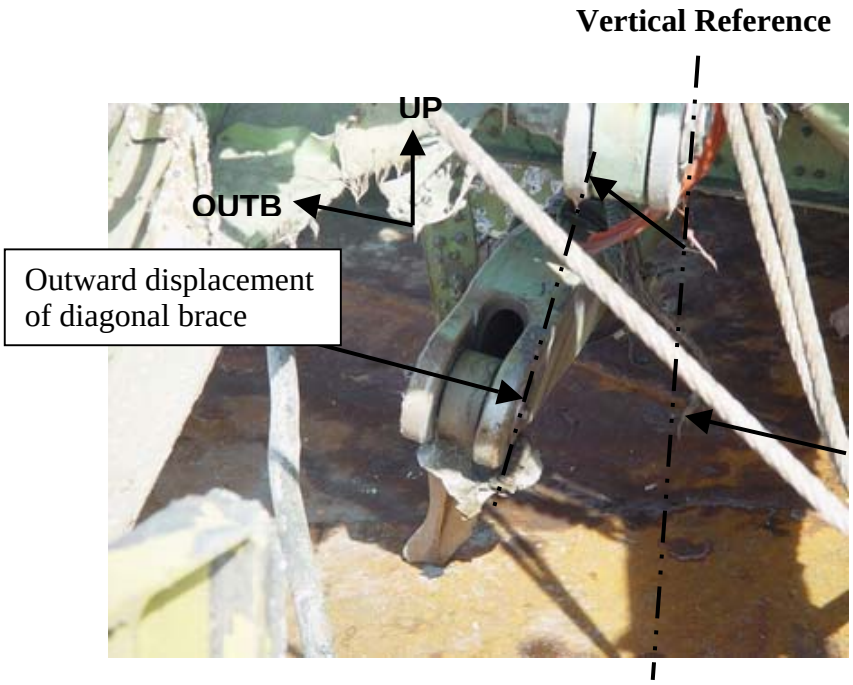

Figure 1.12-59 The forward end of the diagonal brace is bent outboard of its normal position

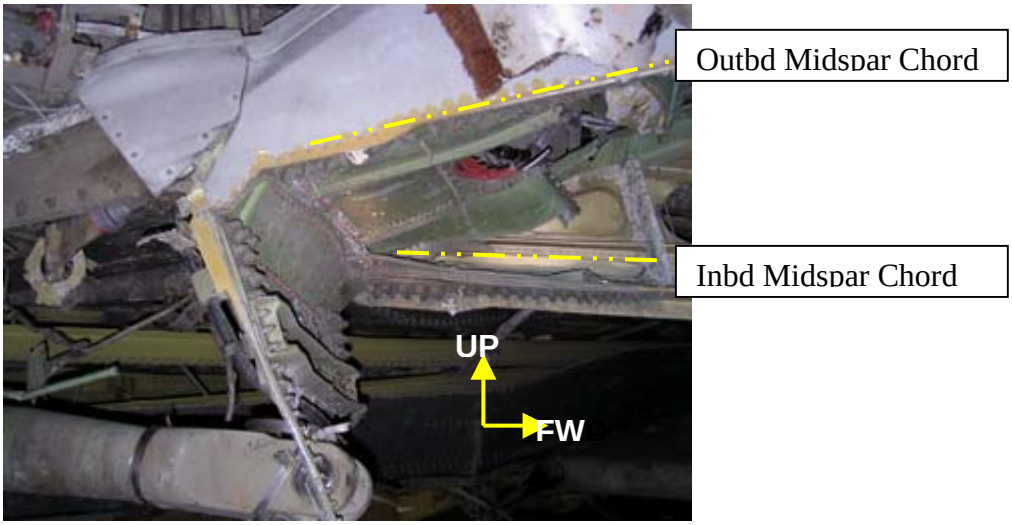

Figure 1.12-60 The outboard mid-spar chord is bent up relative to the inboard mid-spar chord

1.12.6 Additional Metallurgical field examination of recovered structural items

The intend of this additional examination is to warrant further metallurgical field examination of recovered structural items of the fuselage sections 41, 42, 44 and 46, as well as the outboard and center wing sections and keel beam as listed and described in Table 1.12-I. These items were examined in order to note any evidence of pre-existing cracking or corrosion associated with the fractures that could be observed visually.

Detailed visual examination of the fracture surfaces of the structural items listed in Table 1.12-I was accomplished. With the exceptions described 1.12.6.1 and 1.12.6.2,

All fractures examined were characterized as being due to various modes of ultimate ductile separation (i.e. tension, shear, compression, bending). No other evidence of any slow-growth cracking mechanisms or corrosion that was pre-existing prior to the accident flight was observed.

Table 1.12-1 The list of Detailed visual examination of the fracture surfaces of the structural items

Tag No.	Description
546C1	Left Wing Gear with partial Fuselage LH 3 Door with 3 Frame
546C2	Left Wing Gear with partial Fuselage LH 3 Door with 3 Frame
868	LH #2 DOOR
487	Fuselage(station 600 to 800)

545	Cockpit
625	RH Fuselage with #3 Entry Door, 10 windows & connected with partial WCS Front Spar
626C3	LH Fuselage with upper skin No window connected with LH#3 Door & RH #2 Door Frame
626C4	LH Fuselage with upper skin No window connected with LH#3 Door & RH #2 Door Frame
626C5	LH Fuselage with upper skin No window connected with LH#3 Door & RH #2 Door Frame
629	Right fuselage frame sta520 to 740
639	Fuselage skin 46 section from 1320 to 1620
643	RH fuselage skin with #2 Entry Door
650	Partial fuselage skin B.S. 320 to 480 door R1 fwd to aft vertical door frame
652	Partial fuselage skin Sta. 420 to 500, S-16R to 38R
656	Partial fuselage. Skin Sta. 340 to 380, S-23R to -34R
705	Fuselage Skin STA 1000~800
728	LH FUSELAGE SKIN
731	UPPER FUSELAGE WITH BEACON LT ASSY
843	FUSELAGE SKIN(INCLUDE 5 WINDOWS)
911	FUSELAGE SKIN STA 750-1000
1017	STA780~940 Fuselage Skin Segment
547C1	Left Wing inbd Section
547C2	Left Wing Mid Section
547C3	Left Wing outbd Section
628C1	RH WING LWR SKIN
628C2	RH WING LWR SKIN
865	FUSELAGE SKIN PANEL STA 520 TO 620 LH UPPER DECK
526C1	RH WING UPPER SKIN
526C2	RH WING UPPER SKIN
526C3	RH WING UPPER SKIN
526C4	RH WING UPPER SKIN
726	WCS Front Spar
909	WCS Front Spar
2237	WCS Front Spar
2238	WCS Front Spar
2239	WCS Front Spar

835	WCS Spanwise Beam #3
867	WCS Spanwise Beam #3
1069	WCS Spanwise Beam #3
1250	WCS Spanwise Beam #3
2230	WCS Spanwise Beam #3
2231	WCS Spanwise Beam #3
2232	WCS Spanwise Beam #3
1075	WCS Spanwise Beam #2
1258	WCS Spanwise Beam #2
2234	WCS Spanwise Beam #2
2235	WCS Spanwise Beam #2
2236	WCS Spanwise Beam #2 and right Side of Body Rib
2244	WCS Spanwise Beam #2
709	WCS Midspar
908	WCS Midspar
1252	WCS Midspar, Lower Panel and portion of Keel Beam
2229	WCS Midspar
2247	WCS Midspar
1257	WCS Spanwise Beam #1
2240	WCS Spanwise Beam #1
2241	WCS Spanwise Beam #1
2242	WCS Spanwise Beam #1
2243	WCS Spanwise Beam #1
2246	WCS Spanwise Beam #1
864	WCS Rear Spar and portion of Upper Panel
907	WCS Rear Spar
910	WCS Rear Spar, Keel Beam and portion of Upper Panel
642	WCS Upper Panel
1251	WCS Upper Panel
1259	WCS Upper Panel
2228	WCS Upper Panel
549	WCS Lower Panel with portion of SWB#3
606	WCS Lower Panel
628	WCS Lower Panel
725	WCS Lower Panel with portion of Front Spar and left S.O.B. Rib
836	WCS Lower Panel
837	WCS Lower Panel

863	WCS Lower Panel
1254	WCS Lower Panel with portion of Right S.O.B.
1265	WCS Lower Panel with portion of SWB #2
1256	WCS Lower Panel
2233	WCS Lower Panel and portion of Front Spar
1264	WCS Left Side of Body Rib and Front Spar
2239	Right Side of Body Rib
830	Keel Beam
831	Keel Beam
840	Keel Beam
900	Keel Beam
969	Keel Beam
1227	Keel Beam

1.12.6.1 Left Wing Upper Internal Splice Fitting - Left Side of Body (SOB), Rear Spar on item #547C2

Visual examination revealed what appears to be a pre-existing crack on the outboard flange of the Left Wing Upper Internal Splice Fitting common to the left SOB and Rear Spar on item #547C2. The feature appears to be a fatigue crack that initiated on the upper surface of the flange near the aft edge and propagated through the flange thickness and forward to a length of approximately 0.75 inch, where the fracture displayed an abrupt transition from light color associated with a flat profile to a dark colored, slanted profile. The total forward and aft length of the fracture at this location was measured to be approximately 4.0 inches.

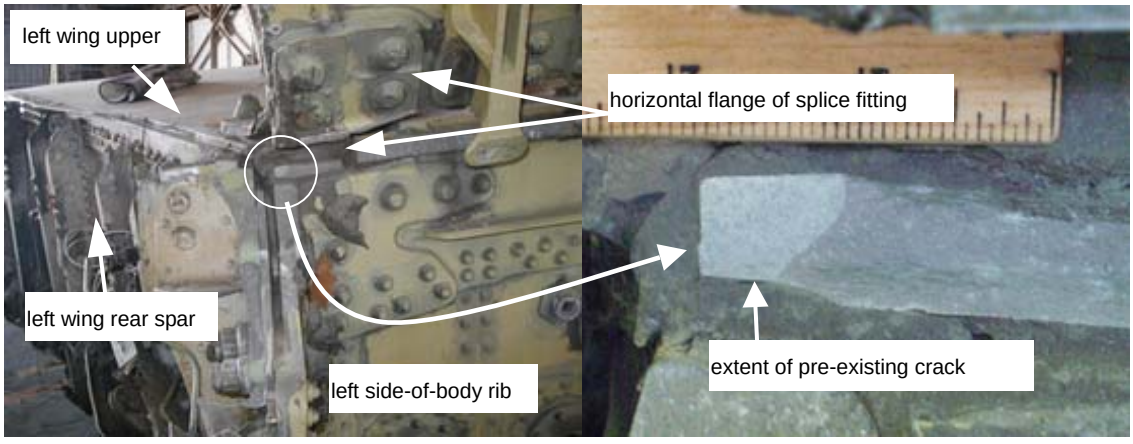

Figure 1.12-61 Left Wing Upper Internal Splice Fitting - Left SOB, Rear Spar on item #547C2

1.12.6.2 Right Wing Front Spar Upper Chord, Wing Station 1115 on Item #526C3

Visual examination of the fracture surface of the Right Wing Front Spar Upper Chord on item #526C3 revealed a possible pre-existing condition at approximately Wing Station 1115. The “woody” appearance of approximately an 8-inch length of the fracture surface in the vertical leg of the upper chord suggests the possibility of a stress corrosion cracking mechanism (SCC). The mating fracture on item #628 was observed to extend additionally several inches into the vertical leg such that it was not completely opened during the break up of the wing structure.

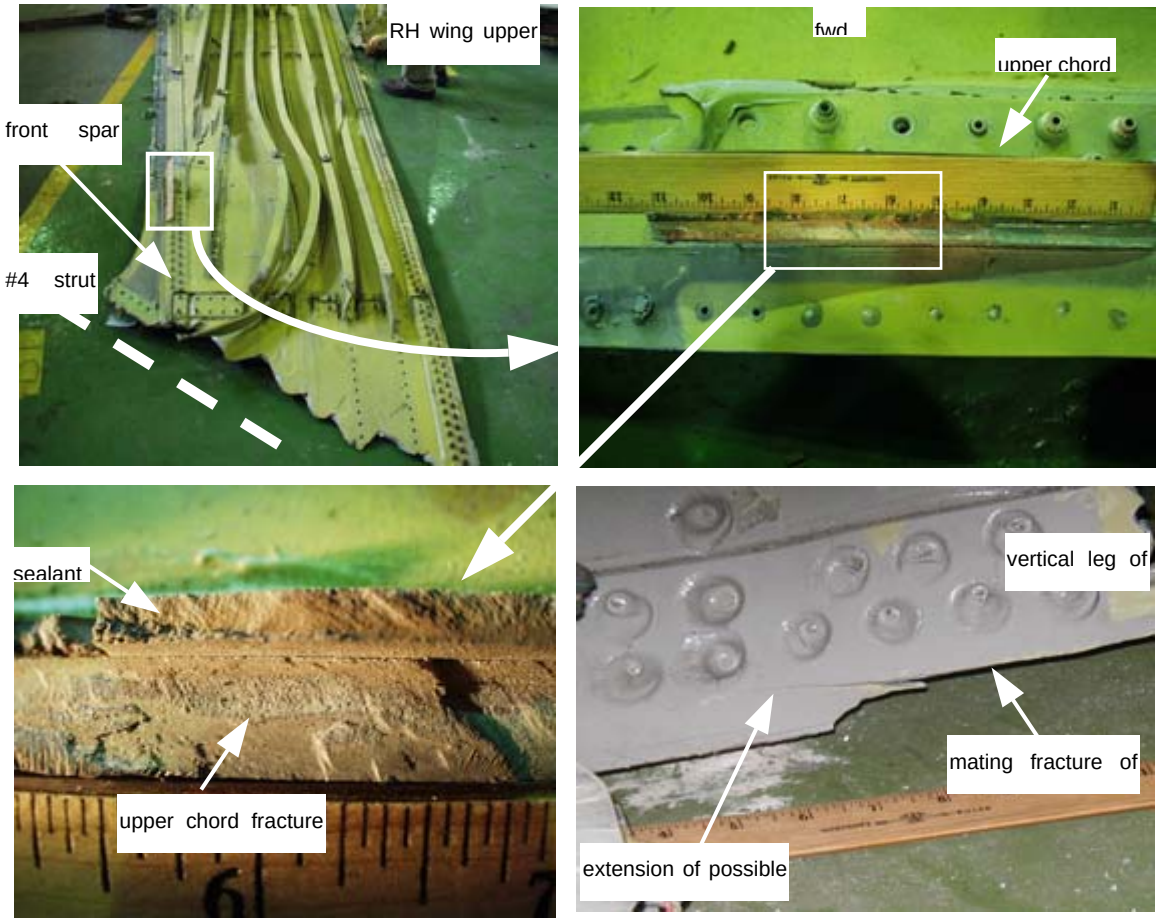

Figure 1.12-62 Right Wing Front Spar Upper Chord, Wing Station 1115 on Item #526C3

1.16.3 Structure and Metallurgical Tests

During detailed wreckage field examination, several pieces of wreckages were of special interest to the investigators. Those wreckage pieces were sent to the metallurgical laboratories of the Chun-San Institute of Science and Technology (CSIST) and Boeing Company.

1.16.3.1 Item 640

Back Ground

On May 25, 2002, a 747-200, B-18255, operated by China Airlines as flight CI611, crashed in the Taiwan Strait on a flight from Taipei, Taiwan to Hong Kong, China. The airplane disappeared from radar at approximately 35,000 feet altitude. There were 206 passengers and a crew of 19 on board the airplane and all received fatal injuries. During the recovery phase of the accident investigation, a fuselage skin panel from Body Station 1920 (STA 1920) to Body Station 2181 (STA 2181), Stringer 23 right (S-23R) to Stringer 49 left (S-49L) was recovered at Latitude - 23 degrees, 58 minutes, 51.702 seconds, Longitude – 119 degrees, 42 minutes, 43.722 seconds on June 30, 2002. This skin panel was given the identification of item 640 by the Aviation Safety Council (ASC) of Taiwan. Field examination of this item revealed a number of areas exhibiting slow crack growth features (e.g. fatigue) along the fracture above S-49L. Two sections of this skin panel containing the fracture above S-49L were sectioned from the wreckage by the ASC and submitted to the Chung Shan Institute of Science and Technology (CSIST) for metallurgical examination. Representatives from Boeing Materials Technology (BMT) participated in the examination of the subject skin panel at the CSIST during the period of July 31, 2002 to September 6, 2002 and ASC, CAL representatives participated periodically in the time frame. An English translation of the CSIST factual report was issued on October 14, 2002.

Subsequent to completion of this work, trawling efforts were undertaken to recover more wreckage. Upon completion of this activity, the ASC requested that the subject fuselage skin panel examined by the CSIST along with all recovered frame segments common to and in the vicinity of the subject skin panel be submitted to BMT for metallurgical examination. Table 1.16-1 provides a description of all the wreckage items submitted by the ASC for

examination. The ASC requested that BMT perform 1) verification of the work conducted by the CSIST on the item 640C1 and C2 skin panel, 2) more extensive determination of crack propagation characteristics of the fatigue cracks present on item 640C1 and 3) examination of all frame segments recovered to date that were common to and in the vicinity of the item 640C1 and C2 skin panel. Representatives from the ASC, NTSB, FAA, CSIST, and China Airlines participated in this examination at the BMT laboratory starting November 6, 2002. An English translation of the BMT factual report was issued on December 18, 2002.

1.16.3.1.1 CSIST metallurgical examination

An overall appearance of ITEM 640 wreckage, submitted to Aero Material Department（AMD） for failure analysis is shown in Figure 1.16-12, which consists of ITEM 640C1 and 640C2. At first, the ITEM 640 wreckage was visually examined and its features were recorded in detail. Further, failure analyses were done as well to identify extent of fatigue area, initiation sites and direction of crack propagation in order to provide valuable information for determining root cause of CI611 plane crash.

Figure 1.16-12 Item 640

Visual Examination

Figures 1.16-13 (a) and 1.16-13 (b), shows both sides of 640C1 and indicates where a repair doubler was attached to the outboard fuselage skin. The range of doubler was approximately within the area between frames STA 2060 and 2180 and stringers S-49L and S-51R, respectively. Figure 1.16-13 (a) indicates that all the frames came off of the skin and were missing except at STA 2160 where a partial frame was attached. However, aside from the section between STA 2120 and STA 2140 of stringer S-50L, almost all stringers were still attached to the fuselage skin. By way of visual examination, the fuselage skin was found to have suspected evidence of fatigue cracking (fracture surface normal to the surface of skin) that was close to, and parallel with, stringer S-49L. This portion of the skin fracture is marked with red arrows in Figure 1.16-13 (a).

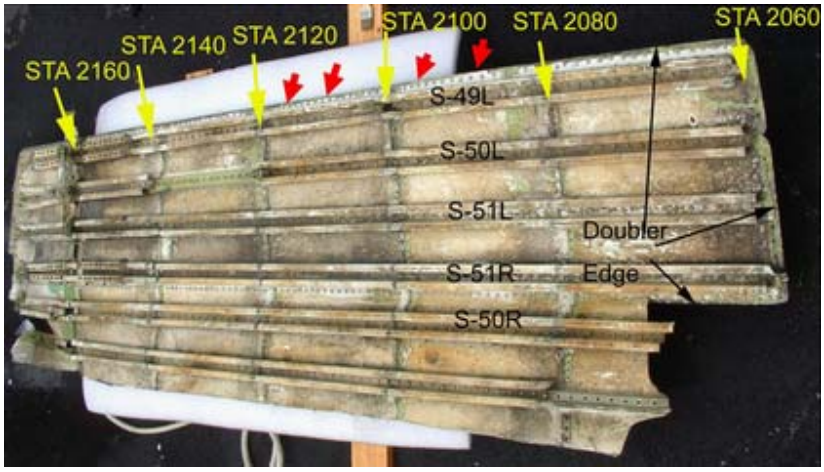

Figure 1.16-13 (a) Inboard side of item 640 indicates that all the frames came off of the skin and were missing except at STA 2160 where a partial frame was attached

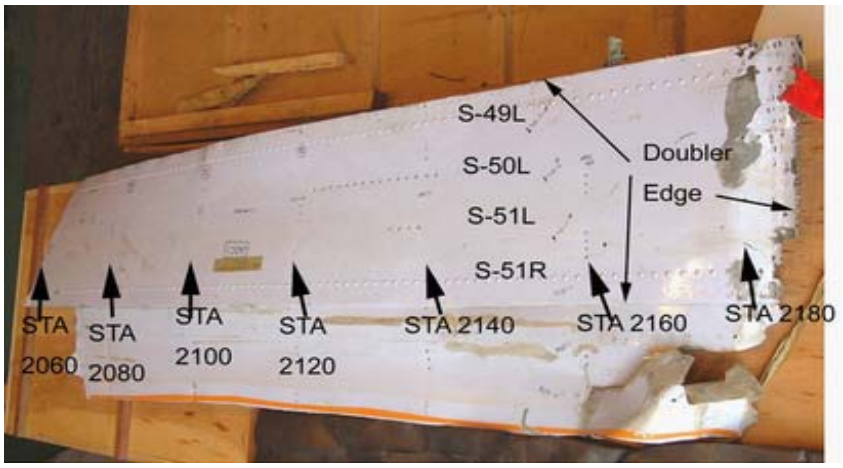

Figures 1.16-13 (b) Out board side of item 640 repair doubler was attached to the outboard fuselage skin

Figure 1.16-14 is composed of 18 photos and shows an overall view of the skin fracture surface along the direction of stringer S-49L. For referencing purposes rivets were identified by the numbers +17 to 91 along the fracture as shown in Figure 1.16-14. The same identification for these rivets was used throughout the report.

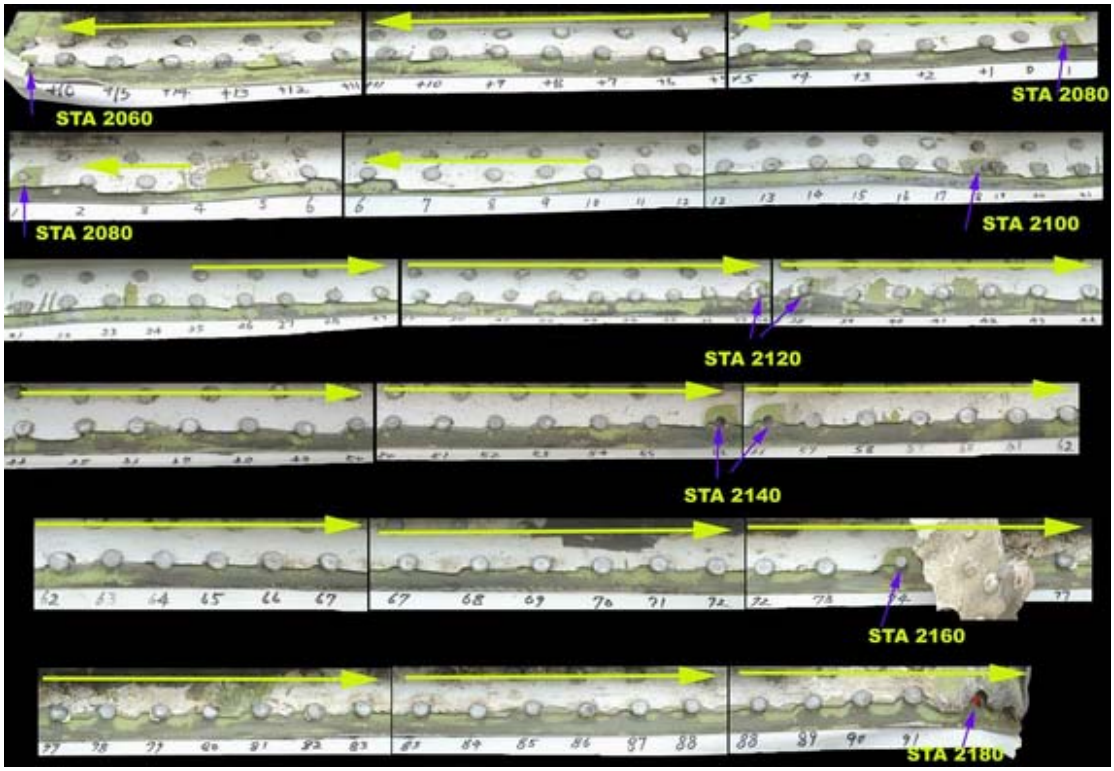

Figure 1.16-14 Shows an overall view of the skin fracture surface along the direction of stringer S-49L

Macroscopic Examination

The fracture surfaces near the rivets from +17 to 91 in Figure 1.16-14 were examined by low-magnification optical (light) microscopy for suspected evidence of fatigue cracking. Three sections of the skin fracture incorporating rivets and doubler sections were removed by saw cutting for macroscopic examination and are shown in Figure 1.16-15. Macro examination using low power optical method was performed at the AMD laboratory while the fracture surfaces were cleaned with a soft bristle brush and acetone during examination. The NTSB Boeing China Airlines（In part from +17 to 38） AMD and ASC representatives participated in macroscopic examination of fracture surface.

Figure 1.16-15 Three sections of the skin fracture incorporating rivets and doubler sections were removed by saw cutting

SEM Examination

The skin fracture near rivets from +17 to 56 was further examined with the aid of a scanning electron microscope (SEM) for the purpose of identifying initial sites the extent of fatigue cracks and the direction of crack propagation. The fracture surfaces associated with the rivets +56~91 were not examined with the SEM.

Before SEM examination, the skin was disassembled（See Figure 1.16-16） and sectioned into many segments that were of an appropriate size so as to fit in the SEM chamber. Moreover, in order not to destroy the skin fracture surface saw cuts, if possible, were made through fastener hole. One exception was the saw cut at a location near rivet number 4.

The disassembly of rivets followed the same general procedure; (1) using a small diameter drill, each rivet head was drilled so as not to damage the rivet hole, (2) a constant diameter punch that was smaller in diameter than the rivet hole was placed in the drilled hole against the remaining rivet shank and driven to pop off the rivet head, (3) the remaining portion of the rivet that contained the tail (formed end) was then liberated from the hole.

Figure 1.16-16 The investigator was disassembling the skin before SEM examination

Due to contamination of the fracture surfaces, the fracture specimens were cleaned prior to SEM examination. Initially, replicating tape with Duco cement was applied to the fracture surface of the specimens and subsequently stripped from the fracture to help remove deposits. This was followed by ultrasonic cleaning of the specimens in acetone. However, even after the fracture surfaces were cleaned by the replica stripping method, the specimens still contained sufficient deposits hindering SEM examination. Ultrasonic agitation in a chromic acid solution offered by the Boeing Company was then used to remove heavy corrosion on the fracture surface for each specimen. A representative of the Boeing Company was present during most of the SEM examination. The results of SEM examination as follow:

(1) The extent of fatigue cracking was determined by SEM examination. The extent of fatigue cracking is shown in Figures 1.16-17 through 22, in which the fatigue propagated from the edge next to the doubler until it reached the black curves shown in these figures. Outside of the fatigue regions the fracture features were typical of an overstress separation. The quantities in Figures 5 through 10 denote the ratio of maximum depth of fatigue crack to the thickness of fuselage skin in the corresponding location. It should be noted that in most circumstances the fatigue initiated at the skin edge next to the doubler and progressed inboard through the direction of skin thickness.

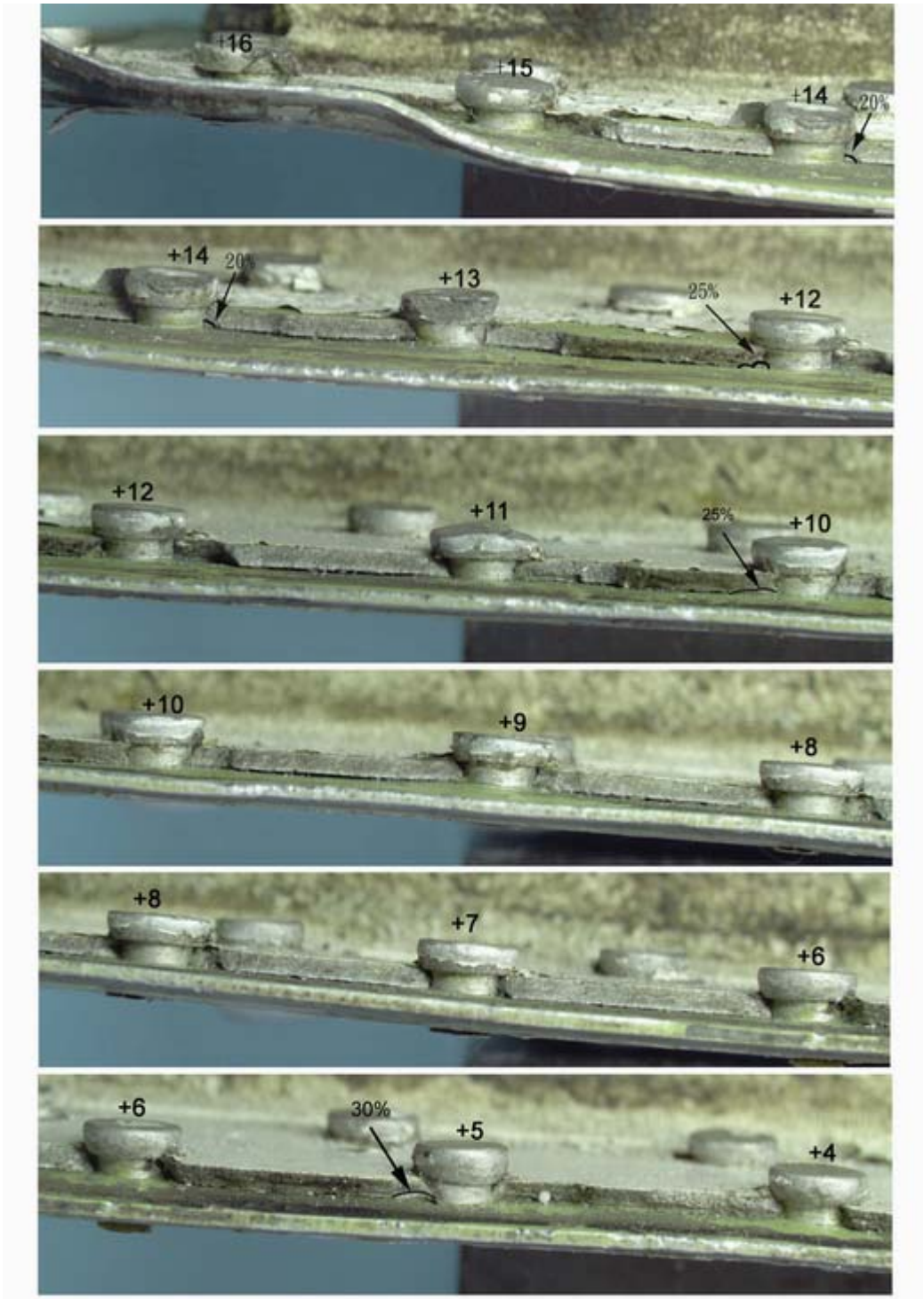

Figures 1.16-17 Shown the extent of fatigue cracking

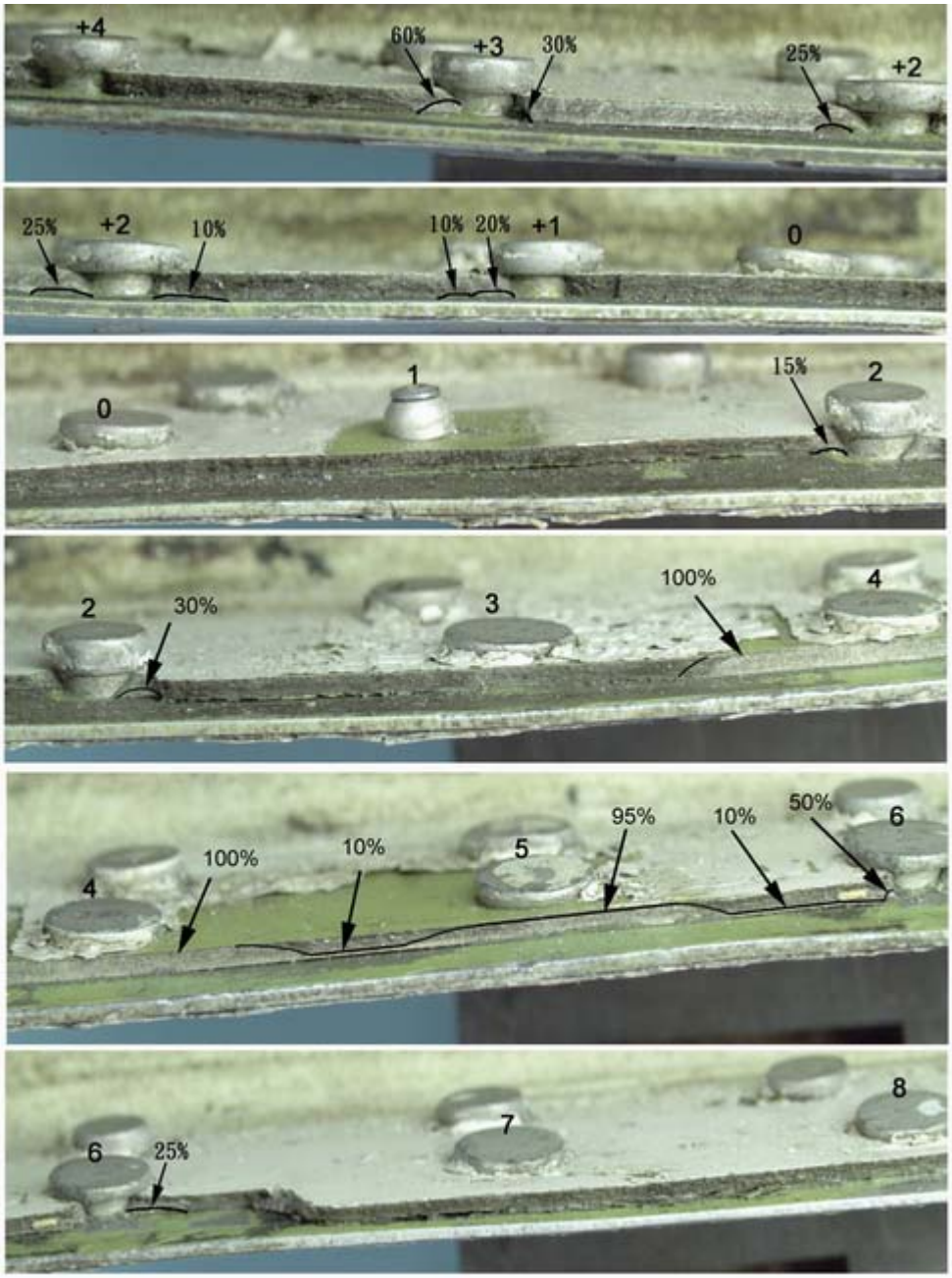

Figures 1.16-18　Shown the extent of fatigue cracking

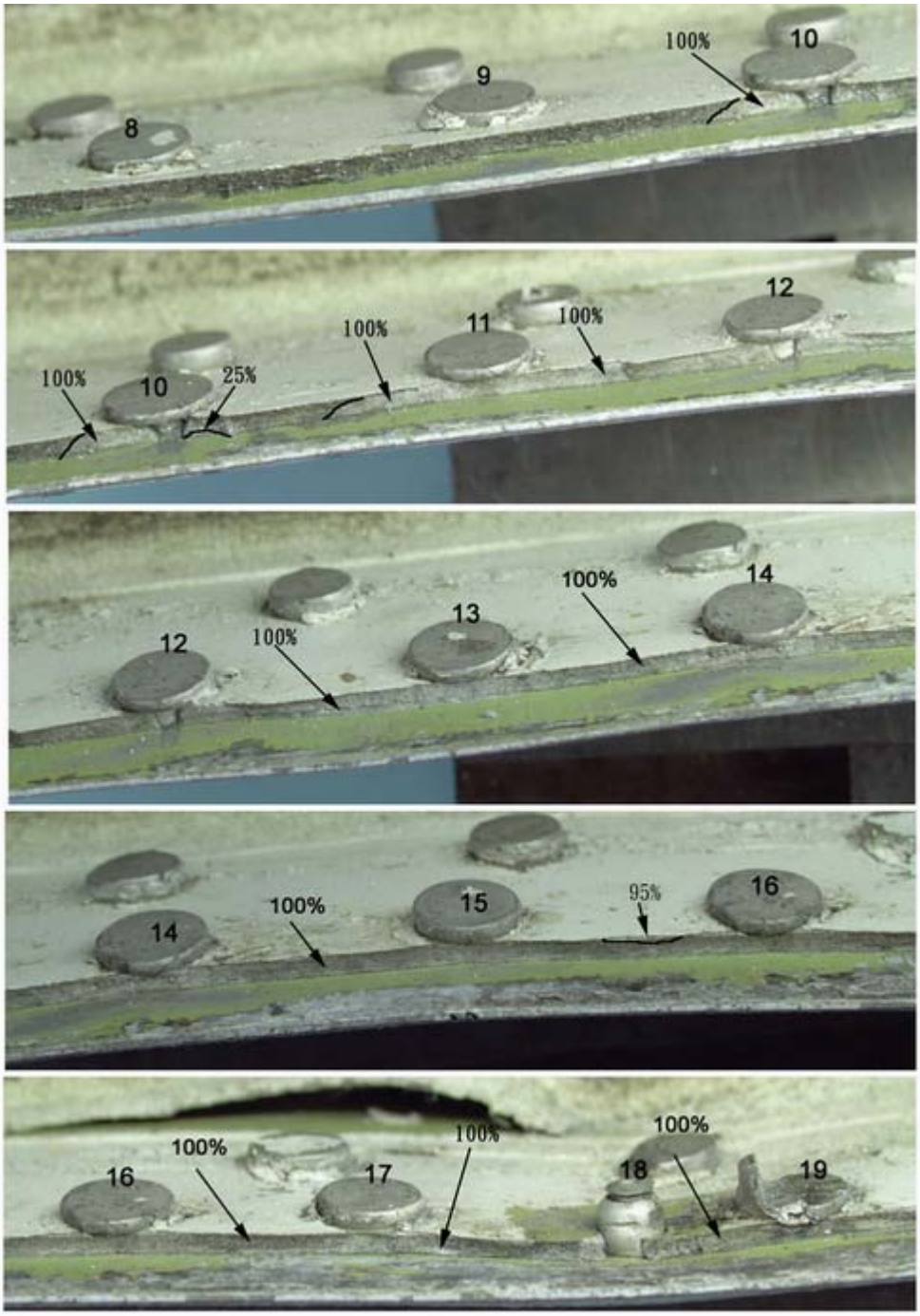

Figures 1.16-19 Shown the extent of fatigue cracking

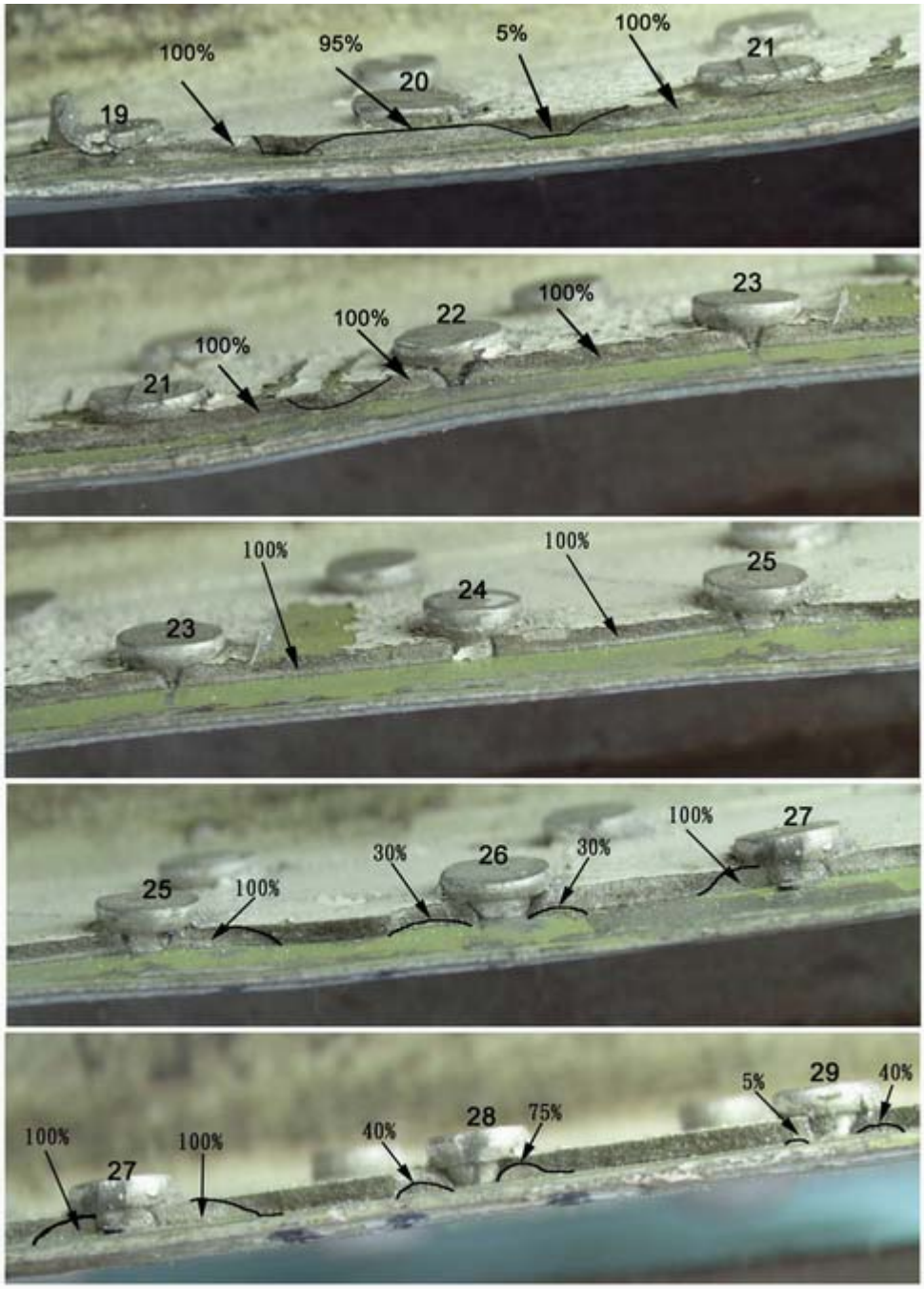

Figures 1.16-20　Shown the extent of fatigue cracking

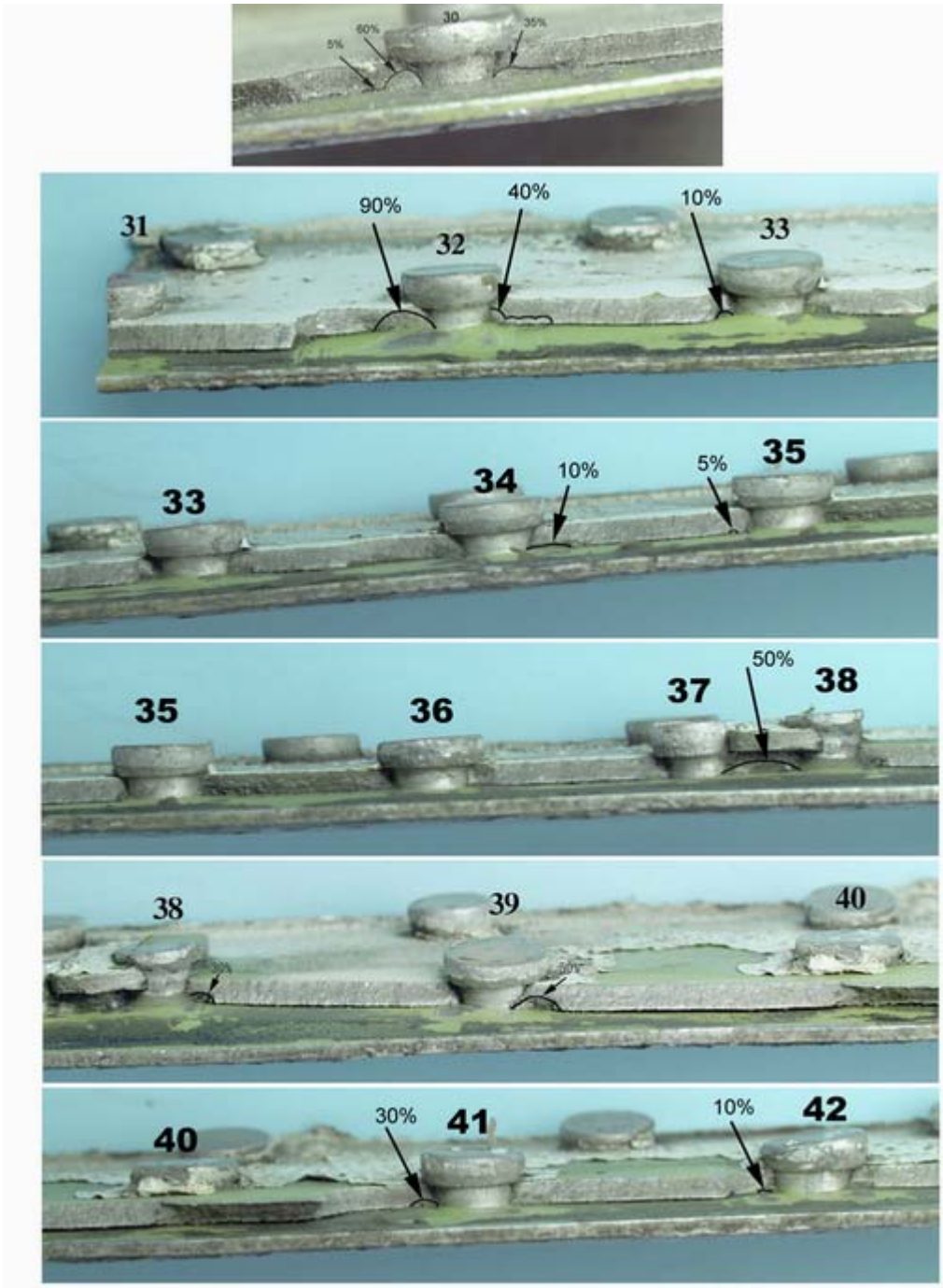

Figures 1.16-21 Shown the extent of fatigue cracking

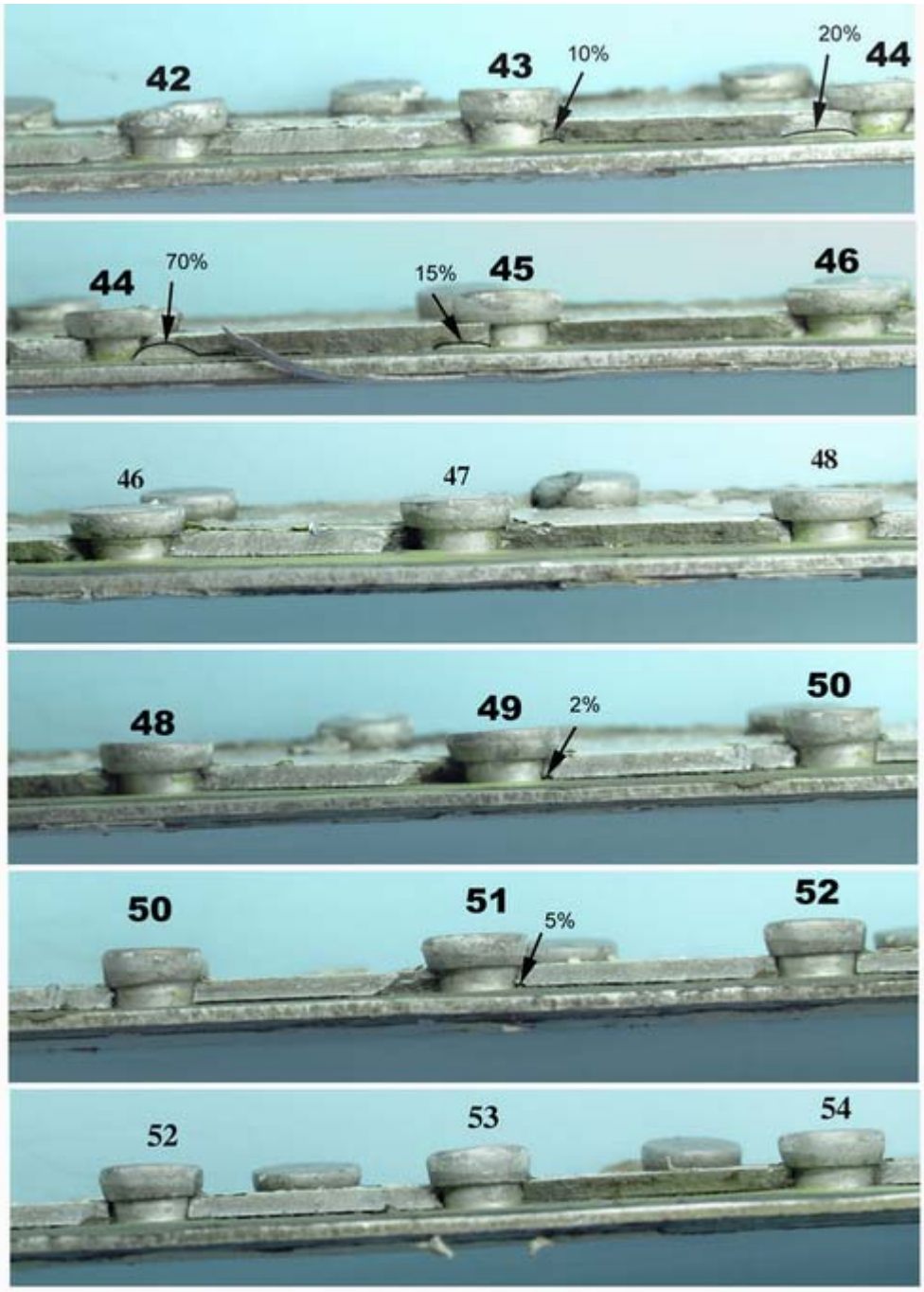

Figures 1.16-22 Shown the extent of fatigue cracking

The majority of the fatigue cracking was associated with frame STA 2100, in the area corresponding to the region of rivets from 10 to 25. Figure 1.16-23 is a drawing (not to scale) indicating the fatigue cracking on the skin fracture surface from rivets +16 through 56.

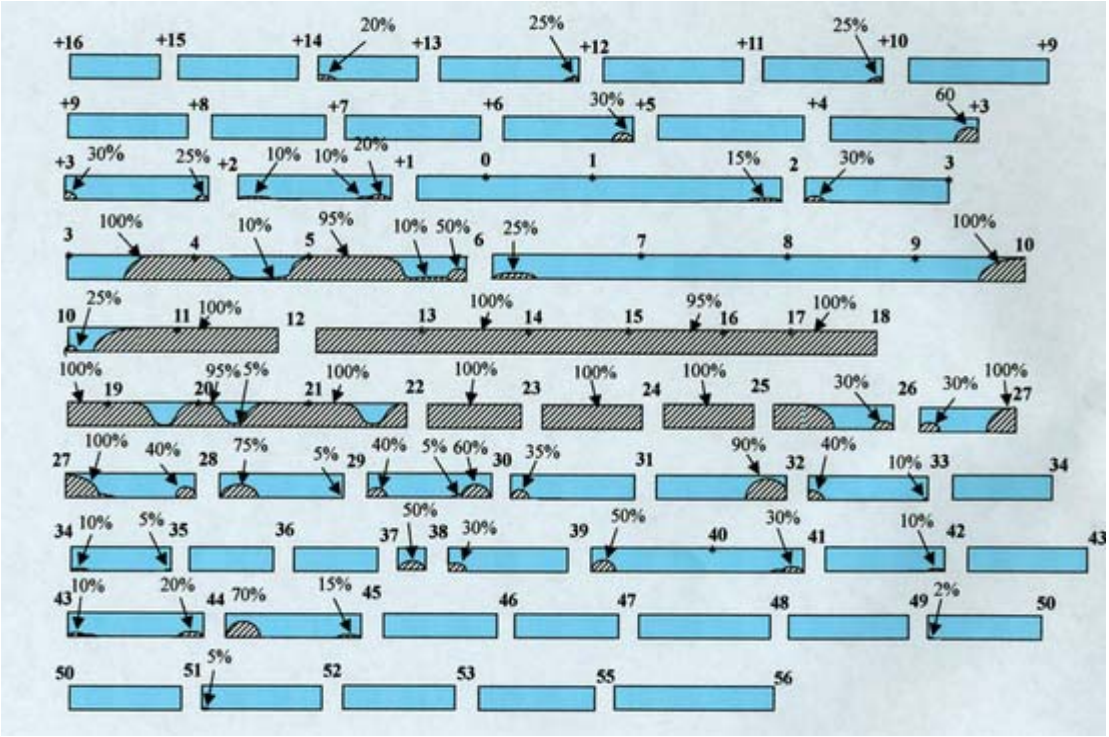

Figure 1.16-23 A drawing (not to scale) indicating the fatigue cracking on the skin fracture surface from rivets +16 through 56.

(2) Five SEM photographs at different magnifications are shown in Figure 1.16-24 for the fracture surface near rivet number 25. Fatigue striations were readily visible in Figures 1.16-24 (e) and 1.16-24 (f), which are the higher magnification SEM views of the area indicated by the white rectangles in Figures 1.16-24 (c). The striations had a characteristic pattern of several less apparent minor striations separating prominent major striations. The spacing of major striations measured about 2 microns. As shown in Figures 1.16-24 (d) and 1.16-24 (e), SEM viewing revealed a mixture of ductile dimples interspersed with patches of fatigue striations. This area was considered as the later stage of fatigue and was at a distance about 200 microns from the inboard edge of skin. Figure 1.16-24 (b) shows that the cracks initiated at the outboard edge next to the doubler and propagated inboard. In addition, numerous ratchet marks indicative of multiple origins for fatigue cracks were seen on the outboard edge of the skin. In Figure 1.16-24 (b), the yellow arrows denote the

direction of crack propagation and the areas indicated by blue arrows are the origins of fatigue. Similarly, the same notations are used in the following.

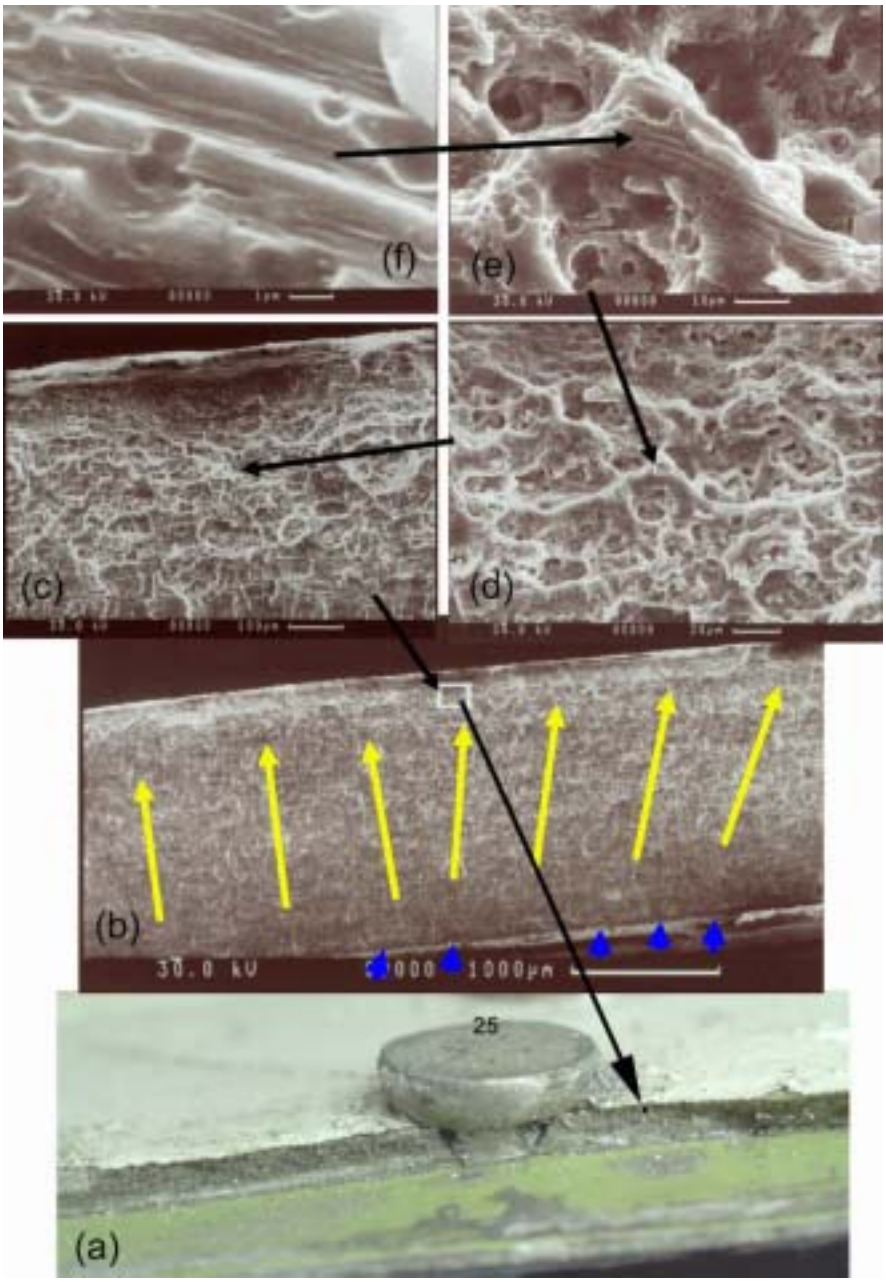

Figure 1.16-24 SEM photographs at different magnifications for the fracture surface near rivet number 25.

(3) As shown in Figure 1.16-25, the SEM photos for the two sides adjoining rivet 25 revealed that ratchet marks, the characteristic of multiple origins

of fatigue cracks, appeared on the edge of the fuselage skin next to the doubler and fatigue propagated across and almost throughout the thickness. The directions of crack propagation indicated the earliest origins of fatigue for each side of the rivet at the approximate locations indicated by the black ellipse in Figure 1.16-25 (b) and 1.16-25 (c). The corresponding points of fatigue cracking through the thickness of the skin are near the periphery of the formed tail end of the rivet.

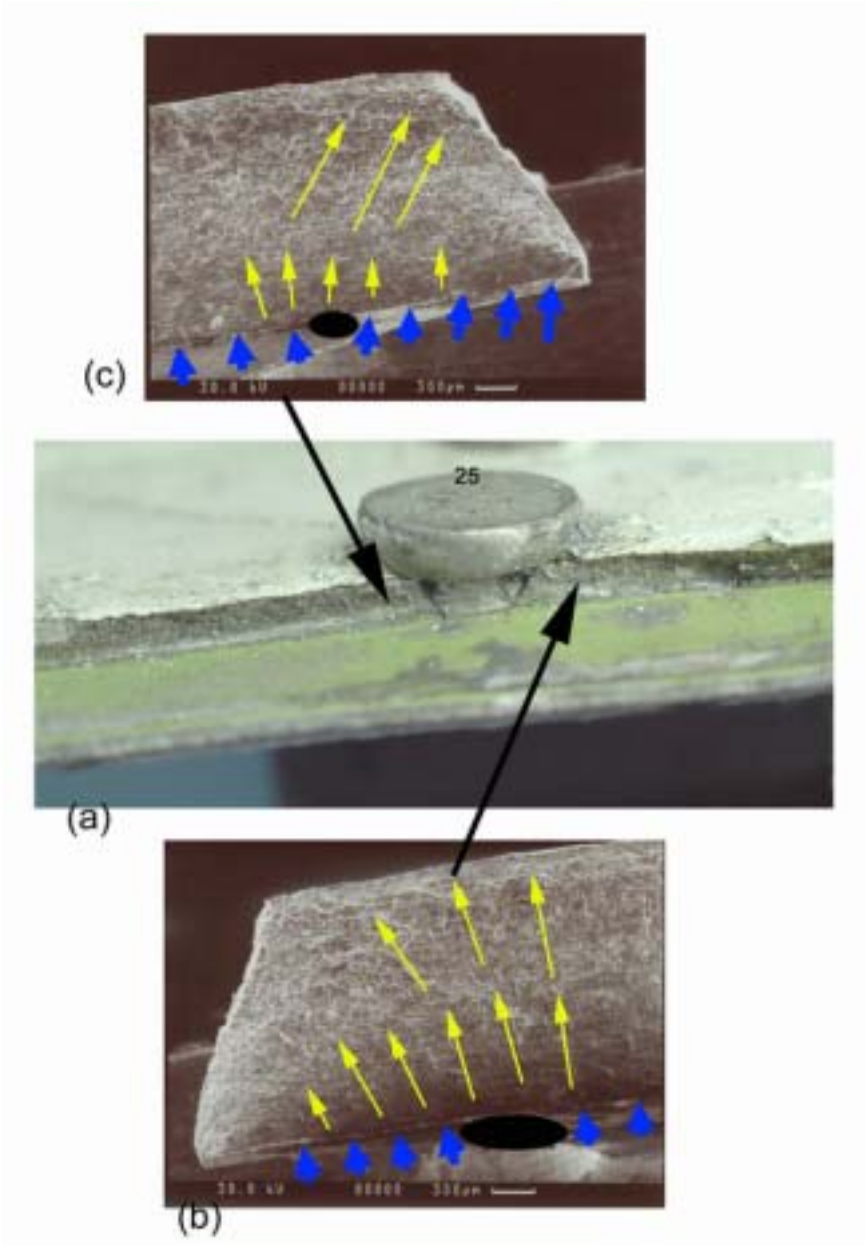

Figure 1.16-25 SEM photos for the two sides adjoining rivet 25

(4) The fracture morphology of fatigue for the area near rivet 14, as shown in Figure 1.16-26, is similar to that found near rivet 25. Figure 1.16-26 (c),

1.16-26 (d) and 1.16-26 (e), denoted by three small black squares, are high magnification photographs for various locations in Figure 1.16-26 (b), showing different spacing of fatigue striations at distances of 250 μm, 1020 μm, and 1480 μm, respectively, away from the skin edge next to doubler. These photographs can be used to measure the striation density at various locations along the crack front. Further, the cycles of loading can be estimated using fracture mechanics.

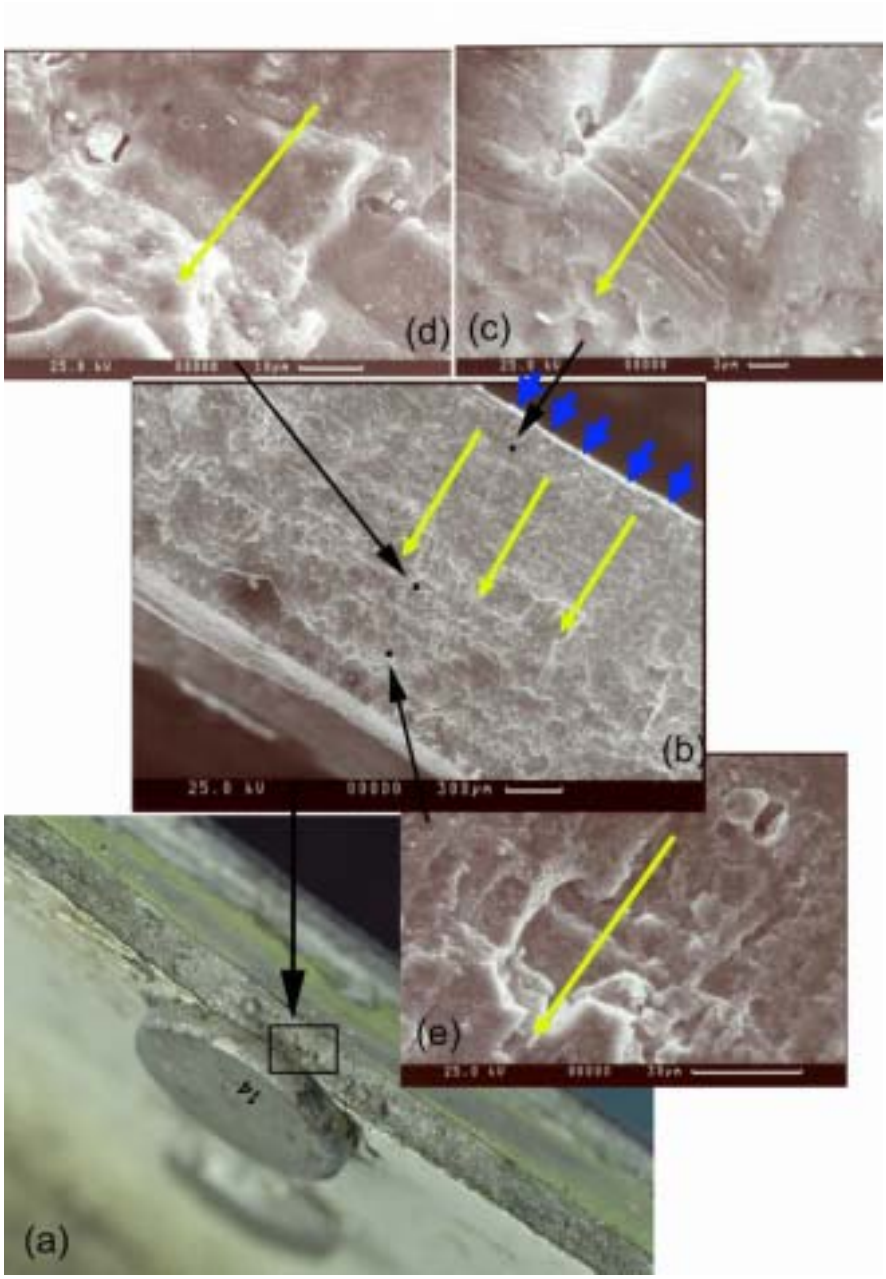

Figure 1.16-26 The fracture morphology of fatigue for the area near rivet 14

(5) SEM photographs shown in Figure 1.16-27 (c) and 1.16-27 (d) are close-up views of the fracture located in the area indicated by the two black squares in Figure 1.16-27 (b). Figure 1.16-27 (c) illustrates visible striations, a typical characteristic of fatigue cracking. In addition, Figure 1.16-27 (d) illustrates dimples, a typical characteristic of overstress. By comparing the proportion of fatigue crack area to overstress area, it is smaller in the area near rivet +5 than those near rivet 25 and 14, in which most areas of fracture surfaces have been identified as fatigue cracking. However, the morphology of fatigue near +5 is similar to those near rivets 25 and 14, such as the direction of crack propagation and the origins of fatigue cracking.

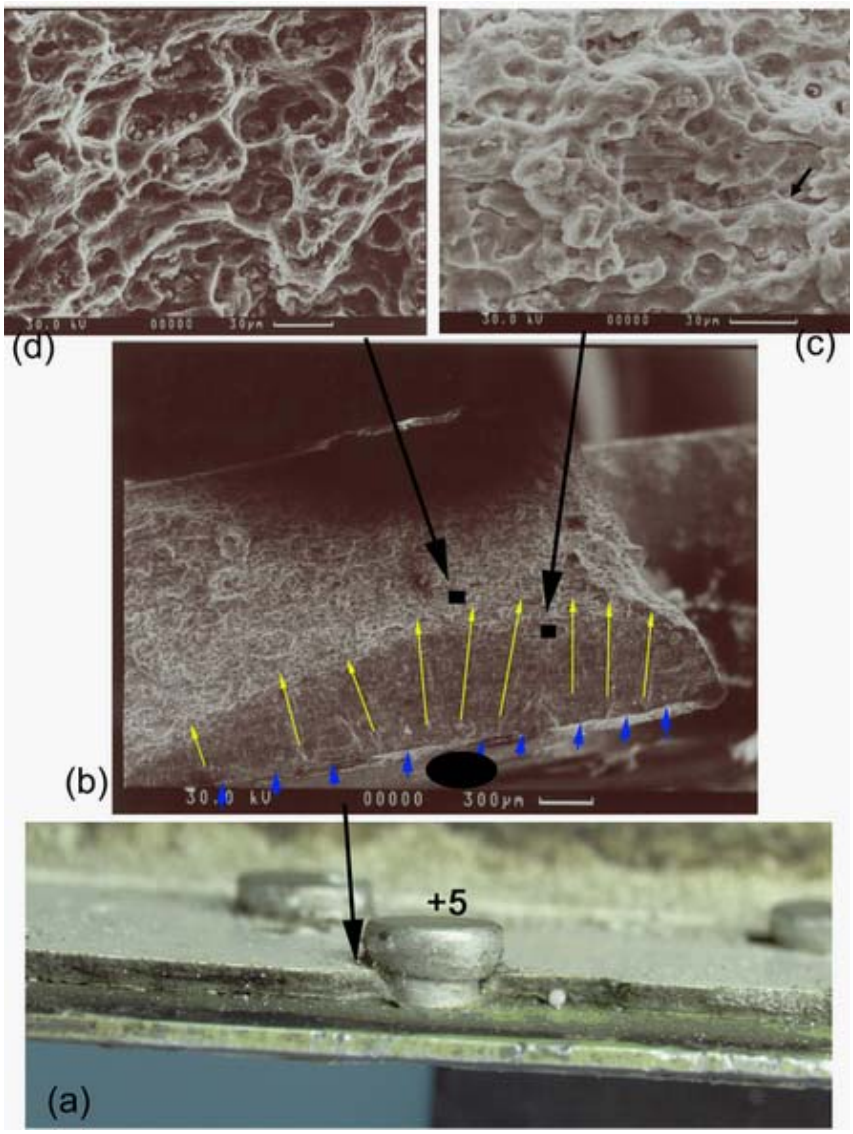

Figure 1.16-27 Illustrates visible striations, a typical characteristic of fatigue cracking and dimples, a typical characteristic of overstress

(6) In general, there were two types of propagation on the fracture surface shown in Figure 1.16-14. One is fatigue which proceeded through the skin thickness, as mentioned above. The other is overstress fracture. Even though the overstress fracture probably propagated along the direction of thickness in some areas, for example, the shear lip in the vicinity of fatigue area, in most areas it propagated along the directions as indicated by the yellow arrows in Figure 1.16-14 about parallel to stringer of S-49L. The overstress cracking generally emanated from the region bounded between rivet 10 through rivet 25. In addition, except for very few areas there is a distinctive feature for the overstress cracking which propagated from hole to hole, as shown in Figure 1.16-14. In the fracture region between rivets 6 and 10, corresponding to rivets 7 through 9, the fracture surface was on a 45^{o} slant plane that was typical of an overstress fracture in tension stress but the fracture did not propagate from hole to hole.

(7) Figures 1.16-28~30, showing macroscopic photographs on both sides of the skin surface around the rivets numbered 19~21, respectively, indicated that many scratches existed on the faying surface of fuselage skin. The scratches were covered with paint. Figure 1.16-28~30 also illustrate that the fatigue cracks at nearby rivets were approximately located around the periphery of the formed tail end of the rivet, in which residual tensile stresses could be induced by the process of riveting. As indicated by black arrows in Figures 1.16-28 and 29, the paths of the fatigue cracks were very straight and always followed the track of scratches along the direction parallel to stringer S-49L.

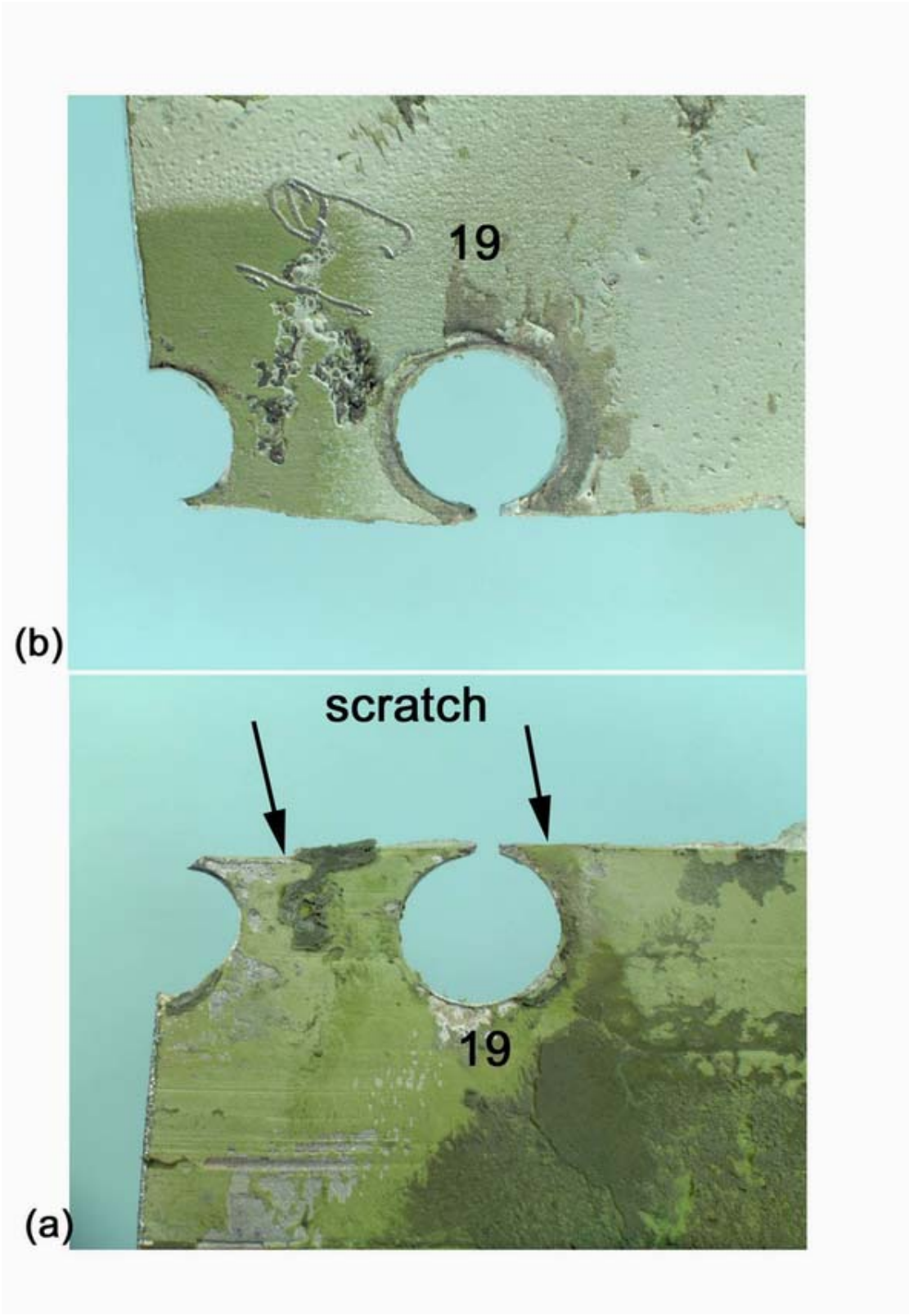

Figure 1.16-28 The skin surface around the rivets 19

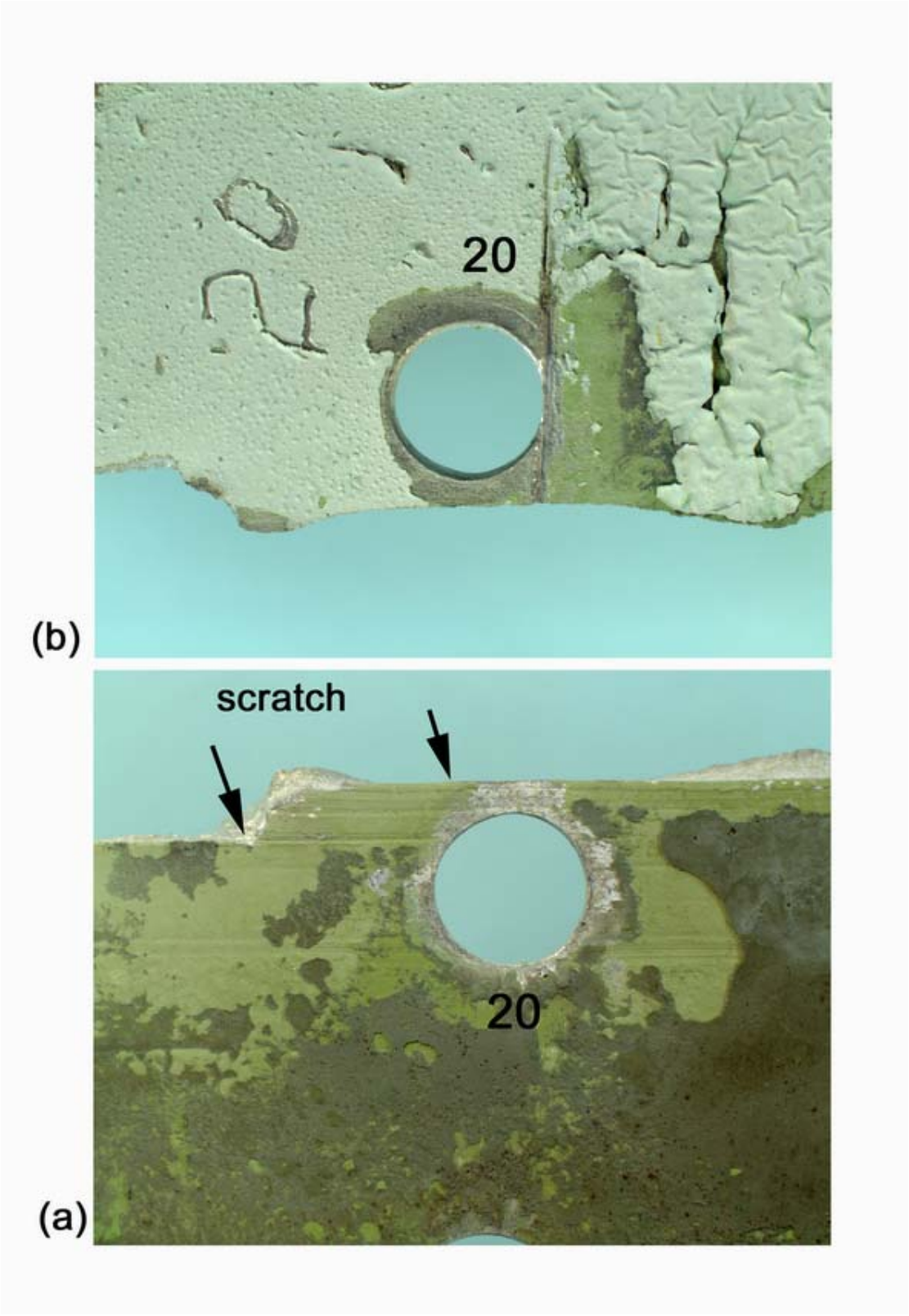

Figure 1.16-29 The skin surface around the rivets 20

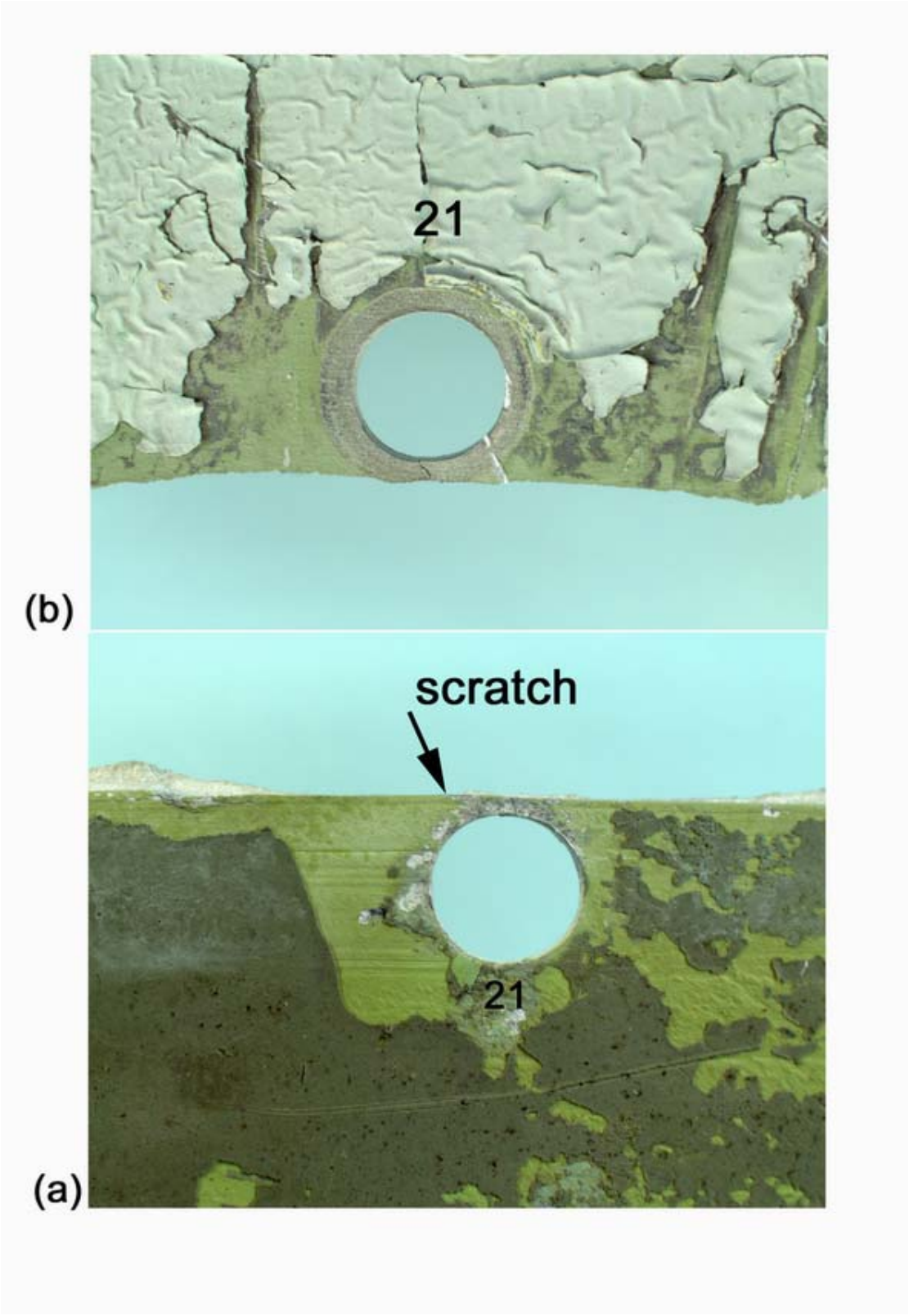

Figure 1.16-30 The skin surface around the rivets 21

(8) Although almost all the fracture surfaces near the rivets from 10 through 28 were dominated by the same through the thickness fatigue fracture, it was found that there were some different features among them. The fatigue cracks associated with rivets 13 through 20 were more close to the edge of doubler and the shanks of these rivets, with the exception of the blind rivet at 18, were not exposed. In comparison, the shank of the rivets on 10, 12 and 22 through 28 were readily visible. In the areas between rivet numbers 22~28, there was a trend for the higher numbered rivets to be associated with a larger portion of exposed rivet shank.

(9) Figure 1.16-31 shows apparent evidences of local deformation near frame of STA 2100. The areas for the most severe deformation corresponded to those areas with the fracture surface having fatigue cracking throughout the skin thickness. The deformation has some features as follows;

- The shape for skin and doubler is outward at frame of STA 2100, two adjacent sides of which were comparatively deformed inward into inboard fuselage. The skin associated with the areas from rivet 13~18 and 22~25 have the most severe inward deformation. However, the skin and doubler corresponded to the region of rivet 19~22 is more flat and the fatigue cracks were not yet throughout the thickness of skin.
- Along the direction parallel to frame STA 2100, the closer to the edge of the doubler the more severe the deformation to the skin and doubler.
- The stringer S-49L contained a fracture at frame STA 2110. Moreover, the sealant peeled off with the skin.
- There was no evidence of contact damage with an object in the area that could account for the local deformation to the skin and doubler.

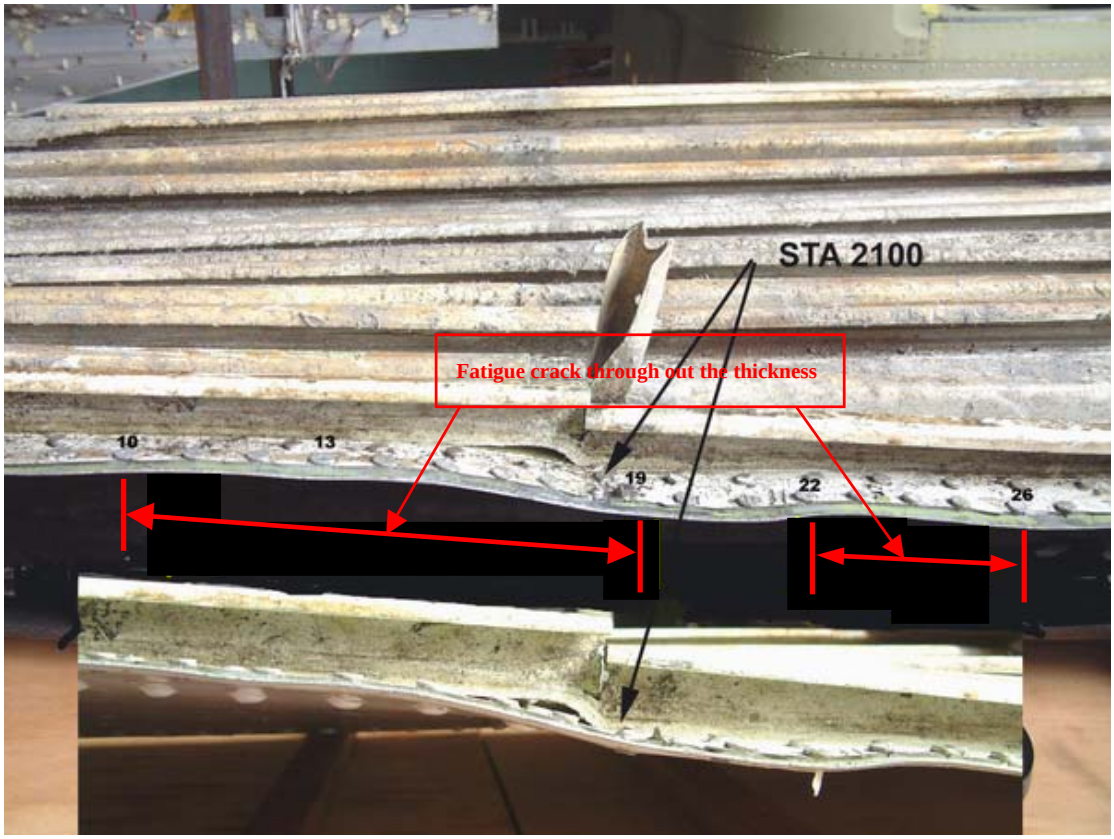

Figure 1.16-31 Show apparent evidences of local deformation near frame of STA 2100

(10) Figure 1.16-32 shows the exterior appearance of the doubler in the area of the local deformation illustrating that the paint around the rivet heads was cracked in some areas. The cracked paint occurred at the location from rivet 14 to 25, which corresponded to the fracture area with the intensive fatigue crack. In the areas with little evidence of fatigue cracking, the exterior paint surface of the doubler was intact around the rivets, such as the locations of rivets beyond number 28.

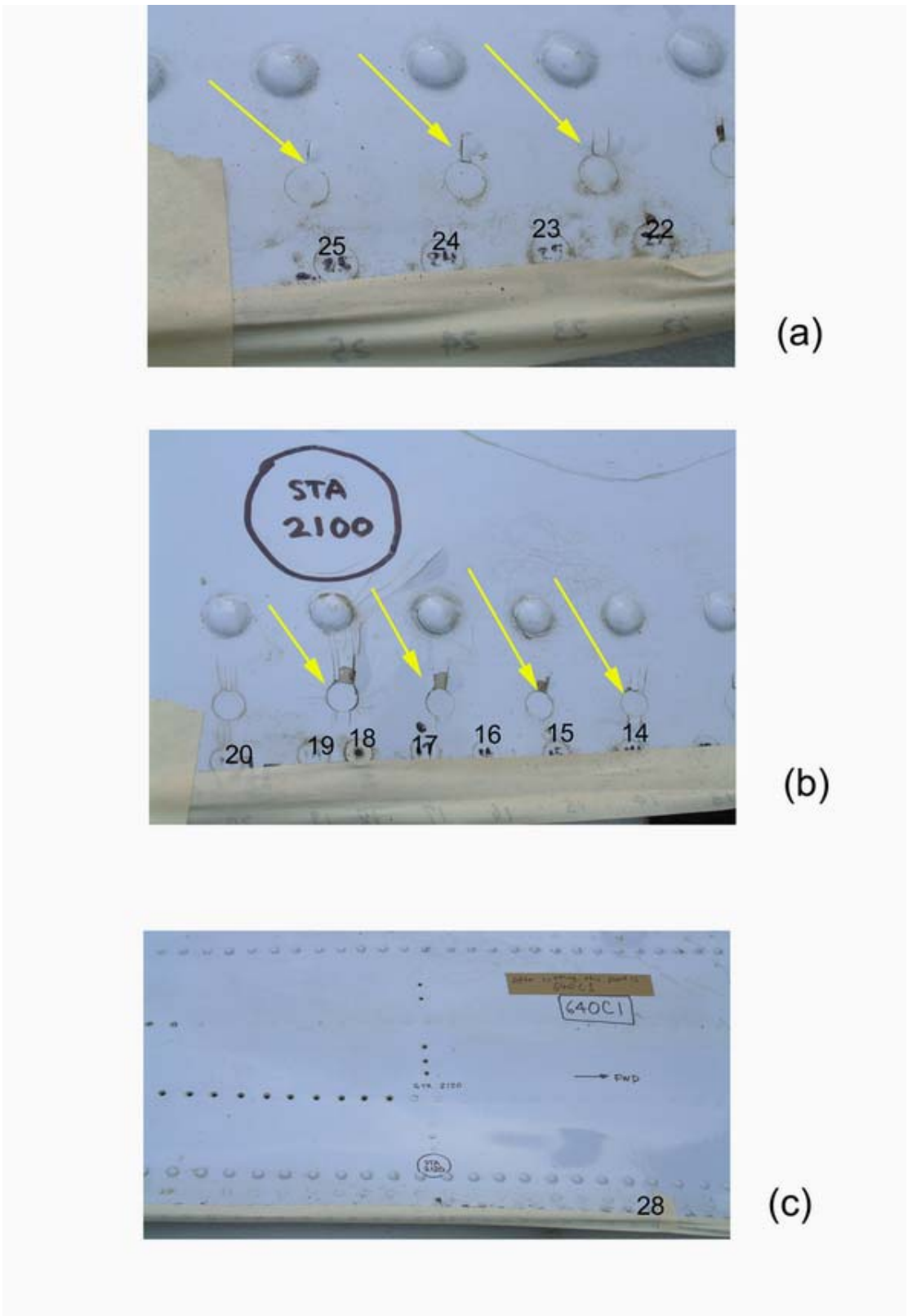

Figure 1.16-32 Show the exterior appearance of the doubler

(11) After removing all rivets and then separating skin from the doubler, many scratches were visible on the faying surface of the skin. Figure 1.16-33 shows this feature after removal of the paint and sealant. Scratches existed almost everywhere. The most severe scratches on the skin surface were located just under the stringers or frames.

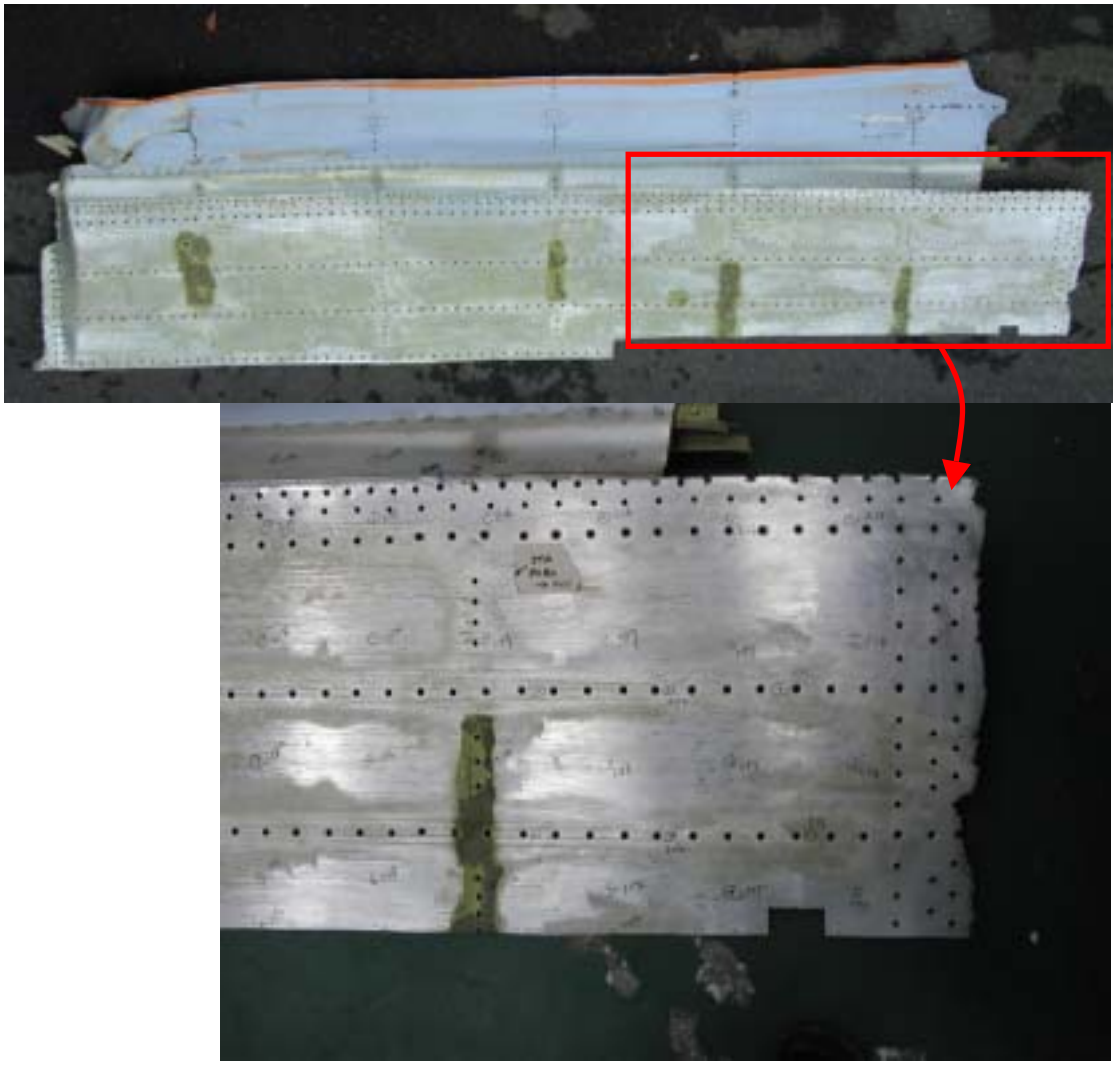

Figure 1.16-33 Show this feature after removal of the paint and sealant

(12) Rub marks produced by abrasion prevailed over the fracture surface near rivet number 1 (Figure 1.16-34). However, in contrast, the fracture surface near rivet +13 contained less evidence of rubbing and so dimples were visible, as shown in Figure 1.16-35.

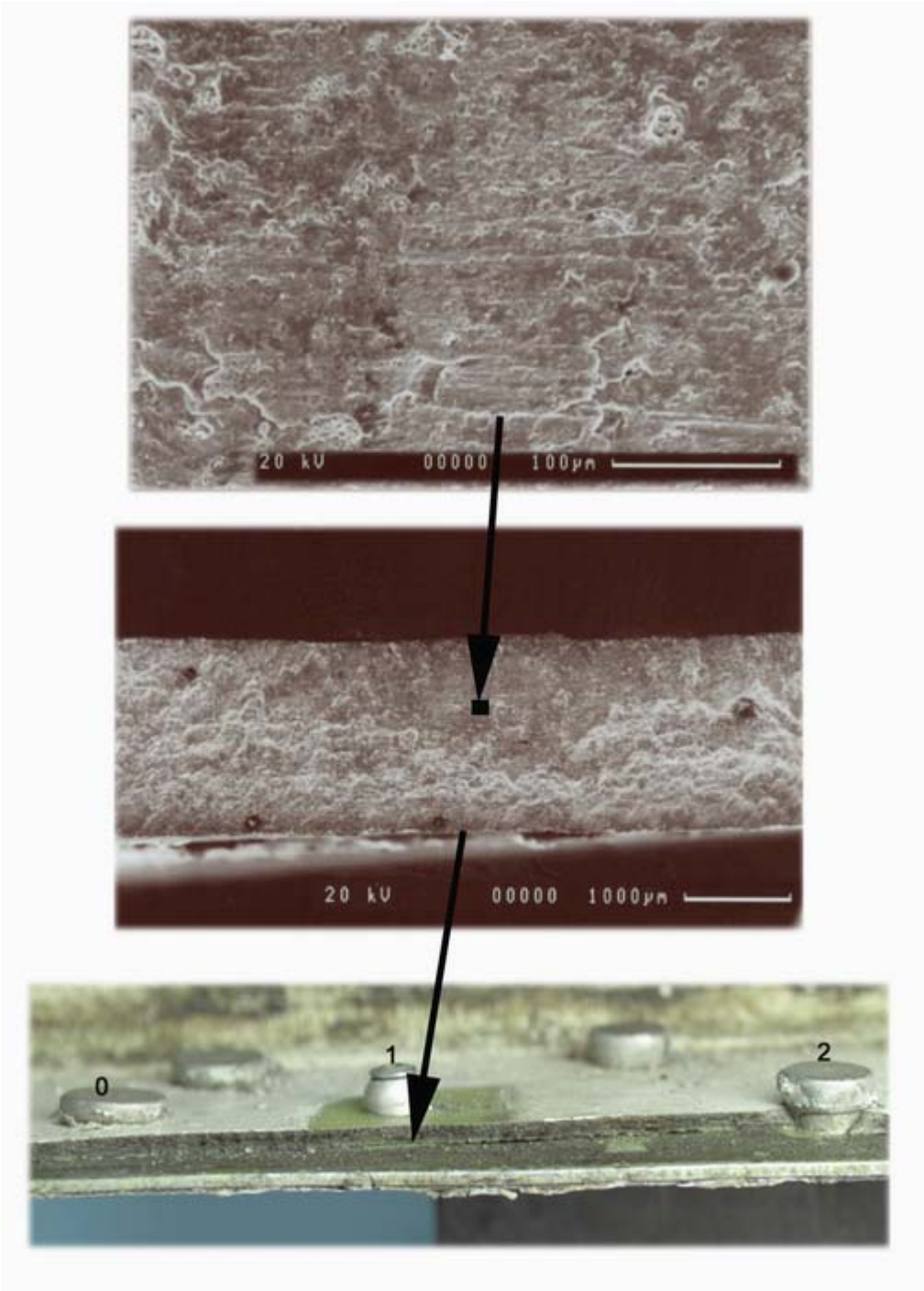

Figure 1.16-34 Rub marks produced by abrasion prevailed over the fracture surface near rivet number 1

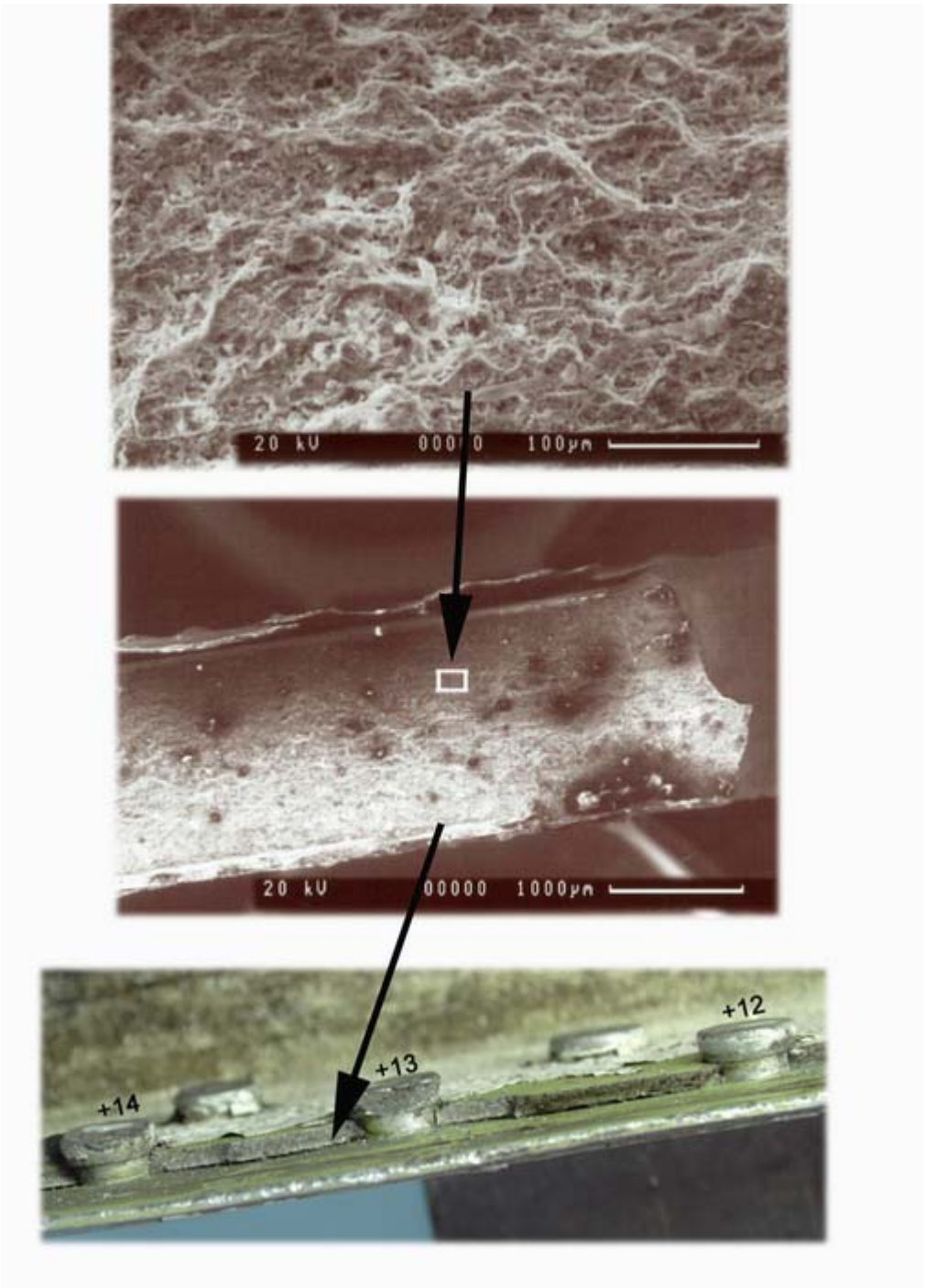

Figure 1.16-35 The fracture surface near rivet +13 contained less evidence of rubbing

(13) Results of Spark spectrum analysis showed that both materials of fuselage skin and doubler were consistent with a 2024 aluminum alloy. Hardness and conductivity measurements associated with skin were individually performed at three locations, and its average was HRB 79 for hardness, is 28.5 %IACS for conductivity. The above values of hardness and conductivity were within specifications for 2024-T3 materials. The doubler was also checked as the same material.

1.16.3.1.2 BMT metallurgical examination

External and Internal Condition of item 640C1 and C2

Field notes were taken in Makung, Taiwan on item 640C1 and C2 fuselage skin panel sections to document the condition of the items prior to shipment to the CSIST. Figure 1.16-36 provides a view of item 640 with the locations of 640C1 and C2 prior to removal in Makung. Figure 1.16-37 provides a view of the interior surface of item 640C1 prior to disassembly at the CSIST laboratory. Item 640C1 contained a 23 inch wide external repair doubler (referred to as the doubler) from approximately STA 2060 to STA 2180 which was installed after a tail strike event was experienced upon landing. The doubler terminated between S-48L and S-49L on one side and between S-50R and S-51R on the other side. The doubler was attached to the skin by two rows of countersunk rivets around its periphery as well as by fasteners common to the stringer and shear tie locations. Universal head rivets were used at S-51R and S-49L while countersunk rivets were used at S-50L and S-51L. Stringer slice repairs were present forward and aft of STA 2160 at S-51R and S-49L. Each of the four splice repairs measured approximately 11 inches in length. At STA 2160 a partial portion of the frame containing three shear ties, the failsafe chord, a fragment of the web, and two stringer clips remained attached to the item 640C1 skin panel. No other frames were attached to either item 640C1 or C2 when the parts arrived in Taichung. However, photographs taken aboard the recovery vessel show that a portion of the STA 2100 frame (item 2015) was attached to item 640C1 when it was recovered. A portion of S-50L between STA 2120 and STA 2140 was missing from item 640C1. Detailed notes were taken prior to disassembly noting the condition of the shear tie and stringer clip attachment to the items 640C1 and C2 skin panels. Table 1.16-2 contains the results of this examination.

Doubler Rivet Spacing and Dimensions

The spacing of the rivets for the two rows used to attach the doubler to the skin above S-49L was measured from the forward edge of the doubler. Figure 1.16-38 provides general information on the spacing of these rows in relationship to S-49L and the edge of the doubler. The driven rivet button diameter and thickness of the two rows of rivets used to attach the doubler above S-49L and S-51R were collected as well. Table 1.16-3 and 4 contain the rivet spacing, driven rivet button diameter, and driven rivet button thickness data for the two rows above S-49L. Table 1.16-5 contains the driven rivet button diameter and thickness data for the two rows above S-51R. The numbering convention assigned to the rivets was established to provide a correlation to the field notes on this item. Reference to the body station location at particular rivet locations is provided for easier identification. All rivets installed in the two rows above S-49L and S-51R were ¼ inch diameter with the exception of a few blind rivets and smaller diameter solid rivets at certain shear tie locations (see Tables 1.16-3, 4, and 5 for details). Figure 3 of SRM 51-30-02 (See Maintenance Records Group Report Attachment 9-6), “Dimensions for Driving Non-Fluid-Tight Solid Shank Rivet” provides requirements for the minimum driven rivet button diameter and minimum driven rivet button thickness for installed rivets. For ¼ inch diameter rivets, the limits are 0.325 inch and 0.100 inch, respectively. The majority of rivets in the two rows above S-49L and S-51R did not satisfy these SRM requirements (see Tables 1.16-3, 4, and 5 for details).

Examination Conducted at Boeing

The following information documents the results of the examination conducted at Boeing in the presence of representatives from the ASC, NTSB, FAA, CSIST, and China Airlines during the period of November 6 to 22, 2002.

Examination of Fracture Surfaces above S-49L

The fracture surface common to the second row of rivets above S-49L between holes +17 and 93 were examined with a combination of visual, low power optical (up to 30X magnification), high power optical (up to 1000X), and Scanning Electron Microscopic (SEM) methods. This examination confirmed fatigue cracks at all the locations reported by CSIST and identified three more fatigue cracks at holes +11 aft, 33 aft, and 34 aft. Figures 1.16-39 and 40

provide a detailed map of all fatigue cracks confirmed during examination at Boeing. This figure incorporates the rivet spacing recorded in Table 1.16-3 and 1.16-4 as well. The length of the main fatigue crack centered about STA 2100 was 15.1 inches. Table 1.16-6 provides the detailed crack lengths of all the fatigue cracks presented in Figures 1.16-39 and 40. The cumulative length of fatigue cracking along the exterior surface of the skin was 25.4 inches. Low power optical examination was also performed to determine the origin of the fatigue cracks. This examination determined that all of the fatigue cracks initiated from longitudinal scratches on the faying surface of the skin with the doubler (original exterior surface of skin) from multiple origins except for the following cracks: +14 aft, +12 aft, + 11 aft, +5 fwd, 33 fwd, 37 aft, 38 fwd, 38 aft, 39 aft, 41 fwd, 42 fwd, 43 aft, 49 aft, and 51 aft. The propagation direction of all fatigue cracks was through the thickness of the skin. The extent of through-thickness propagation and origin location of the fatigue cracks is provided in Table 1.16-6. Figures 1.16-41 and 42 provide views of some of the scratches present on the faying surface of the skin to the doubler in relationship to the fatigue cracks. During examination a number of secondary fatigue cracks were also observed initiating from the longitudinal scratches.

From Hole 4 to Hole 26 the fracture surface generally maintained a flat profile through the skin thickness, with the exception of an intermediate segment between Holes 6 and 10 where the fracture assumed a slanted profile. The forward and aft end of the flat profile fatigue fracture surfaces displayed transition zones where the cracking mechanism changed from plane strain to plane stress conditions. Large transition zones were associated with the forward and aft extension of the main fatigue cracking between holes 10 and 25, as well as the forward extension of the fatigue cracking between holes 4 and 6 (see Figures 1.16-43 through 45). Generally, the smaller flat profile fatigue regions forward of hole 3 and aft of hole 32 displayed relatively brief transition zones. Figures 1.16-46 through 48 demonstrate the very small transition zones at holes +3 and 39.

Beyond the flat profile and transition zones of the main fatigue areas, the fracture surface contained numerous segments that displayed indications of incremental crack growth that could be observed visually or with the aid of low power optical instrumentation (Figures 1.16-49 and 1.16-50). In general, these indications were observed to increase in spacing as the distance from the flat profile fatigue regions increased in both the forward and aft directions. Such features were also observed on the fracture face between holes 6 and 10 with

increasing spacing in the forward direction (Figure 1.16-51). Incremental crack growth indications were observed as far forward as approximately STA 2055 and as far aft as hole 56 (STA 2140).

Rubbing of the fracture surface and associated compression deformation of the cladding was observed along the faying surface. Figure 1.16-52 shows the visible appearance of the fracture surface near holes 57, 58, and 59. The significant amounts of cladding were missing in the area of the panel coincident with the scratches. However, all areas where cladding remained forward and aft of the main fatigue cracking displayed compressive deformation consistent with crack closure as far forward as hole +17 and as far aft as hole 62. Figures 1.16-53 through 55 are SEM photographs showing the appearance of such aluminum cladding deformation. The remaining fracture aft of hole 62 displayed “necking”, which is typical of continuous tensile loading to ultimate tensile separation (Figure 1.16-56). The distance from the forward most incremental crack growth indication (STA 2055) to hole 62 is approximately 93.75 inches.

Striation Counts

Although much of the fracture suffered from heavy corrosion, fatigue striations were resolved by SEM in many local areas of the fatigue cracking regions as described in Figures 1.16-39 and 1.16-40. Striation counting was performed at a number of locations along the flat profile fatigue regions of the fracture. Since the fracture surface was not continuous from a single fatigue initiation origin to the ultimate extent of stage II (striation producing) cracking, it was not possible to estimate a time of initiation. Instead, the nature of cracking on this detail provided numerous initiation sites along scratches on the faying surface, with subsequent propagation in the through-thickness direction. Because cyclic cabin pressure is the prevailing driving force for cracking at this detail, each striation is considered to represent the microscopic crack advancement during one flight cycle of the airplane. Thus, striation counting was performed in order to obtain an estimate of the number of flight cycles that contributed to the fatigue crack propagation through the material thickness. CSIST reported the observation of “major” and “minor” striations. These minor striation-like features are shown in Figure 1.16-57 and were ignored for striation counting purposes.

Fatigue cycle estimates were obtained at the locations on the fracture listed in Table 1.16-7 along with the calculated results. For each location, a traverse

across the fracture at several points between the skin surfaces was made by sampling striation spacing with SEM photographs (Figure 1.16-58). For determining the crack length at each sample point, x and y Cartesian coordinates generated by the SEM stage were recorded and compared with a reference slope using an analytical geometrical approach. Striation spacing was determined by direct measurement from a photograph at each sampling location. The data was reduced and calculated by employing a trapezoidal integration method, whereby the number of cycles between two successive data points is equal to the distance divided by the average striation spacing (half of the sum of the growth rates at the two points). Although this approach may not precisely represent actual cracking behavior, it removes some of the subjectivity of assigning best-fit curves to widely scattered data points and can provide useful information, given an understanding of its limitations.

In each case, there was a distance between the initiation site and the nearest location where striations could be resolved. On the other end of each traverse, there was a distance between the inner surface of the skin, labeled “end of cracking” (EOC) for striation counting purposes, and the point where striations were observed. Hence, growth rates in those regions could not be determined. Since these distances were sometimes a significant portion of the actual crack propagation, the results are reported in two columns in Table 1.16-7. One column, “Total Cycles (Point)”, shows the estimated number of striations (or flight cycles) between the first and last obtainable data point. Another column, “Total Cycles (Ext.)”, includes that, as well as the unknown regions. This information is extrapolated by assuming constant growth rate from the initiation site to, and equal to, the first obtainable data point. Again, such extrapolation may not accurately represent actual fatigue cracking behavior, but it is presented here for discussion purposes to account for an estimate of flight cycles that may have contributed to the cracking up to that point and may be considered a minimum. The raw data collected, as well as the integrated calculations are provided in the attached Appendix 7-I.

Examination of Skin

Photographs showing features of the as-received item 640 C1 skin inboard and outboard (repair faying surface) surfaces are shown in Figures 1.16-59 and 60 respectively. Protective finishes had previously been removed from much of the repair faying surface at the CSIST to enable examination of skin damage consistent with a tail strike event. Close-up photographs displaying the extent of damage consistent with a tail strike are shown in Figures 1.16-61

through 70. This damage consists primarily of fore to aft (longitudinal) scratching with the most severe scratching typically occurring at the location of skin stiffening members such as skin stringers and body frame shear ties. Figure 1.16-71 displays the location of the most severe skin damage. As noted in this photograph, the most severe damage consistent with a tail strike occurred on the left hand side of the airplane in the area covered by the repair doubler. Evidence of rework sanding marks was noted over much of the repair surface.

A surface replication medium was applied at five locations on the skin repair faying surface as shown in Figure 1.16-72 to examine scratch geometry and depth. The locations were chosen to display surface features typical to areas exhibiting major scratching. This medium creates a “positive” of the surface it is applied to, enabling direct feature measurement from the replica. The maximum scratch depth measured with this technique was 0.0096 inch. Composite photographs exhibiting scratch profiles at locations noted above are shown in Figures 1.16-73 and 74.

The thickness of the skin was measured ultrasonically at several locations. Thickness measurements were recorded in millimeters directly on the skin at point of measurement and are documented in Figures 1.16-75 through 80. The ultrasonic unit was calibrated using a reference sample and ultrasonic measurements were also verified using a calibrated micrometer.

Corrosion was noted at several shear tie locations on the skin inboard surface sometimes penetrating completely through the skin thickness. Photographs displaying these corrosion features are shown in Figures 1.16-81 through 1.16-83. Table 1.16-8 records visual observations of these features.

Open hole High Frequency Eddy Current (HFEC) inspection of the skin was performed on the outer two rows of fastener holes associated with attachment of the repair doubler above S- 51R. A total of ten crack indications were identified, nine occurred in the second fastener row above S-51R and one occurred in the first fastener row above S-51R. Open hole HFEC inspection of the second row of fastener holes above S-51R had previously been performed by a China Airlines inspector with three holes indicating cracking. The skin/doubler sealant fillet region was inspected by HFEC using a surface probe. Visual examination of this area previously identified longitudinal scratches in the skin in this region that were different in appearance and severity (less severe) relative to probable tail strike scratches. No evidence of cracking was

identified in this region. This result was consistent with HFEC surface probe testing previously done at the CSIST.

”Cookie cuts” were excised from the skin at HFEC crack indications to enable further examination. Figures 1.16-84 through 87 document the location of cookie cut samples. Cookie cuts 1 and 4 were inadvertently damaged during removal, destroying all fastener bore features. The remaining excised samples were penetrant inspected and optically examined to 50X. Cracking was visually identified on three of the remaining cookie cuts (#3, #7and #9). Cracks in cookie cuts #3 and # 9 were successfully opened, while #7 proved too small to open. Crack features were examined from low to high magnification in a Scanning Electron Microscope (SEM). Figures 1.16-88 through 91 display the crack features. Cracking in cookie cut #3 was the due to fatigue originating from multiple origins at the skin faying surface, away from the fastener bore (Figure 1.16-88). The crack length was 0.028 inch and maximum crack penetration through the skin thickness was 0.011 inch. Cracking in cookie cut #9 was also due to fatigue but initiated from the fastener bore from an origin near the bore/skin repair faying surface interface (Figure 1.16-90). The crack length and its propagation through the skin thickness were both 0.044 inch. (Figures 1.16-89 and 91).

A metallographic specimen was removed from plane A-A (Figure 1.16-85) to examine scratch features associated with sealent fillet seal scratching. A composite photograph of this section is shown in Figure 1.16-92. Maximum scratch depth was measured at 0.0037 inch. Plane AA also traversed the only area of probable tail strike damage associated with the right hand side of the repair. The damage at this location was much less severe than the skin damage on the left hand side of the repair. Figure 1.16-93 displays surface features associated with the outer fastener row of the repair. A maximum scratch depth of 0.0008 was measured optically in this location.

Full size longitudinal (L) and long transverse (LT) tensile specimens were excised from the skin in the vicinity of STA 2080, between stringers S-48R and S-50R. The specimens were tested to destruction and tensile test results are recorded in Table 1.16-9. All values met minimum property requirements per QQ-A-250/5 for clad 2024-T3 sheet as specified by the engineering drawing. Specimen geometry and test procedures were per ASTM B557.

Remnants of two ¼ inch diameter countersunk doubler repair rivets previously removed and labeled at the CSIST were selected at random to determine their

alloy and temper. These rivets were identified as E64 and D51, however their location relative to installation in the repair was not provided. Spectrochemical analysis verified the rivet alloy was 2017 per aluminum QQ-A-430 as recorded in Table 1.16-11. Hardness and conductivity measurements were indicative of the T4XXX temper as noted in Table1.16-12.

The thickness of the fuselage skin was measured along the fracture above S-49L at intervals of 0.10 inch from hole +17 to 56 using a calibrated point contact micrometer. The drawing required thickness at this location is 0.071 inch with a tolerance of + 0.010 inch, – 0.004 inch. The measured skin thickness ranged from 0.062 inch at hole 19 to 0.078 inch between hole 24 and 25. A number of localized areas with below drawing allowed thickness were measured and were most likely due to the presence of a scratch or localized rework. This thickness data was plotted along the length of the crack from hole +17 to 56 (See Figure 1.16-94 for details).

Metallographic specimens were taken through the main fatigue region to characterize the depth and geometry of the longitudinal scratches initiating the through-thickness fatigue cracks. The cross sections were taken in the vicinity of STA 2100 between holes 18 and 19 and between holes 19 and 20. Figure 1.16-95 provides the location of the cross section taken between holes 18 and 19. At this location two longitudinal scratches were visible with one being the initiation site for the primary fatigue crack forward of hole 19 and another scratch being the site for initiation of the primary fatigue crack aft of hole 18. A secondary fatigue crack under that primary fatigue crack aft of hole 18 was also present. Evidence of rework blending (sanding) was present in the vicinity of the scratches. To accurately determine the depth of these scratches a line was projected back to an area of undisturbed clad material. At this location the depth of the scratches measured from 0.0043 inch (110 microns) to 0.0046 inch (118 microns) (see Figure 1.16-96). The cross section taken between hole 19 and 20 represented an area with a number of scratches where the primary fatigue crack aft of hole 20 and secondary fatigue crack initiated. Figure 1.16-97 provides the location where the cross section was taken. Rework sanding was also present at this location and therefore a similar projection technique was employed to accurately determine the depth of the scratches in this area. The depth of scratches ranged from 0.0056 inch (143 microns) at the primary fatigue crack to 0.0025 inch (63 microns) at the secondary fatigue crack origin (see Figure 1.16-98)

<u>Examination of Repair Doubler:</u>

Visual examination revealed a light colored deposit on the overhanging portion of the faying surface of the doubler (mating surface with skin) above the fracture surface at S-49L. Low power optical examination of this area revealed that this light colored deposit had a similar appearance to the light blue exterior paint applied to the doubler. This light colored deposit was on top of what appeared to be the sealant used during installation of the doubler to the skin. The deposit was present between holes 10 and 25 with the largest area observed between holes 14 and 22 (see Figures 1.16-99 and 100). Two samples of this deposit were removed in the vicinity of hole 18 (STA 2100) and subjected to organic analysis utilizing Fourier Transform Infrared Spectroscopy (FT-IR). A sample of the exterior paint on the doubler was also removed as well as the sealant on the faying surface for baseline comparisons. FT-IR analysis of the deposit revealed that the spectra of the light colored deposit was an excellent match to the reference light blue exterior paint on the doubler (see Figure 1.16-101). Optical examination of the deposits showed that the paint had cured in place and therefore must have flowed between the doubler and skin while wet. As noted in the CSIST report the doubler in the vicinity STA 2100 was deformed locally in an outward direction with the fractured skin.

Numerous areas of the overhanging portion of the faying surface of the doubler exhibited signs of localized damage as if the skin moved against the doubler above the S-49L fracture surface. The furthest forward and aft portions of this localized damage was observed at hole +16 (~STA 2061) to hole 49 (~STA 2132) with the most significant degree present between holes 8 and 43. Low power optical examination determined the damage resulted from hoop-wise movement of the skin against the doubler. The degree and position of this hoop wise fretting is documented in Table 1.16-10 with photographic examples provided in Figure 1.16-102 and 103.

Examination of Frame Segments:

All the recovered frame segments in the vicinity of the item 640C1 and C2 skin panel were submitted to BMT for: 1) examination of all the fracture surfaces to determine fracture modes, evidence of pre-existing damage, and fracture propagation direction; 2) examination of all shear ties for evidence of separation direction from the skin panel; 3) material and temper verification of critical frame members (failsafe chord, inner chord, and shear ties). A total of five frame segments from STA 2160, 2100, 2060, 2040, and 1940 were received for examination (see Table 1.16-1 for details). The following provides the results of this examination on each of these frame segments:

STA 2160 Frame Segment Between S-51L to S-48L:

This frame segment was part of the recovered item 640C1 skin panel and was removed during disassembly at the CSIST laboratory (see Figure 1.16-104). The overall condition of the submitted frame segment as received by BMT is shown in Figures 1.16-105 and 106. The frame segment contained three shear ties, the failsafe chord, a portion of a stringer clip and a portion of the web. A repair existed at the shear tie between S-51L and S-50L. The repaired shear tie exhibited no corrosion, however, the mating interior surface of the fuselage skin as previously described in Figure 1.16-93 displayed two pockets of exfoliation corrosion with corresponding cracks visible on the exterior surface of the original skin (faying surface with repair doubler). A significant lump of sealant was found attached to the aft side of the shear tie free flange and skin flange. An impression of the skin corrosion was evident in the surface of the sealant faying with the interior surface of the skin. The shear tie between S-50L and S-49L was heavily corroded with no remaining skin flange attachment provided for examination. The associated mating interior surface of the fuselage skin displayed no evidence of corrosion. The shear tie between S-49L and S-48L was heavily corroded with no remaining skin flange attachment. The skin at this location was free of corrosion on the interior surface mating with the shear tie skin flange, however this represents only a small portion of the mating interior surface. The rest of associated mating interior surface has not been recovered to date.

Visual and low power optical examination of the failsafe chord fractures at both forward and aft ends of this frame segment revealed slanted fracture profiles with fracture morphologies consistent with ductile separation. No evidence of any pre-existing damage (i.e. slow crack growth or corrosion) was present. A considerable degree of post fracture mechanical damage (i.e. rub) was observed at the failsafe chord fracture common to S-48L. Closer examination of the two shear ties between S-50L and S-48L revealed a considerable degree of pre-existing exfoliation corrosion primarily at the mid thickness plane of the shear tie (see Figures 1.16-107 and 108). Low power optical examination of these fracture surfaces revealed further fragmentation by exfoliation corrosion or slanted type fractures with no evidence of any slow crack growth.

The one shear tie with the skin flange still intact on the submitted frame segment (between S-51L and S-50L) exhibited a compressed free flange and rivets pushed in the upward direction. The skin flange rivets were fractured at

the countersink head by what appeared to be straight tension type load. Prior to disassembly of this frame segment from the Item 640C1 skin panel, notes were taken at the CSIST laboratory (see Table 1.16-2) indicating that this shear tie was still attached to the skin but that the rivets were completely pulled through the doubler but remained in the skin. This shear tie was also reported to exhibit up and aftward deformation.

Spectrochemical analysis confirmed the failsafe chord was fabricated from 7075 aluminum alloy in accordance with the drawing requirements (see Table 1.16-11). Hardness and conductivity measurements verified the drawing required T6 type temper (see Table 1.16-12 for details). The same techniques determined that the material for the shear tie repair was 2024 aluminum alloy in the T4 type temper. The drawing required thickness, material, and temper for this shear tie is 0.063 inch thick 7075-T62 aluminum alloy. The thickness of this repair shear tie was measured by use of a micrometer to be 0.071 inch.

STA 2100 Frame Segment Between S-49L to S-48R (Item 2015):

The overall condition of this frame segment as received by BMT is presented in Figures 1.16-109 and 110.

The fracture to the S-49L end of this frame segment was common to the failsafe chord, shear tie, web and intermediate chord. Visual and low power optical examination of these fracture surfaces revealed slanted fracture profiles with fracture morphologies consistent with ductile separation. No evidence of pre-existing damage (slow crack growth or corrosion) was observed. The fractured end common to S-49L exhibited deformation of the shear tie member in the forward direction and deformation of the web at the intermediate chord location in the aft direction (refer to Figure 1.16-111). In addition, the hole in the shear tie at the fracture location was elongated in the upward direction. No evidence of compressed or buckled members at this area was noted.

Examination of the remaining fracture surfaces for the failsafe chord, shear ties, inner chord, and stringer clips by visual and low power optical techniques revealed slanted fracture profiles with fracture morphologies consistent with ductile separation. No evidence of any pre-existing slow crack growth or corrosion on these fractures was observed.

The shear ties present on this frame segment were examined for evidence of separation direction from the skin. The shear tie skin flange and skin

attachment rivets were examined using visual and low power optical techniques to determine if any evidence of loading direction was present. The shear tie between S-49L and S-50L was fractured in the free flange and therefore no separation direction observations were made or assessment of pre-existing corrosion in the skin flange. As previously noted extensive corrosion existed through the thickness of the skin at this shear tie location. The shear tie between S-50L and S-51L had a small portion of the skin flange at the inboard most fastener hole remaining. The remnants of this fastener hole exhibited deformation in the downward direction indicative of a tensile pull through of the fastener. The shear tie between S-51L and S-51R exhibited deformation at all three fastener holes common to the skin in the downward direction as well. The skin flange of the shear tie between S-51R and S-50R was not fractured but the inboard most fastener hole was deformed in the downward direction with the rivet missing (See Figure 1.16-112). The remaining two rivets were fractured at the countersink and exhibited fracture and deformation characteristics that indicated a forward component of this tensile load. Similar results of the fracture and deformation characteristics indicative of a forward acting tensile load were observed in the all three rivets common to the skin flange for the shear tie between S-50R and S-49R. The shear tie between S-49R and S-48R had Hi-Loks installed at the skin flange. The Hi-Loks were not fractured but the holes in the shear tie skin flange containing these fasteners were loose. The holes in the mating skin at this shear tie location were deformed in the upward direction on the aft side of the hole with witness marks on the forward side of the skin (see Figure 1.16-113). These observations were consistent with all others for this frame indicating a forward acting tensile load on the shear ties of this frame segment.

Spectrochemical analysis, hardness and conductivity measurements performed on samples of the failsafe chord and inner chord of this frame segment confirmed that the failsafe chord and inner chord were fabricated from the drawing required 7075 aluminum alloy in the T6 type temper. The shear tie sampled was verified using the same methods as 2024 aluminum alloy in the T4 type temper in accordance with the drawing requirements (see Table 1.16-11 and 12 for details).

STA 2060 Frame Segment Between S-49L to S-51R (Item 2014):

The as-received condition of this frame segment is shown in Figures 1.16-114 and 1.16-115. This frame segment contained three stringer clips, two shear ties, the failsafe chord, the intermediate chord and a portion of the web.

The fracture at S-49L was common with the failsafe chord and web. The shear tie at this location fractured through one fastener hole inboard of this location. Visual examination of the fracture surface of the failsafe chord revealed a slanted fracture profile, however, a heavy, dark deposit in a localized area of the fracture precluded complete examination (see Figure 1.16-116). Attempts to remove this deposit using surfactants and solvents were unsuccessful. The remainder of this fracture surface was examined with the use of low power optical techniques to reveal a fracture morphology characteristic of ductile separation. No evidence of pre-existing corrosion or any fracture features indicative of slow crack growth was present. The hole in the failsafe chord where the fracture propagated through exhibited elongation in the inboard/outboard direction suggesting a tensile stress causing the fracture. The fracture surfaces of the web and shear tie at this location were characterized by slanted profiles with fracture topographies typical of ductile separation.

The other end of this submitted frame segment was fractured at S-51R through the failsafe chord, shear tie and web. All of the fractures exhibited significant post fracture damage consisting of mechanical damage (i.e. rub) and corrosion due to immersion in salt water. The preserved fracture surfaces exhibited slanted fracture profiles with overall fracture topographies consistent with ductile separation when viewed using visual and low power optical techniques.

Visual examination of the shear ties from this frame segment was performed to determine the direction of separation from the skin. The shear tie between S-51R and S-51L was missing the skin attachment rivets and contained no fractures, however, the skin flange was bent in the downward direction. The shear tie between S-51L and S-50L was fractured at the inboard most fastener hole common to the skin flange. The middle fastener hole was deformed in the downward direction. The outboard most rivet remained in the skin flange with the manufactured countersink head pulled off (see Figure 1.16-117). This shear tie also exhibited downward deformation of the skin flange. The shear tie between S-50L and S-49L was also missing the skin attachment rivets and exhibited downward deformation of the middle skin flange fastener hole. In addition, the stringer clip at S-51L exhibited a bearing fracture through one of the attachment lugs. All these observations were consistent with the application of a straight tensile load on the shear ties of this frame segment.

Spectrochemical analysis, hardness, and conductivity testing of samples of the failsafe chord and shear tie confirmed the drawing required materials of

7075-T62 and 2024-T42 aluminum alloys, respectively. Results of this testing are provided in Tables 1.16-11 and 12.

STA 2040 Frame Segment Between S-50L to S-42R (Item 740):

Figure 1.16-118 and 119 provide overall views of the aft and forward faces of this frame segment submitted for examination.

The failsafe chord, web, and shear tie all were fractured at S-51L. At S-42R the fracture was common with the failsafe chord and web. Examination of these fracture surfaces with the use of visual and low power optical techniques revealed slanted fracture profiles with no evidence of any pre-existing corrosion or slow crack growth regions. The overall fracture morphologies were consistent with ductile separation. At S-51R, the failsafe chord was fractured at the free flange radius with deformation consistent with compression buckling (see Figure 1.16-120). All of the inner chord fractures exhibited slanted fracture profiles with fracture morphologies consistent with ductile separation as well.

All of the shear ties on this frame segment with the exception of the two at the far right side (between S-42R and S-44R) exhibited no fractures. The extruded “T” shear tie between S-42R and S-43R was fractured through the forward skin flange while the sheet metal shear tie between S-43R and S-44R was fractured through the free flange. Visual and low power optical examination of these fracture surfaces revealed slanted fracture profiles with fracture morphologies typical of ductile separation. The remainder of the shear ties on this frame experienced skin flange rivet fractures. These rivet fractures were examined to help determine the direction of loading during separation from the skin. The skin flange rivets present on the three shear ties between S-45R and S-48R exhibited evidence of loading in the forward to forward/inboard direction (See Figure 1.16-121) while the four shear ties between S-48R and S-51L exhibited evidence of loading in the aft/outboard direction (note the direction of loading for the shear tie between S-51R and S-51L was identical to the other three shear ties) (See Figure 1.16-122). All these shear ties exhibited no deformation except for the location between S-45R and S-46R which exhibited forward deformation.

Spectrochemical analysis, hardness and conductivity measurement performed on samples of the failsafe chord and inner chord from this frame segment confirmed these items were fabricated from the drawing required 7075 aluminum alloy in the T6 type temper. The shear tie sampled was verified

using the same methods as 2024 aluminum alloy in the T4 type temper in accordance with the drawing requirements (see Table 1.16-11 and 12 for details).

STA 1940 Frame Segment between S-50L and S-43L (Item 2086):

The as-received condition of this frame segment is shown in Figure 1.16-123 and 124. This frame segment contained two repairs of shear tie locations and one repair to the web. The shear ties were repaired between S-50L and S-49L with the use of a doubler (See Figure 1.16-125) and between S-46L and S-44L with the use of a replacement shear tie/doubler combination (See Figure 1.16-126). The web was repaired with the use of a doubler placed on the aft side under the cut-out between S-50L and S-49L (See Figure 1.16-127).

The frame segment was fractured at the failsafe chord, web, and shear tie at S-50L. Visual and low power optical examination of all of these fracture surfaces revealed slanted fracture profiles with fracture topographies consistent with ductile separation. No evidence of pre-existing cracking or corrosion was observed on any of these fractures. The inner chord at S-50L was also fractured and exhibited a slanted fracture profile. Low power optical examination of this fracture surface revealed a considerable degree of post fracture mechanical damage (i.e. rub), however, localized areas that could be viewed exhibited a fracture morphology consistent with ductile separation. The inner chord was also fractured through the free flange between S-50L and S-48L. Examination of these fracture surfaces also revealed slanted profiles with fracture morphologies typical of ductile separation. Between S-44L and S-43L the fracture was common to the failsafe chord and web. The fractures at this location exhibited slanted profiles, however, a very heavy deposit existed precluding a closer examination to determine the fracture morphology. Attempts to remove this deposit using surfactants and solvents were unsuccessful. No obvious signs of deformation that would indicate a direction of loading or fracture were observed on any of these fractures. Localized deformation was observed on the failsafe chord in the upward direction just outboard of S-49L and in the downward direction just outboard of S-48L and S-46L.

The shear ties present on this frame segment were examined for evidence of separation direction from the skin. This frame segment exhibited fractured shear ties at two locations: between S-45L and S-44L and between S-45L and S-46L. The repair shear tie between S-45L and S-44L was fractured through

the inboard most hole by what appeared to be a bearing type fracture. The deformation was observed at this location in the outboard direction. The remaining skin flange attachment rivets were fractured in an outboard direction as well (See Figure 1.16-128). The shear tie between S-46L and S-45L was fractured through the free flange of the production shear tie and therefore no separation direction observations were made. Visual and low power optical examination of this fracture surface revealed a slanted profile with a morphology consistent with ductile separation. The remaining shear ties were not fractured but exhibited either fractured skin flange attachment rivets or deformation. These skin flange attachment rivets were examined using visual and low power optical techniques to determine if any evidence of loading direction was present. On the shear tie between S-50L and S-49L three of the skin flange attachment rivets were fractured in the forward to outboard direction while the inboard most rivet exhibited evidence of an inboard direction of loading (See Figure 1.16-129). All the skin flange attachment rivets of the shear tie between S-49L and S-48L showed signs of fracture in the forward to inboard direction (See Figure 1.16-130). The skin flange attachment rivets for the shear tie between S-48L and S-47L were not fractured but the shear tie exhibited general deformation in the aft direction. On the shear tie between S-47L and S-46L the two outboard most skin flange attachment rivets were fractured in the forward to outboard direction while the two inboard most rivets exhibited evidence of an aft to outboard direction of loading (See Figure 131).

Between S-47L and S-44L the stringer clips were missing from this frame segment. The rivet fractures and or hole deformation at these locations were examined to determine if any evidence of separation direction was present. At all of these stringer clip locations the rivets were fractured and remained in the shear tie except at the lower attachment hole at S-47L which was missing the rivet. All of the fractured rivets that could be viewed (some of the fractures existed at the web/shear tie interface) exhibited signs of loading in the downward direction. The lower attachment hole at S-47 exhibited elongation in the downward direction as well (See Figure 132).

Spectrochemical analysis, hardness and conductivity measurement performed on samples of the failsafe chord and inner chord from this frame segment confirmed these items were fabricated from the drawing required 7075 aluminum alloy in the T6 type temper. The shear tie sampled was verified

using the same methods as 2024 aluminum alloy in the T4 type temper in accordance with the drawing requirements (see Tables 1.16-11 and 12 details).

Table 1.16-1 Description of wreckage items submitted to BMT for examination

Description of wreckage items submitted to BMT for examination.

ASC Assigned Item Number	General Description	Boeing Part Number	Boeing Part Name	Material & Heat Treat	Material Specification	Finish
640C1	Section 46 Skin Panel – STA 2060 to 2180, S-49L to S-49R	65B04152	Skin Panel Instl – STA 1961.10 to STA 2181.10, S-46L to S-46R	Skin – Clad 2024-T3	Skin – QQ-A-250/5	Interior surface - chromic acid anodize + one coat of BMS 10-11 primer + BMS 10-11 enamel
	Frame Segment – STA 2160, S-49L to S-51L	65B04345	Frame Instl – Body STA 2160, Lower Lobe	Shear Ties – 7075-T62 Failsafe Chord - 7075-T62	Shear Ties – QQ-A-250/12 Failsafe Chord QQ-A-200/11	Same as Item 2015
640C2	Section 46 Skin Panel – STA 2046 to 2060, S-49L to S-49R	65B04152	Skin Panel Instl – STA 1961.10 to STA 2181.10, S-46L to S-46R	Skin – Clad 2024-T3	Skin – QQ-A-250/5	Same as 640C1
2015	Frame Segment – STA 2100, S-49L to S-48R	65B04342	Frame Instl – STA 2100, Lower Lobe	Shear Ties – 2024-T42 Inner Chord – 7075-T6511 Failsafe Chord – 7075-T62	Shear Ties – QQ-A-250/4 Inner Chord – QQ-A-200/11 Failsafe Chord QQ-A-200/11	Alodine or chromic acid anodize + one coat of BMS 10-11 primer + BMS 10-11 enamel
2014	Frame Segment – STA 2060, S-49L to S-51R	65B04340	Frame Instl – STA 2060, Lower Lobe	Shear Ties – 2024-T42 Failsafe Chord – 7075-T62	Shear Ties – QQ-A-250/4 Failsafe Chord QQ-A-200/11	Same as Item 2015
740	Frame Segment – STA 2040, S-50L to S-42R	65B04339	Frame Instl – Body Station 2060, Lower Lobe	Same as Item 2015	Same as Item 2015	Same as Item 2015
2086	Frame Segment – STA 1940, S-50L TO S-43L	65B04334	Frame Instl – Body Station 1940, Lower Lobe	Same as Item 2015	Same as Item 2015	Same as Item 2015

Figure 1.16-36 Item 640C1 and C2 Skin panel segments prior to removal from the parent item 640 wreckage in Makung, Taiwan.

Figure 1.16-37 Interior surface of Item 640C1 as received at CSIST laboratory in Taichung, Taiwan.

Table 1.16-2 Schematic representation of shear tie and stringer clip attachment to item 640C1 and C2 skin sections.

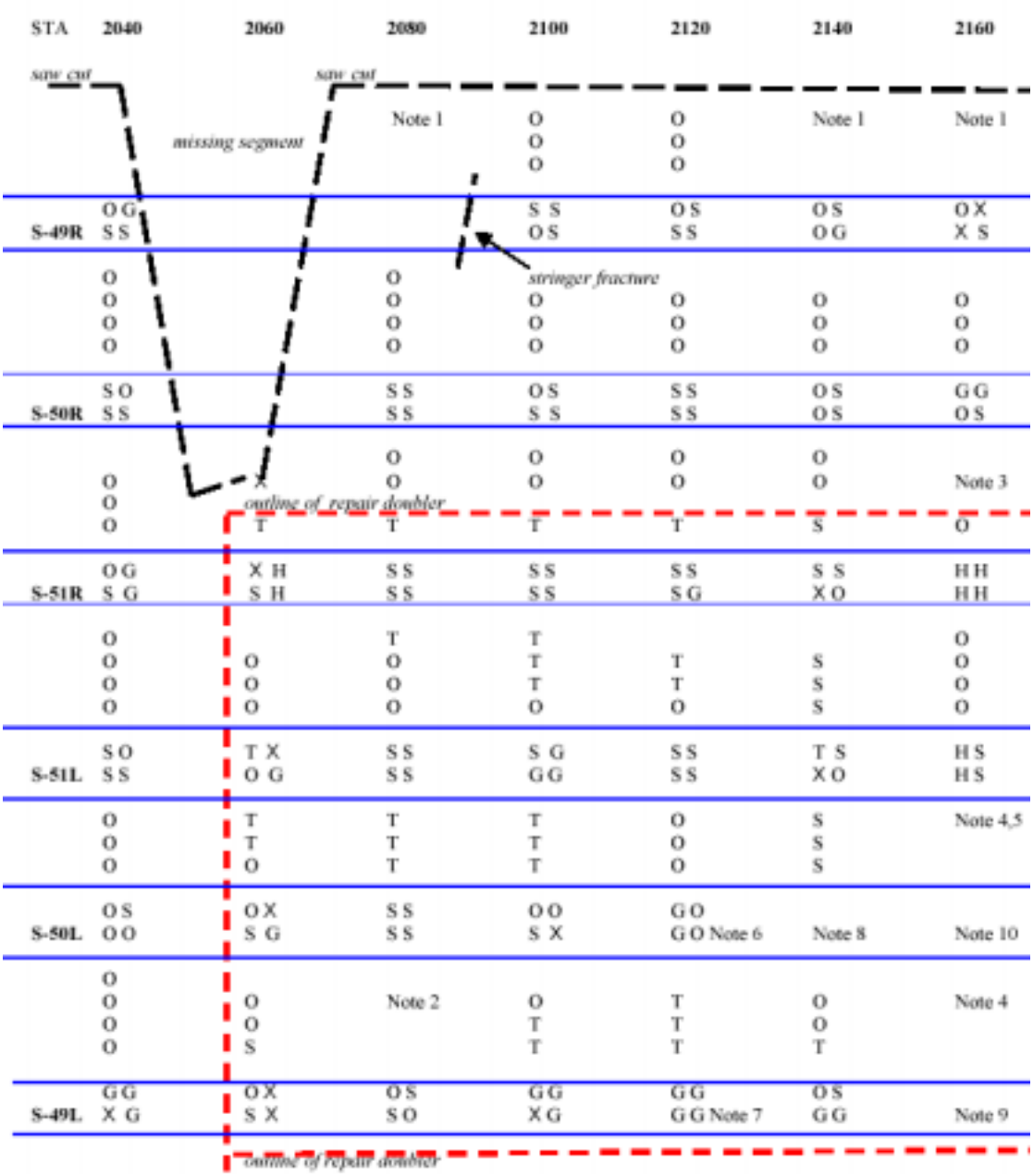

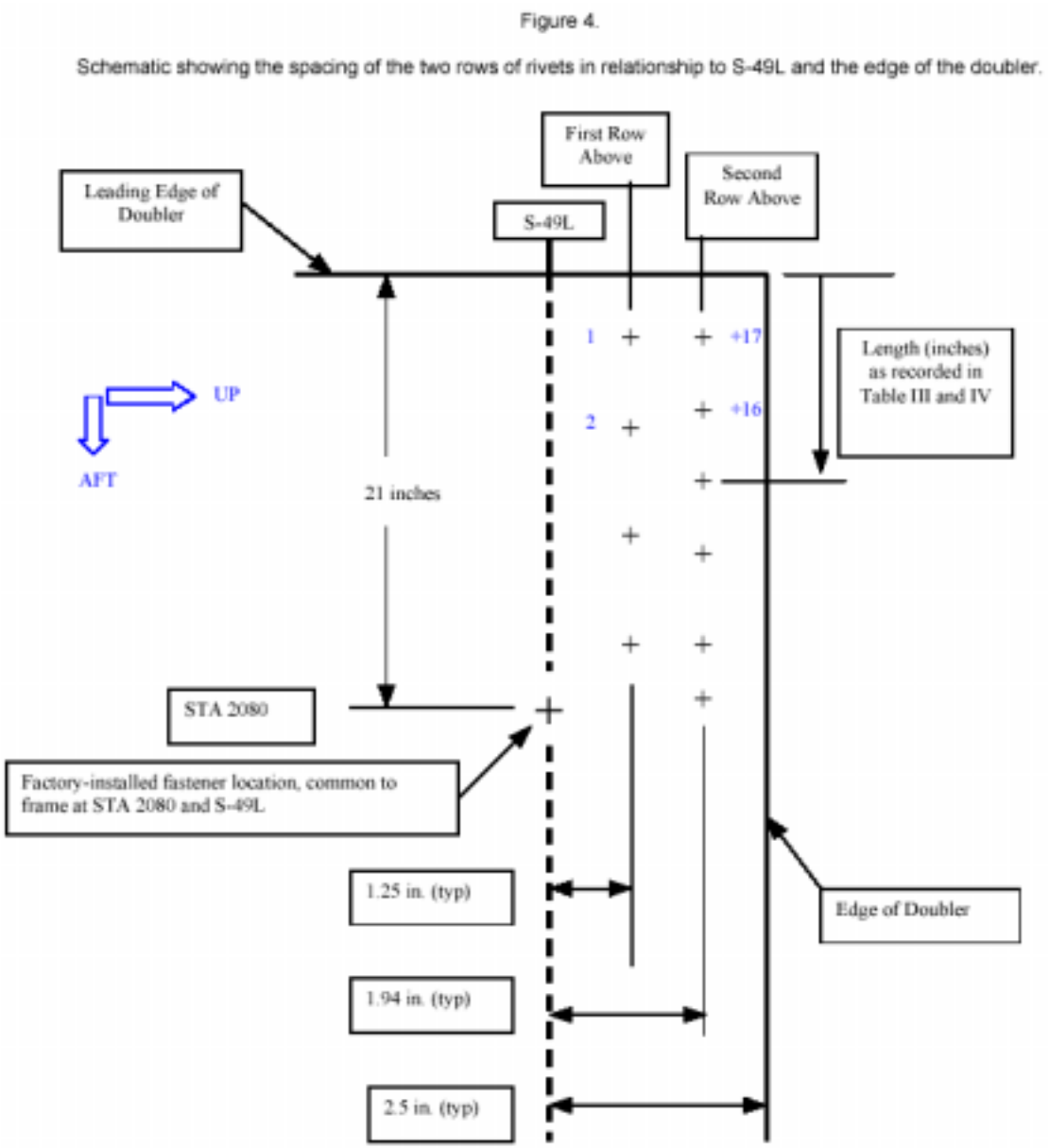

Figure 1.16-38 Schematic showing the spacing of the two rows of rivets in relationship to S-49L and the edge of doubler

Table 1.16-3 Repair doubler rivet spacing and driven rivet dimensions for first row above S-49L.

Rivet No.	Body Station Reference	Length from Leading Edge of Doubler (inches)	Driven Rivet Button Diameter (inch)	Driven Rivet Button Thickness or Height (inch)	Notes
1		0.69	0.322	0.103	underdriven
2		1.44	0.300	0.124	underdriven
3		2.50	0.343	0.070	overdriven
4		3.88	0.325	0.068	overdriven
5		5.31	0.350	0.060	overdriven
6		6.69	0.337	0.060	overdriven
7		8.06	0.339	0.060	overdriven
8		9.50	0.340	0.060	overdriven
9		10.81	0.337	0.060	overdriven
10		12.25	0.339	0.060	overdriven
11		13.69	0.344	0.070	overdriven
12		15.00	0.337	0.071	overdriven
13		16.38	0.337	0.069	overdriven
14		17.69	0.327	0.103	
15		19.06	0.313	0.082	overdriven
16		20.38	0.365	0.078	overdriven
17	~2081	21.38	0.388	0.073	overdriven
18		23.50	0.325	0.084	overdriven
19		25.06	0.337	0.081	overdriven
20		26.38	0.387	0.065	overdriven
21		27.63	0.318	0.093	overdriven
22		29.06	0.339	0.068	overdriven
23		30.38	0.338	0.071	overdriven
24		31.75	0.300	0.101	
25		33.25	0.325	0.096	overdriven
26		34.63	0.331	0.076	overdriven
27		36.00	0.336	0.062	overdriven
28		37.56	0.358	0.058	overdriven
29		38.94	0.331	0.076	overdriven
30		40.38	0.373	0.061	overdriven
31	2100	41.75	0.391	0.077	overdriven

32		43.19	0.315	0.115	underdriven
33		44.56	0.37	0.076	overdriven
34		45.94	0.36	0.065	overdriven
35		47.25	0.35	0.067	overdriven
36		48.75	0.38	0.064	overdriven
37		50.19	0.35	0.068	overdriven
38		51.63	0.33	0.068	Overdriven
39		52.94	0.32	0.082	overdriven
40		54.44	0.342	0.060	overdriven
41		55.88	0.327	0.069	overdriven
42		57.38	0.335	0.067	overdriven
43		58.75	0.337	0.075	overdriven
44		60.25	0.348	0.061	overdriven
45		61.50	0.334	0.066	overdriven
46	~2121	63.00	0.307	0.087	overdriven
47		64.38	0.331	0.060	overdriven
48		65.75	0.344	0.055	overdriven
49		67.06	0.328	0.056	overdriven
50		68.44	0.324	0.075	overdriven
51		69.88	0.327	0.065	overdriven
52		71.25	0.335	0.068	overdriven
53		72.63	0.336	0.067	overdriven
54		74.00	0.332	0.057	overdriven
55		75.50	0.356	0.063	overdriven
56		76.94	0.348	0.061	overdriven
57		78.19	0.370	0.058	overdriven
58		79.50	0.348	0.050	overdriven
59		80.75	0.355	0.053	overdriven
60	2140	82.44	0.343	0.053	overdriven
61		83.94	0.357	0.118	
62		85.25	0.349	0.095	overdriven
63		86.63	0.360	0.090	overdriven
64		88.00	0.351	0.060	overdriven
65		89.56	0.340	0.095	overdriven
66		90.88	0.341	0.096	overdriven
67		92.25	0.317	0.100	
68		93.69	0.358	0.100	

69		95.00	0.320	0.100	underdriven
70		96.38	0.370	0.095	overdriven
71		97.88	0.367	0.100	
72		99.25	0.382	0.090	overdriven
73		100.63	0.370	0.110	
74		102.00	0.330	0.150	
75	~2161	103.63	0.298	0.150	underdriven
76		104.88	0.321	0.160	underdriven
77		106.19	0.332	0.105	
78		107.56	0.350	0.094	overdriven
79		109.00	0.370	0.092	overdriven
80		110.44	0.390	0.087	overdriven
81		111.75	0.367	0.127	
82		113.19	0.378	0.107	
83		114.69	0.364	0.116	
84		116.13	0.350	0.100	
85		117.38	0.368	0.085	overdriven
86		118.88	0.396	0.082	overdriven
87		120.13	0.361	0.080	overdriven
88		121.13	0.358	0.083	overdriven
89		122.00	0.401	0.094	overdriven
90		123.25	missing	missing	
91		124.19	missing	missing	
AFT Edge of Doubler		124.81	n/a	n/a	

Table 1.16-4 Repair doubler rivet spacing and driven rivet dimensions for second row above S-49L.

Rivet No.	Body Station Reference	Length from Leading Edge of Doubler (inches)	Driven Rivet Button Diameter (inch)	Driven Rivet Button Thickness or Height (inch)	Notes
+17		0.31	missing	missing	
+16	~2061	1.50	0.367	0.091	overdriven
+15		2.50	0.359	0.085	overdriven
+14		3.56	0.334	0.101	
+13		4.56	0.357	0.113	
+12		5.81	0.349	0.100	
+11		7.06	0.400	0.080	overdriven
+10		8.19	0.345	0.095	overdriven
+9		9.38	0.357	0.095	overdriven
+8		10.50	0.368	0.095	overdriven
+7		11.63	0.357	0.088	overdriven
+6		12.81	0.356	0.096	overdriven
+5		14.00	0.331	0.105	
+4		15.25	0.350	0.105	
+3		16.56	0.333	0.114	
+2		17.88	0.393	0.070	overdriven
+1		19.25	0.356	0.100	
0		20.06	0.371	.1035/.0835	overdriven
1	2080	21.00	0.213	0.138	blind rivet
2		22.50	0.319	0.111	half bucked
3		23.81	0.421	0.076	overdriven
4		25.00	0.397	0.062	overdriven
5		26.44	0.389	0.091	overdriven
6		27.63	0.393	.0805/.094	overdriven
7		29.19	0.422	0.077	overdriven
8		30.75	0.389	.0735/.0835	overdriven
9		32.00	0.395	.0725/.095	overdriven
10		33.19	0.428	0.080	overdriven
11		34.38	0.400	0.077	overdriven
12		35.44	0.385	0.075	overdriven
13		36.63	0.400	0.079	overdriven

14		37.69	0.399	0.077	overdriven
15		38.75	0.374	0.088	overdriven
16		39.81	0.401	0.075	overdriven
17		40.81	0.373	0.088	overdriven
18	2100	41.63	0.237	0.136	blind rivet
19		42.19	0.399	0.058	overdriven
20		43.25	0.424	0.074	overdriven
21		44.50	0.413	0.081	overdriven
22		45.56	0.384	0.087	overdriven
23		46.56	0.380	.0975/.08	overdriven
24		47.63	0.348	.0955/.0925	overdriven
25		48.63	0.370	.0855/.095	overdriven
26		49.81	0.383	0.073	overdriven
27		50.81	0.377	0.070	overdriven
28		52.06	0.355	0.100	
29		53.25	0.358	0.095	overdriven
30		54.44	0.369	0.072	overdriven
31		55.63	0.326	0.110	
32		56.75	0.340	0.094	overdriven
33		57.81	0.357	0.081	overdriven
34		58.81	0.352	0.088	overdriven
35		59.81	0.346	0.103	
36		60.69	0.364	0.082	overdriven
37		61.50	.3125/.289	0.100	underdriven
38	2120	62.00	0.277	0.121	7/32 rivet
39		63.19	0.360	0.109	
40		64.38	0.351	0.096	overdriven
41		65.31	0.347	0.100	
42		66.44	0.358	.111/.0725	overdriven
43		67.56	0.338	0.108	
44		68.75	0.376	0.089	overdriven
45		70.06	0.361	0.100	
46		71.13	0.375	0.088	overdriven
47		72.19	0.364	0.102	
48		73.38	0.372	0.093	overdriven
49		74.50	0.365	0.084	overdriven
50		75.56	0.312	0.109	underdriven

51		76.63	0.342	0.100	
52		77.69	0.330	0.102	
53		78.75	0.333	0.096	overdriven
54		79.88	0.350	0.100	
55		80.31	0.322	0.106	underdriven
56	2140	82.50	missing	missing	hole cut during disassembly
57		83.50	0.355	0.102	
58		84.63	0.407	0.096	overdriven
59		85.75	0.365	0.104	
60		86.75	0.378	0.100	
61		87.81	0.394	0.080	overdriven
62		88.94	0.386	0.086	overdriven
63		89.94	0.358	0.089	overdriven
64		90.88	0.361	0.087	overdriven
65		91.88	0.370	0.076	overdriven
66		92.94	0.394	0.082	overdriven
67		94.06	0.365	0.083	overdriven
68		95.50	0.350	0.088	overdriven
69		96.63	0.363	0.085	overdriven
70		97.88	0.386	0.079	overdriven
71		99.00	0.361	0.088	overdriven
72		100.13	0.388	0.075	overdriven
73		101.38	0.381	0.076	overdriven
74	2160	102.94	0.259	0.165	3/16 rivet
75		104.19	0.318	0.104	underdriven
76		105.25	0.379	0.072	overdriven
77		106.38	0.347	0.091	overdriven
78		107.38	0.346	0.103	
79		108.50	0.336	0.111	
80		109.56	0.352	0.110	
81		110.63	0.344	0.100	
82		111.75	0.372	0.075	overdriven
83		112.75	0.353	0.100	
84		114.00	0.353	0.100	
85		115.13	0.352	0.100	

86		116.25	0.365	0.086	overdriven
87		117.38	0.361	0.090	overdriven
88		118.50	0.377	0.100	
89		119.75	0.374	0.080	overdriven
90		120.81	0.381	0.075	overdriven
91		121.88	0.400	0.080	overdriven
92		123.31	missing	missing	
93		124.19	missing	missing	
AFT edge of doubler		124.81	n/a	n/a	

Table 1.16-5 Repair doubler driven rivet dimensions for first and second rows above S-51R.

First Row Above S-51R					Second Row Above S-51R				
Rivet No.	Body Station Reference	Driven Rivet Button Diameter (inch)	Driven Rivet Button Thickness or Height (inch)	Notes	Rivet No.	Body Station Reference	Driven Rivet Button Diameter (inch)	Driven Rivet Button Thickness or Height (inch)	Notes
1		0.30	N/A		+16		missing	missing	
2		0.33	0.12		+15		0.303	0.152	underdriven
3		0.32	0.08	Overdriven	+14		0.327	0.121	
4		0.35	0.08	Overdriven	+13		0.335	0.106	
5		0.43	0.10		+12		0.352	0.103	
6		0.33	0.09	Overdriven	+11		0.328	0.127	
7		0.33	0.08	Overdriven	+10		0.341	0.115	
8		0.31	0.09	Overdriven	+9		0.341	0.108	
9		0.32	0.08	Overdriven	+8		0.341	0.109	
10		0.31	0.10		+7		0.349	0.091	overdriven
11		0.32	0.09	Overdriven	+6		0.329	0.109	
12		0.35	0.09	Overdriven	+5		0.335	0.118	
13		0.35	0.09	Overdriven	+4		0.320	0.131	underdriven
14		0.34	0.15		+3		0.352	0.117	
15		0.35	0.08	Overdriven	+2		0.316	0.130	underdriven
16	~2081	0.35	0.09	Overdriven	+1		0.333	0.134	
17		0.35	0.08	Overdriven	+0		0.362	0.107	
18		0.36	0.08	Overdriven	1	2080	0.299	0.153	3/16 rivet
19		0.34	0.08	Overdriven	2		0.331	0.114	
20		0.36	0.08	Overdriven	3		0.344	0.120	
21		0.33	0.11		4		0.344	0.114	
22		0.35	0.08	Overdriven	5		0.362	0.104	
23		0.34	0.16		6		0.355	0.106	
24		0.33	0.07	Overdriven	7		0.356	0.103	
25		0.34	0.08	Overdriven	8		0.383	0.095	overdriven

26		0.34	0.07	Overdriven	9		0.384	0.070	overdriven
27		0.35	0.08	Overdriven	10		0.349	0.106	
28		0.34	0.08	Overdriven	11		0.349	0.107	
29		0.35	0.09	Overdriven	12		0.375	0.090	overdriven
30	2100	0.32	0.10		13		0.354	0.100	
31		0.37	0.08	Overdriven	14		0.368	0.100	
32		0.34	0.09	Overdriven	15		0.360	0.089	overdriven
34		0.34	0.10		17		0.377	0.086	overdriven
35		0.35	0.09	overdriven	18		0.376	0.087	overdriven
36		0.34	0.08	overdriven	19		0.392	0.084	overdriven
37		0.34	0.10		20		0.362	0.103	
38		0.32	0.10		21	2100	0.266	0.152	3/16 rivet
39		0.32	0.10		22		0.391	0.091	overdriven
40		0.35	0.14		23		0.372	0.085	overdriven
41		0.34	0.07	overdriven	24		0.352	0.101	
42		0.35	0.07	overdriven	25		0.385	0.093	overdriven
43		0.320	0.080	overdriven	26		0.363	0.098	overdriven
44		0.350	0.080	overdriven	27		0.386	0.079	overdriven
45	~2121	0.30	0.100	underdriven	28		0.372	0.086	overdriven
46		0.35	0.07	overdriven	29		0.367	0.080	overdriven
47		0.35	0.090	overdriven	30		0.393	0.081	overdriven
48		0.33	0.090	overdriven	31		0.385	0.082	overdriven
49		0.36	0.09	overdriven	32		0.371	0.090	overdriven
50		0.35	0.07	overdriven	33		0.385	0.079	overdriven
51		0.33	0.08	overdriven	34		0.389	0.075	overdriven
52		0.32	0.08	overdriven	35		0.387	0.079	overdriven
53		0.32	0.09	overdriven	36		0.387	0.073	overdriven
54		0.33	0.08	overdriven	37		0.409	0.073	overdriven
55		0.32	0.08	overdriven	38		0.410	0.075	overdriven
56		0.32	0.08	overdriven	39		0..396	0.081	overdriven
57		0.36	0.08	overdriven	40	2120	0.267	0.126	3/16 rivet
58		0.34	0.07	overdriven	41		0.343	0.119	
59	2140	0.33	0.09	overdriven	42		0.372	0.092	overdriven
60		0.34	0.08	overdriven	43		0.409	0.096	overdriven
61		0.32	0.09	overdriven	44		0.391	0.079	overdriven
62		0.31	0.10		45		0.370	0.087	overdriven
63		0.34	0.08	overdriven	46		0.383	0.092	overdriven

64		0.36	0.07	overdriven	47		0.362	0.087	overdriven
65		0.32	0.09	overdriven	48		0.362	0.087	overdriven
66		0.35	0.10		49		0.340	0.103	
67		0.35	0.08	overdriven	50		0.361	0.077	overdriven
68		0.34	0.07	overdriven	51		0.339	0.105	
70		0.36	0.07	Overdriven	53		0.336	0.100	
71		0.35	0.08	Overdriven	54		0.352	0.092	overdriven
72		0.36	0.10		55		0.354	0.087	overdriven
73		0.35	0.10		56		0.342	0.093	overdriven
74	2160	0.36	0.09	Overdriven	57		0.335	0.105	
75		0.36	0.07	Overdriven	58		0.396	0.086	overdriven
76		0.360	0.08	Overdriven	59		0.365	0.080	overdriven
77		0.37	0.08	Overdriven	60	2140	missing?	Missing?	3/16 hole
78		0.32	0.10		61		0.348	0.112	
79		0.35	0.07	Overdriven	62		0.371	0.087	overdriven
80		0.35	0.09	Overdriven	63		0.367	0.100	
81		0.37	0.10		64		0.333	0.093	overdriven
82		0.37	0.10		65		0.360	0.087	overdriven
83		0.35	0.11		66		0.377	0.077	overdriven
84		0.36	0.07	Overdriven	67		0.448	0.062	overdriven
85		0.37	0.07	Overdriven	68		0.386	0.093	overdriven
86		0.38	0.10		69		0.354	0.097	overdriven
					70		0.384	0.084	overdriven
					71		0.377	0.087	overdriven
					72		0.386	0.090	overdriven
					73		0.390	0.078	overdriven
					74		0.393	0.075	overdriven
					75		0.391	0.055	overdriven
					76		0.408	0.072	overdriven
					77		0.414	0.083	overdriven
					78		0.399	0.078	overdriven
					79	2160	0.314	N/A	3/16 hole
					80		0.299	0.153	underdriven
					81		0.409	0.083	overdriven
					82		0.406	0.083	overdriven
					83		0.403	0.079	overdriven

84		0.403	0.069	overdriven
85		0.395	0.083	overdriven
86		0.383	0.086	overdriven
87		0.383	0.071	overdriven
89		0.403	0.075	overdriven
90		0.393	0.081	overdriven
91		0.395	0.075	overdriven
92		0.345	0.100	
93		0.360	0.086	overdriven
94		0.360	0.083	overdriven
95		0.392	N/A	
96		0.393	N/A	
97		missing	missing	

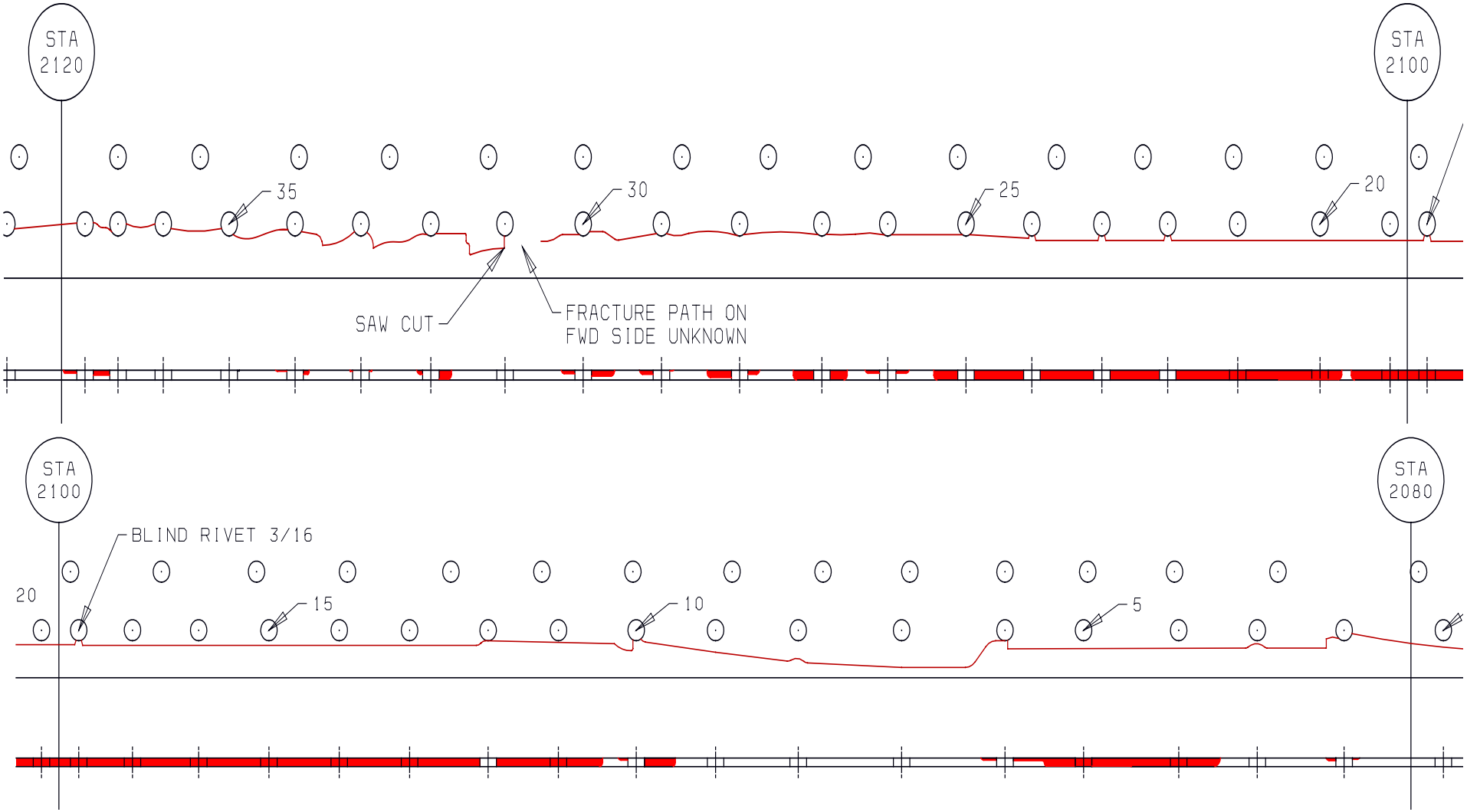

Figure 1.16-39 A detailed map of all fatigue cracks confirmed during examination at Boeing- STA 2060~2120

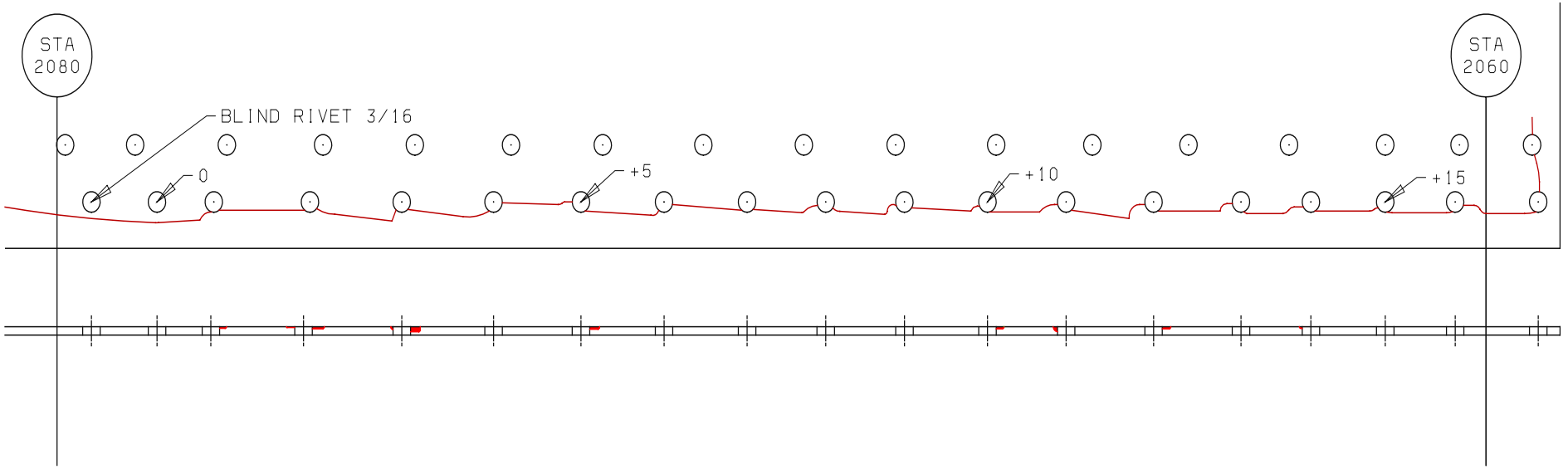

Figure 1.16-39 (Cont) A detailed map of all fatigue cracks confirmed during examination at Boeing- STA 2060~2120

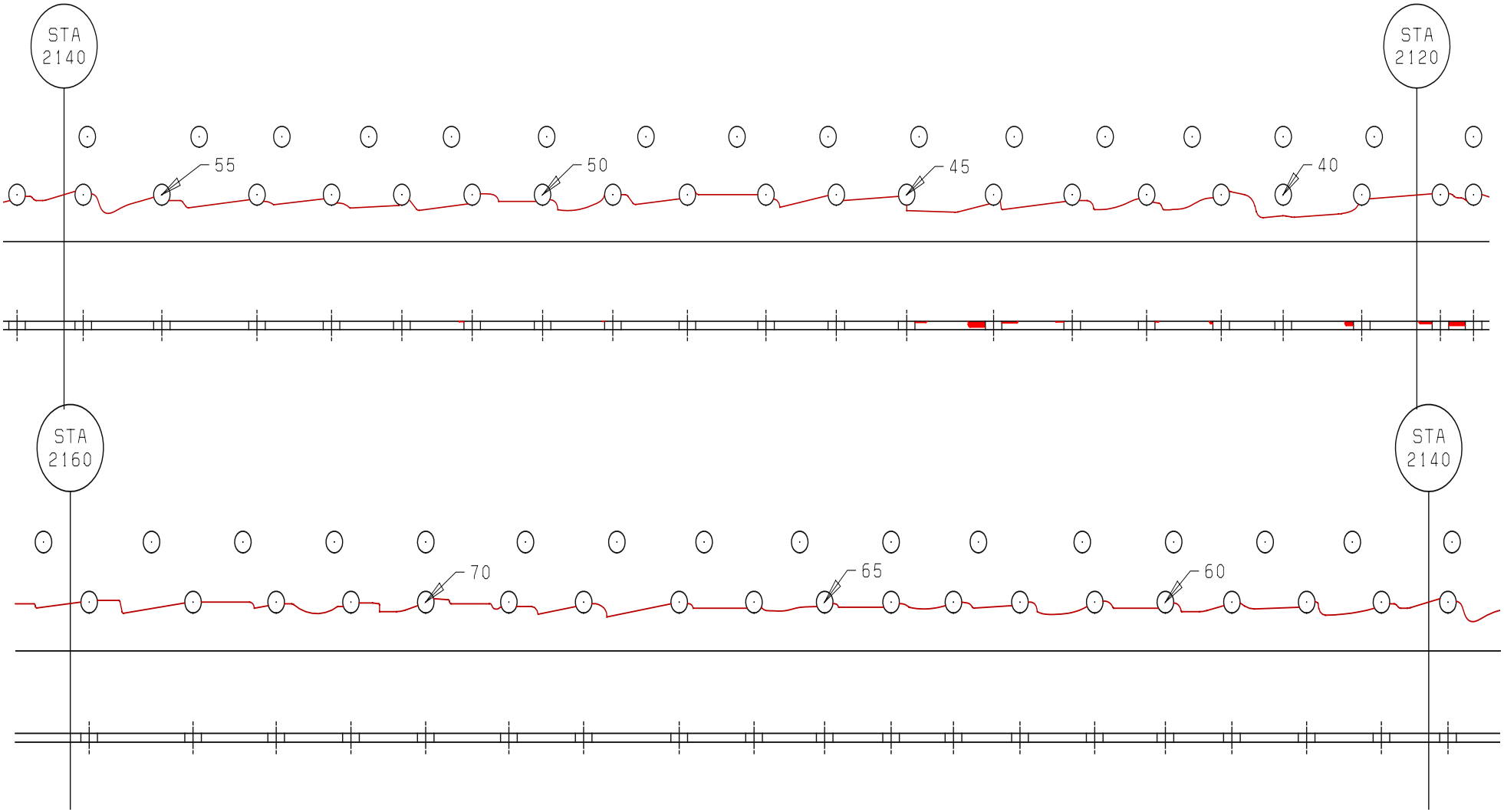

Figure 1.16-40 A detailed map of all fatigue cracks confirmed during examination at Boeing- STA 2120~2180

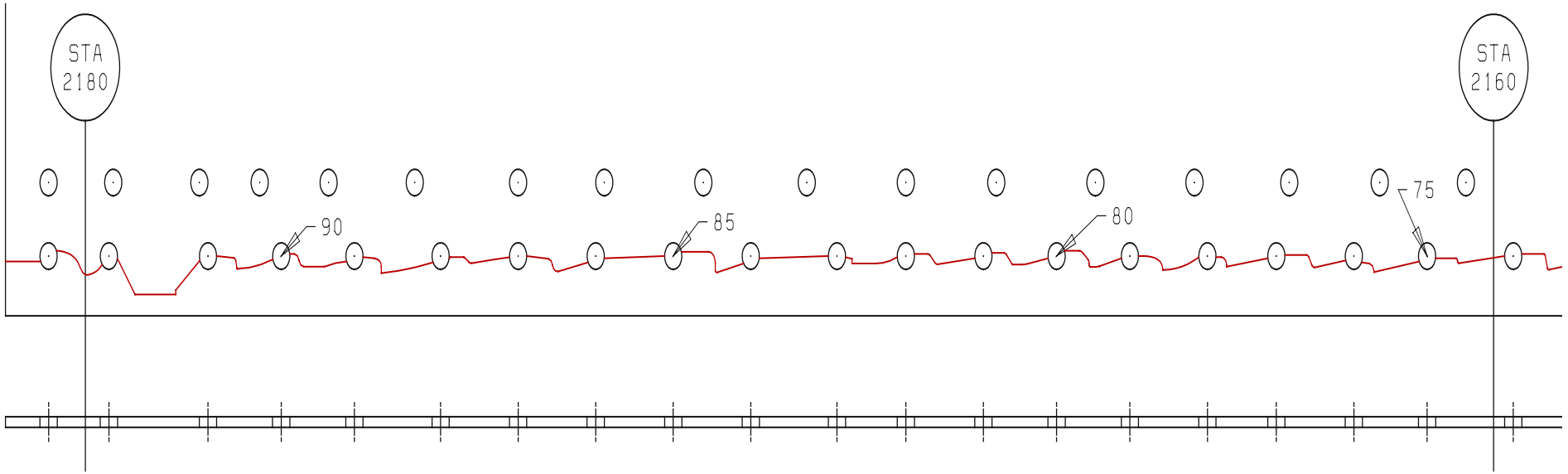

Figure 1.16-40 (Cont) A detailed map of all fatigue cracks confirmed during examination at Boeing- STA 2120~2180

Table 1.16-6 Length, depth and origin location of fatigue cracks on fracture above S-49L.

Location	Length of Fatigue Crack (inch)	Depth of Fatigue Crack (%)	Origin of Fatigue Crack
Aft of hole +14	0.04	20	Faying surface – no scratch
Fwd of hole +12	0.12	25	Faying surface – no scratch
Aft of hole +11	0.06	60	Corner of hole at faying surface
Fwd of hole +10	0.11	25	Scratch on faying surface
Fwd of hole +5	0.14	30	Faying surface – no scratch
Fwd of hole +3	0.14	60	Scratch on faying surface
Aft of hole +3	0.03	30	Scratch on faying surface
Fwd of hole +2	0.17	25	Scratch on faying surface
Aft of hole +2	0.12	10	Scratch on faying surface
Fwd of hole 2	0.11	15	Scratch on faying surface
Aft of hole 2	0.15	30	Scratch on faying surface
Fwd of hole 4 to aft of hole 6	3.50	25-100	Scratch on faying surface
Fwd of hole 10	0.47	100	Scratch on faying surface
Aft of hole 10	0.15	25	Scratch on faying surface
Fwd of hole 11 to aft of hole 25	15.14	*95-100	Scratch on faying surface
Fwd of hole 26	0.20	30	Scratch on faying surface
Aft of hole 26	0.22	30	Scratch on faying surface
Fwd of hole 27	0.26	100	Scratch on faying surface
Aft of hole 27	0.39	100	Scratch on faying surface
Fwd of hole 28	0.18	40	Scratch on faying surface
Aft of hole 28	0.37	75	Scratch on faying surface
Fwd of hole 29	0.03	5	Scratch on faying surface
Aft of hole 29	0.21	40	Scratch on faying surface
Fwd of hole 30	0.26	60	Scratch on faying surface
Aft of hole 30	0.21	35	Scratch on faying surface
Fwd of hole 32	0.22	90	Scratch on faying surface
Aft of hole 32	0.09	40	Scratch on faying surface
Fwd of hole 33	0.04	10	Faying surface – no scratch
Aft of hole 33	0.04	10	Faying surface – no scratch
Fwd of hole 34	0.09	40	Scratch on faying surface
Aft of hole 34	0.17	10	Scratch on faying surface
Fwd of hole 35	0.02	5	Scratch on faying surface
Aft of hole 37 to fwd of hole 38	0.50	50-60	Faying surface – no scratch
Aft of hole 38	0.09	30	Countersink bore
Aft of hole 39	0.14	50	Faying surface – no scratch
Fwd of hole 41	0.05	30	Faying surface – no scratch
Fwd of hole 42	0.06	10	Faying surface – no scratch
Aft of hole 43	0.13	10	Faying surface – no scratch
Fwd of hole 44	0.23	20	Scratch on faying surface
Aft of hole 44	0.26	70	Scratch on faying surface
Fwd of hole 45	0.49	15	Scratch on faying surface
Aft of hole 49	0.02	2	Faying surface – no scratch
Aft of hole 51	0.07	5	Faying surface – no scratch

* The crack depth at a local area forward of hole 20 was 5%.

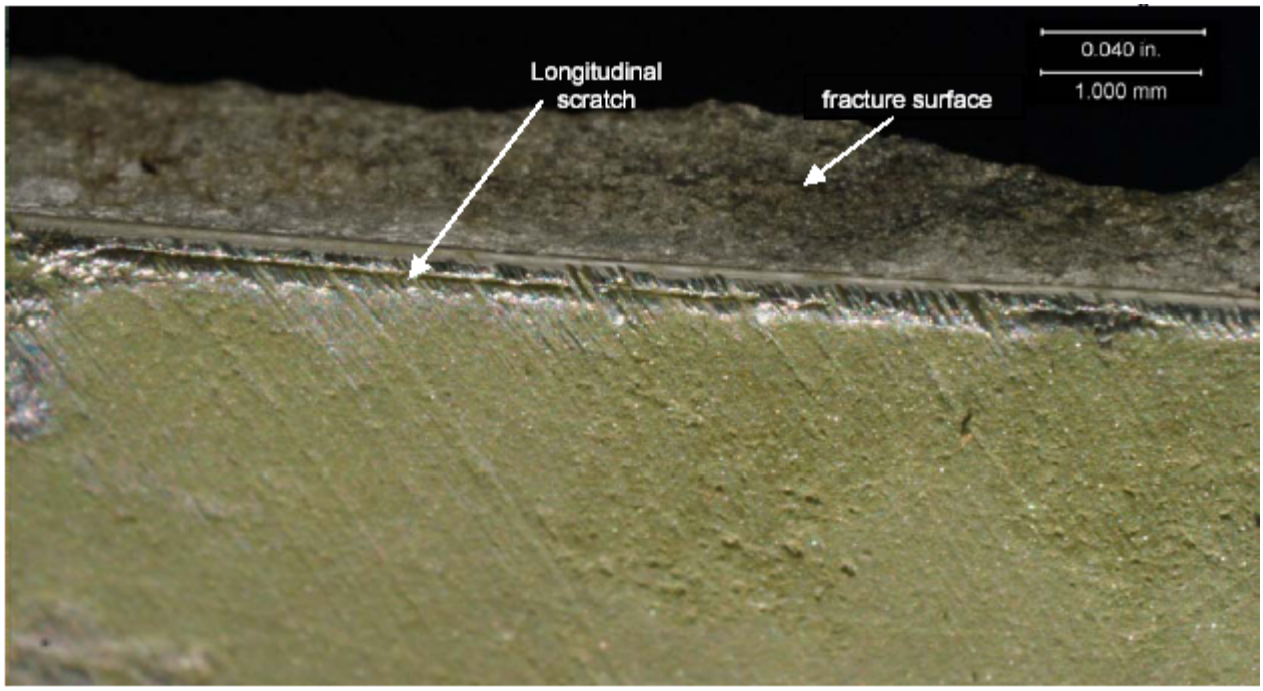

Figure 1.16-41 Surface of skin faying with repair doubler near hole 20 showing the longitudinal scratch where fatigue crack initiation occurred from multiple origins. Also note the sanding marks induced during rework of the skin.

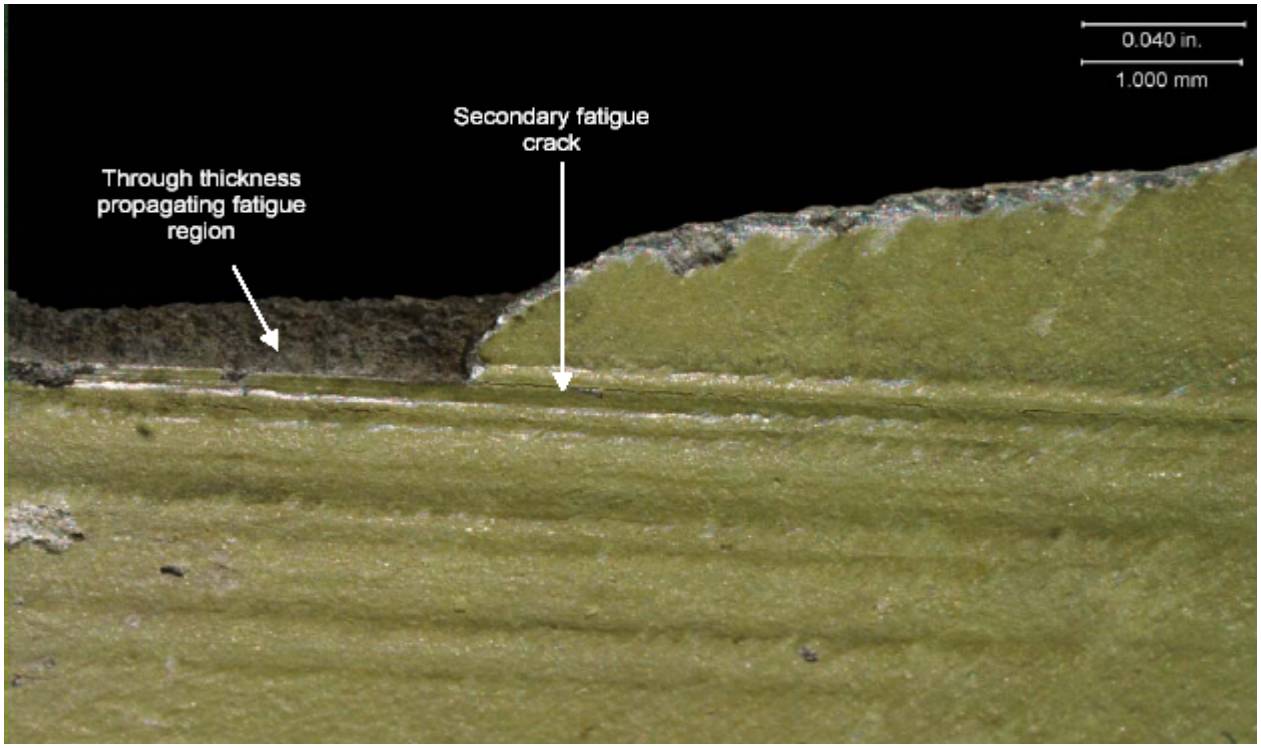

Figure 1.16-42 Surface of skin faying with repair doubler between hole 29 and hole 30 showing the longitudinal scratches in relationship to this fatigue crack. Note the secondary crack extending out of this common scratch.

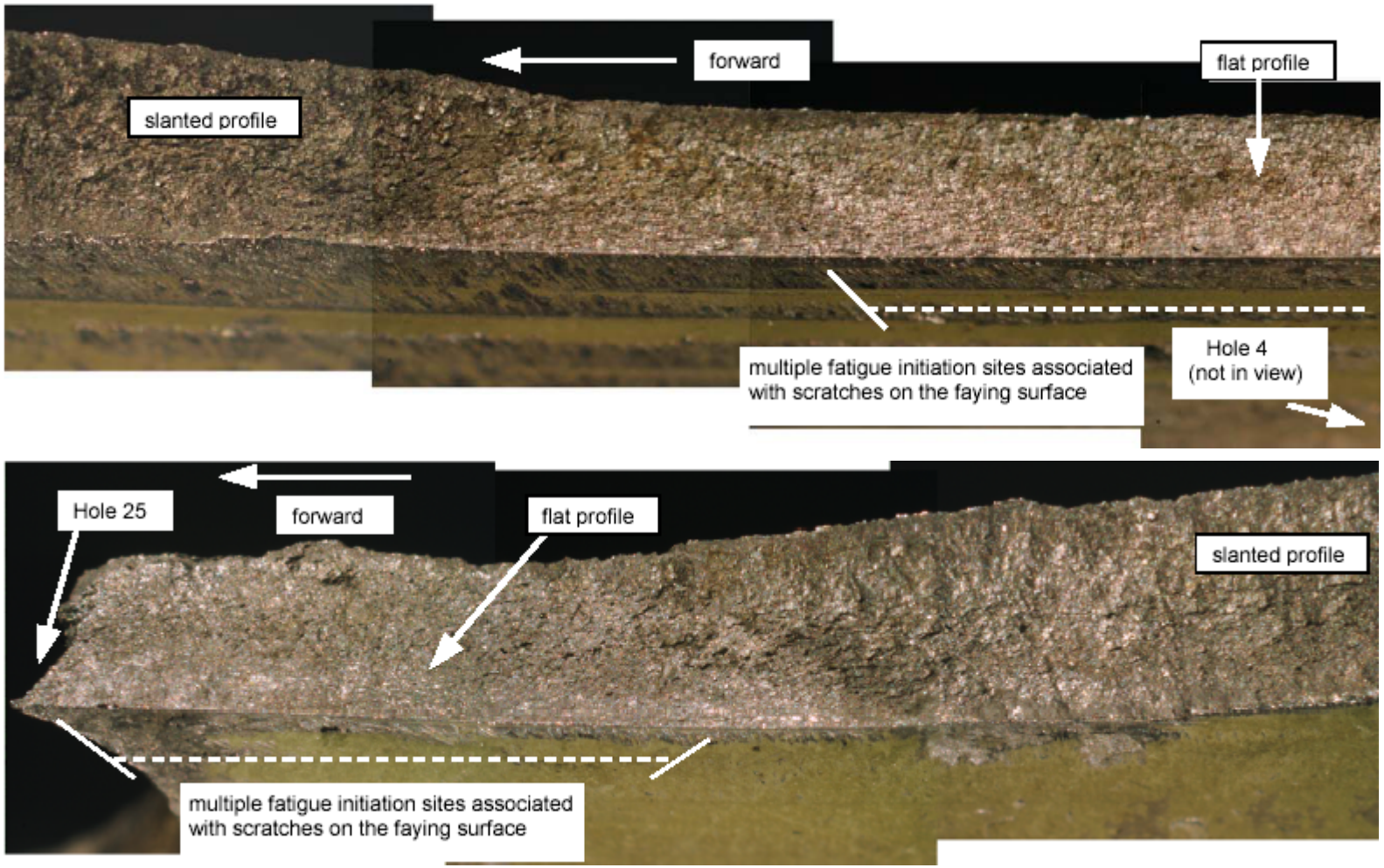

Figure 1.16-43 Photographs showing the transition regions from flat fracture profiles to slanted profiles just forward of fastener Hole 4 (top) and Hole 25 (bottom).

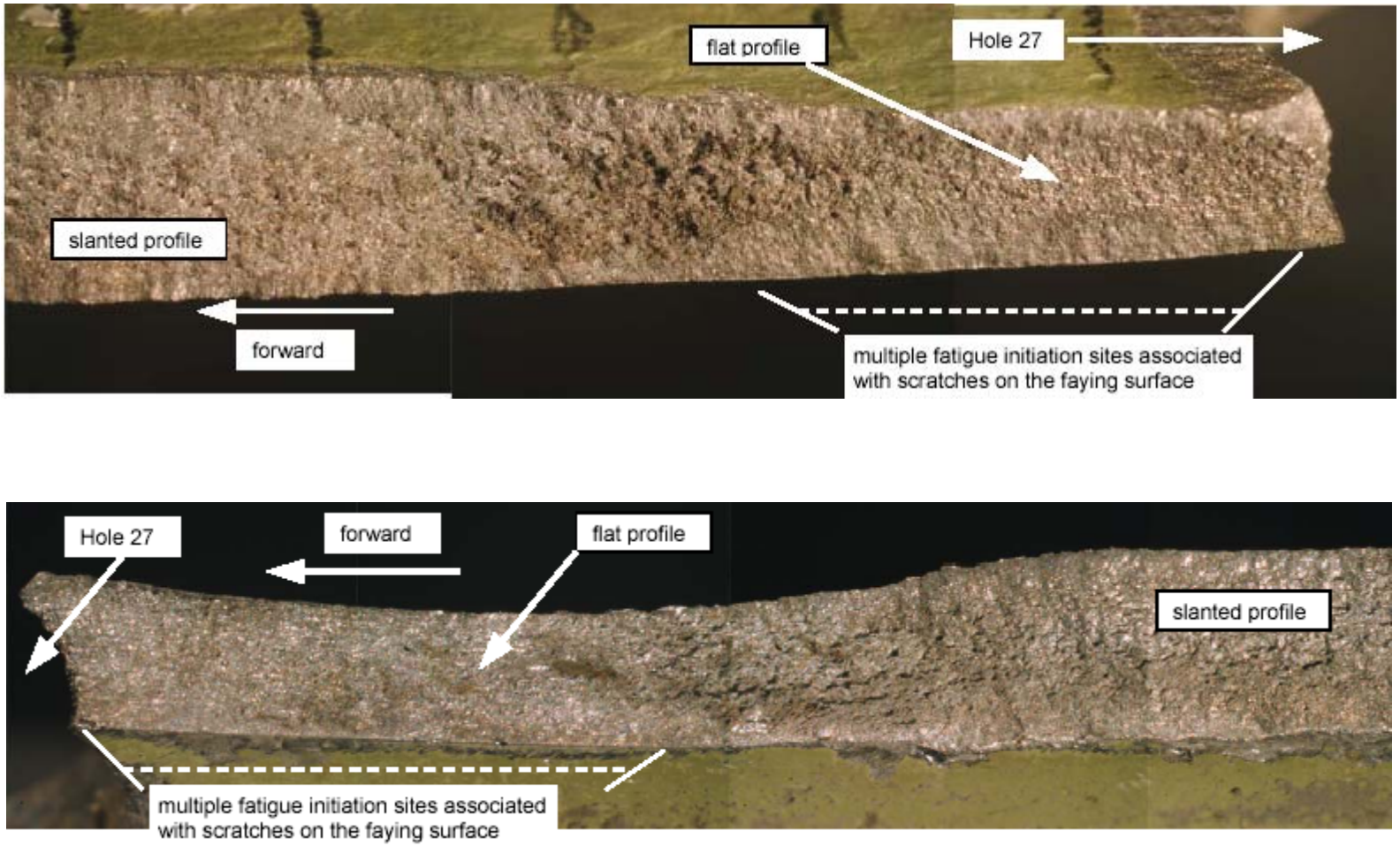

Figure 1.16-44 Photographs showing the transition regions from flat fracture profiles to slanted profiles at fastener Hole 27 in the forward direction (top) and the aft direction (bottom).

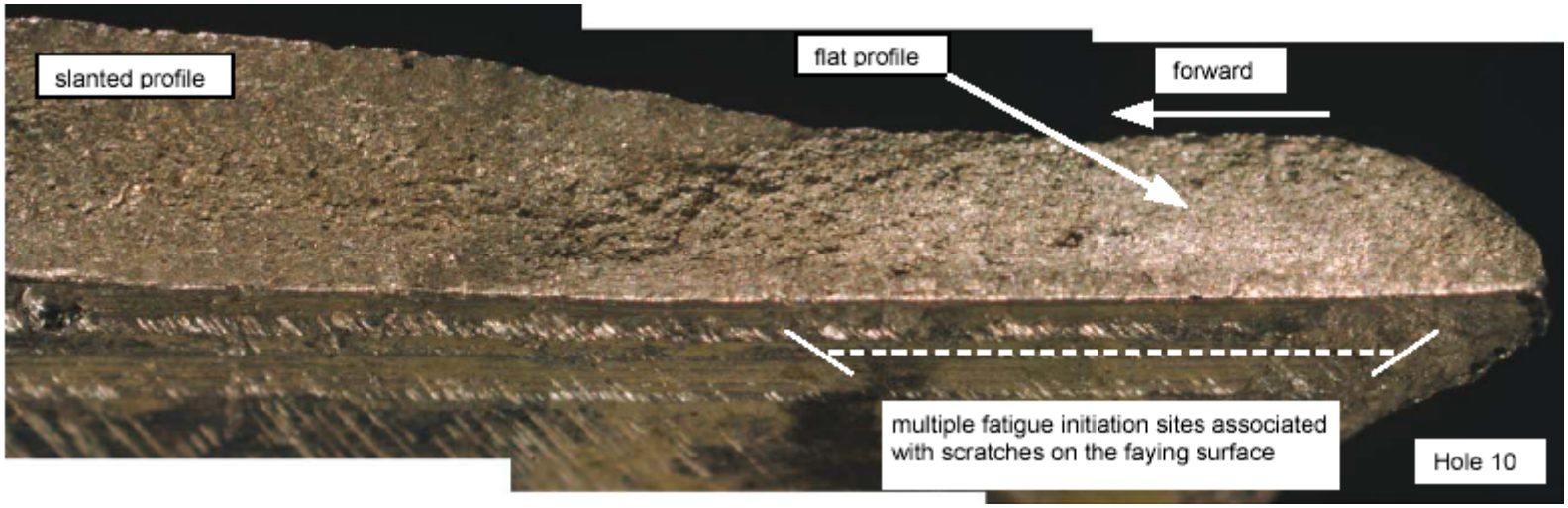

Figure 1.16-45 Photograph showing the transition region from a flat fracture profile to a slanted profile at fastener Hole 10 in the forward direction.

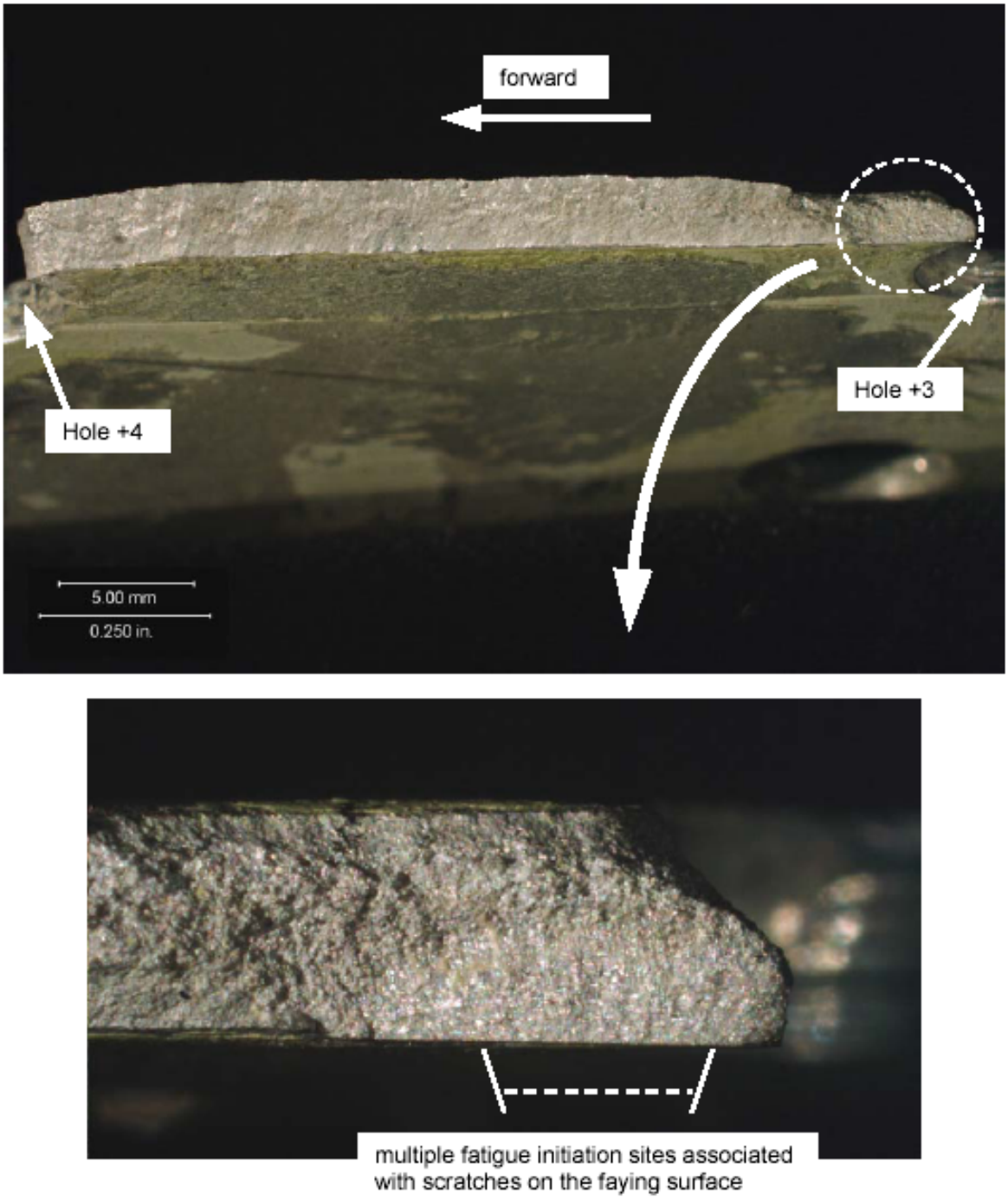

Figure 1.16-46 Photographs of the fracture segment extending from Hole +3 to +4 (top), and closer view of the flat profile fatigue region on the forward side of Hole +3 (bottom).

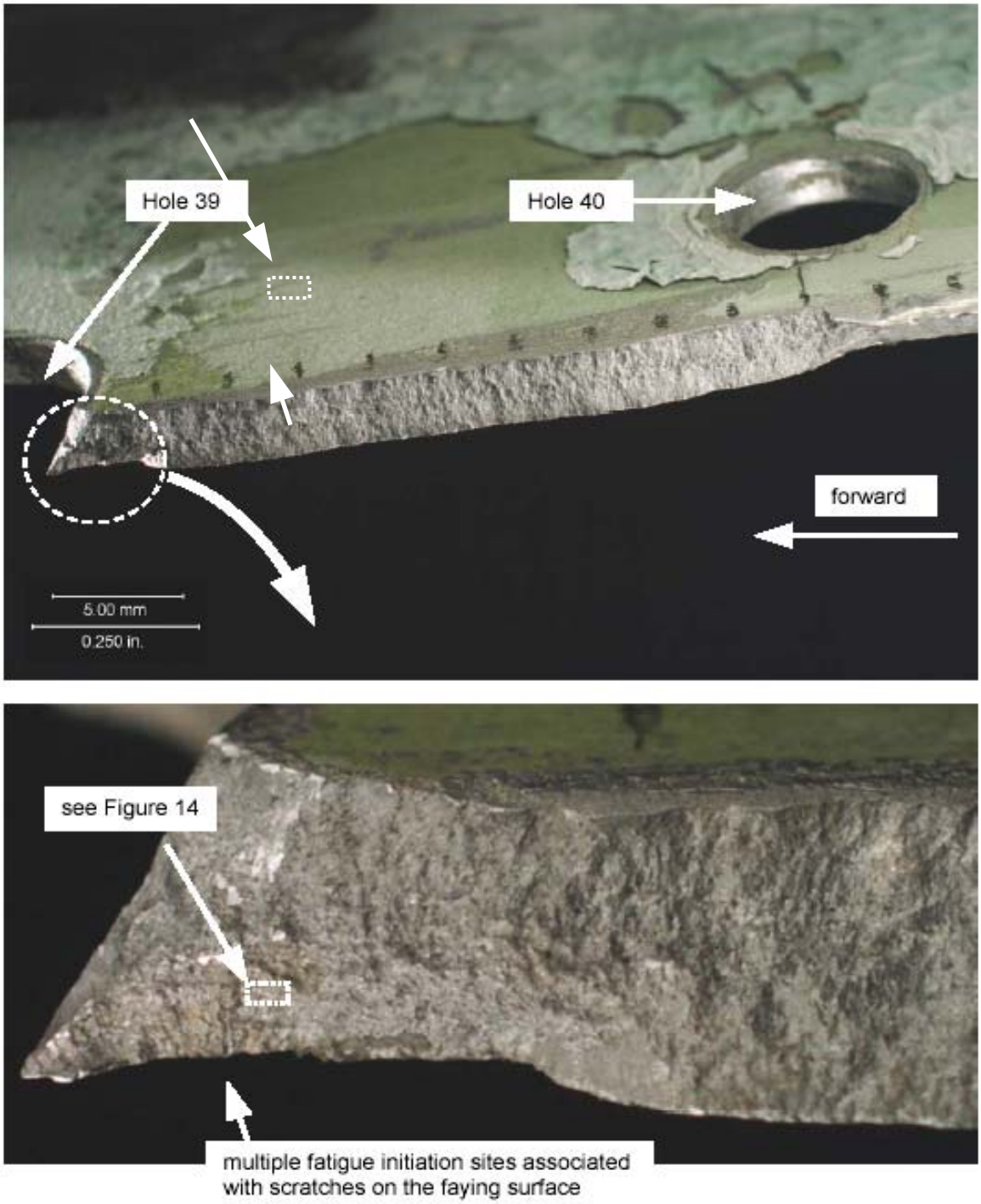

Figure 1.16-47 Photographs of the fracture segment extending from Hole 39 to 40 (top), and closer view of the flat profile fatigue region and short transition zone on the aft side of Hole 39 (bottom). SEM photographs showing an increase in striation spacing near the extent of the flat fracture thumbnail (indicated area) are shown below in Figure 1.16-48.

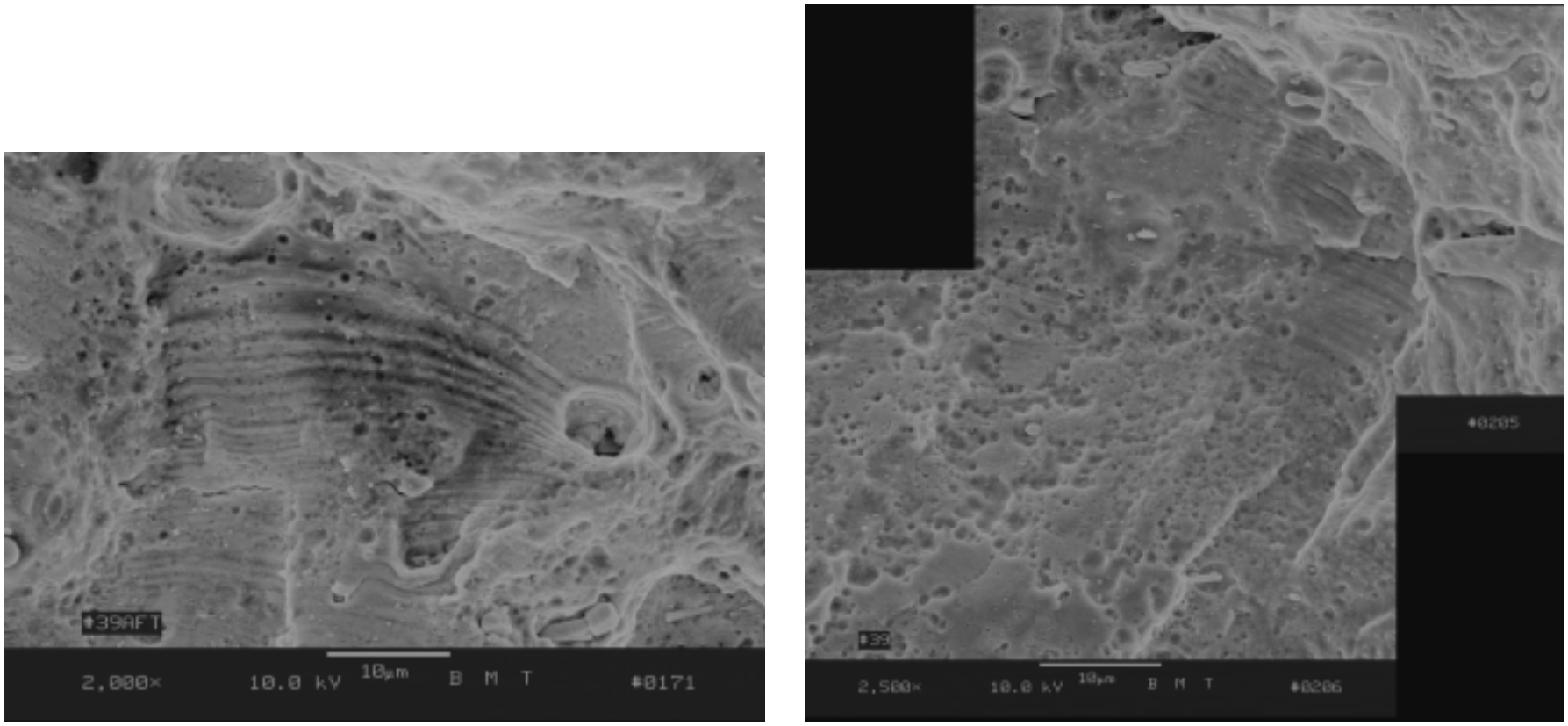

Figure 1.16-48 Scanning electron microscope photographs showing fatigue striations near the end of the flat profile fracture surface aft of Hole 39. Just beyond these regions, the fracture surface was dominated by a dimpled morphology, indicative of the fracture mechanism of micro-void coalescence, or ductile separation. Severe pitting due to corrosion can also be seen.

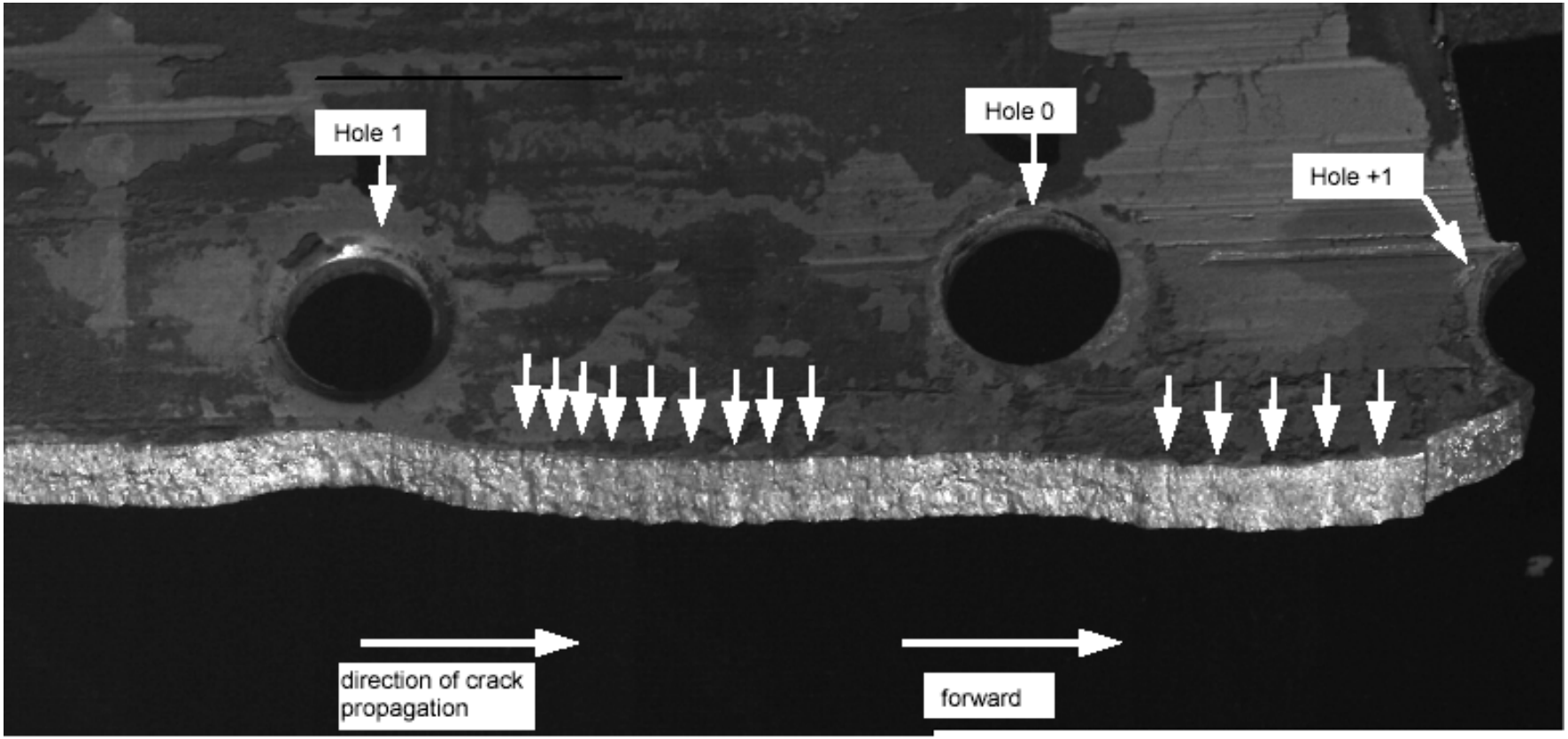

Figure 1.16-49 Photograph showing the incremental crack growth indications on the fracture segment from Hole 1 to Hole +1 with two groups of them identified with arrows. This area is just a few inches forward of the flat profile fatigue and transition areas of Hole 4 shown in Figure 1.16-21. Note that the regular spacing generally increases as the distance increases from the main cracking system at Holes 4 through 26

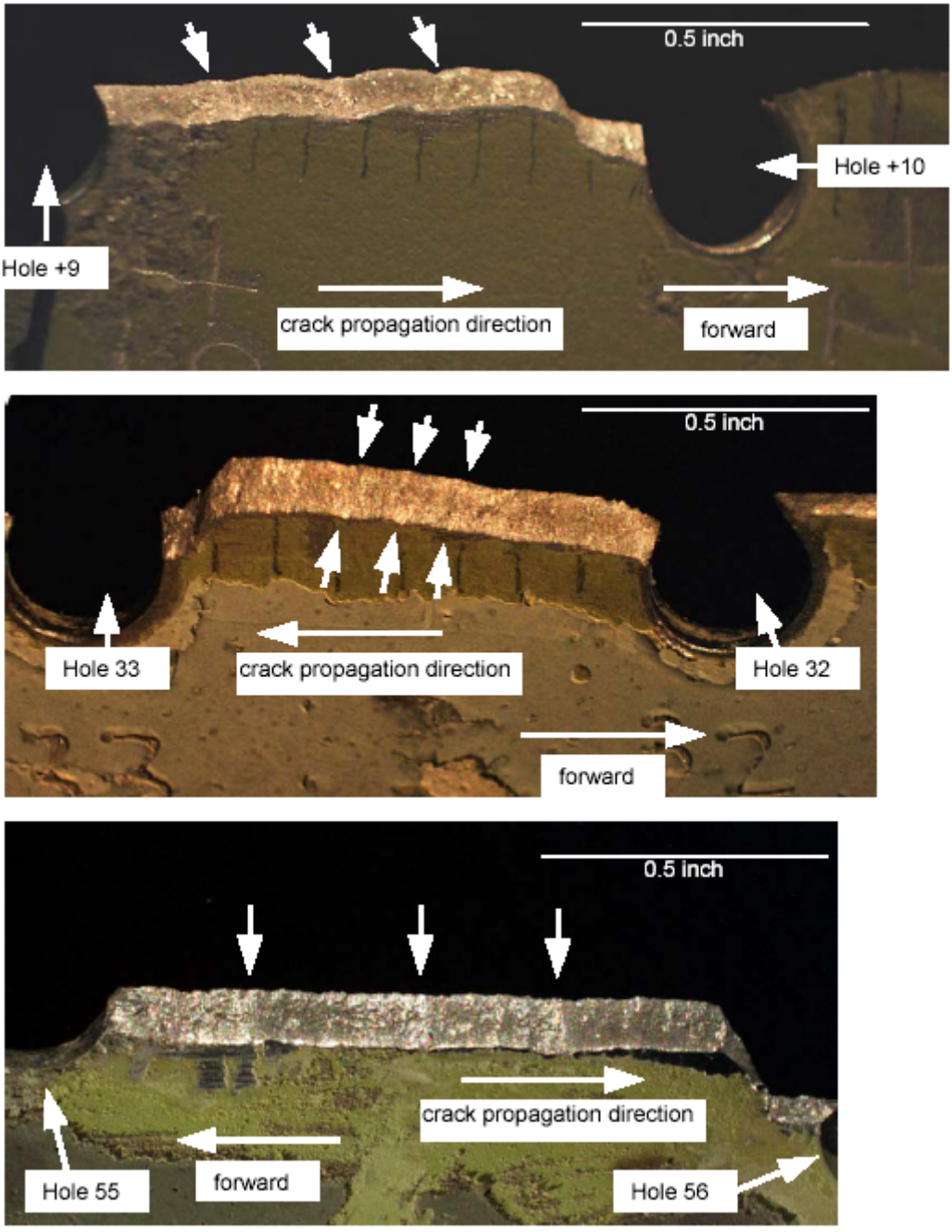

Figure 1.16-50 Photographs showing the incremental crack growth indications on the fracture segments between Holes +9 and +10 (top), Holes 32 and 33 (center), and Holes 55 and 56 (bottom).

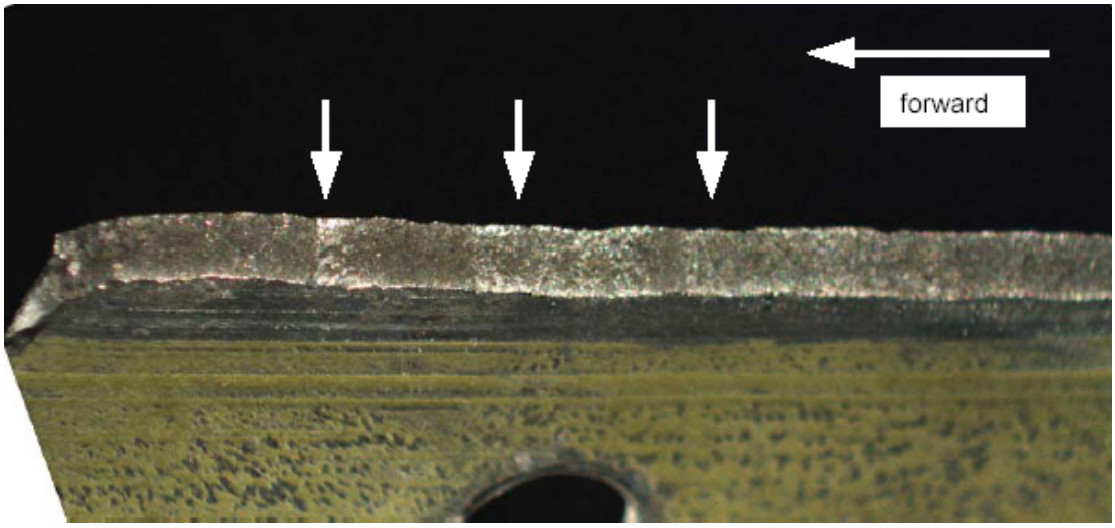

Figure 1.16-51 Photograph showing the incremental crack growth indications (arrows) on the fracture segment near Hole 7, which is between the two main fatigue cracking systems at Holes 4 and 5 and Holes 10 through 25.

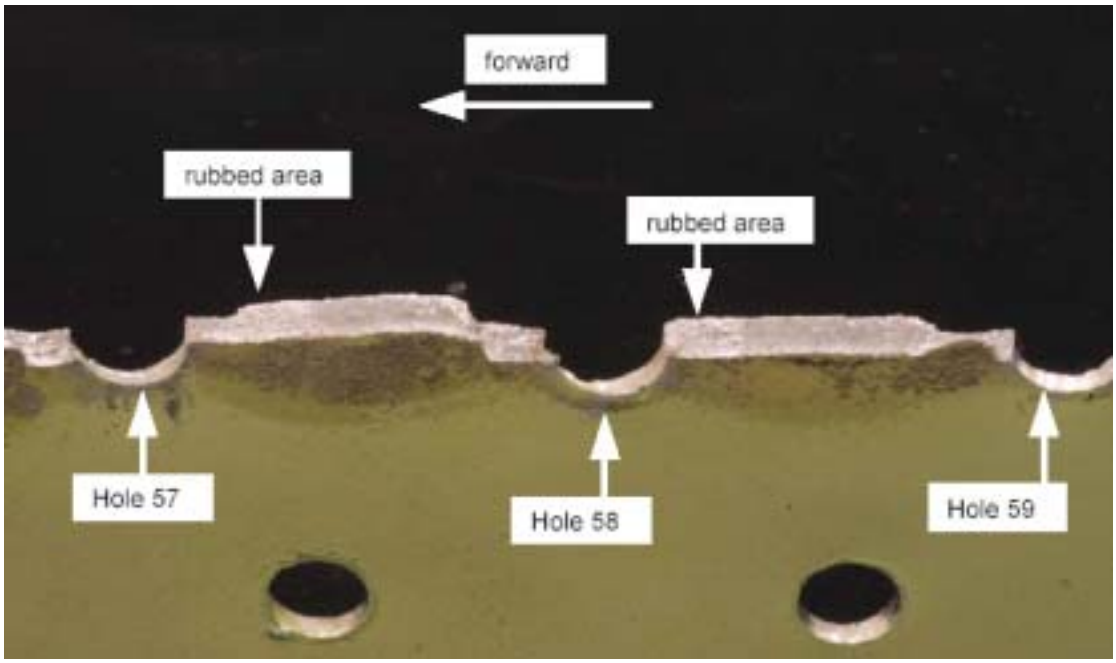

Figure 1.16-52 Photograph of the fracture surface at Holes 57, 58, and 59. The shiny areas are indicative of rubbing with the mating fracture surface and appeared consistently forward of this area, but were not present aftward beyond Hole 62.

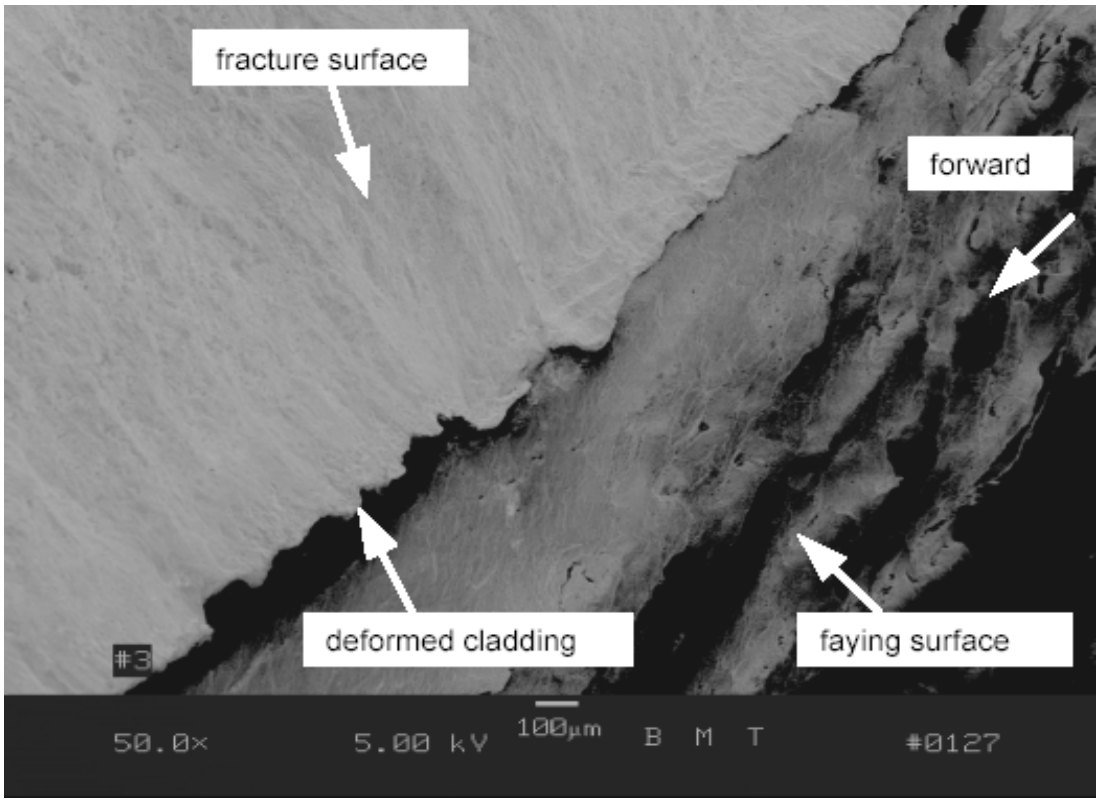

Figure 1.16-53 Scanning electron microscope photograph along the edge of the fracture common to the faying surface where the aluminum cladding remained near Hole 3. The fracture surface profile was slanted here.

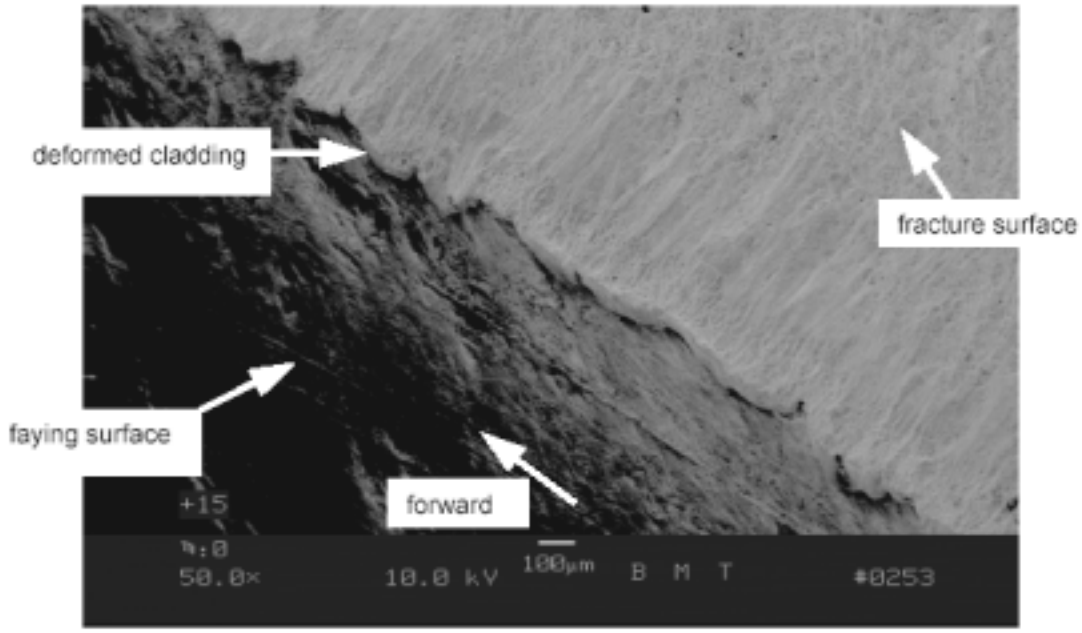

Figure 1.16-54 SEM photograph showing the compressive deformation of the cladding just forward of Hole +15.

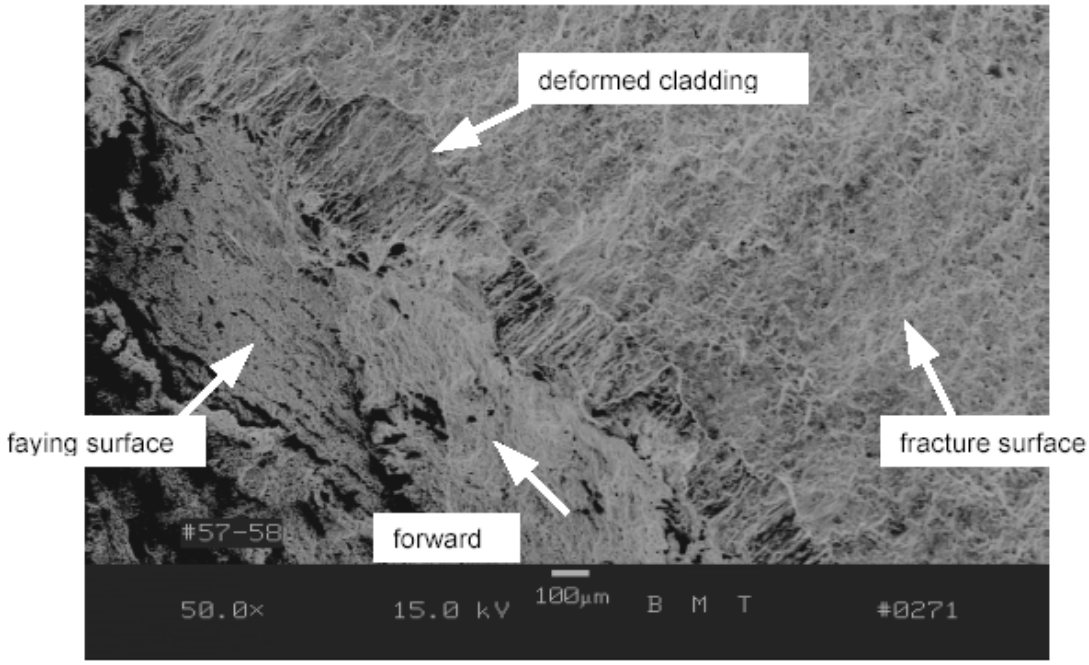

Figure 1.16-55 SEM photograph showing the compressive deformation of the cladding between Holes 57 and 58. Note that the degree of compressive damage is less severe than that observed closer to the main cracking system, Figure 1.16-53 for example.

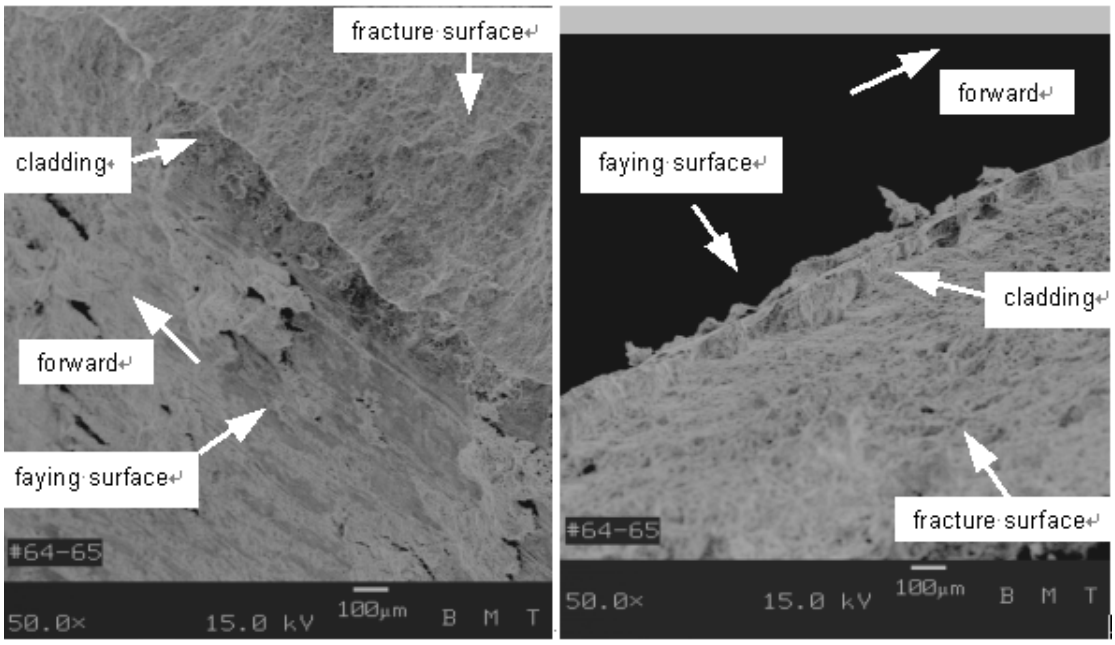

Figure 1.16-56 Opposing angle SEM photographs of the fracture segment between Holes 64 and 65 showing the cladding on the faying surface retaining its upward profile from the necking process during ultimate tensile separation without subsequent crack closure.

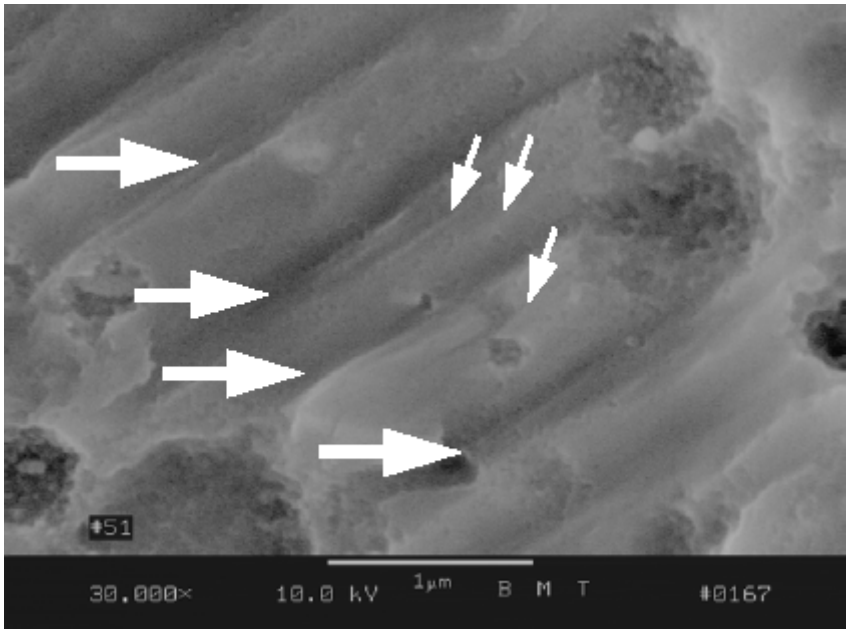

Figure 1.16-57 SEM photograph showing minor striation-like features (indicated withsmaller arrows).

Table 1.16-7 Striation Count Results

Location Title	Location of Traverse	Total Cycles (Point)	Total Cycles (Ext.)
Hole # +3	.15 inch fwd of hole centerline	8,000	11,000
Hole # 5	Centerline of hole	6,700	9,400
Hole # 12	.10 inch aft of hole centerline	1,600	2,800
Hole # 13	Centerline of hole	5,400	6,300
Hole # 13	.55 inch aft of hole centerline	2,000	2,400
Hole # 15	.10 inch aft of hole centerline	3,100	5,800
Hole # 16-17	.50 inch aft of hole centerline	2,600	3,300
Hole # 17-18	.45 inch aft of hole centerline	1,300	2,400
Hole # 19	.10 inch fwd of hole centerline	6,400	9,000
Hole # 21	Centerline of hole	8,300	10,200
Hole # 23	.15 inch aft of hole centerline	9,100	10,900
Hole # 25	.20 inch aft of hole centerline	1,700	4,000
Hole # 27 Fwd	.15 inch aft of hole centerline	5,500	7,700

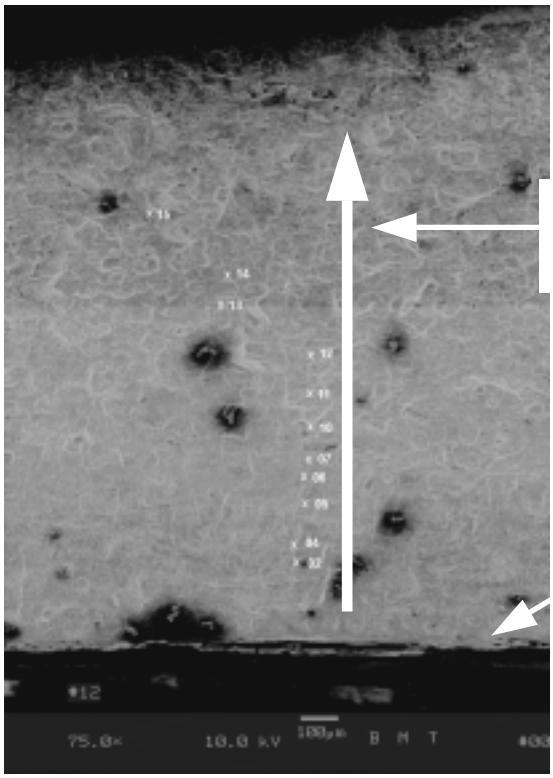

Figure 1.16-58 SEM photograph showing the locations through the skin thickness that were sampled for crack growth rate at Hole 12. The approach was repeated for other through-thickness areas

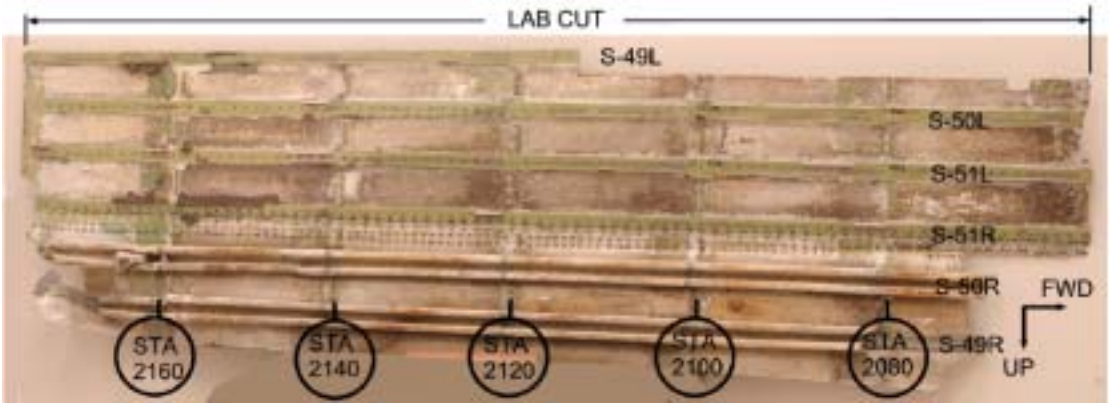

Figure 1.16-59 As received item 640 CI skin inboard surface- the S-49L fracture segment was removed at the CSIST during the initial examination.

Figure 1.16-60 As received item 640 CI skin outboard surface – the approximate location of the repair doubler is shown with dotted lines. Protective finishes were removed from the repair faying surface at the CSIST.

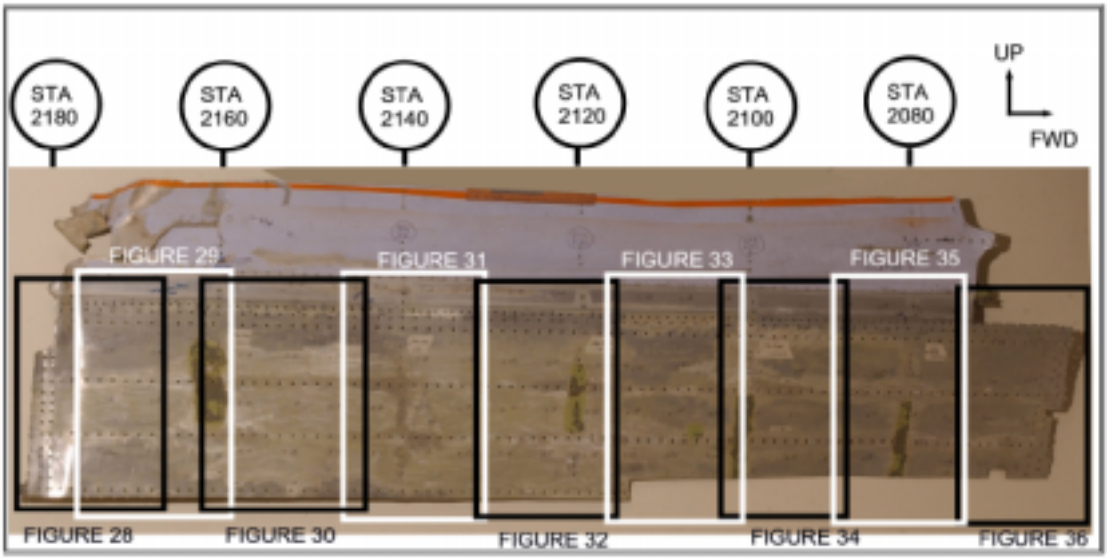

Figure 1.16-61 Scratch photograph legend– This illustration identifies the location of following photographs that document scratch features observed on the skin repair faying surface. Scratches are fore/aft in orientation and characteristic of a tail strike event.

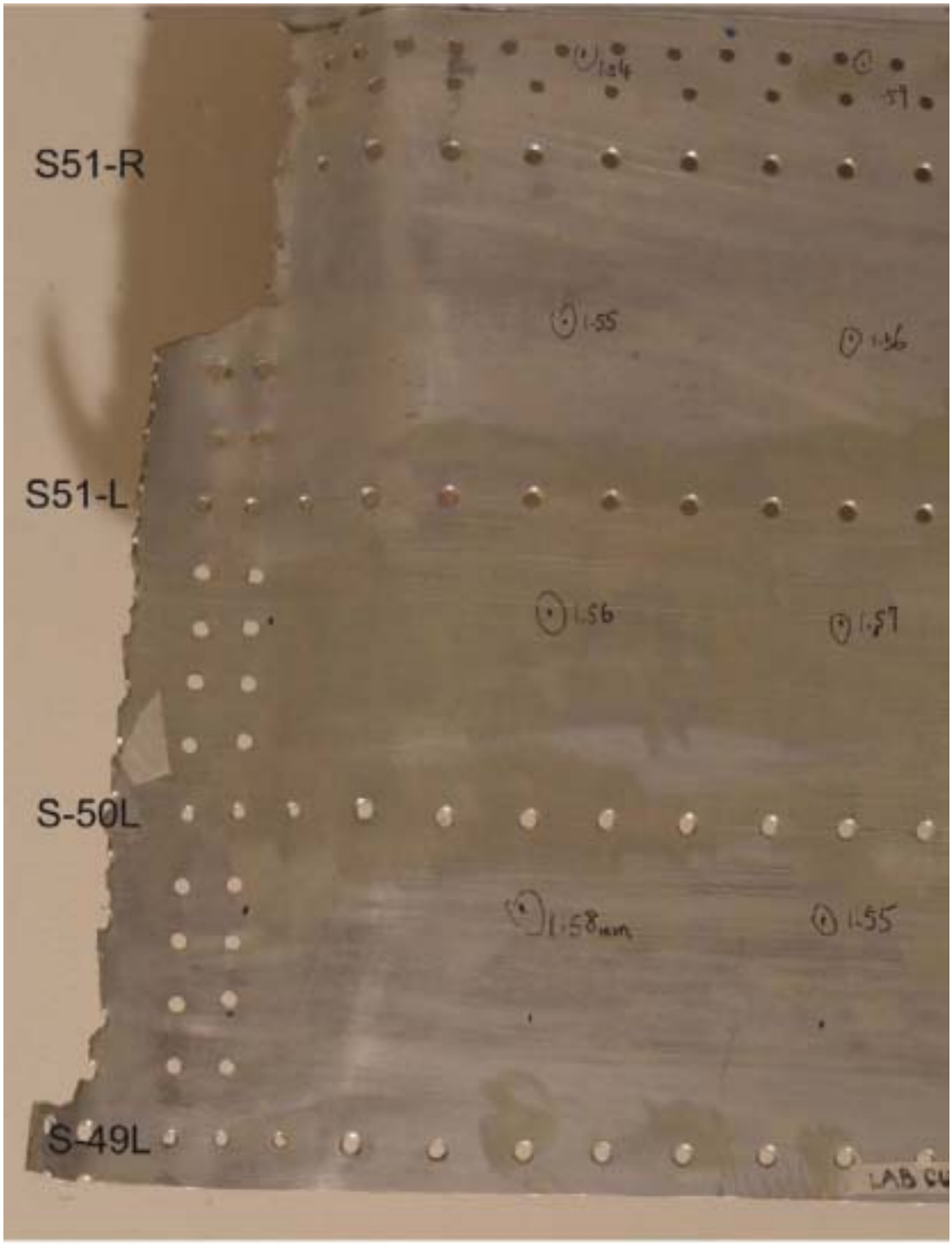

Figure 1.16-62 Extent of damage consistent with a tail strike– Scratches may be noted at S-50L and S-51L. Numerical information on skin are results of thickness measurements at the CSIST. Scratch severity increases as you move forward on the panel as shown in the following photographs.

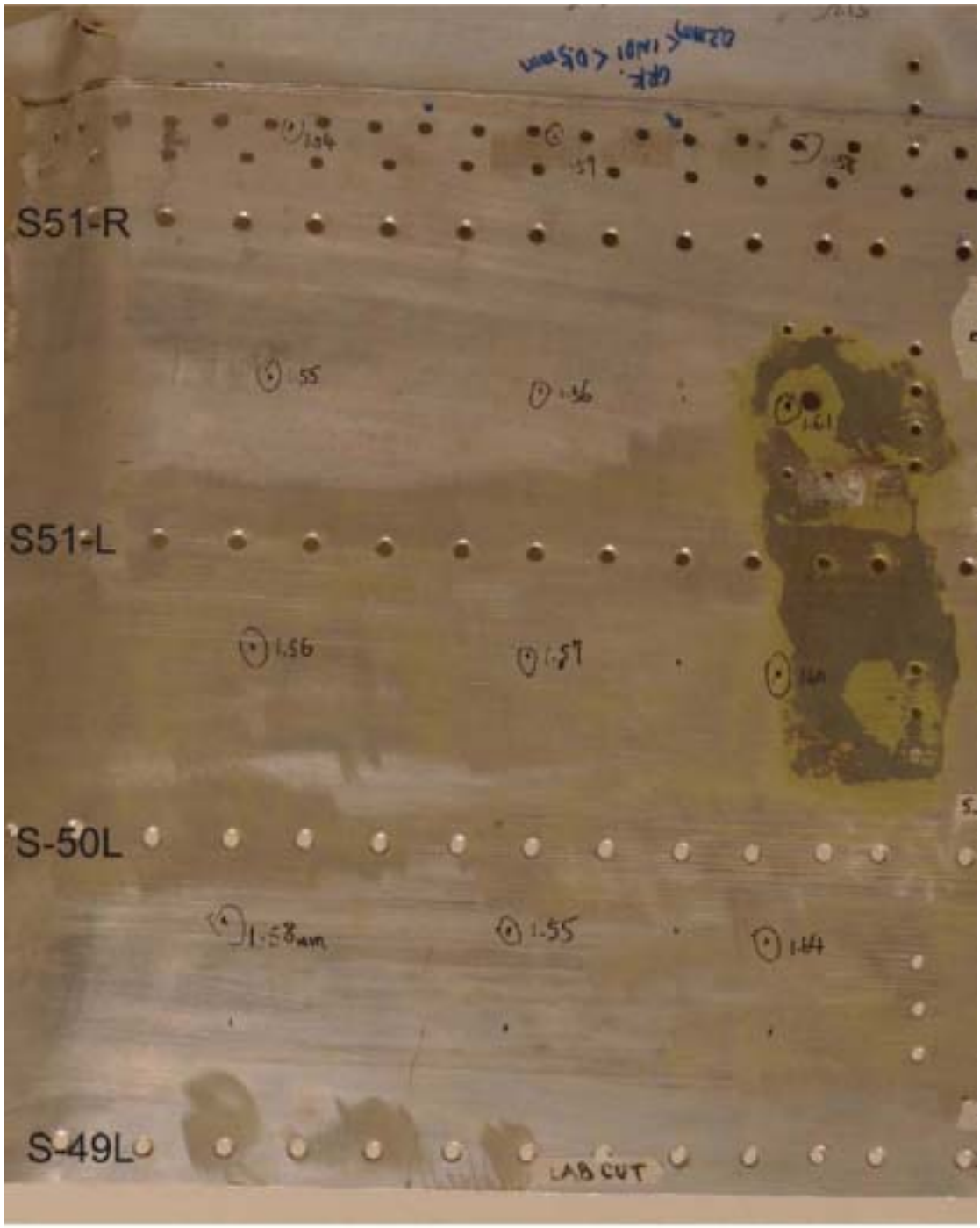

Figure 1.16-63 Extent of damage consistent with a tail strike– Scratches may be noted at S-50L and S-51L. Scratches may also be noted at the shear tie between S-49L and S-50L.

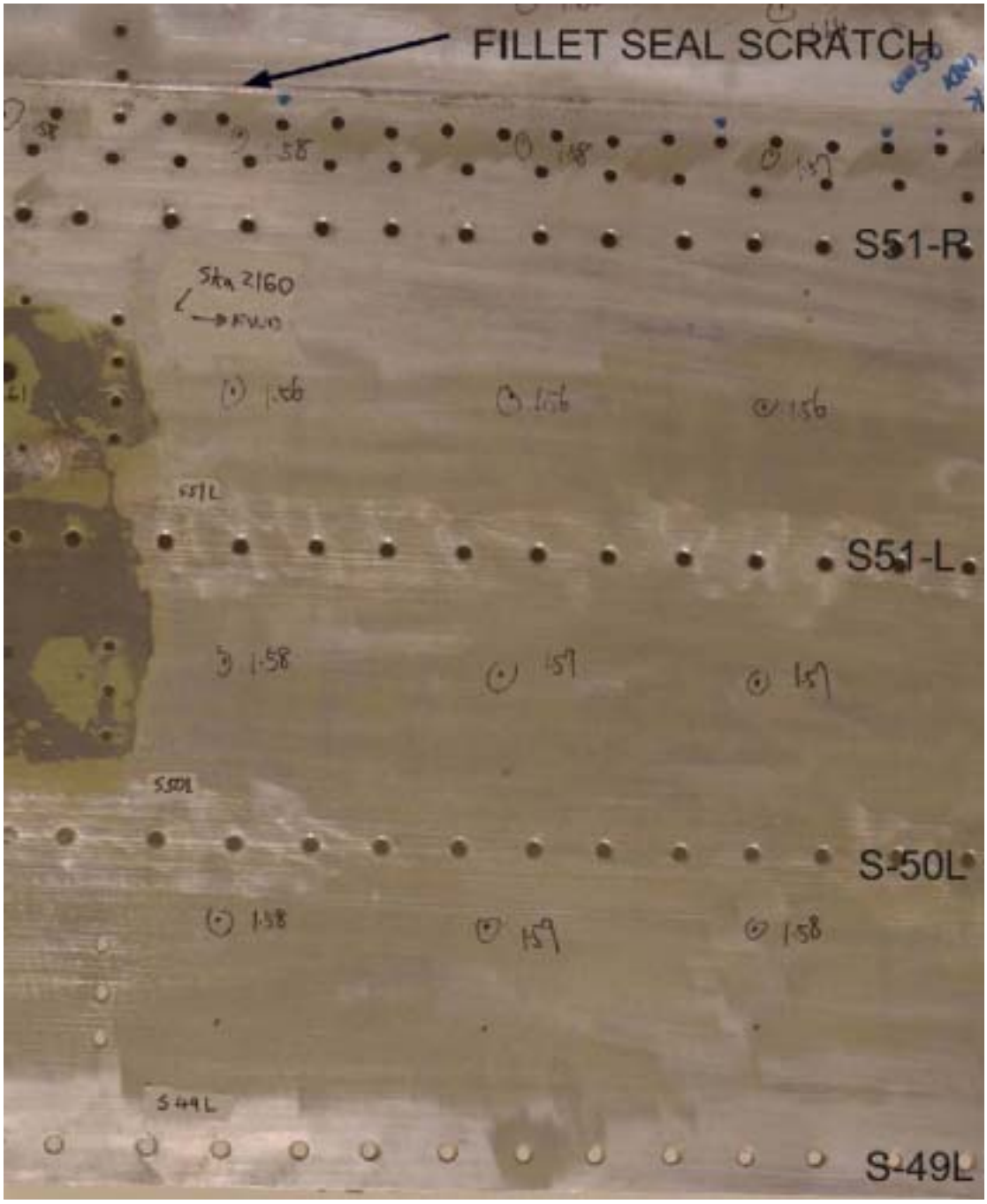

Figure 1.16-64 Extent of damage consistent with a tail strike- Note that minimal damage occurs on the right hand side of the repair area. Scratching in the doubler fillet seal area may also be seen in this photo.

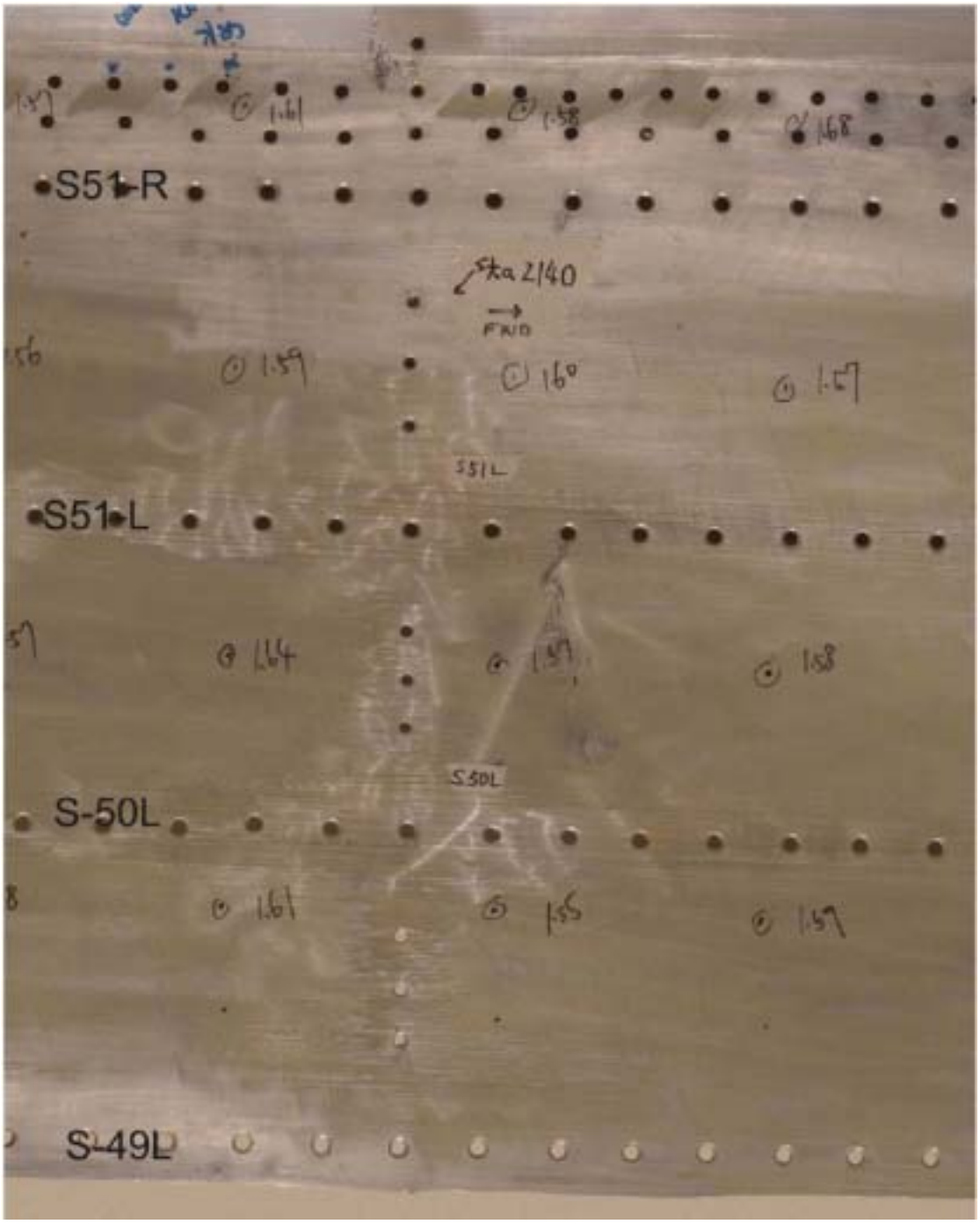

Figure 1.16-65 Extent of damage consistent with a tail strike

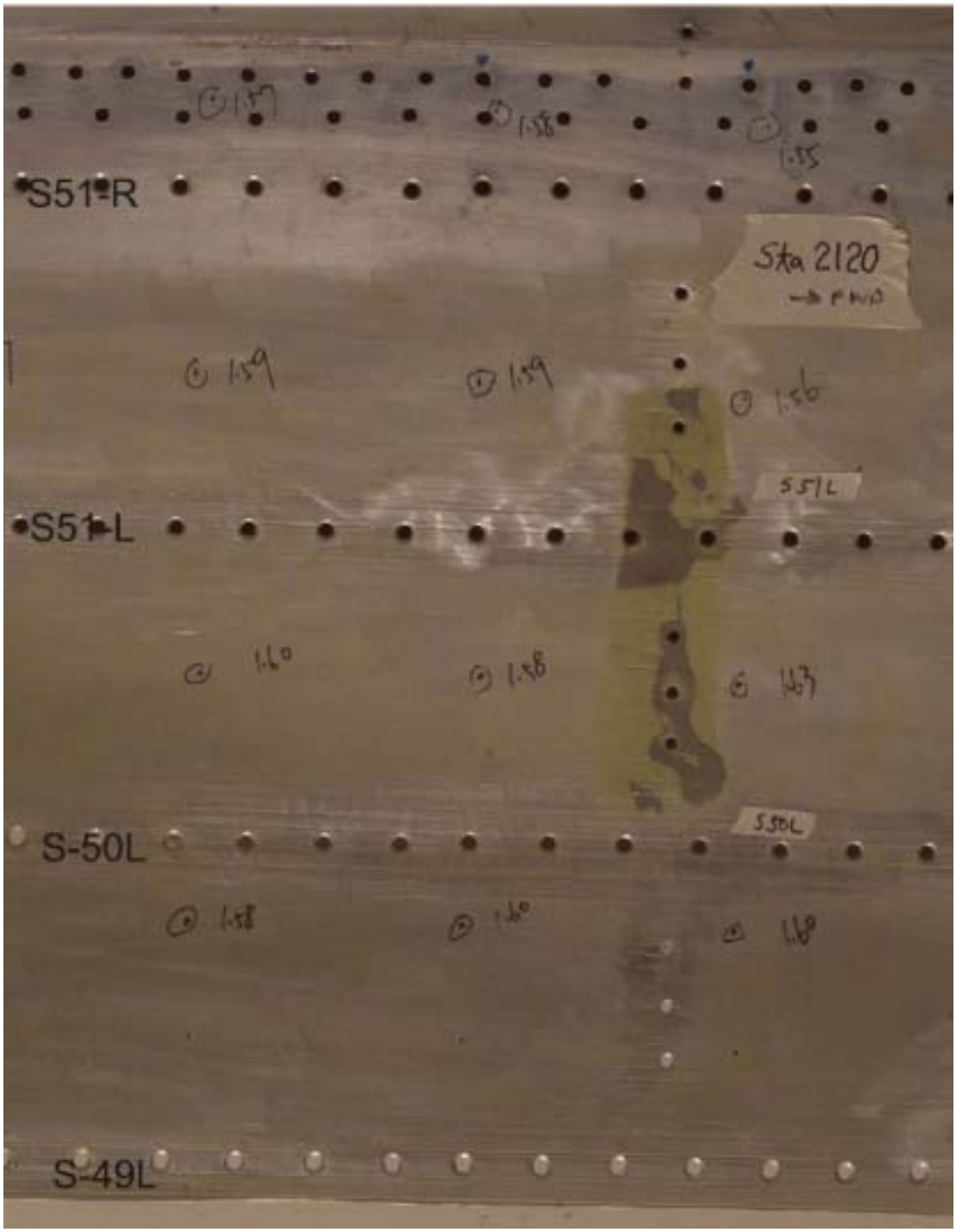

Figure 1.16-66 Extent of damage consistent with a tail strike- Deep scratches can be noted at S-49L, S-50L, AND S-51L.

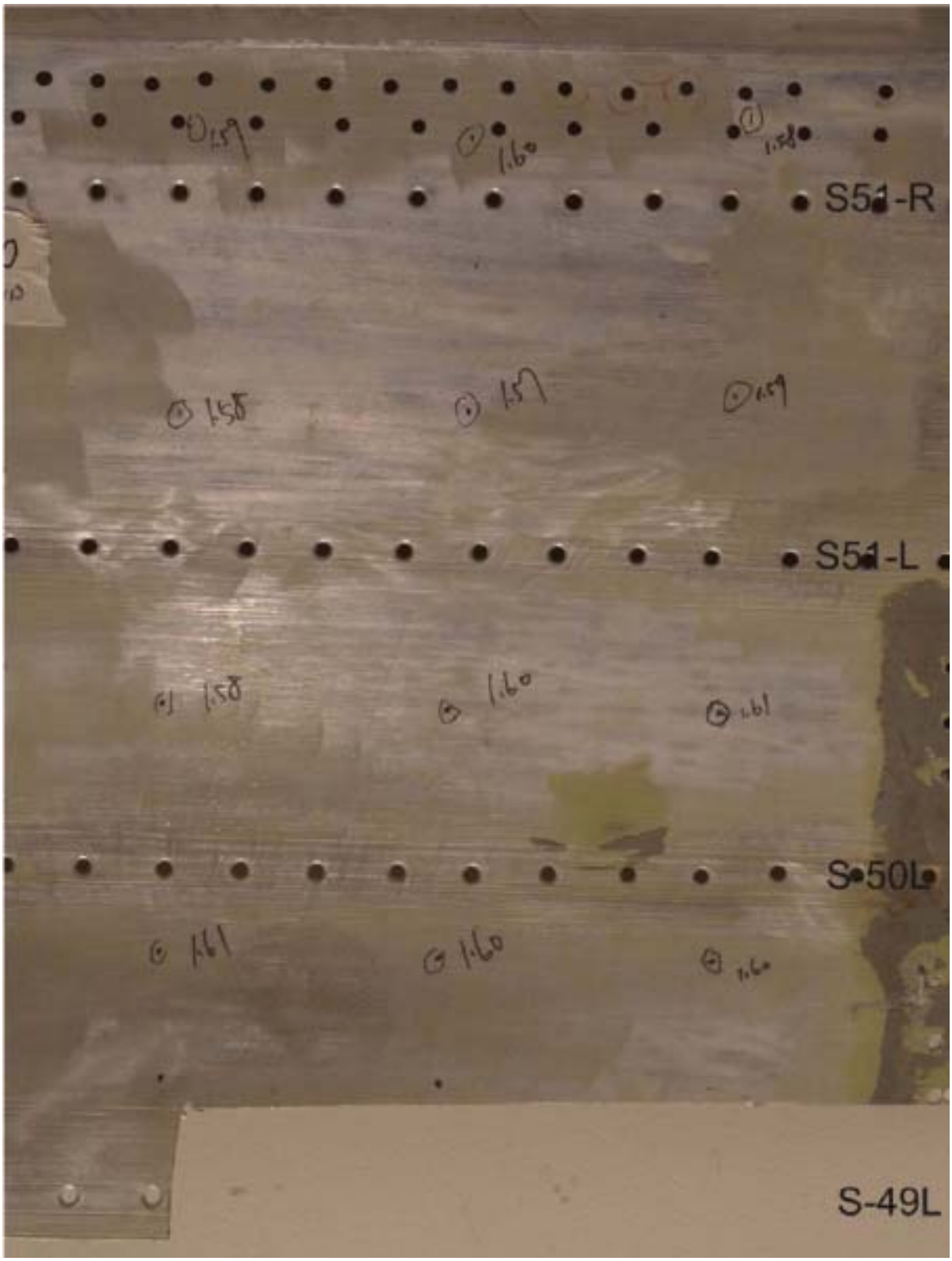

Figure 1.16-67 Extent of damage consistent with a tail strike

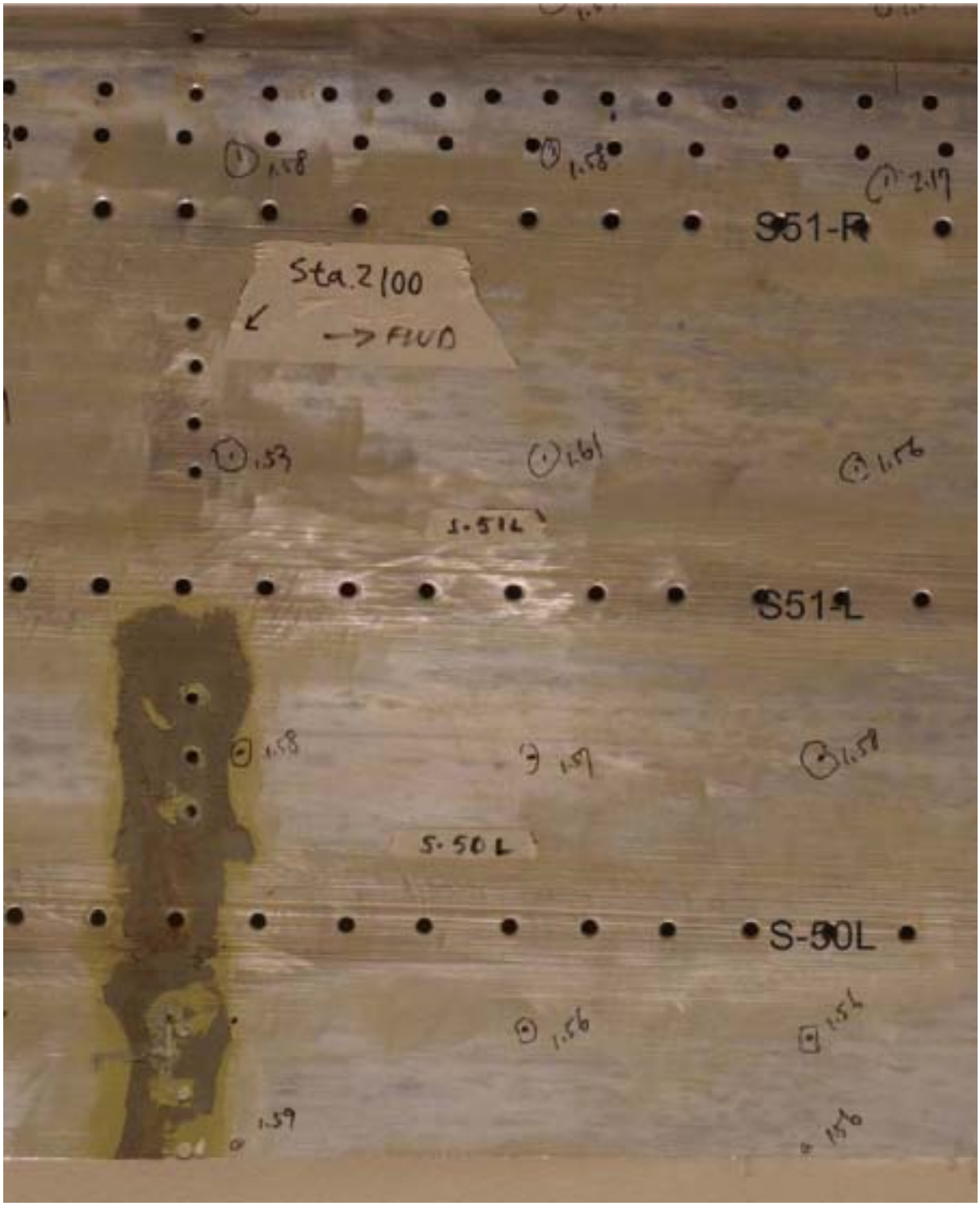

Figure 1.16-68 Extent of damage consistent with a tail strike

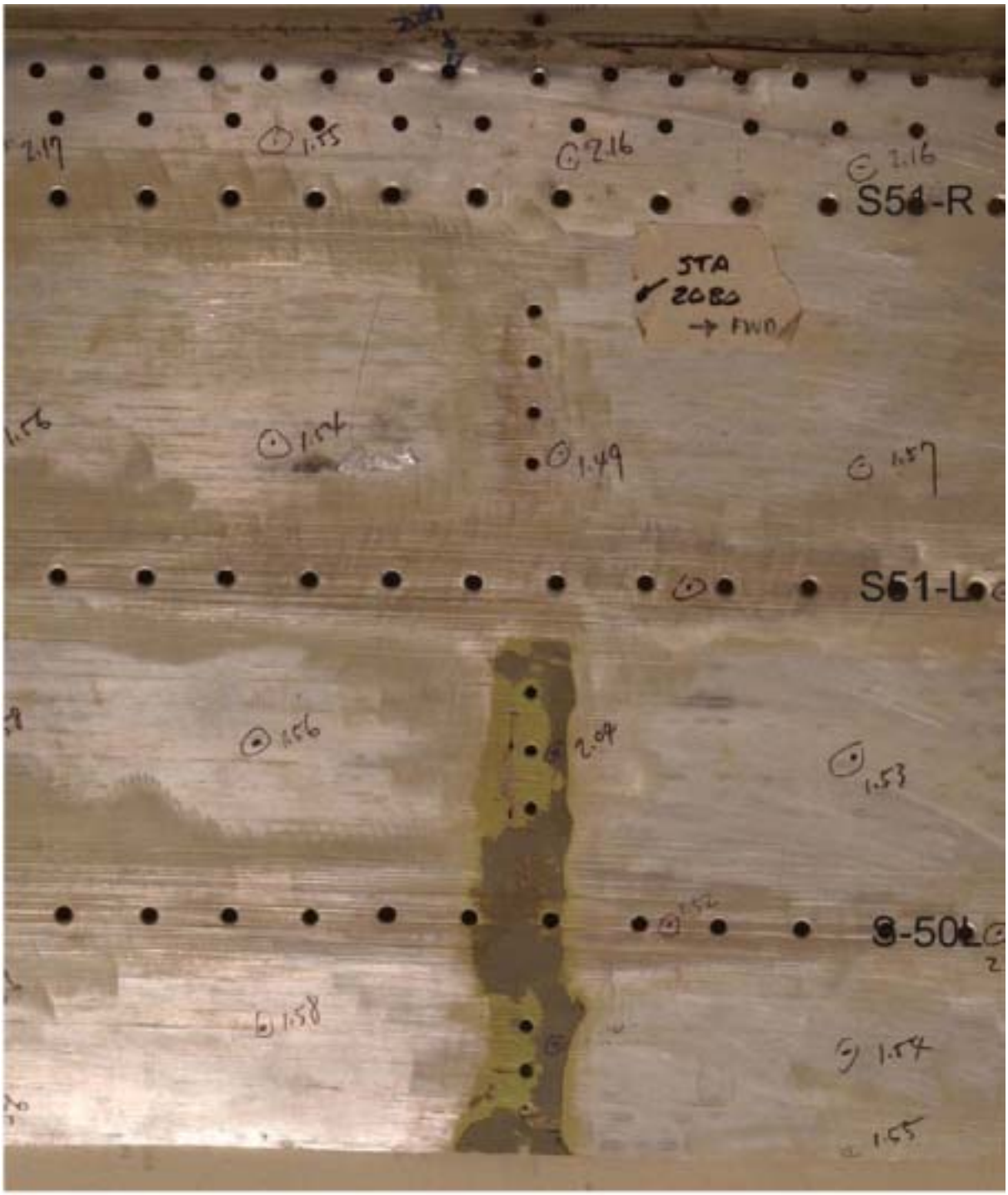

Figure 1.16-69 Extent of damage consistent with a tail strike- Note the severity of damage in this photo

Figure 1.16-70 Extent of damage consistent with a tail strike

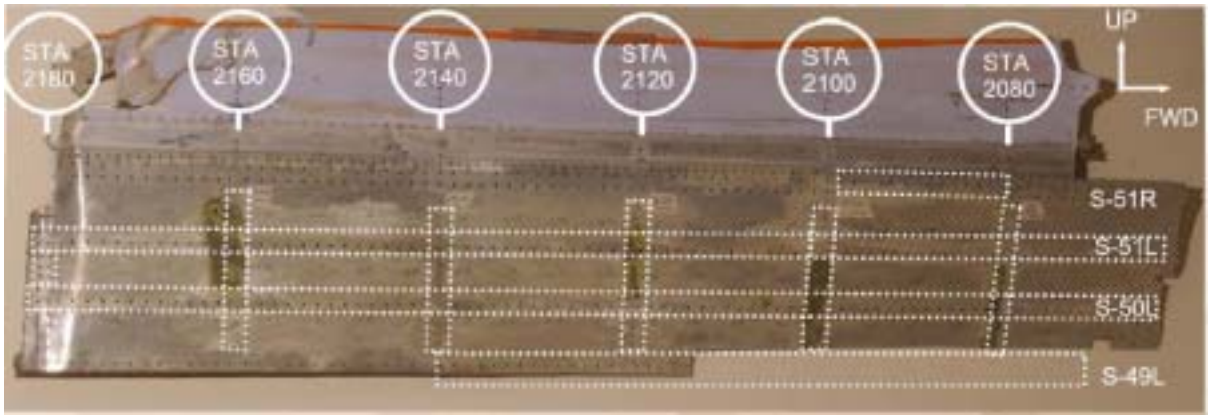

Figure 1.16-71 Areas of most severe skin damage- Scratch severity was greatest in the left hand/forward area of the skin.

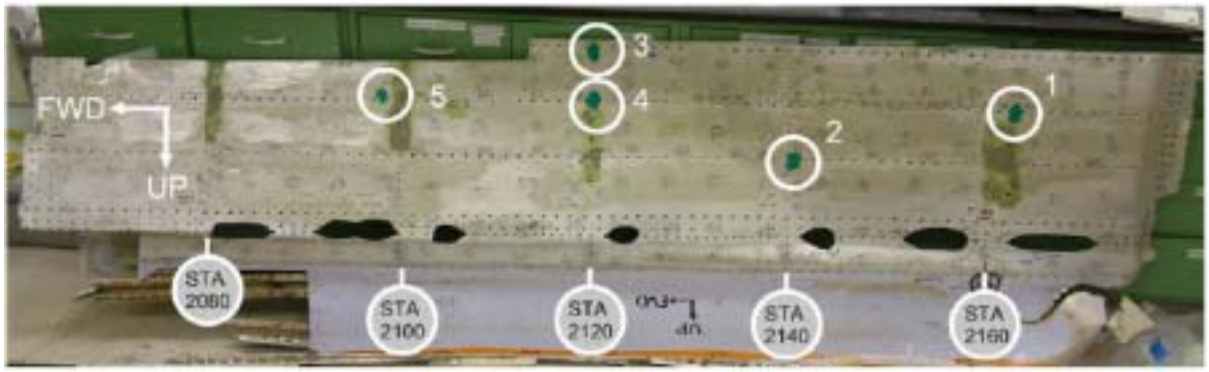

Figure 1.16-72 Location of scratch replication areas

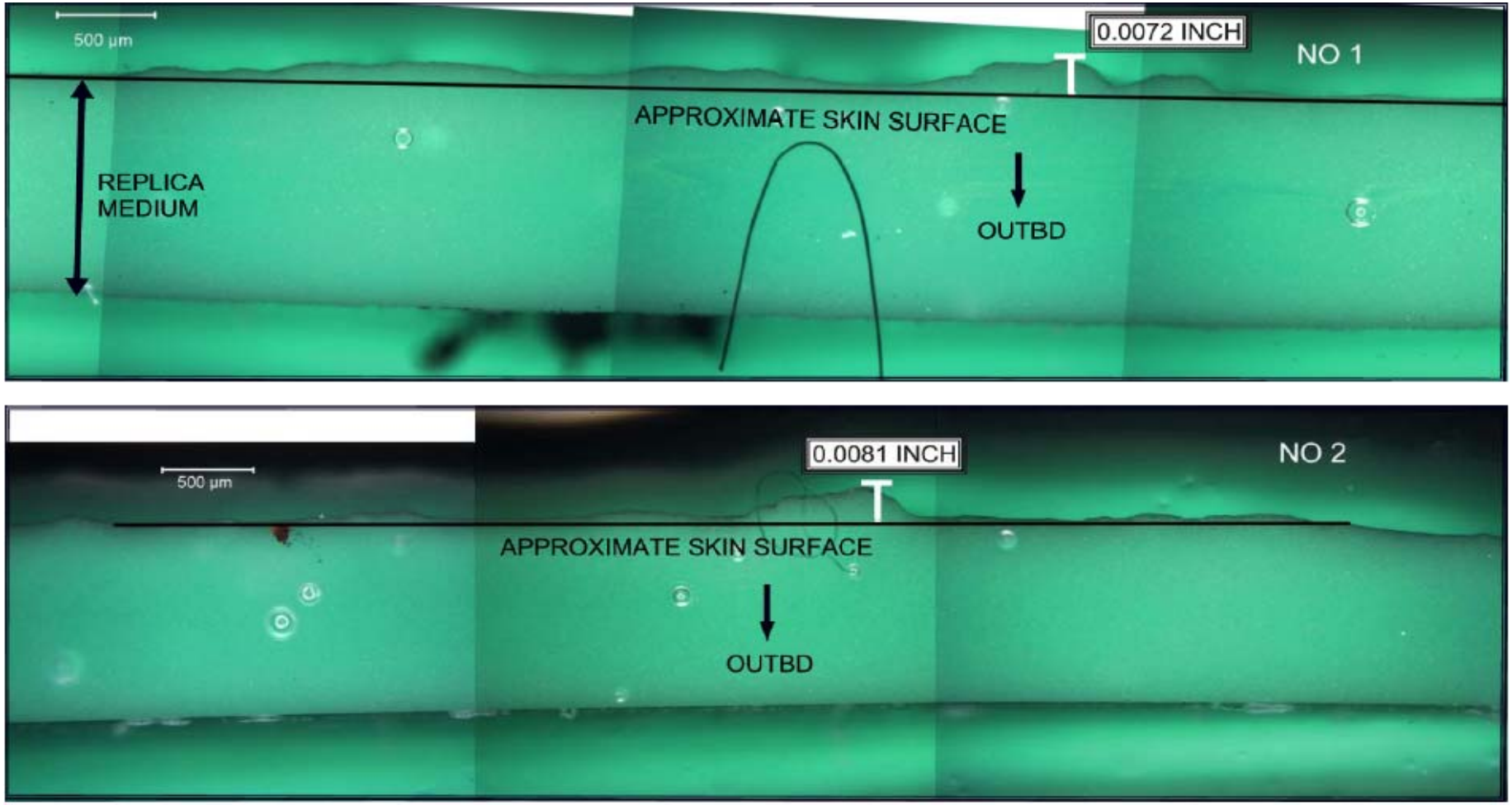

Figure 1.16-73 Scratch profile composite photographs- the replication medium creates a “positive” of the skin scratches. Scratch features of replica locations 1 and 2 are shown above.

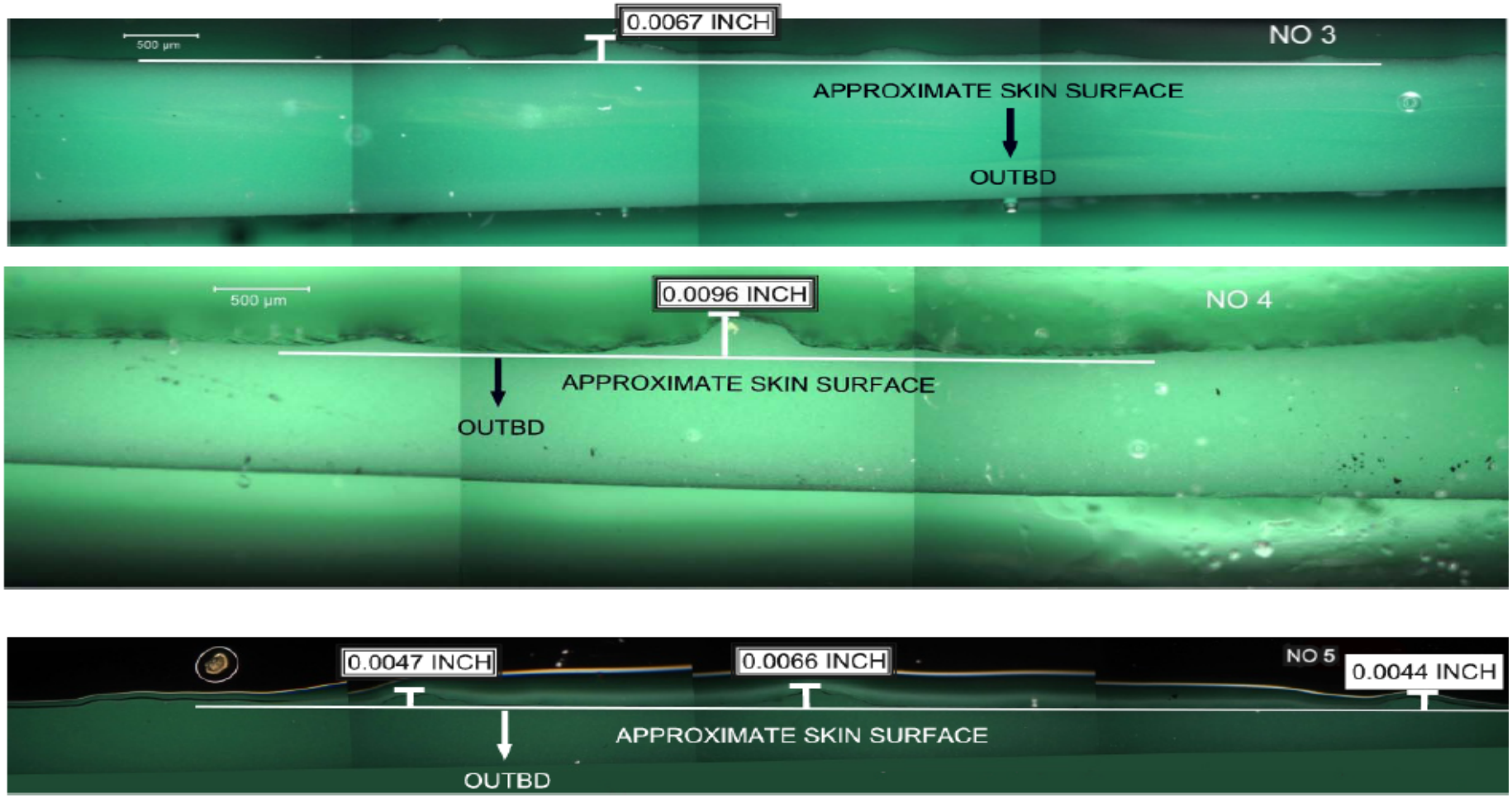

Figure 1.16-74 Scratch profile composite photographs– Shown above are replicas from locations 3,4, and 5. Location 4 presented the deepest scratch found using this technique

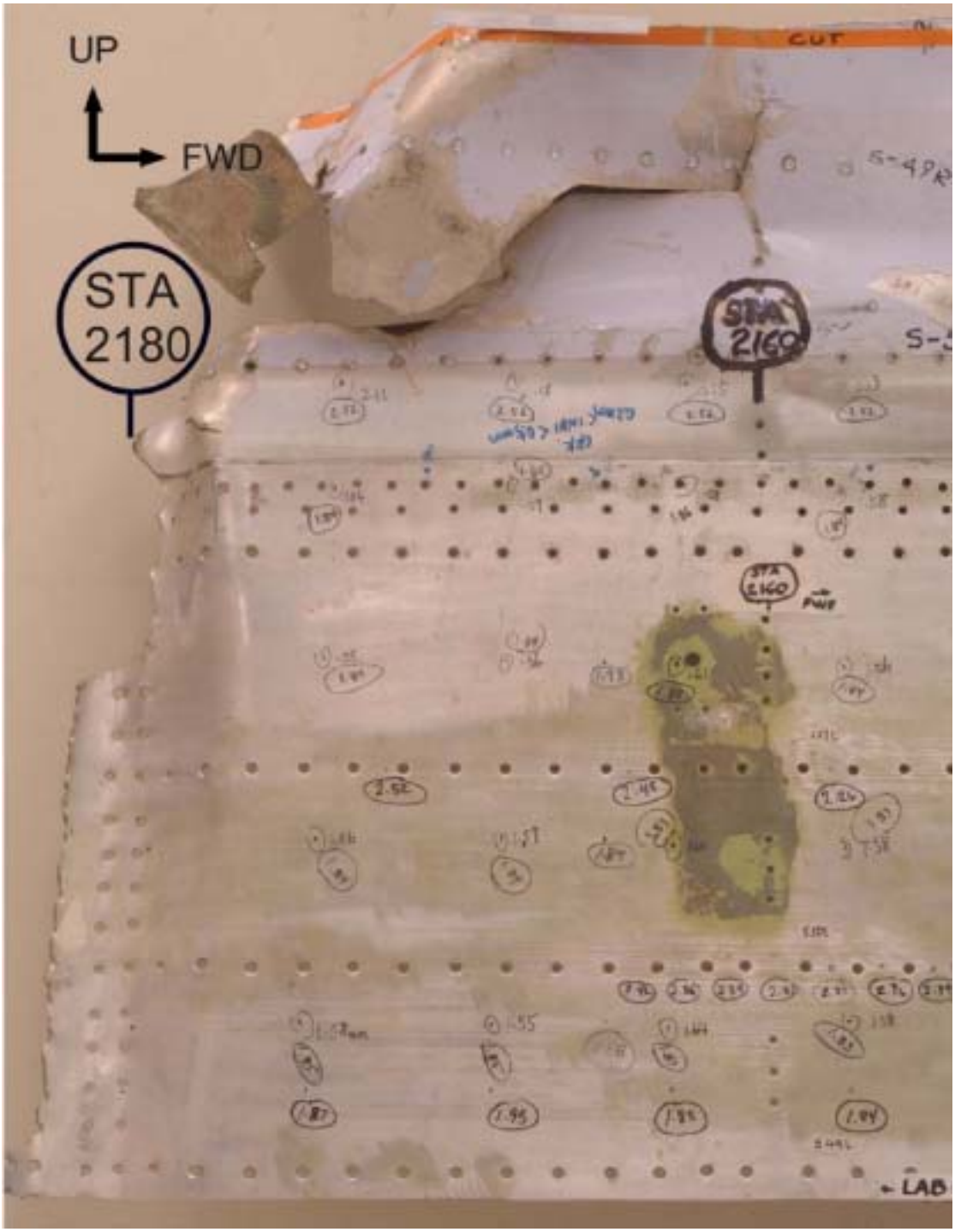

Figure 1.16-75 Skin thickness measurements- All measurements are in millimeters. Circled values were performed at Boeing

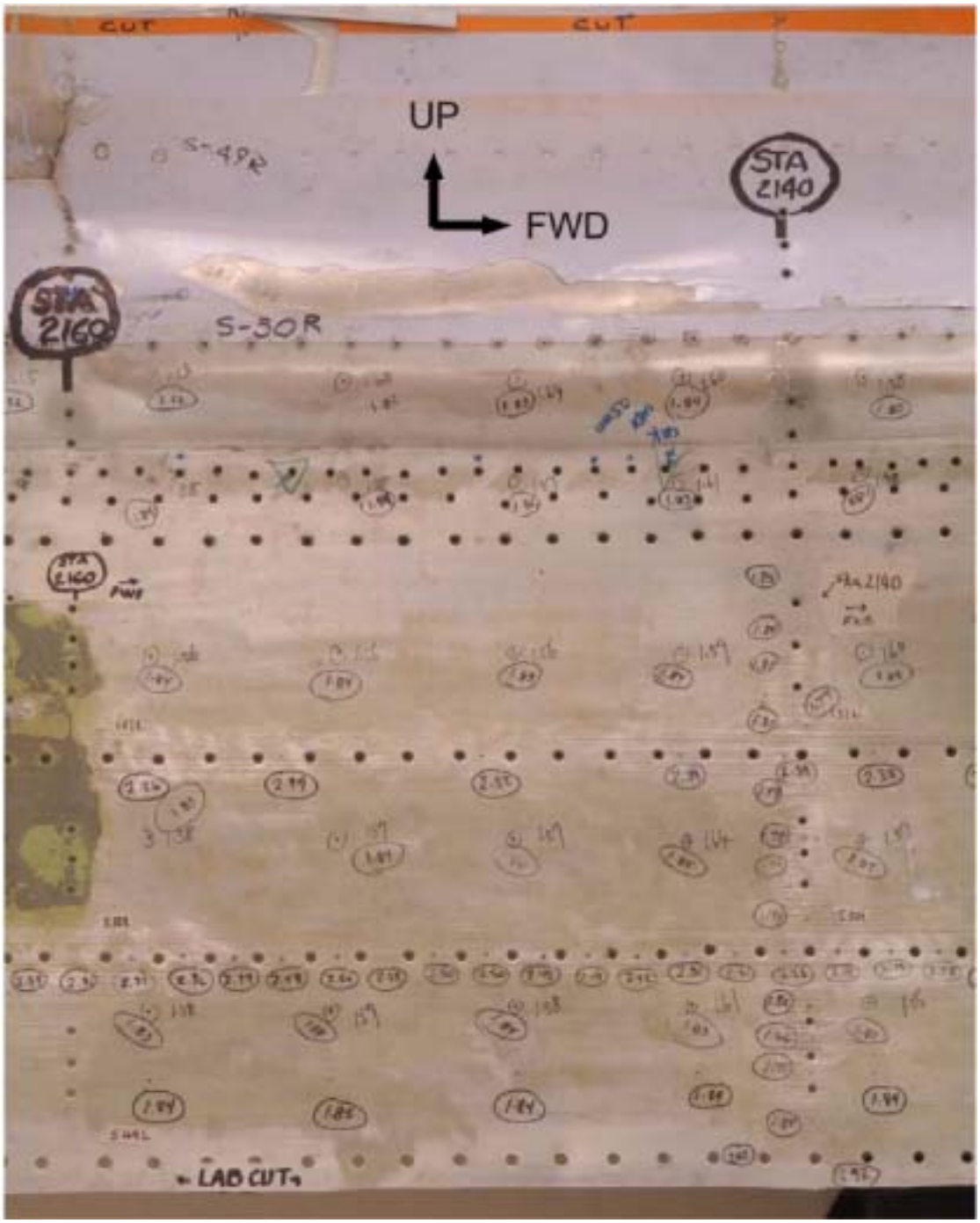

Figure 1.16-76 Skin thickness measurements- All measurements are in millimeters. Circled values were performed at Boeing.

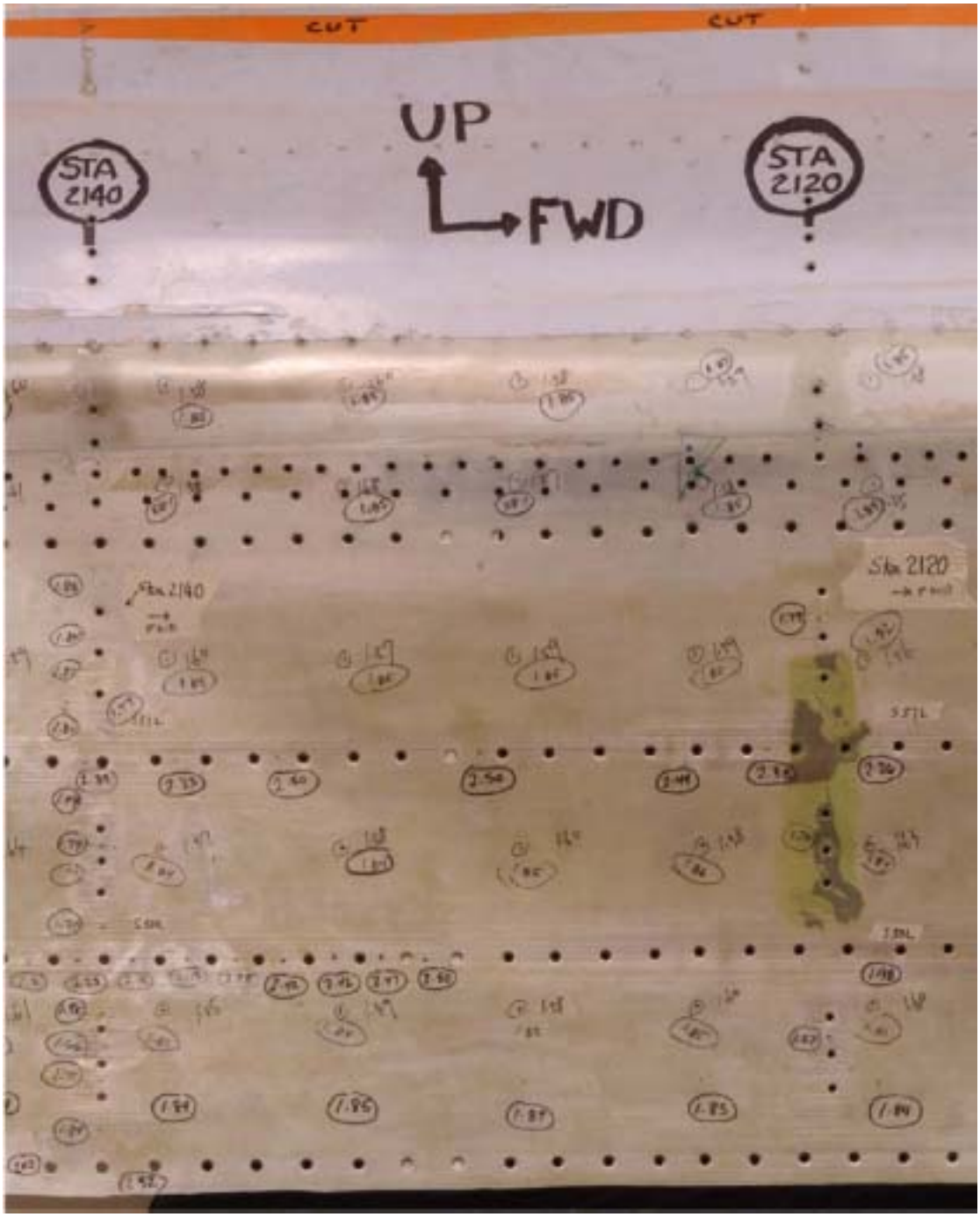

Figure 1.16-77 Skin thickness measurements- All measurements are in millimeters. Circled values were performed at Boeing.

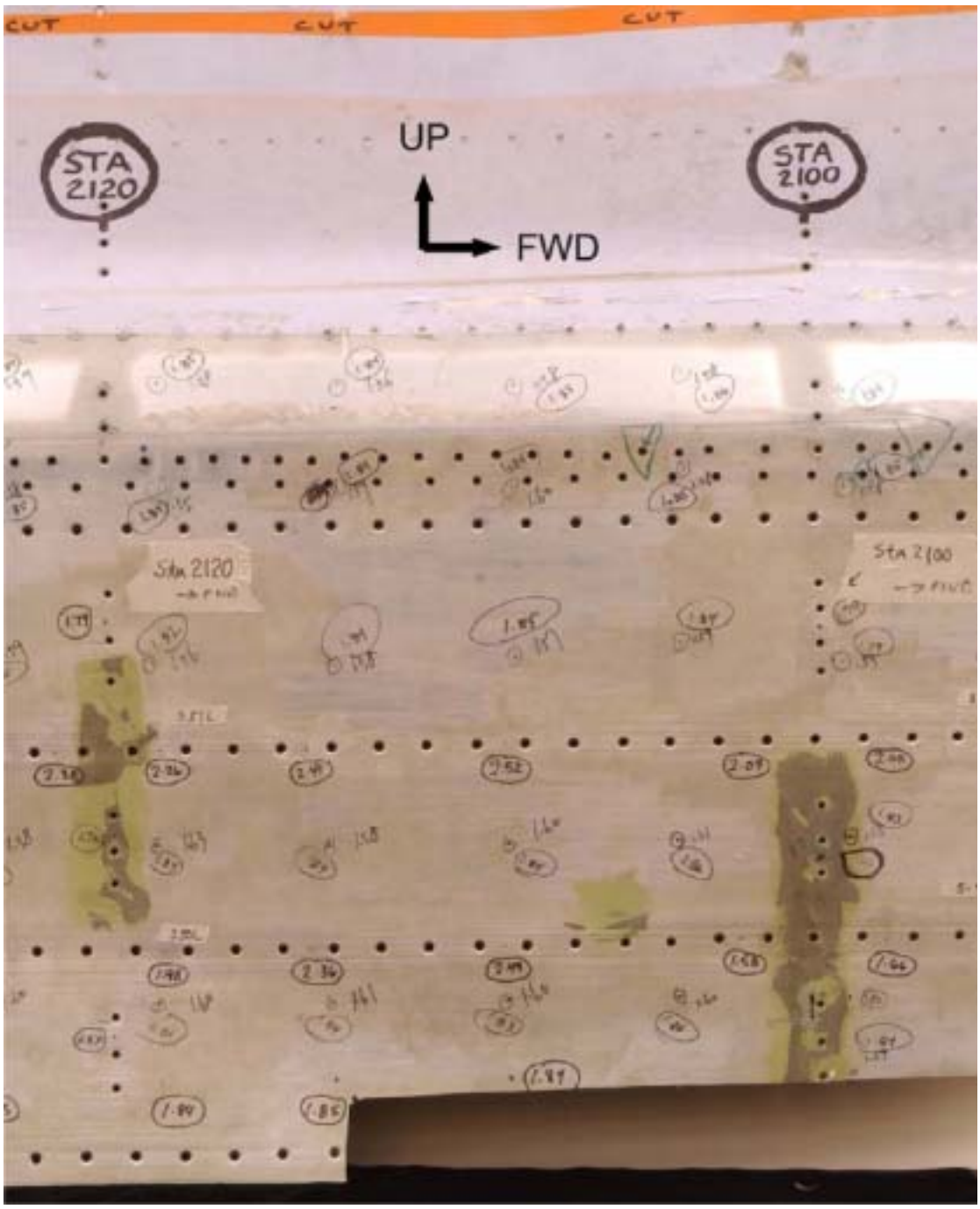

Figure 1.16-78 Skin thickness measurements- All measurements are in millimeters. Circled values were performed at Boeing.

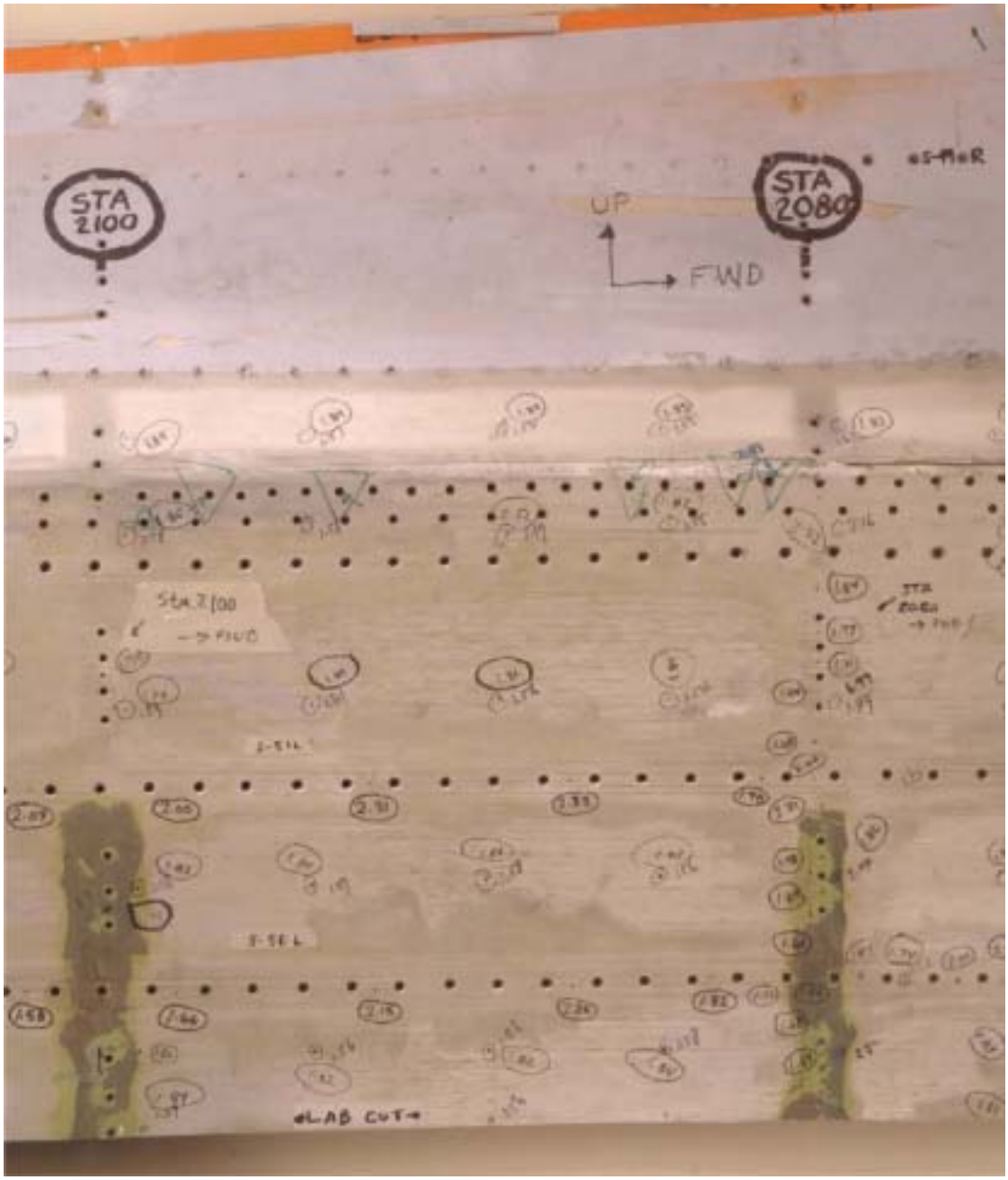

Figure 1.16-79 Skin thickness measurements- All measurements are in millimeters. Circled values were performed at Boeing.

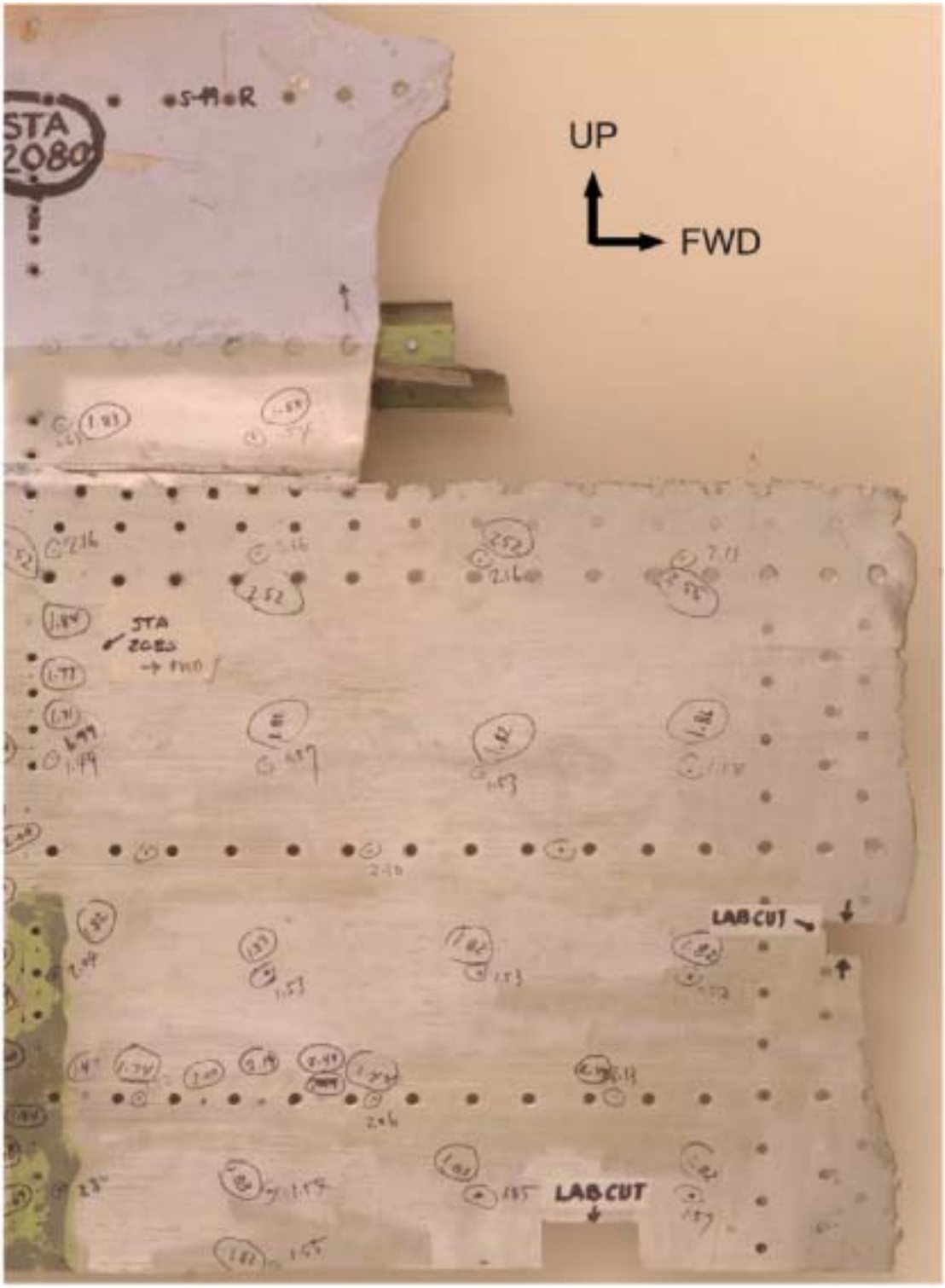

Figure 1.16-80 Skin thickness measurements- All measurements are in millimeters. Circled values were performed at Boeing.

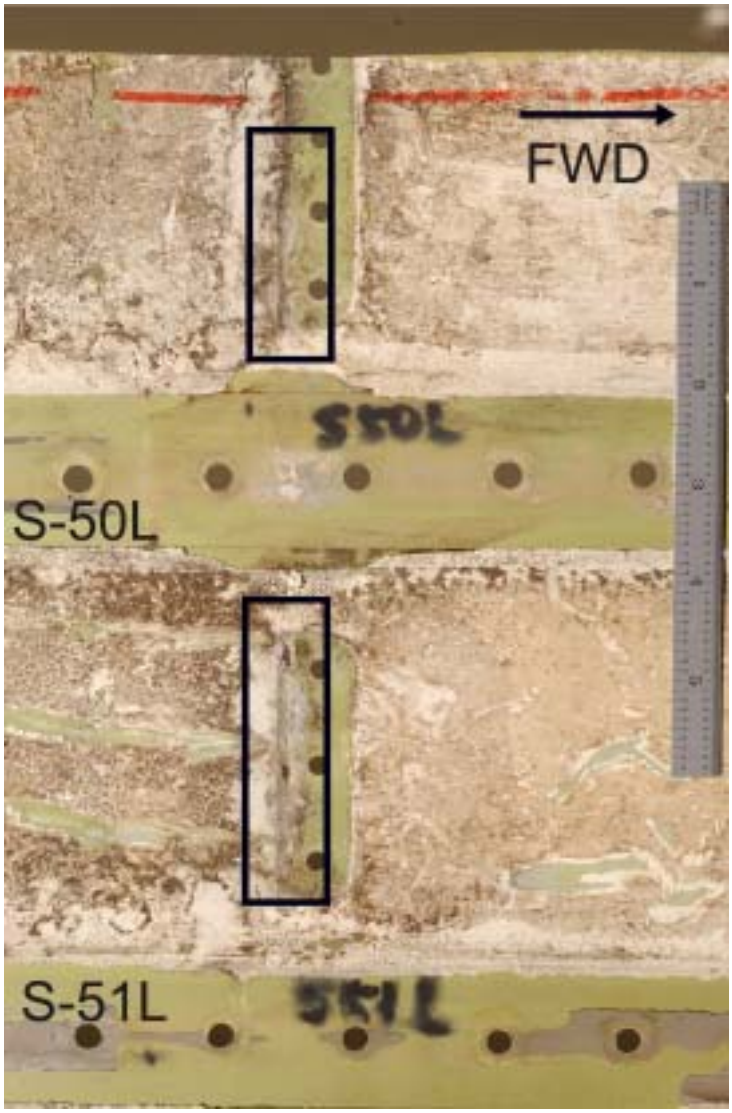

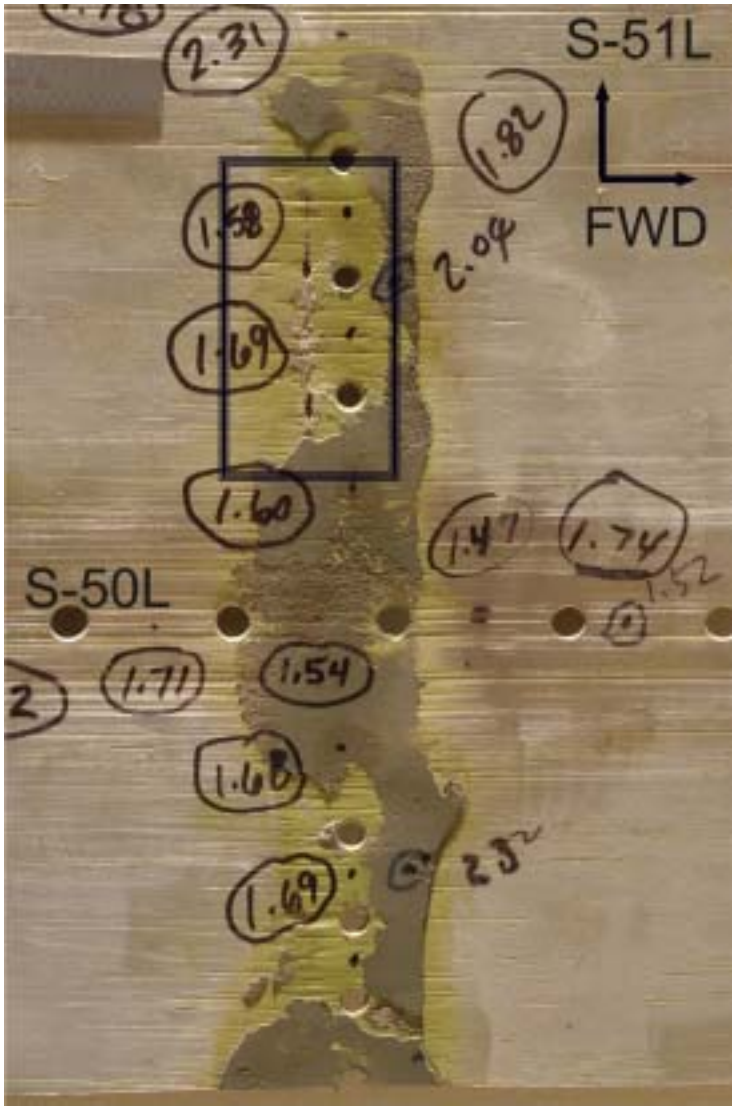

SKIN INBOARD SURFACE SKIN REPAIR FAYING SURFACE

Figure 1.16-81 Skin corrosion features at STA 2080 - Areas of corrosion are identified with rectangles above. Corrosion penetrated completely through the skin thickness at the shear tie located between S-50L and S-51L.

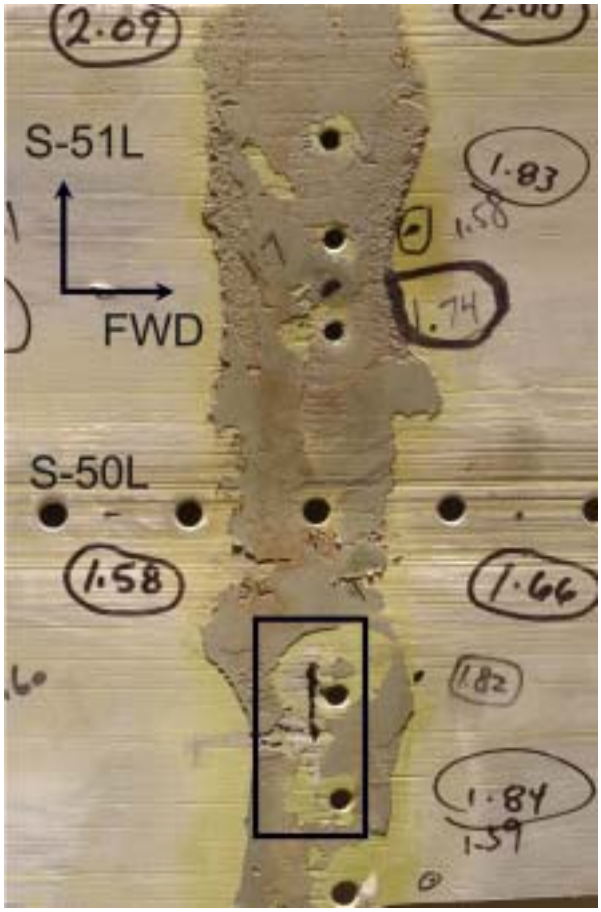

SKIN INBOARD SURFACE REPAIR FAYING SURFACE

Figure 1.16-82 Skin corrosion features at STA 2100 - Areas of corrosion are highlighted with rectangles. Corrosion penetrated completely through the skin thickness between S-49L and S-50L.

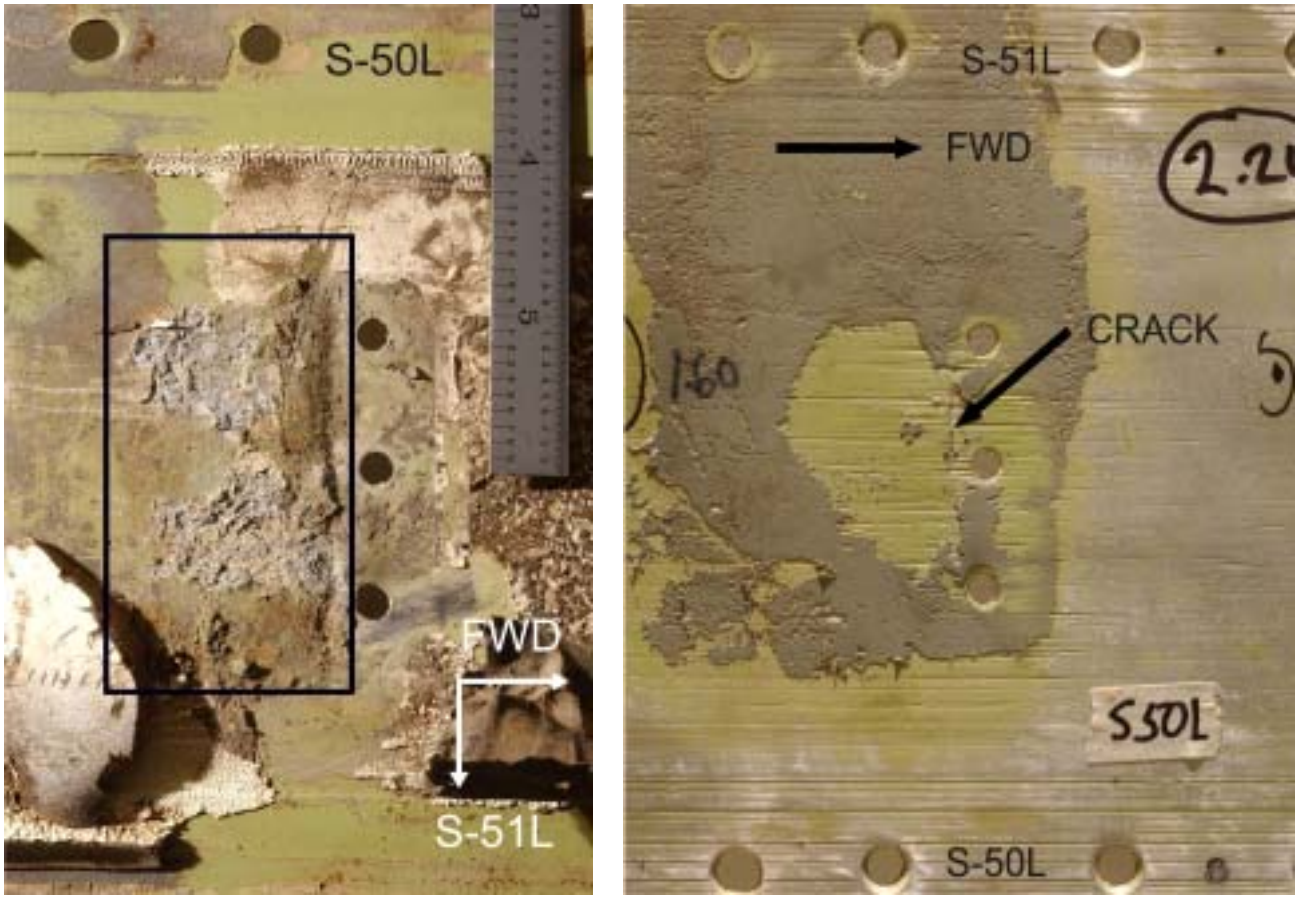

SKIN INBOARD SURFACE SKIN REPAIR FAYING SURFACE

Figure 1.16-83 Corrosion features at STA 2160, inboard surface - The area of corrosion is identified with a rectangle above. A crack noted on the skin faying surface may have been the result of exfoliation corrosion penetrating from the skin inboard surface.

Table 1.16-8 Item 640 C1 skin inboard surface corrosion details

STA	**STRINGER BAY**	**CORROSION THROUGH SKIN THICKNESS**	**APPROXIMATE AREA (INCH^2)**
2080	49L-50L	NO	0.24
2080	50L-51L	YES	0.44
2100	49L-50L	YES	1.44
2100	50L-51L	NO	0.64
2160	50L-51L	YES	2.28

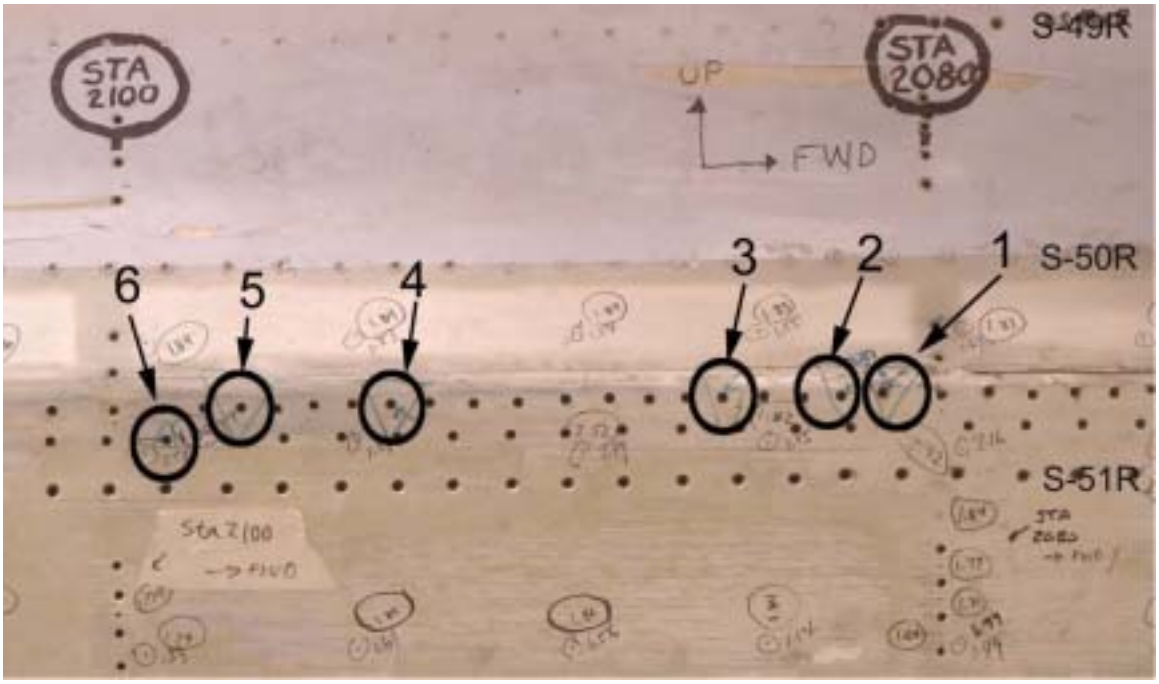

Figure 1.16-84 Cookie cut locations

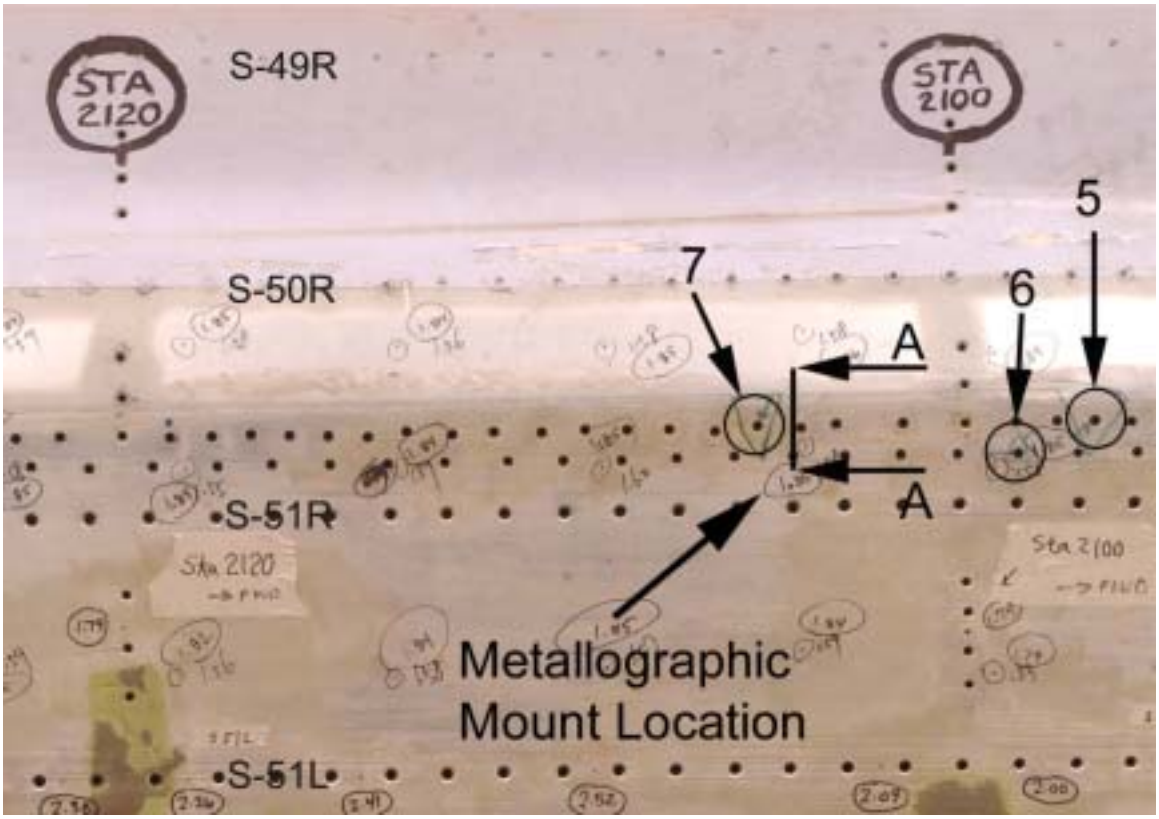

Figure 1.16-85 Cookie cut locations

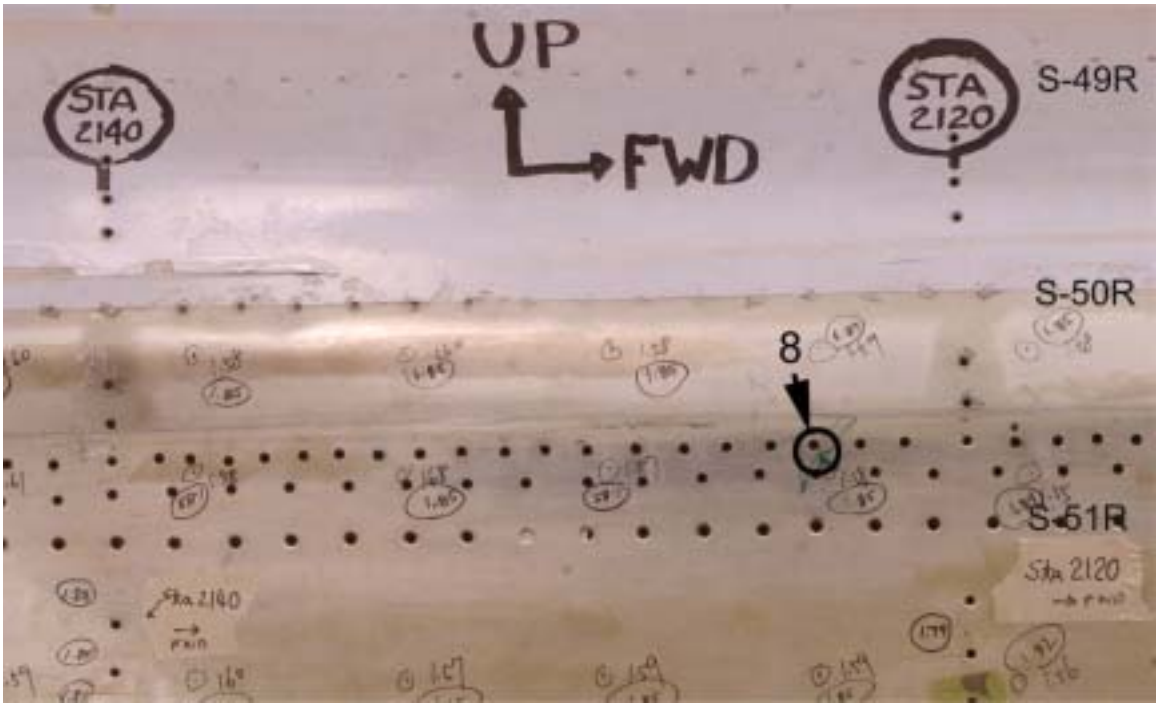

Figure 1.16-86 Cookie cut locations

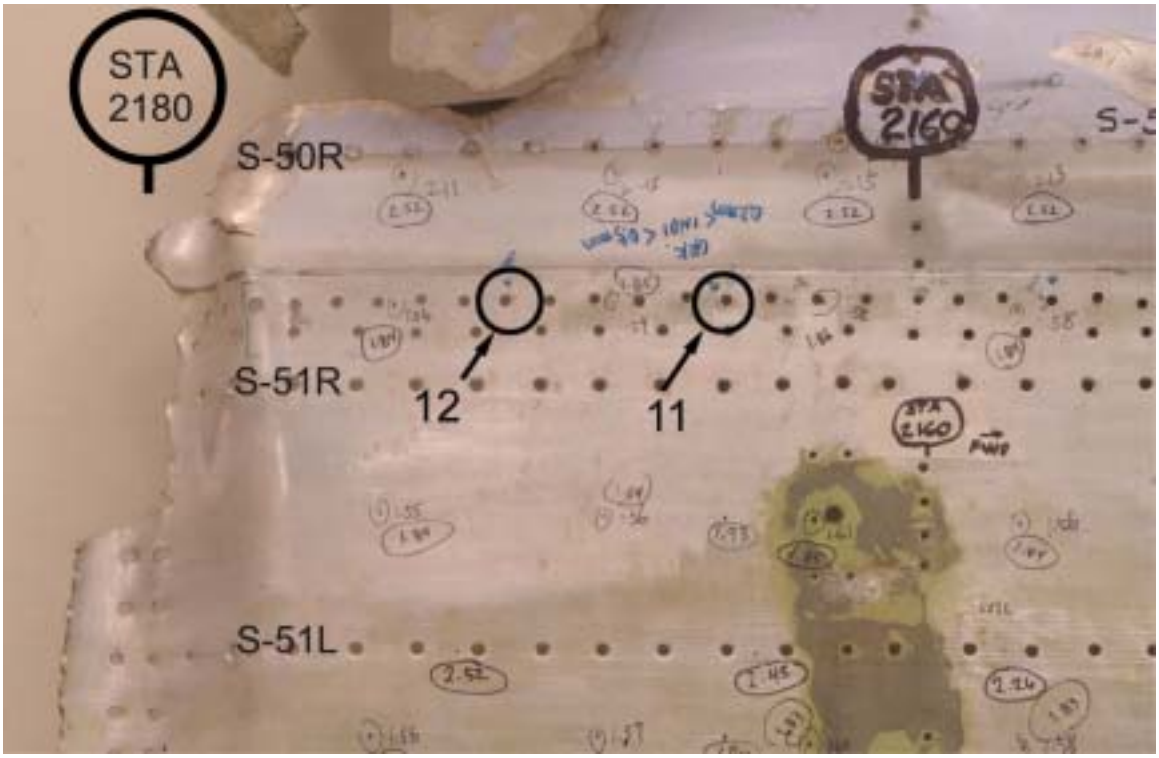

Figure 1.16-87 Cookie cut locations

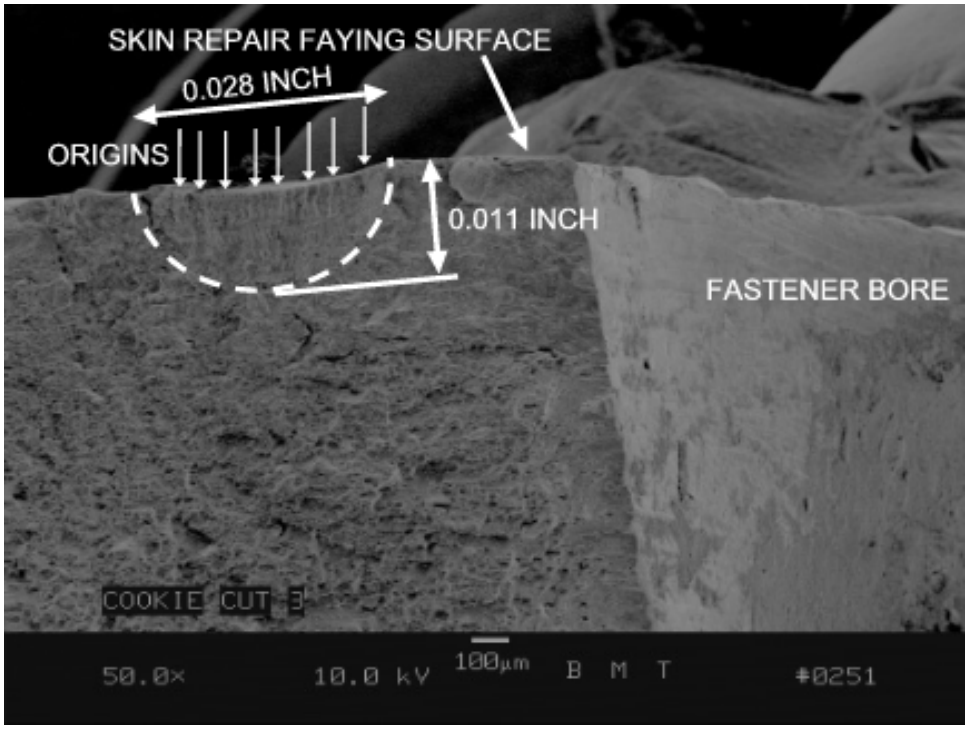

Figure 1.16-88 Cookie cut # 3 fatigue crack features – The extent of fatigue cracking is identified with a dashed line. Multiple fatigue origins are denoted with arrows.

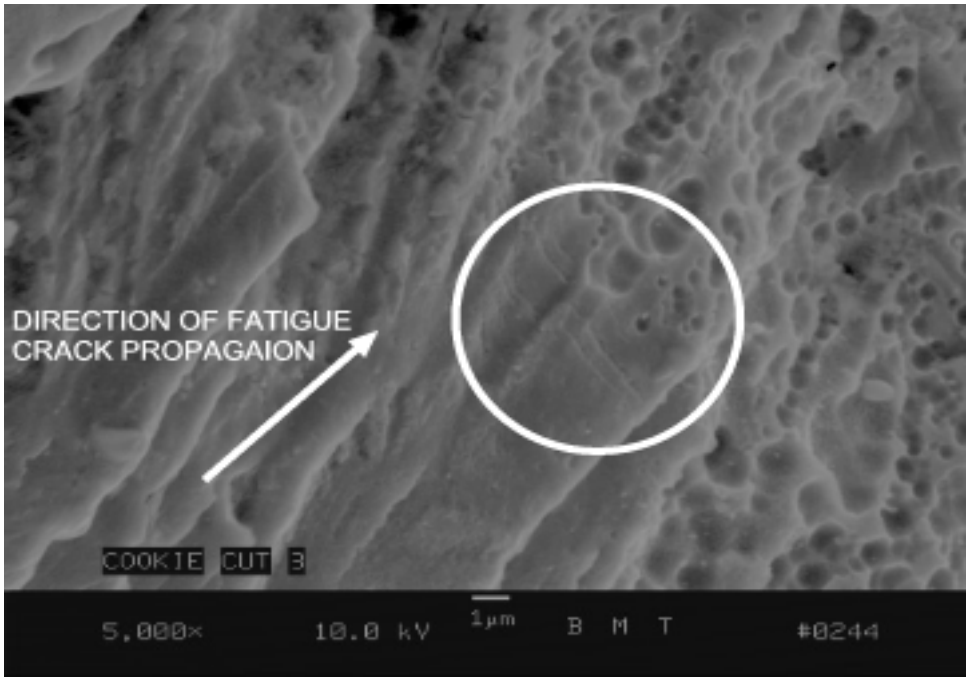

Figure 1.16-89 FATIGUE FEATUES FOUND IN CRACK AT COOKIE CUT #3 - Circled area identifies typical fatigue striations characteristic of fuselage pressure cycles observed at the maximum depth of cracking in Cookie Cut #3

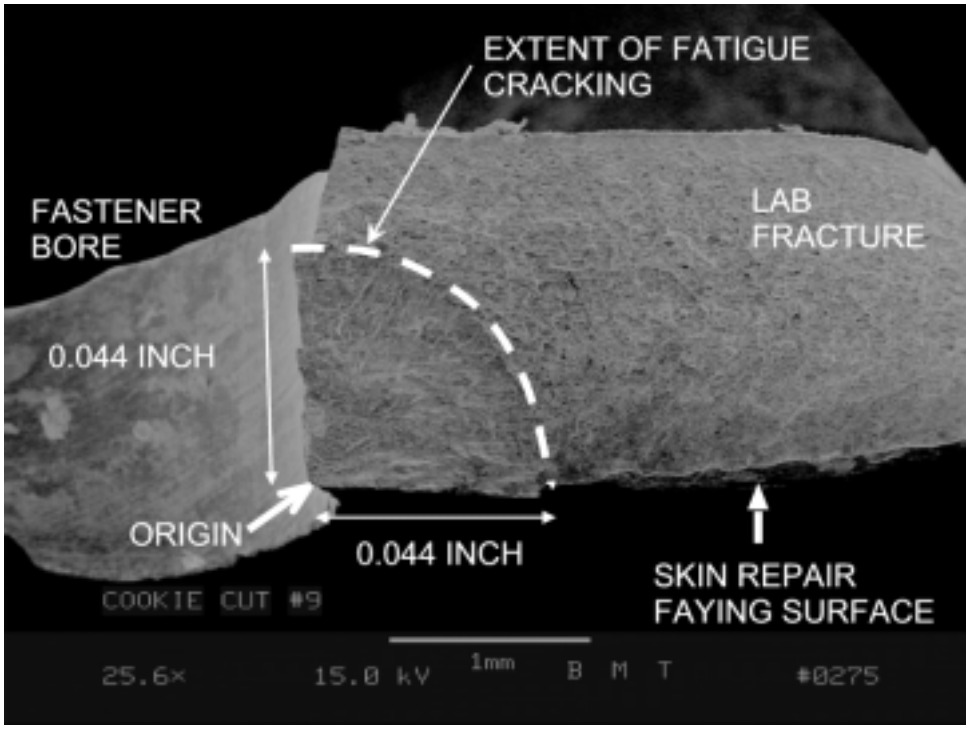

Figure 1.16-90 COOKIE CUT #9 FATIGUE CRACK FEATURES - Cracking initiated from the single origin noted above.

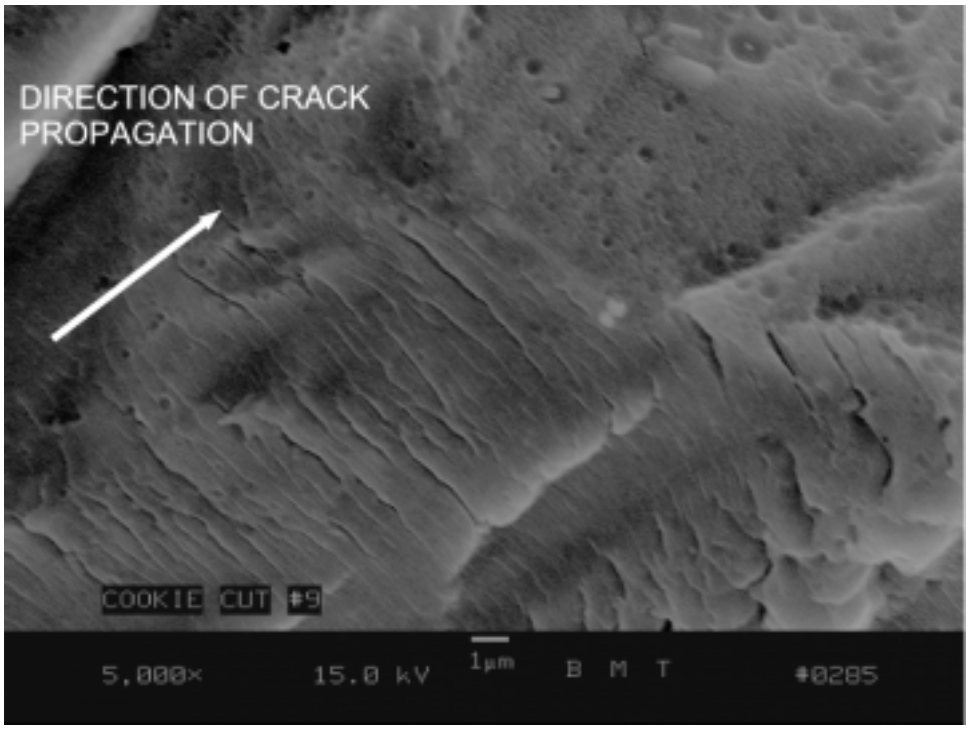

Figure 1.16-91 COOKIE CUT #9 FATIGUE STRIATIONS – The above features were located at the maximum extension of the fatigue crack.

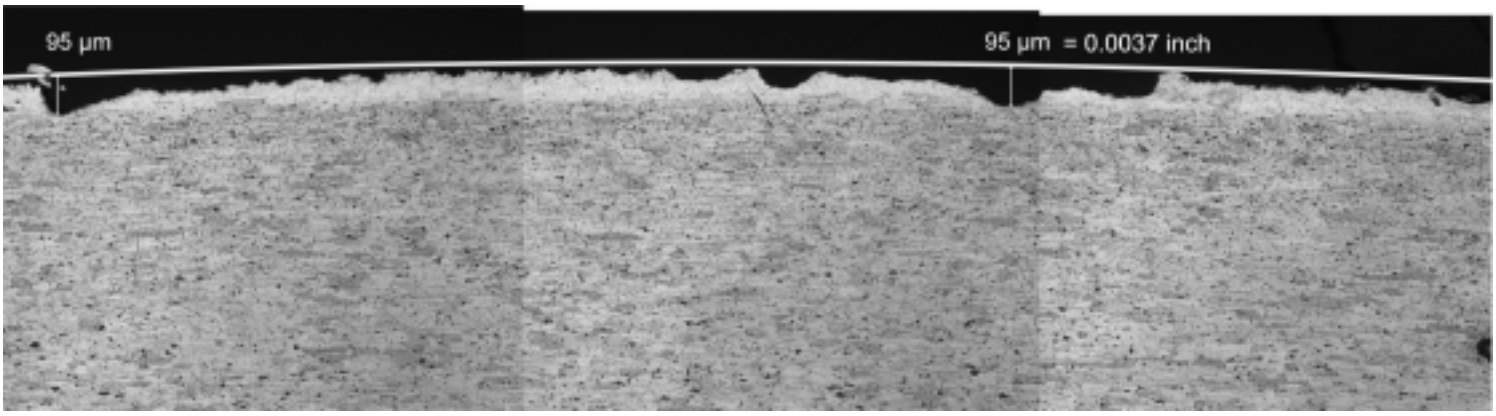

Figure 1.16-92 FILLET SEAL SCRATCH FEATURES - These skin surface features were observed at Plane A-A Figure. The clad layer of the skin appears to be penetrated at both measurement locations.

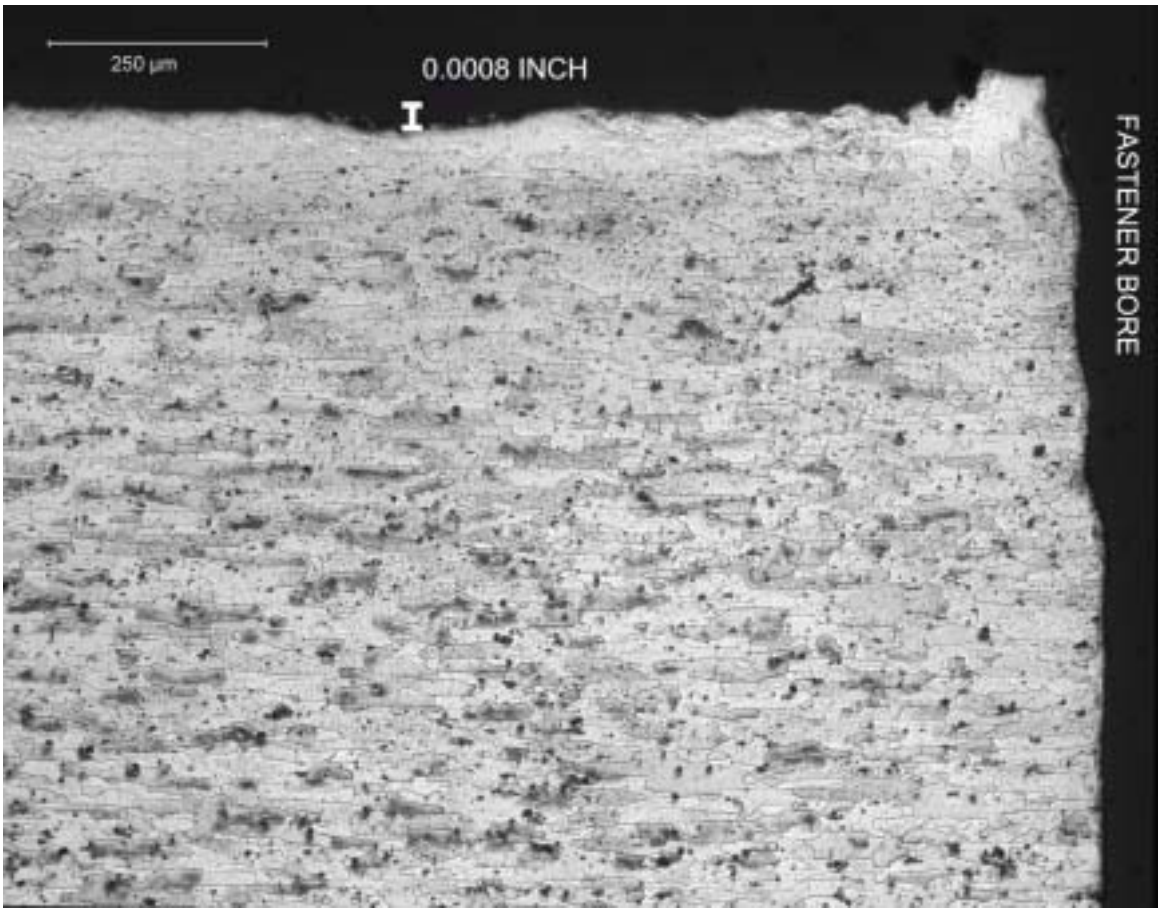

Figure 1.16-93 OUTER FASTENER ROW SCRATCH FEATURES AT PLANE A-A – Skin damage at this location was much less severe than on the left hand side of repair doubler. Skin cladding was not compromised by surface damage in this view.

Table 1.16-9 MECHANICAL PROPETERY TESTS RESULTS FOR THE ITEM 640 C1 SKIN

LONGITUDINAL PROPERTIES

SAMPLE	**TENSILE ULTIMATE STRENGTH F_{tu} (KSI)**	**TENSILE YIELD STRENGTH F_{ty} (KSI)**	**PERCENT ELONGATION (2.00 INCH GAGE)**
L1	68.7	54.0	19.2
L2	68.6	53.0	19.4
L3	69.9	53.6	19.6
REQUIRED 1	61.0	40.0	15.0

LONG TRANSVERSE PROPERTIES

SAMPLE	**TENSILE ULTIMATE STRENGTH F_{tu} (KSI)**	**TENSILE YIELD STRENGTH F_{ty} (KSI)**	**PERCENT ELONGATION (2.00 INCH GAGE)**
LT1	67.4	46.8	9.9
LT2	67.0	46.4	9.8
LT3	67/4	46.8	10.0
REQUIRED 1	N/A	N/A	N/A

NOTE 1 – QQ-A-250/5, “Aluminum Alloy Alcad 2024. Plate and Sheet”, for T3 sheet 0.063 to 0.128 inch thick

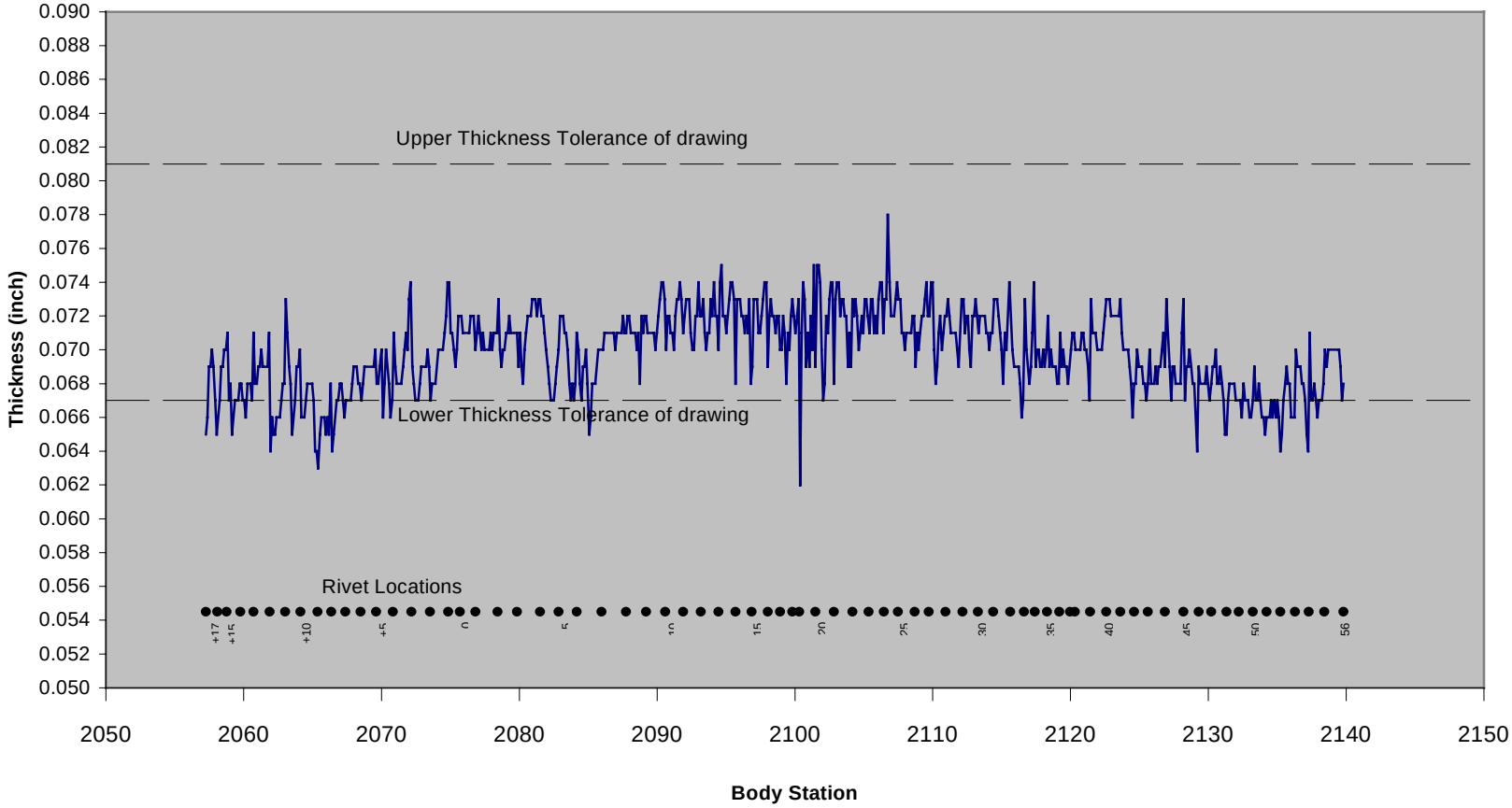

Figure 1.16-94 Thickness measurements taken along the fracture surface above S-49L.

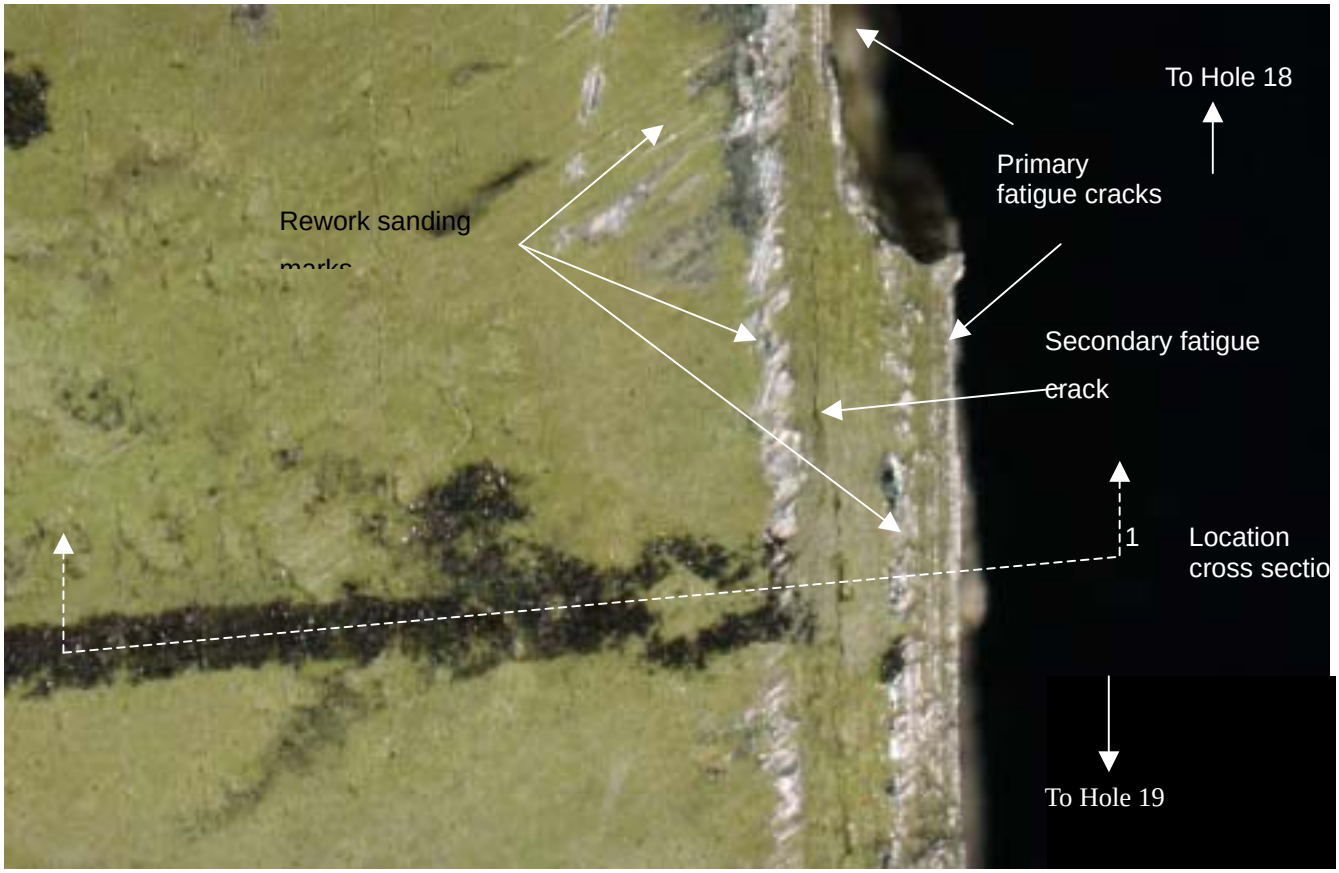

Figure 1.16-95 Location of cross section taken to characterize the scratch depth and geometry in the main fatigue region between holes 18 and 19.

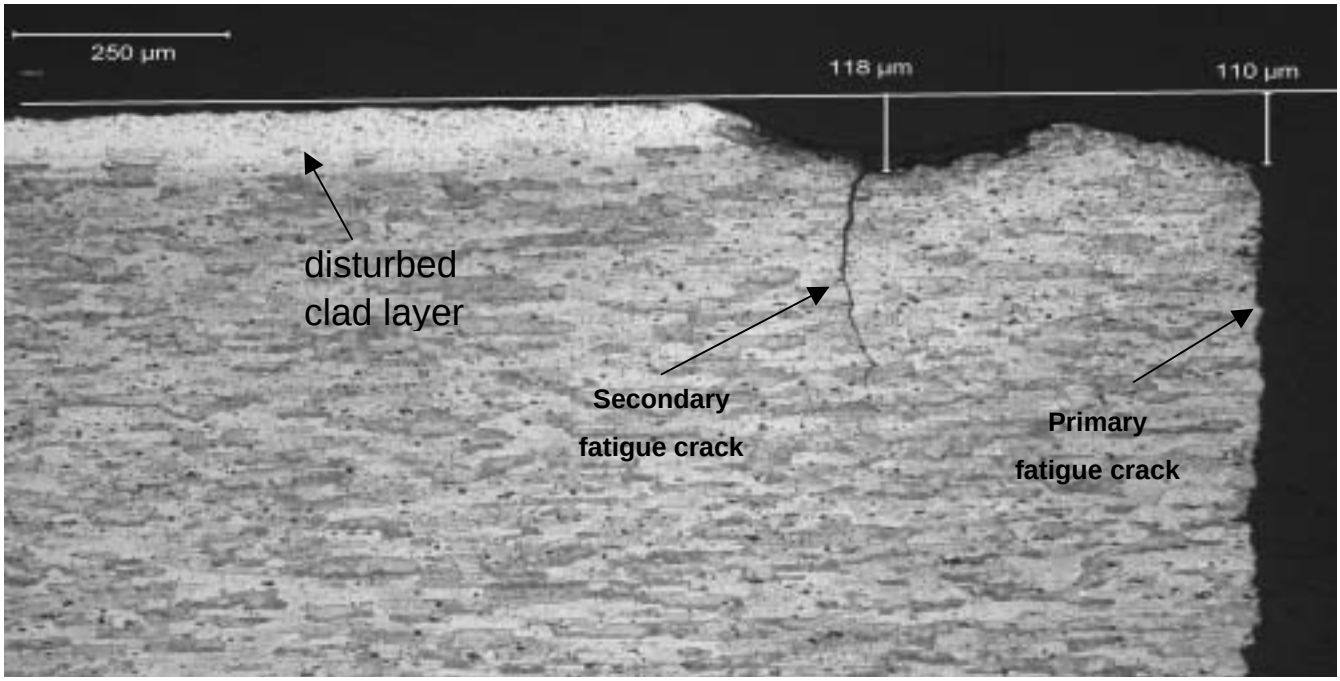

Figure 1.16-96 Metallographic specimen through the area indicated in Figure 1.16-73 above. The line shown was projected back to an area of undisturbed clad material to determine the depth of the scratches at the primary and secondary fatigue cracks present in this area.

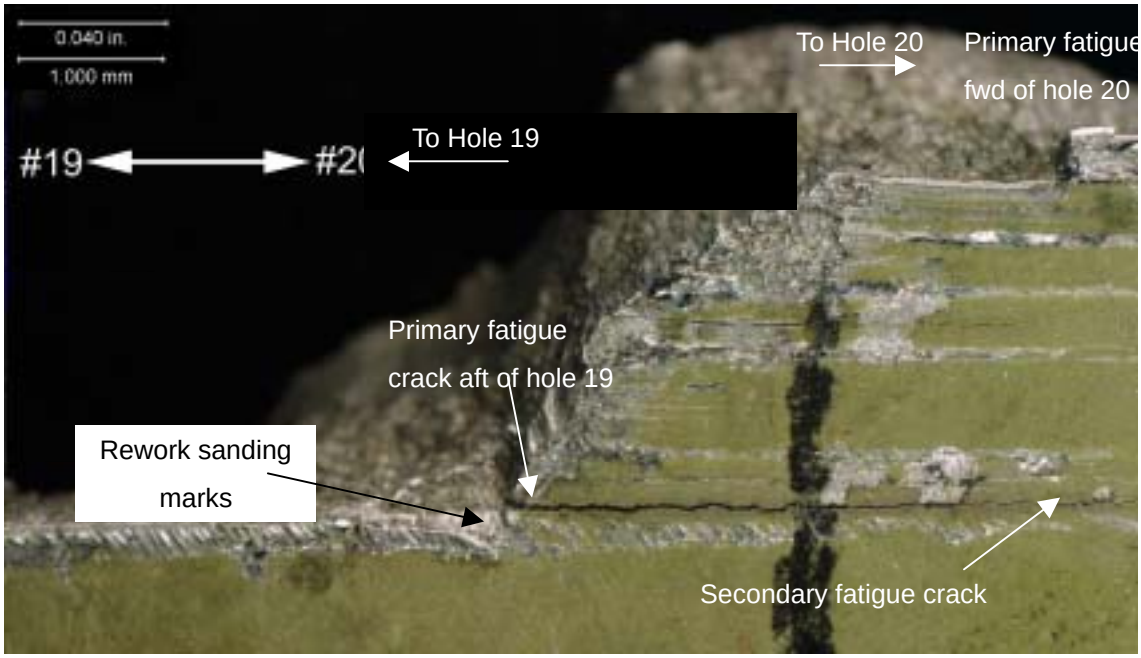

Figure 1.16-97 Location of cross section taken to characterize the scratch depth and in the main fatigue region between holes 19 and 20.

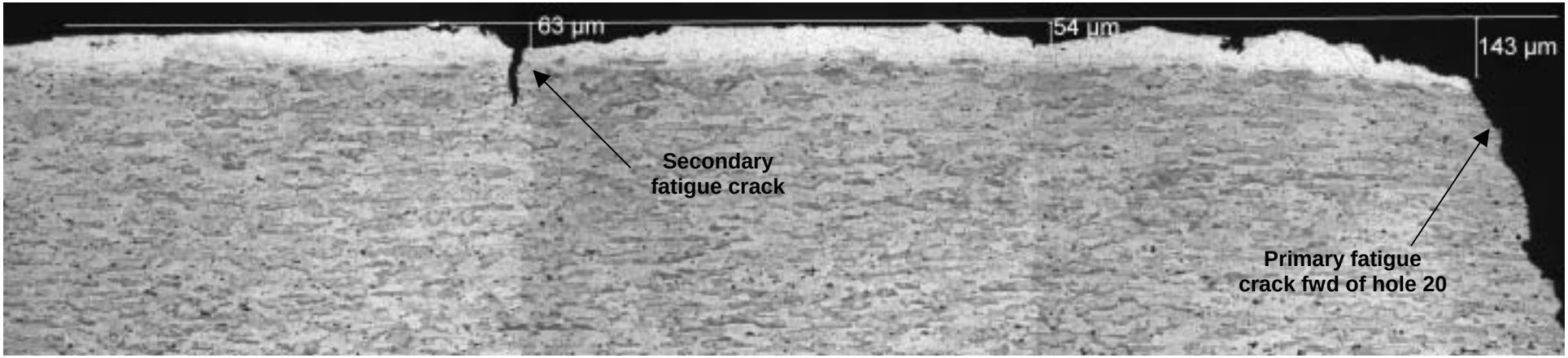

Figure 1.16-98 Metallographic montage through the area indicated in Figure 1.16-75 above. The line shown was projected back to an area of undisturbed clad material to determine the depth of the scratches at the primary and secondary fatigue cracks present in this area.

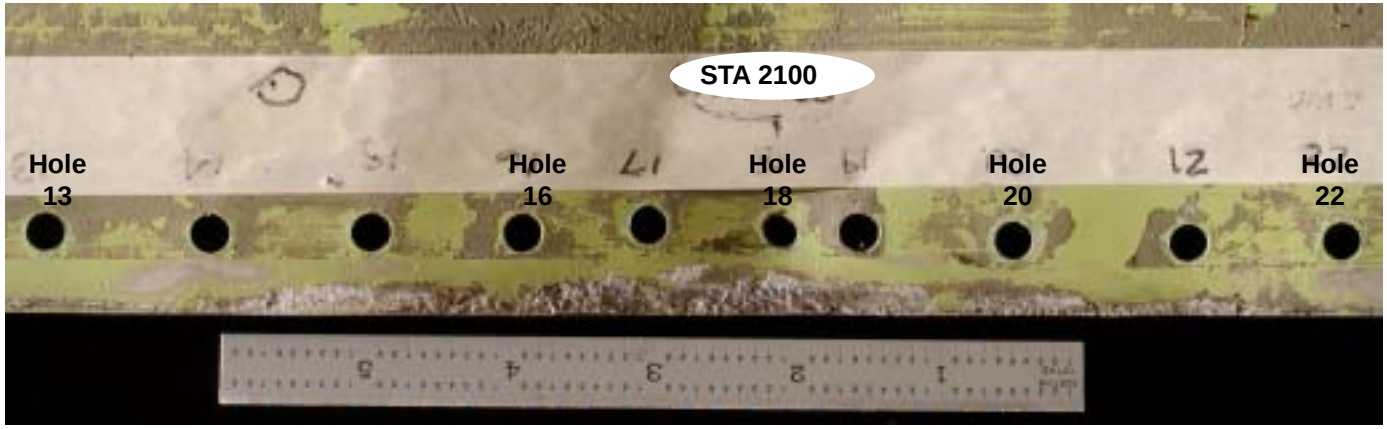

Figure 1.16-99 Faying surface of doubler with skin showing the light colored deposit present from hole 14 to 22

Figure 1.16-100 Higher magnification image of light colored deposit on faying surface of doubler in the vicinity of hole 15. Note the smooth bubbled appearance of the deposit adjacent to the edge of the doubler.

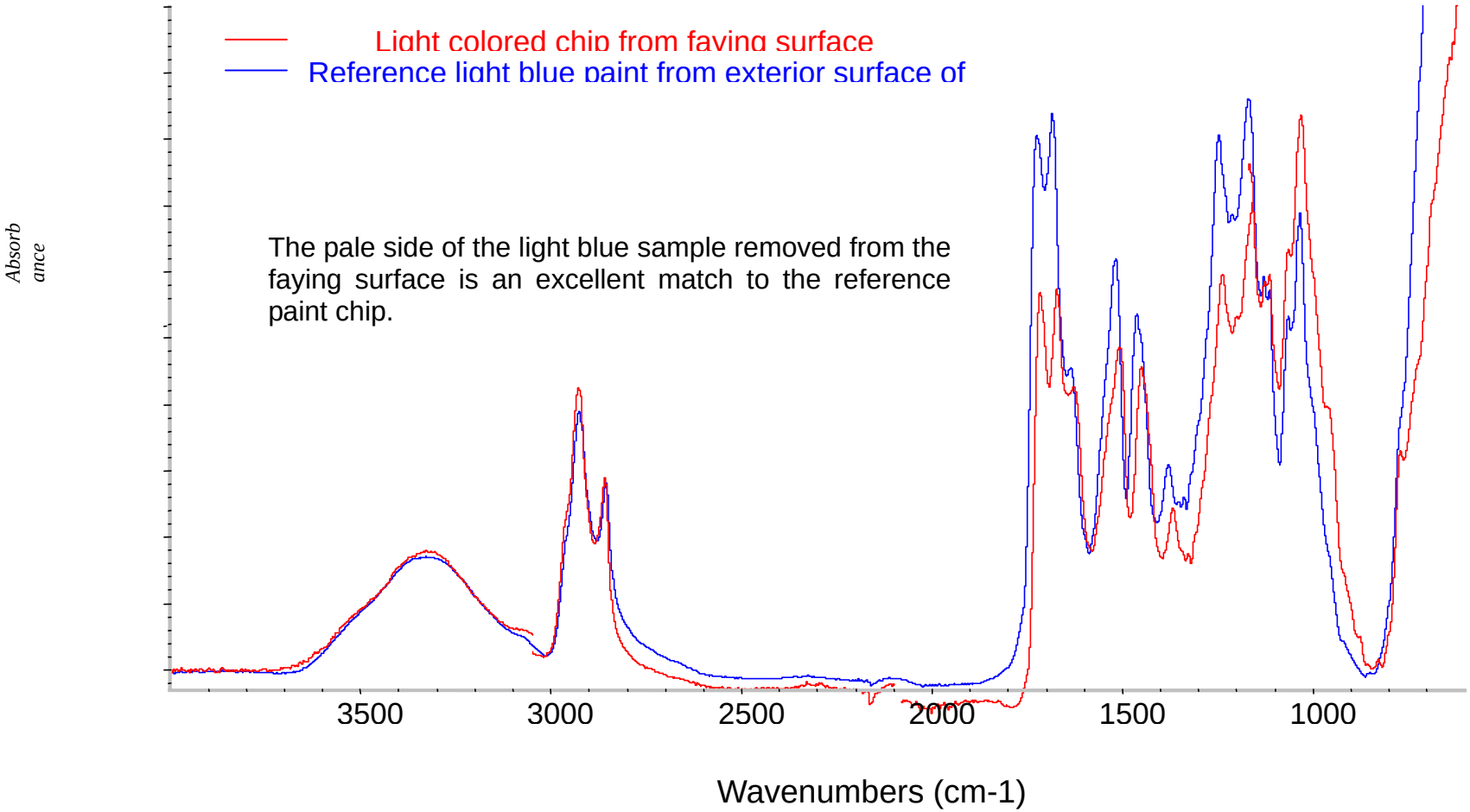

Figure 1.16-101 FT-IR analysis spectra of light colored material removed from overhanging portion of doubler faying surface adjacent to hole 18 and spectra from light blue exterior pain on the doubler. These spectra are baseline corrected and scaled to make an easier comparison.

Table 1.16-10 Degree and position of fretting damage present on overhanging portion of the faying surface of the repair doubler above the S-49L fracture surface.

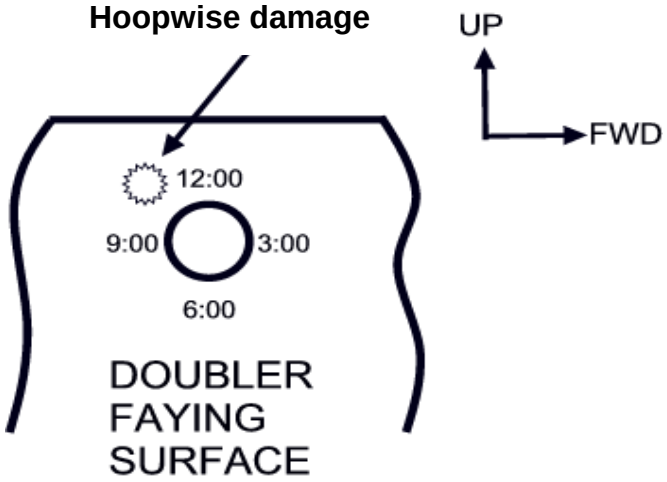

FASTENER HOLE	DEGREE OF DAMAGE	CLOCK POSITION OF FRETTING	FASTENER HOLE	DEGREE OF FRETTING	CLOCK POSITION OF FRETTING
+16	Minor	10:00	18	Minor	10:00 and 2:00
+15	Minor	9:00	19	Significant	10:00
+14	Minor	11:00	20	Minor	11:00
+13	Minor	10:00	22	Significant	10:00 to 2:00
+12	Minor	9:00 to 10:00	23	Minor	12:00
+11	Minor	10:00 and 1:00	25	Significant	10:00 to 2:00
+10	Minor	10:00 and 1:00	26	Significant	11:00 to 1:00
+9	Minor	10:00 and 1:00	27	Minor	12:00
+8	Minor	10:00 and 1:00 to 2:00	28	Significant	12:00 to 2:00
+7	Minor	10:00	29	Significant	12:00
+6	Minor	10:00 and 1:00	30	Significant	10:00 to 2:00
+4	Minor	2:00	32	Significant	10:00 to 2:00
+3	Minor	1:00	34	Significant	10:00 to 2:00
+2	Minor	1:00	35	Minor	2:00
0	Minor	10:00 and 2:00	36	Minor	2:00
1	Minor	12:00	37	Minor	1:00 to 2:00
6	Significant	10:00 to 11:00 and 12:00 to 1:00	38	Significant	10:00 to 2:00
7	Minor	12:00	39	Significant	12:00 to 3:00
8	Significant	10:00 to 1:00	41	Significant	10:00 to 12:00

9	Significant	10:00 to 12:00	42	Significant	10:00 to 2:00
10	Significant	11:00 to 1:00	43	Significant	10:00 and 12:00
11	Minor	12:00	44	Minor	1:00
12	Significant	10:00 to 2:00	46	Minor	2:00
14	Significant	10:00 to 2:00	47	Minor	2:00
15	Significant	10:00 to 2:00	49	Minor	1:00
16	Minor	2:00			

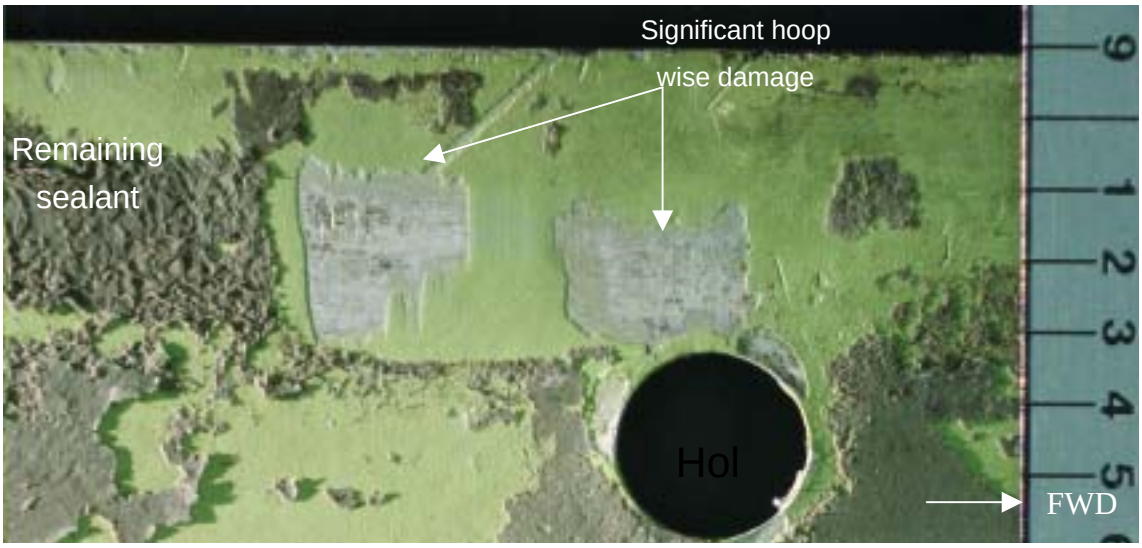

Figure 1.16-102 Faying surface of doubler in the vicinity of hole 6 showing an example of significant hoop wise damage at the 10:00 to 11:00 and 1:00 to 2:00 clock positions.

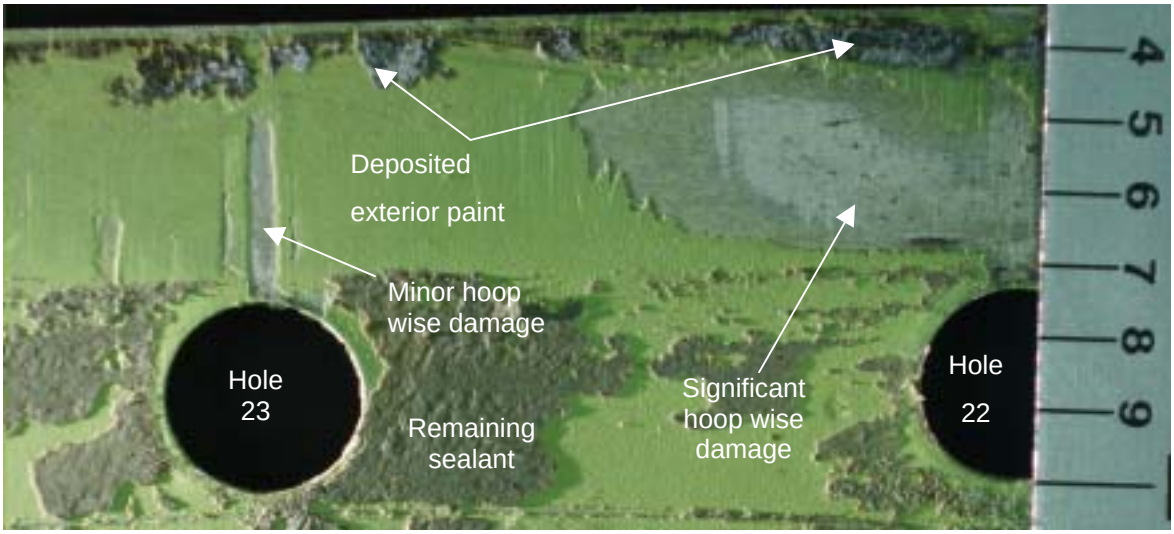

Figure 1.16-103 Faying surface of the doubler showing an example of minor hoop wise damage at the 12:00 clock position of hole 23 and significant hoop wise damage at the 10:00 to 12:00 clock position of hole 22. Note the presence of deposited paint near the edge of the doubler.

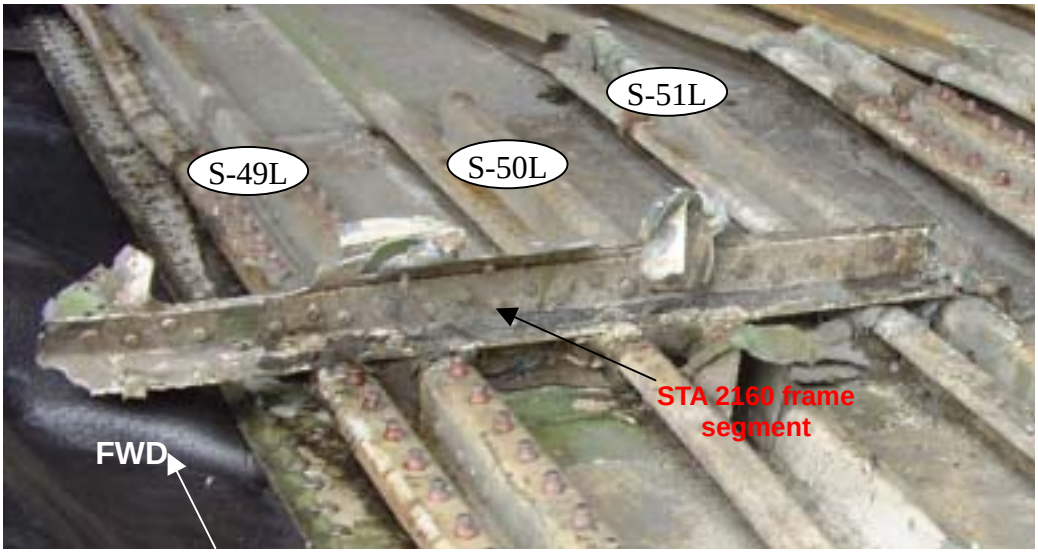

Figure 1.16-104 Condition of the STA 2160 frame segment prior to disassembly from the Item 640C1 skin panel at the CSIST.

Figure 1.16-105 As received condition of the STA 2160 frame segment submitted for examination. The aft surface is shown in this view.

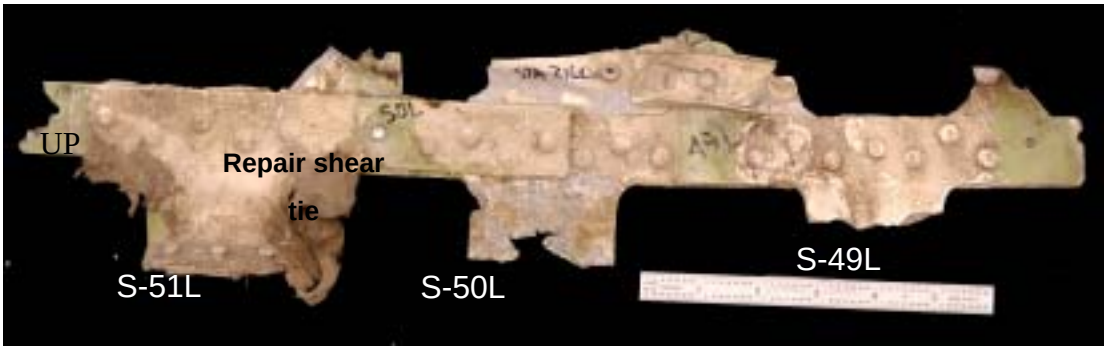

Figure 1.16-106 As received condition of the STA 2160 frame segment submitted for examination. The forward surface is shown in this view.

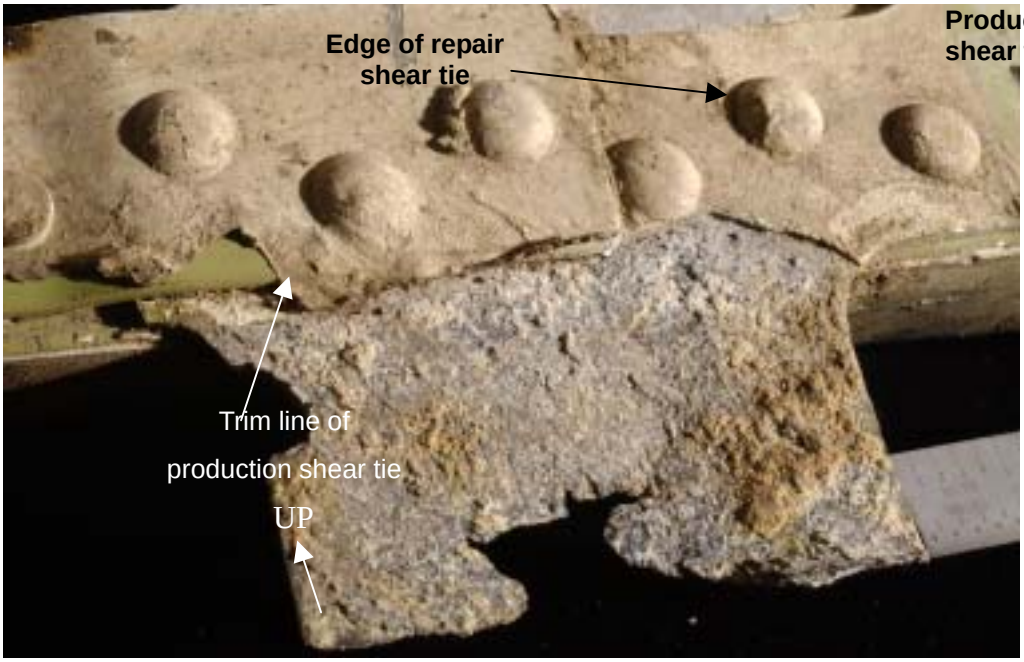

Figure 1.16-107 Exfoliation corrosion present at shear tie between S-50L and S-49L of STA 2160 frame segment.

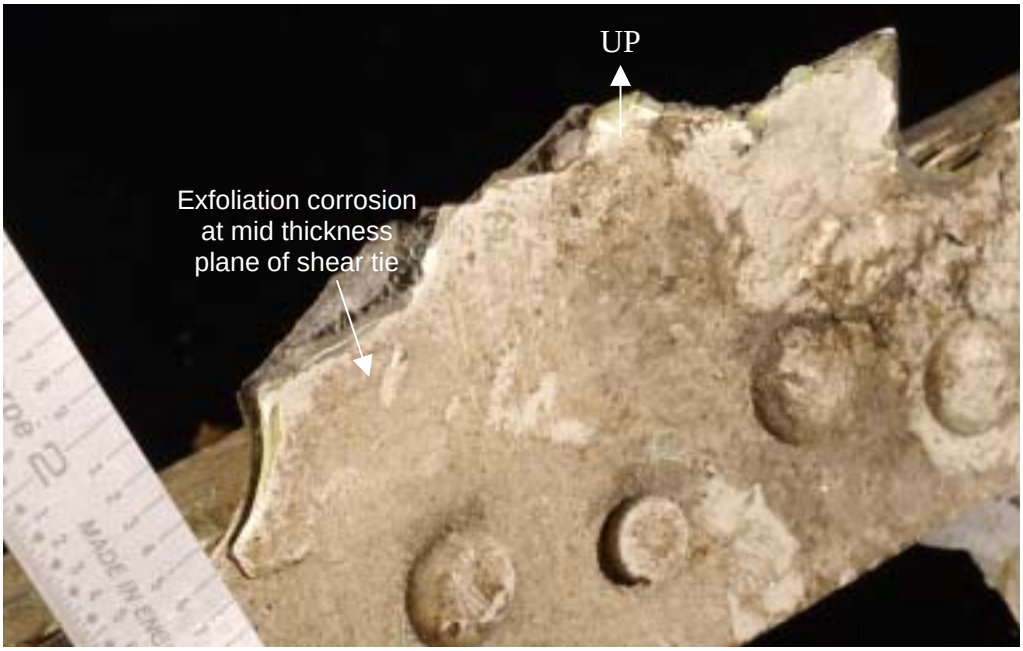

Figure 1.16-108 Exfoliation corrosion present at shear tie between S-49L and S-48L of STA 2160 frame segment.

Table 1.16-11 Spectrochemical analysis results

		Chemical Composition (Percent)									Confirmed Alloy
Frame	**Member**	**Zn**	**Mg**	**Cu**	**Cr**	**Fe**	**Si**	**Mn**	**Ti**	**Al**	
STA 2160	Shear Tie (repair)	0.14	1.49	4.46	0.02	0.22	0.09	0.62	0.01	remainder	2024
	Failsafte Chord	5.29	2.43	1.34	0.23	0.27	0.12	0.00	0.02	remainder	7075
STA 2100	Shear Tie	0.11	1.42	4.28	0.03	0.34	0.11	0.58	0.01	remainder	2024
	Inner Chord	5.60	2.31	1.34	0.22	0.26	0.18	0.03	0.04	remainder	7075
	Failsafe Chord	5.15	2.59	1.36	0.24	0.31	0.10	0.00	0.03	remainder	7075
STA 2060	Shear Tie	0.08	1.55	4.11	0.03	0.33	0.11	0.58	0.01	remainder	2024
	Failsafe Chord	5.55	2.56	1.43	0.23	0.24	0.12	0.00	0.01	remainder	7075
STA 2040	Shear Tie	0.22	1.36	3.87	0.02	0.29	0.10	0.56	0.02	remainder	2024
	Inner Chord	5.71	2.44	1.37	0.23	0.27	0.19	0.04	0.03	remainder	7075
	Failsafe Chord	5.29	2.50	1.35	0.22	0.25	0.11	0.00	0.01	remainder	7075
STA 1940	Shear Tie	0.07	1.68	4.10	0.03	0.34	0.11	0.63	0.01	remainder	2024
	Inner Chord	5.51	2.58	1.50	0.24	0.28	0.09	0.00	0.03	remainder	7075
	Failsafe Chord	5.44	2.62	1.50	0.25	0.31	0.15	0.06	0.02	remainder	7075
Countersunk Rivets for Repair Doubler		0.06	0.50	4.40	0.03	0.53	0.35	0.50	0.02	remainder	2017
		0.05	0.71	3.72	0.02	0.52	0.48	0.61	0.03	remainder	2017

	Chemical Composition (Percent)								
Material Specification Requirements	**Zn**	**Mg**	**Cu**	**Cr**	**Fe**	**Si**	**Mn**	**Ti**	**Al**
2024 Alloy per QQ-A-250/4	0.25 max	1.2 - 1.8	3.8 - 4.9	0.10 max	0.50 max	0.50 max	0.30- 0.09	0.15 max	remainder
7075 Alloy per QQ-A-200/11	5.1 to 6.1	2.1 - 2.9	1.2 - 2.0	0.18- 0.28	0.50 max	0.40 max	0.30 max	0.20 max	remainder
2017 Alloy per QQ-A-430	.25 max	0.40- 0.80	3.5 - 4.5	0.10 max	0.70 max	0.20 -0.80	0.40 - 0.80	0.15 max	remainder

Table 1.16-12 Temper inspection results for frame segments

Frame	Member	Average Hardness (Rockwell B)	Average Conductivity (%IACS)	Confirmed Alloy* & Temper
STA 2160	Shear Tie (repair)	74.0	30.3	2024-T4X
	Failsafe Chord	90.9	32.3	7075-T6XXX
STA 2100	Shear Tie	68.8	30.5	2024-T4X
	Inner Chord	90.1	32.1	7075-T6XXX
	Failsafe Chord	90.7	31.9	7075-T6XXX
STA 2060	Shear Tie	71.6	29.3	2024-T4X
	Failsafe Chord	92.0	31.8	7075-T6XXX
STA 2040	Shear Tie	71.0	30.1	2024-T4X
	Inner Chord	92.3	32.6	7075-T6XXX
	Failsafe Chord	90.8	32.6	7075-T6XXX
STA 1940	Shear Tie	69.0	30.8	2024-T4X
	Inner Chord	92.1	32.5	7075-T6XXX
	Failsafe Chord	90.8	31.0	7075-T6XXX

COUNTERSUNK REPAIR RIVETS

Rivet Number	Average Hardness (Rockwell B)	Average Conductivity (%IACS)	Confirmed Alloy* & Temper
E64	79.2	35.0	2117-T4XXX
D51	72.7	34.5	2117-T4XXX

BAC 5946 "Temper Inspection of Aluminum Alloys" Requirements	Hardness (Rockwell B)	Conductivity (%IACS)
2017-T4XXX	68 - 80	31.5 - 35.0
2024-T4X	63 - 83.5	28.5 - 32.0
7075-T6XXX	83.5 - 94	30.0 - 35.0

* See previous table for spectrochemical analysis results

Figure 1.16-109 As received condition of the STA 2100 frame segment submitted for examination. The aft surface is shown in this view.

Figure 1.16-110 As received condition of the STA 2100 frame segment submitted for examination. The forward surface is shown in this view.

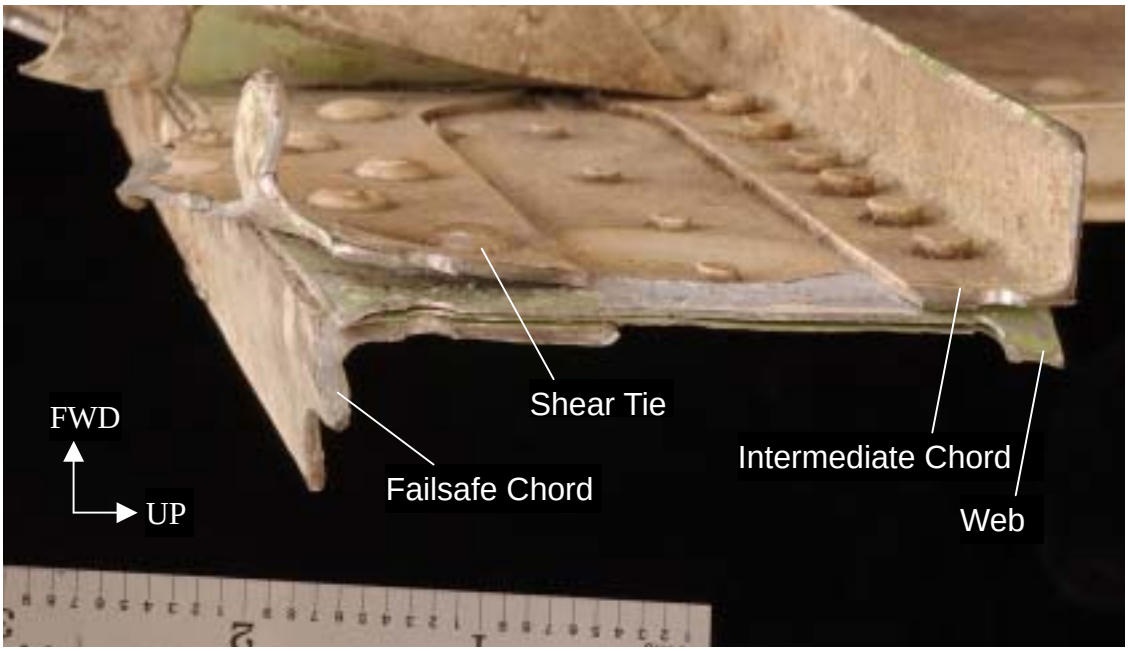

Figure 1.16-111 Fracture at S-49L of the STA 2100 frame segment showing deformation in shear tie and web.

Figure 1.16-112 Shear tie between S-51R and S-50R of the STA 2100 frame segment showing downward deformation in skin flange and pull through of the fastener hole at the inboard most fastener hole.

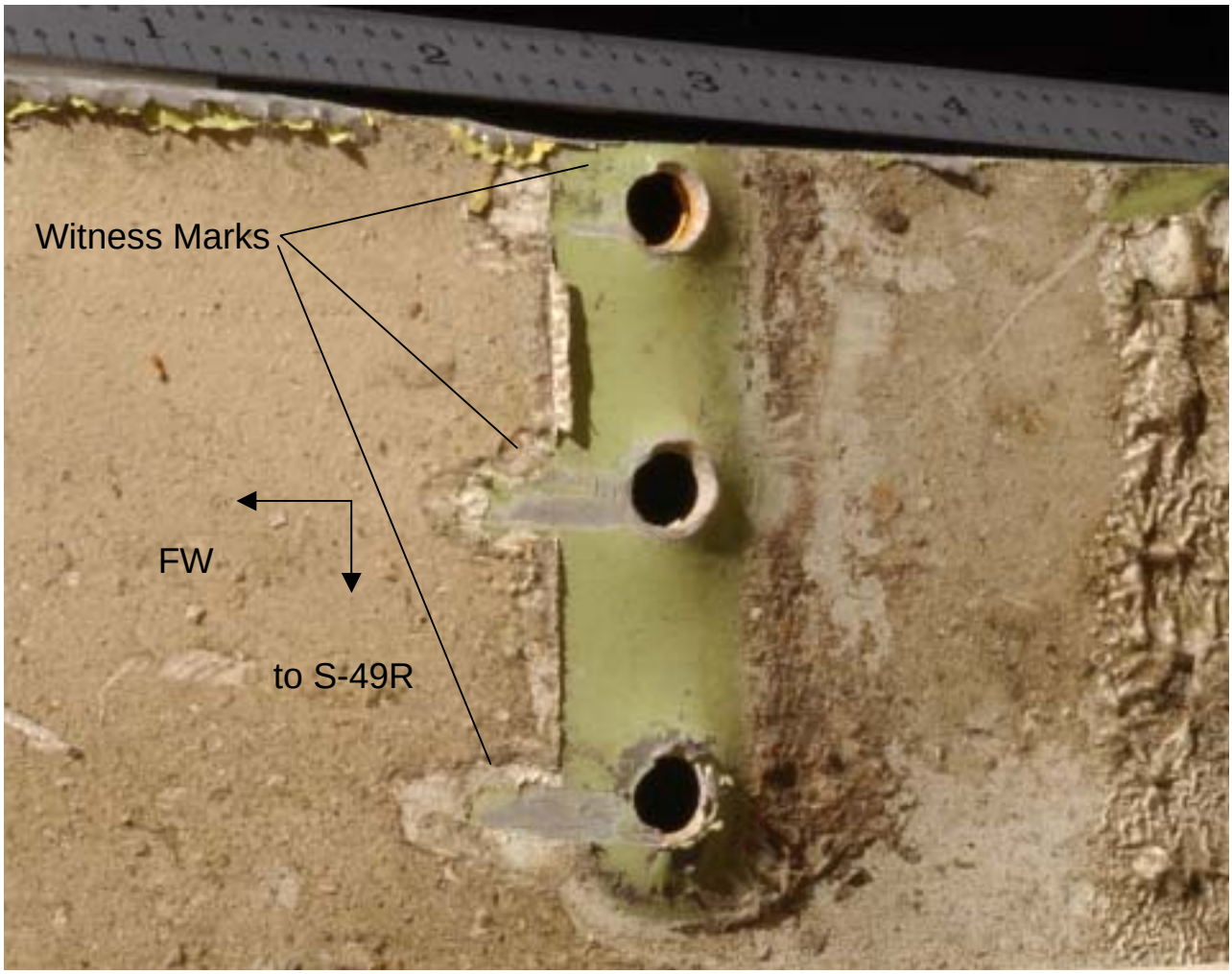

Figure 1.16-113 Witness marks and deformation in skin at shear tie fastener holes common to S-49R /S-48R at STA 2100

Figure 1.16-114 As received condition of the STA 2060 frame segment. The aft surface is shown in this view.

Figure 1.16-115 As received condition of the STA 2060 frame segment. The forward surface is shown in this view.

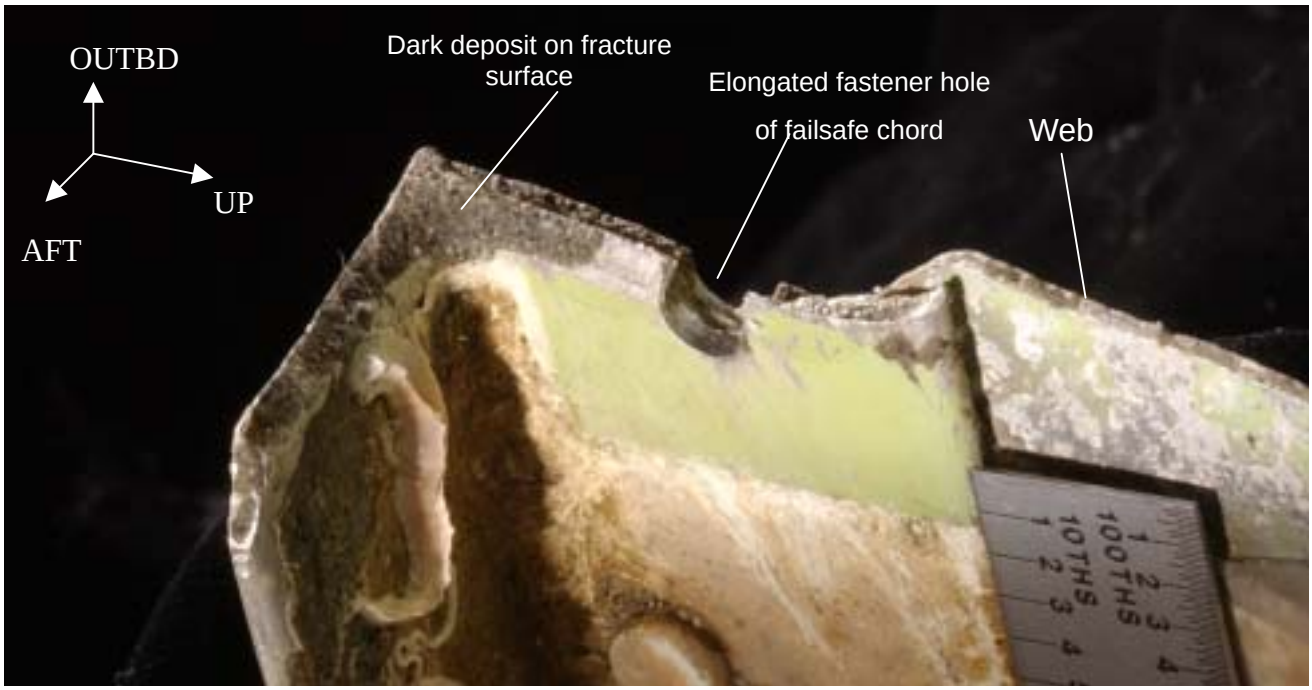

Figure 1.16-116 Fracture surface of failsafe chord and web common to S-49L of the STA 2060 frame segment.

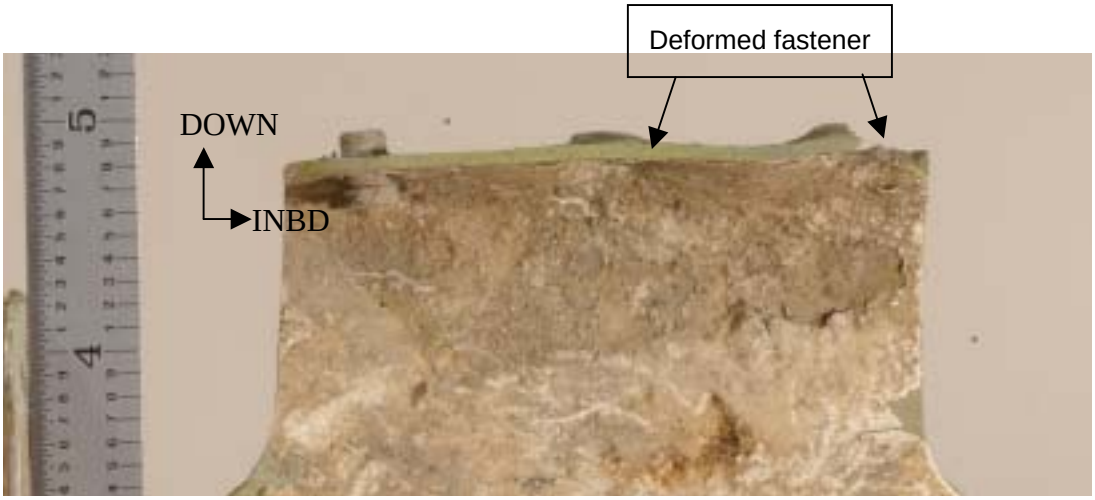

Figure 1.16-117 Shear tie between S-51L and S-50L of the STA 2060 frame segment showing deformation of skin flange fastener holes in the downward direction.

Figure 11.16-118 As received condition of the STA 2040 frame segment submitted for examination. The aft surface is shown.

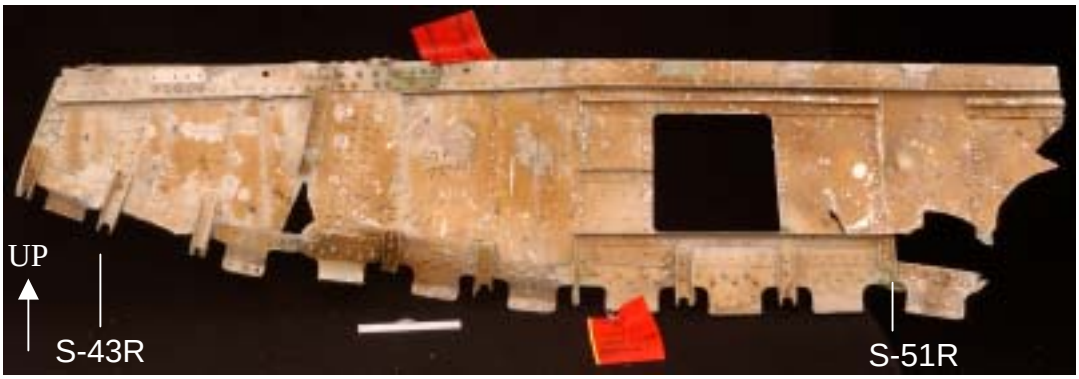

Figure 1.16-119 As received condition of the STA 2040 frame segment submitted for examination. The forward surface is shown in this view.

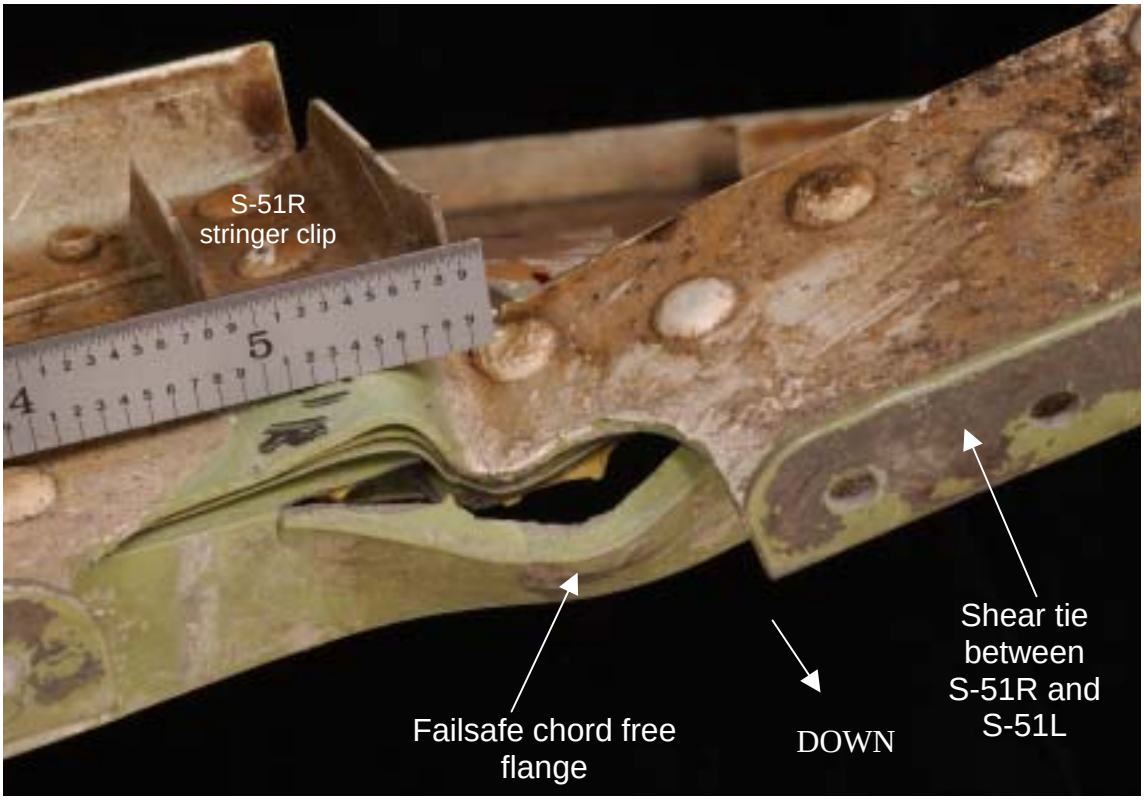

Figure 1.16-120 Fracture in failsafe chord free flange radius at S-51R of the STA 2040 frame segment.

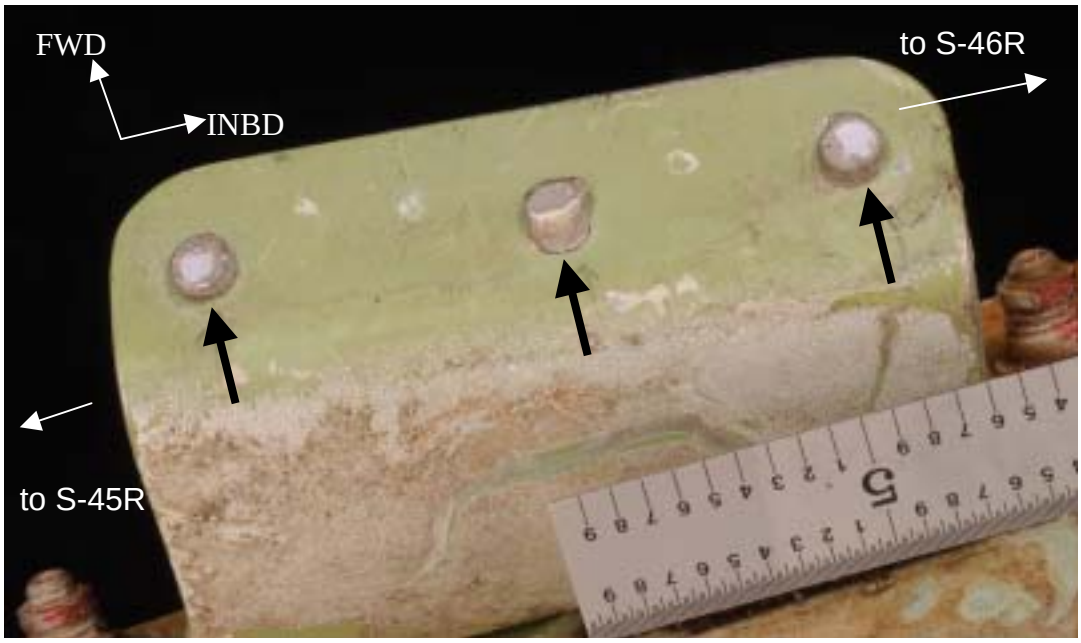

Figure 1.16-121.Skin flange rivet fractures at shear tie between S-45R and S-46R of the STA 2040 frame. Black arrows indicate the direction of loading.

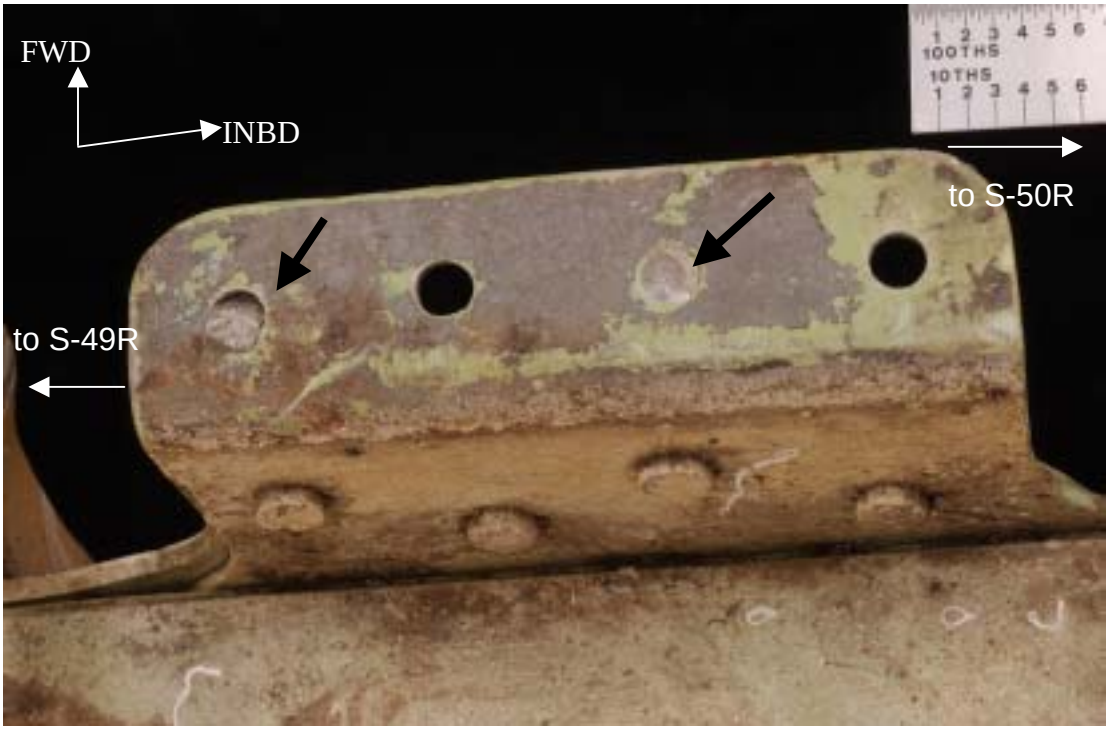

Figure 1.16-122 Skin flange rivet fractures at shear tie between S-49R and S-50R of the STA 2040 frame segment. Black arrows indicate the direction of loading.

Figure 1.16-123 As received condition of the STA 1940 frame segment submitted for examination. The aft surface is shown in this view.

Figure 1.16-124 As received condition of STA 1940 frame segment submitted for examination. The forward surface is shown in this view.

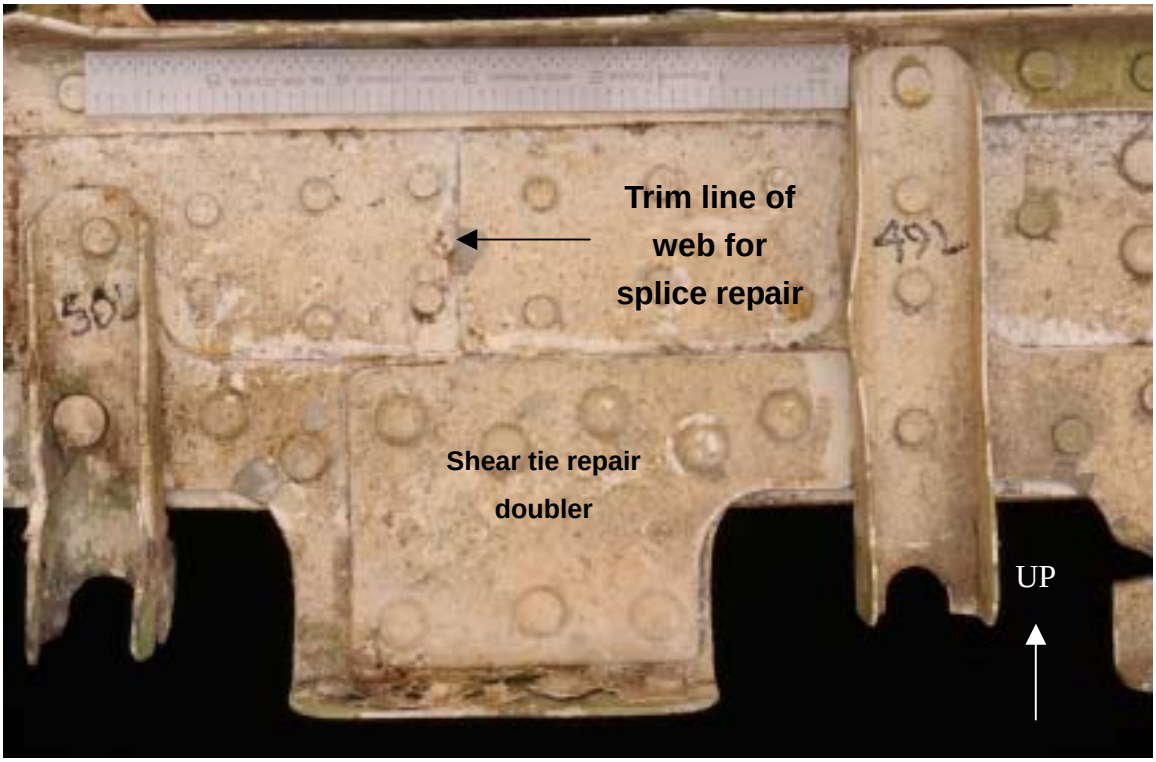

Figure 1.16-125 STA 1940 frame segment showing the shear tie repair doubler and web splice repair at the location between S-50L and S-49L.

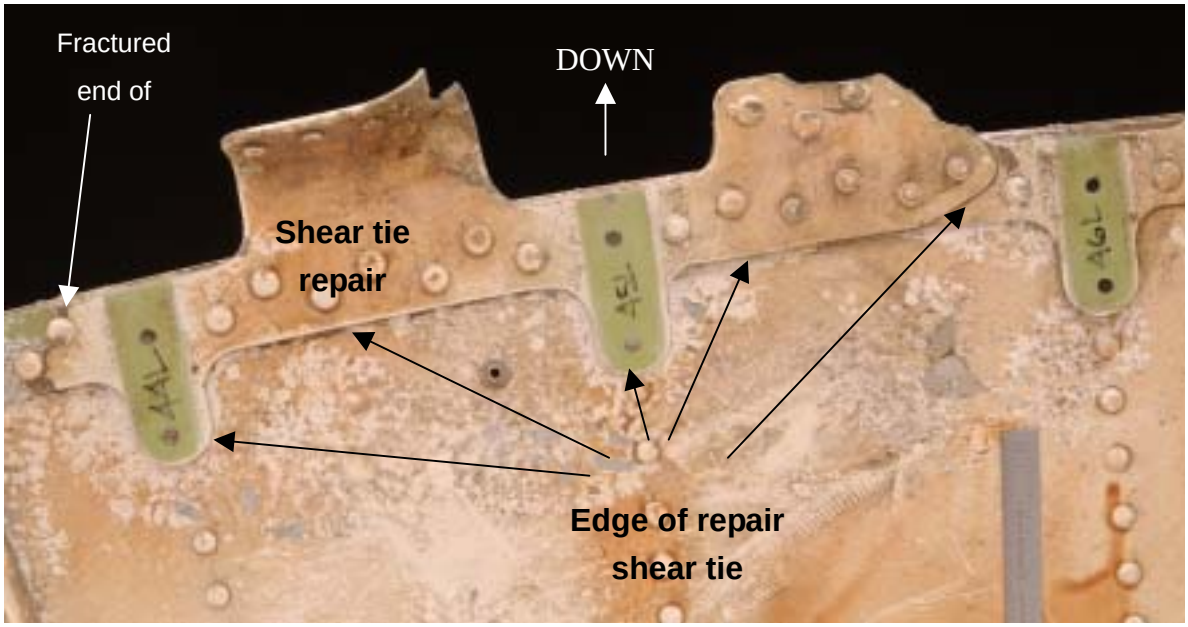

Figure 1.16-126 STA 1940 frame segment showing the shear tie repair between S-46L and S-44L.

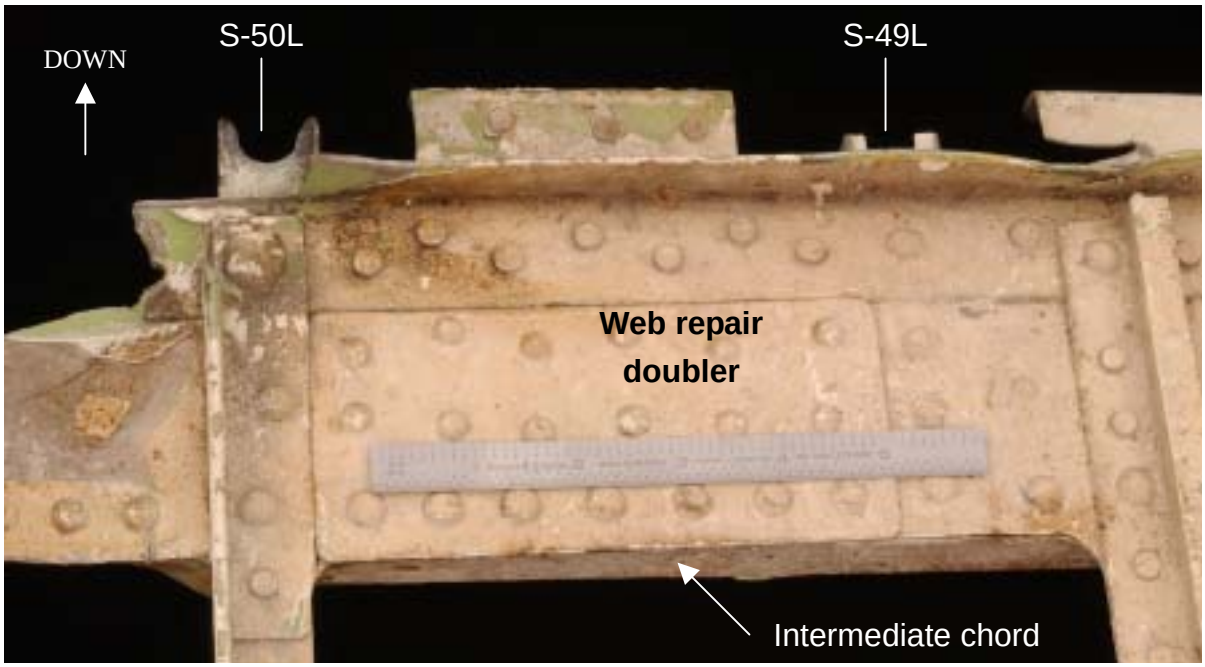

Figure 1.16-127 STA 1940 frame segment showing the web repair doubler on the aft side between S-50L and S-49L.

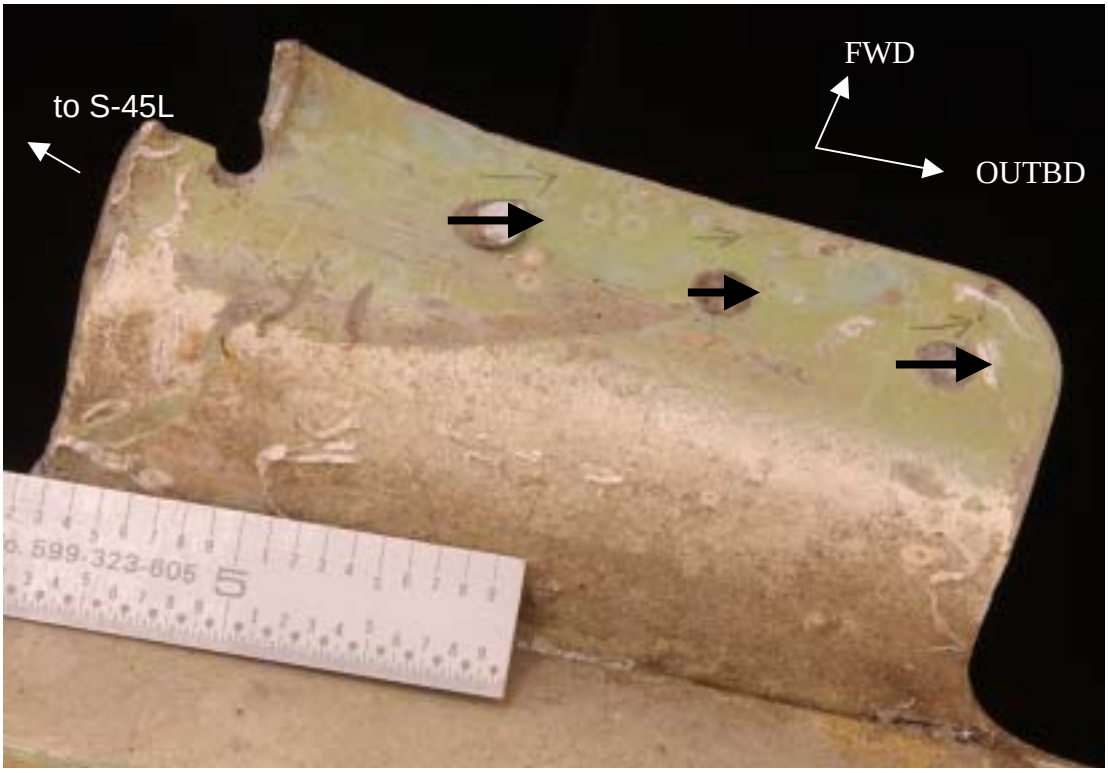

Figure 1.16-128 Shear tie between S-45L and S-44L of STA 1940 frame segment. Black arrows indicate the direction of loading.

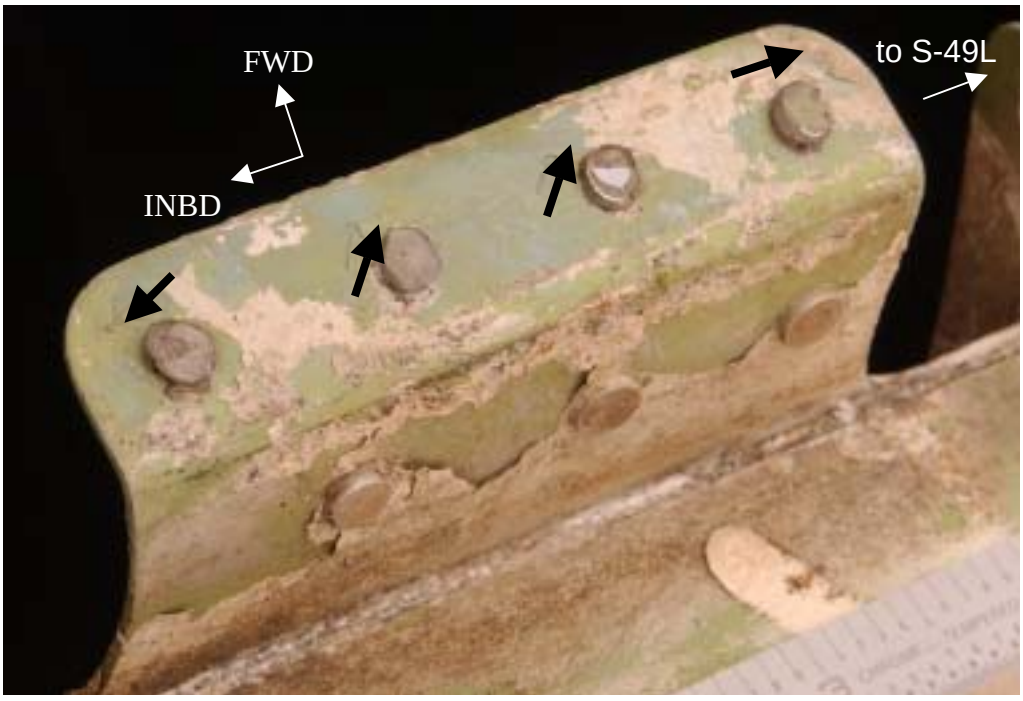

Figure 1.16-129 Shear tie between S-50L and S-49L of STA 1940 frame segment. Black arrows indicate the direction of loading.

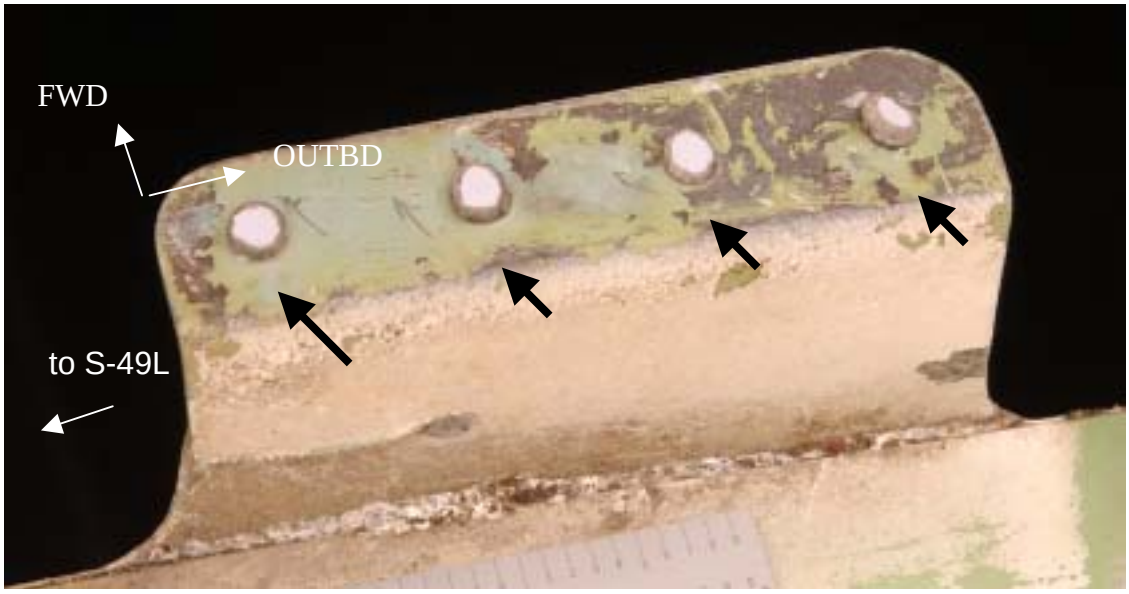

Figure 1.16-130 Shear tie between S-49L and S-48L of STA 1940 frame segment. Black arrows indicate the direction of loading.

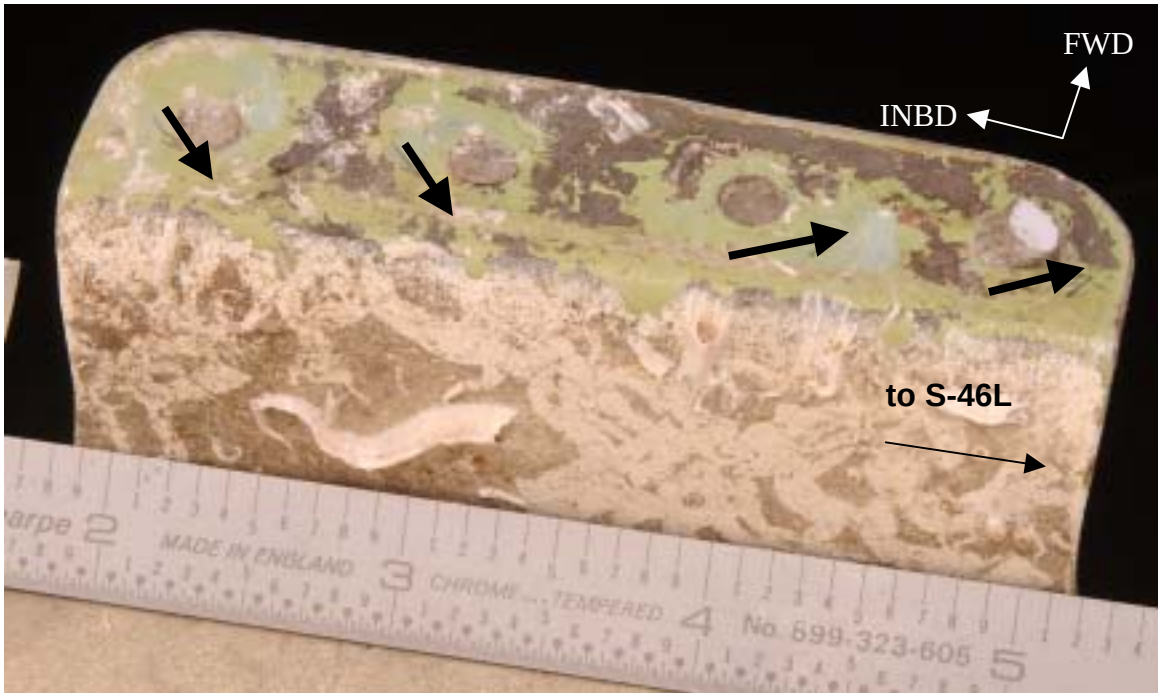

Figure 1.16-131 Shear tie between S-47L and S-46L of STA 1940 frame segment. Black arrows indicate the direction of loading.

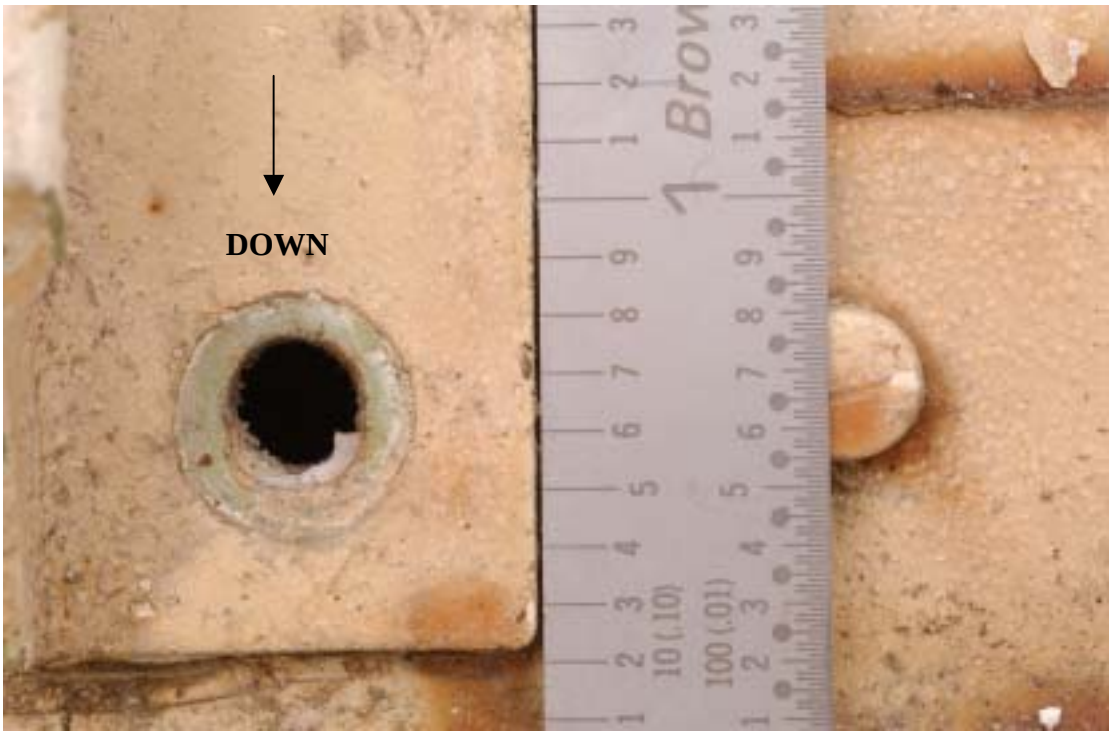

Figure 1.16-132 FWD view of STA 1940 frame segment showing downward deformation of the lower attachment hole of shear tie at S-47L clip.

1.16.3.2 Item 626 tested by CSIST

Background

One failed part of ITEM 626C1 of flight No. CI-611 was fractured. The failed part was submitted by Aviation Safety Council (ASC) to Aero Materials Department for conducting dimensional measurement and examination of corrosion pit in order to gather all the evidences and make a final judgment for the incident.

Results

(1) Macro Observation and photograph Figure 1.16-133 showed that the overall appearance of item 626 C1, there are 6 corrosion pits as arrows indicate. Those initial site of corrosion evidences were occurred at the interface of sealant and splice plate as in Figure 1.16-134 through Figure 1.16-138. It is believed that this is typical of morphology of crevice corrosion as in Figure 1.16-134 through Figure 1.16-138.

(2) Dimensional measurement and examination of corrosion pit Figure 1.16-139 through Figure 1.16-143 showed that the higher magnification of corrosion pit after cleaning by acetone and steel ruler, which were taken from area #1 through #5 as in Figure 1.16-133, respectively. The corrosion was not observed by 6X magnifier to extend under the splice plate, therefore no further inspection was required. Figure 1.16-144 through Figure 1.16-148 showed that the dimensional measurement of corrosion, which were taken from area #1 through #5 as in Figure 1.16-139 through Figure 1.16-143, respectively.

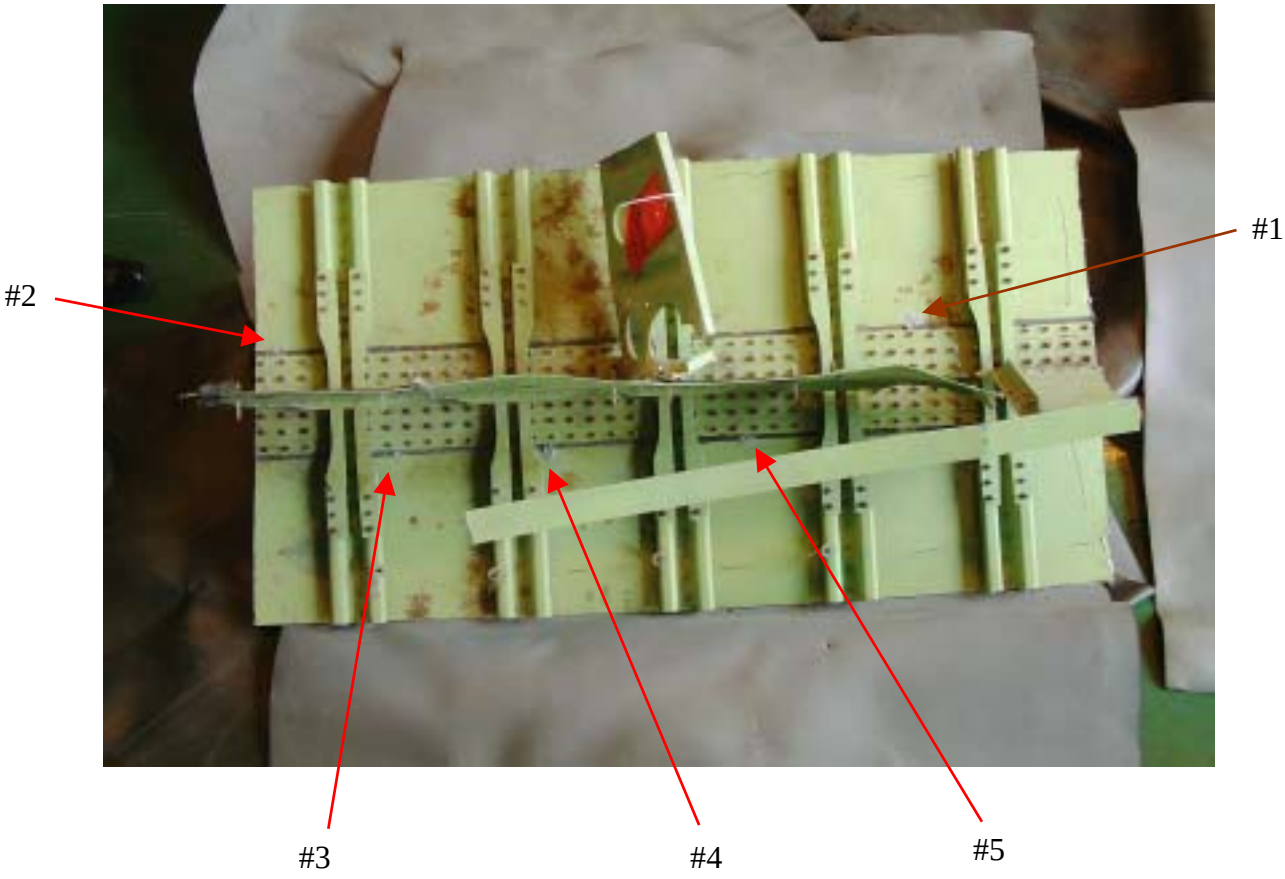

Figure 1.16-133 Overall appearance of ITEM 626 C1.(0.09X)

Figure 1.16-134 Higher magnification of #1 corrosion pit, before cleaning (0.71X)

Figure 1.16-135 Higher magnification of #2 corrosion pit, before cleaning (1.52X)

Figure 1.16-136 Higher magnification of #3 corrosion pit, before cleaning (1.56X)

Figure 1.16-137 Higher magnification of #4 corrosion pit, before cleaning (1.27X)

Figure 1.16-138 Higher magnification of #5 corrosion pit, before cleaning (1.46X)

Figure 1.16-139 Higher magnification of #1 corrosion pit, after cleaning (0.99X)

Figure 1.16-140 Higher magnification of #2 corrosion pit, after cleaning (1.40X)

Figure 1.16-141 Higher magnification of #3 corrosion pit, after cleaning (1.73X)

Figure 1.16-142 Higher magnification of #4 corrosion pit, after cleaning (1.22X)

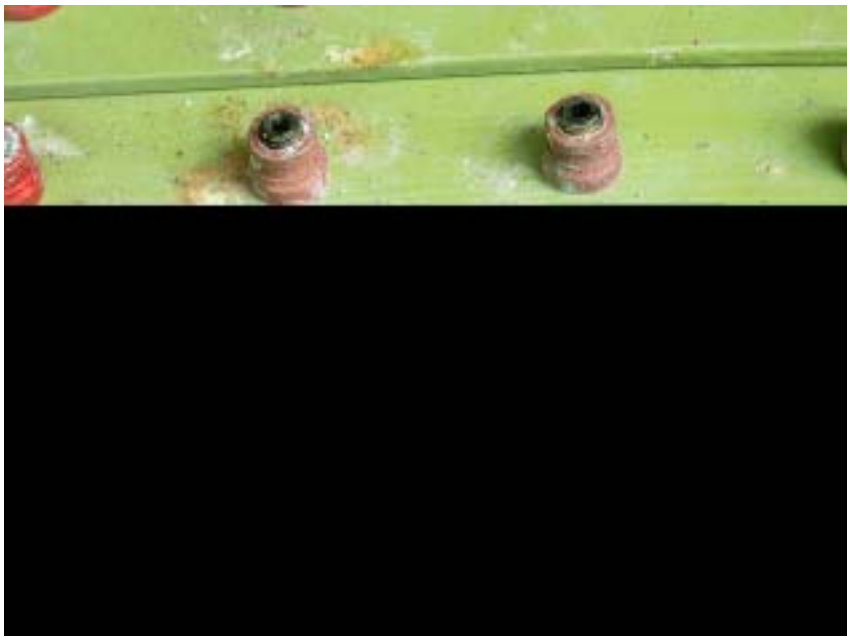

Figure 1.16-143 Higher magnification of #5 corrosion pit, after cleaning (1.44X)

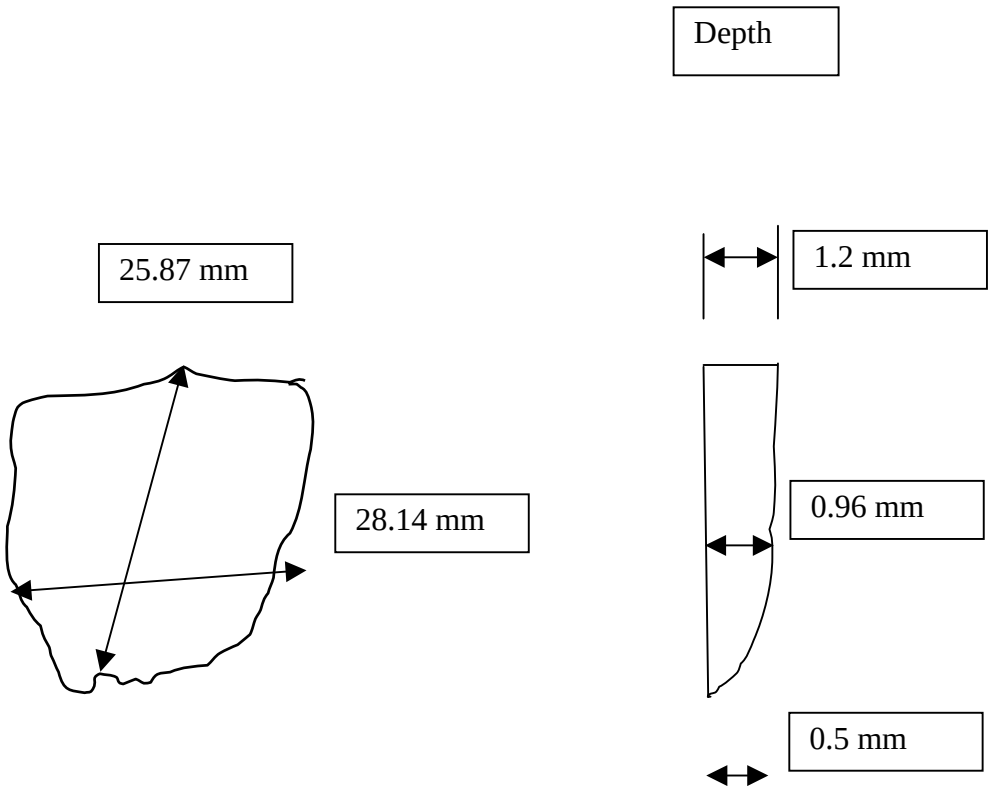

Figure 1.16-144 Sketch of #1 corrosion pit dimensional measurement.

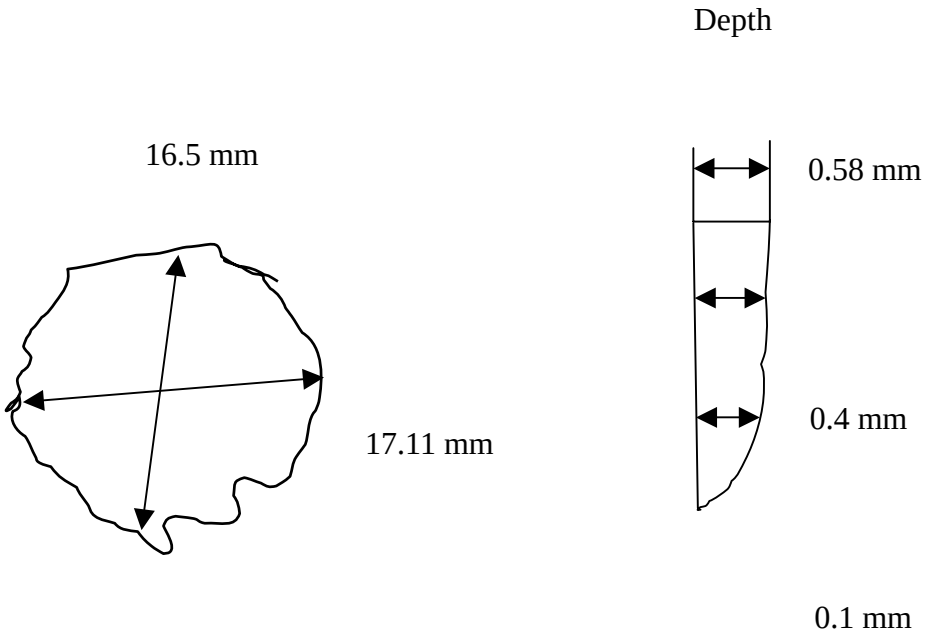

Figure 1.16-145 Sketch of #2 corrosion pit dimensional measurement.

The depth of corrosion pit on
left hand site can’t measure.

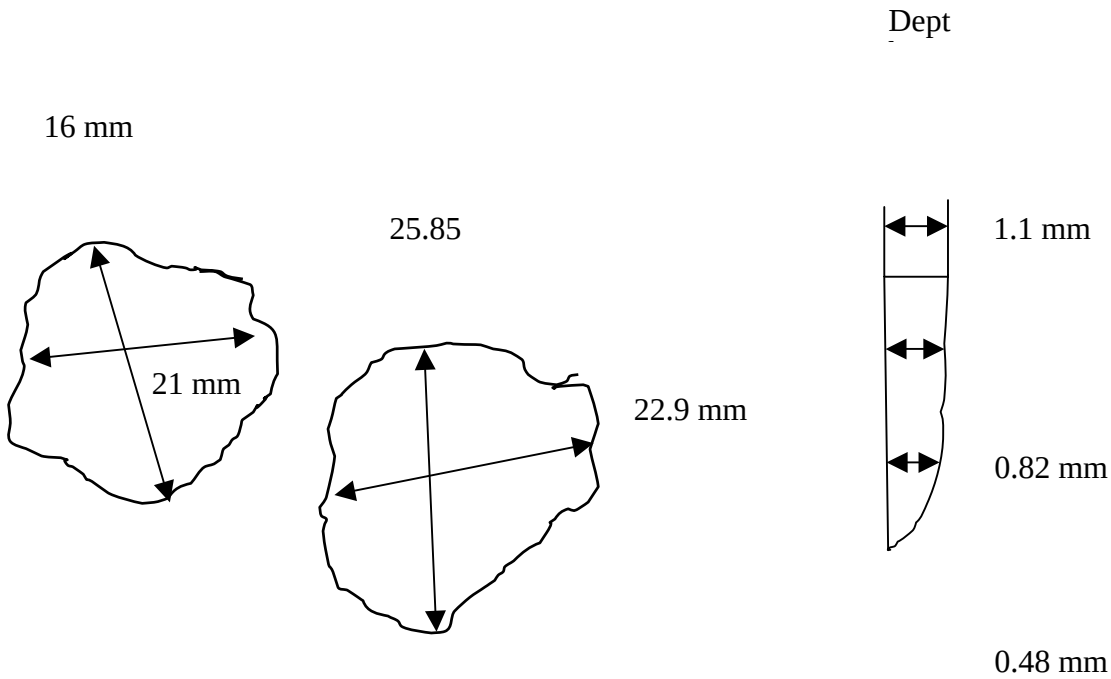

Figure 1.16-146 Sketch of #3 corrosion pit dimensional measurement.

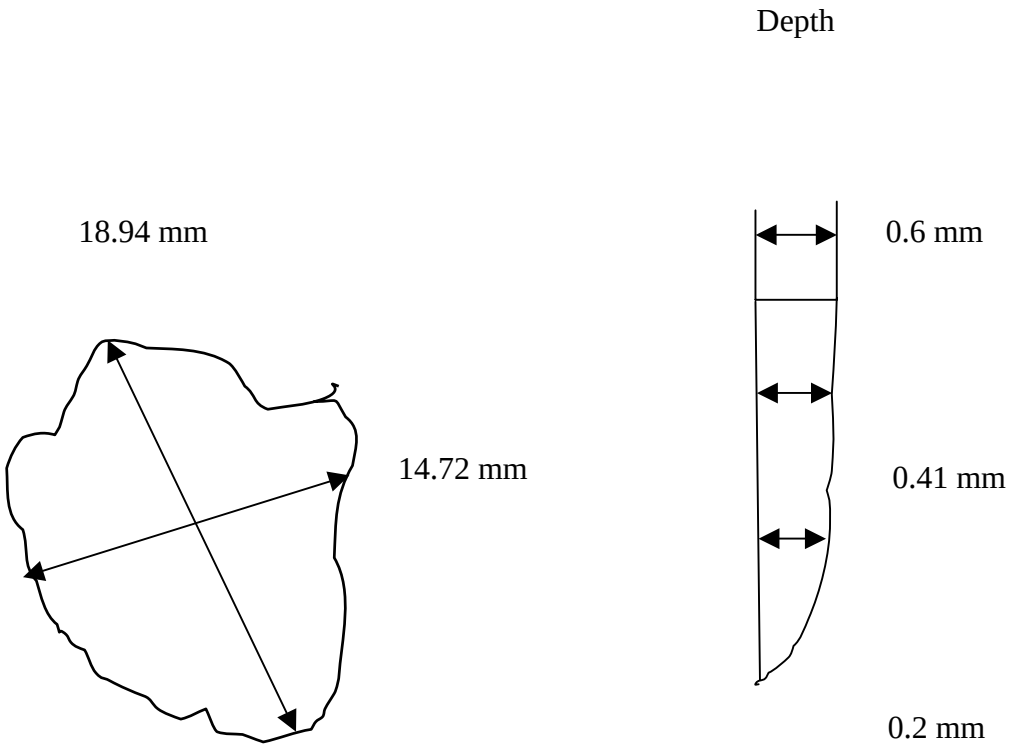

Figure 1.16-147 Sketch of #4 corrosion pit dimensional measurement.

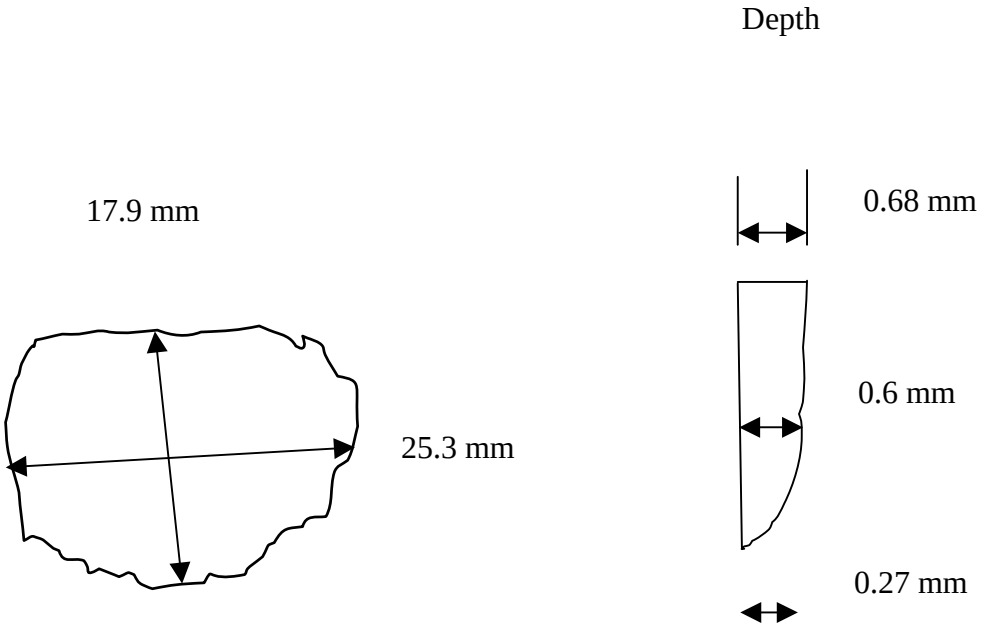

Figure 1.16-148 Sketch of #5 corrosion pit dimensional measurement.

1.16.3.3 Item 751 tested by CSIST

Background

One failed part of #5 LH entry door, ITEM 751 of flight No. CI-611, was fractured. The failed part was submitted by Aviation Safety Council (ASC) to Aero Materials Department for conducting examination and analysis on fracture surface in order to gather all the evidences and make a final judgment for the incident.

ITEM 751

- FUSELAGE SKIN
- #5 LH ENTRY DOOR
- STA 2120 2230
- 1S-25L-S-17L

ITEM 751 C1

- DOOR REVEAL
- STA 2190 2240
- S-16L-S23L

Results

(1) Macro Observation and photograph

Figure 1.16-149 showed that the overall appearance of #5 LH entry door and basically the fractography can be divided into three examination focuses, No. A revealed the examination of the fractured door reveal, No. B revealed the examination of patch, and No. C revealed 5 different crack evidences caused by impact stress (torn) as arrows indicate in Figure 1.16-149. The fractured door reveal has two fractographys, one is upper fractography (Figure 1.16-150) and the other is lower fractography (Figure 1.16-151). Some suspicious fatigue evidences were found in macro examination on left hand side of the upper fractography and it need to do the further inspection and analysis in next paragraph. Fractography of lower door reveal as in Figure 1.16-151 showed

that the fractured surface was at about 45 ° slant to the maximum tensile stress and it means the typical overload fractography of soft metal and no further inspection was required. Only 4 rivets left and patch was deformed as shown in figure 4. Figure 1.16-152 revealed that the bonding rivet was disappeared and both of the aluminum alloy sheet and rivet were torn apart as arrow indicates.

(2) Fractographic examination on fracture surface of door reveal

The fractography of upper door reveal was composed of 3 parts which were upper (UP)、left (LH)，and right (RH) as shown in figure 2, respectively. The fractography of upper (UP) and right (RH) of the upper fractography as in figure 2 showed that the fracture plane was at about 45 ° slant to the maximum tensile stress. It means the typical overload fractography of soft metal and no further inspection was required. Fractographic examination (fracture surface was covered with severe corrosion) of LH of upper door reveal (Figure 1.16-150) was performed by 6X magnifier and the results were shown in Figure 1.16-153. Fracture surface can be divided into two zones, one is more flatness and the other is more roughness. Fracture surface exhibiting beach marks (more flat plane、light color , and covers about 48% of the fracture surface) indicate that cracking was initiated and propagated by fatigue until an overload stage was reached. The critical crack length was about 0.95 inches as measured from free edge of left hand side of the extrusion part to the extend of fatigue crack and which was described more detailed in Figure 1.16-154, and also it was about 0.62 inches as measured from the center of the fastener hole of the extrusion part to the extent of fatigue crack. The color of final-fracture region, more rough plane, looked more dark and the final-fracture region covered about 52% of the fracture surface and it was at about 45 ° slant to the maximum tensile stress. That’s the characteristic of typical overload fractography of soft metal.

(3) Fractographic examination on patch (doubler)

Four rivets were removed out by using handy grinder to disassemble the patch and then measured its dimension. The patch’s dimension of length、width、thickness were 5.053 ” X 4.146 ” X 0.032 ” 0.033 ”, respectively. Fractography of door reveal where under the patch as in Figure 1.16-155 showed that the fracture surface was at about 45 ° slant to the maximum tensile stress and it means the characteristic of typical overload fractography of soft metal and no further inspection was required.

(4) Chemical composition analysis by EDS (Energy Dispersive Spectrum) for door reveal and patch

The material of door reveal (LH) was determined to be 7075 aluminum alloy by EDS analysis and analysis results were listed in Table 1.16-13. The material of patch was determined to be 17-7 PH stainless steel by EDS analysis and analysis results were listed in Table 1.16-14. The material of patch also has magnetism response by a magnet.

(5) Metallography、conductivity and Hardness testing

Metallographic examination of door reveal as in Figure 1.16-156 and compare to ASM handbook volume 9, it is believed that this is typical of microstructure of 7075-T6 Aluminum alloy. The actual average hardness reading was 82.8 HRB and it conforms to AMS-H-6088 specification requirements.(7075-T6≧78 HRB) The conductivity testing results of door reveal were described as follows, 【UP】 are 32.8 IACS、32.4 IACS；【LH】are 31.6 IACS、31.4 IACS, and 【RH】 are 32.1 IACS、32.2 IACS, respectively. Those conductivity results conform to AMS-H-6088 specification requirements.(conductivity of 7075-T6 at 30.5 36.0 IACS) The Boeing company's engineer said that the material and heat treatment condition was 7075-T6511.

Metallographic examination of patch as in Figure 1.16-157 and compare to ASM handbook volume 9, it is believed that this is typical of microstructure of 17-7 Stainless steel with solution treated and precipitation hardened to 177ksi (39HRC). The actual average hardness reading was 39 HRC (converted from 391 H_k) and it conforms to AMS 5528 specification requirements.(hardness of 17-7 with ST+PH at 38 46HRC, approximately tensile strength shall be 150ksi minimum)

(6) SEM examination for failure mode determination

Figure 1.16-158 and 159 showed that SEM photographs of upper door reveal(LH), which were taken from area A and B as in figure 6, respectively. Fracture surface as described above was covered with severe corrosion so that we can't perform any further inspection by SEM. Figure 1.16-160 showed that the lower magnification of SEM photograph of upper door reveal (LH), which was taken from suspicious fatigue fracture area as in Figure 1.16-154. Corroded residues, light-colored spot, were also occurred on the fracture surface as in Figure 1.16-160 and the features cannot be observed clearly. Figure 1.16-161 and 1.16-162 showed that the typical fatigue fractography of

upper door reveal (LH), striations as arrows indicate, which were taken from area D and E as in Figure 1.16-154, respectively. The typical overload fractography of upper door reveal(LH), dimple structure, cannot be observed due to severe corrosion.

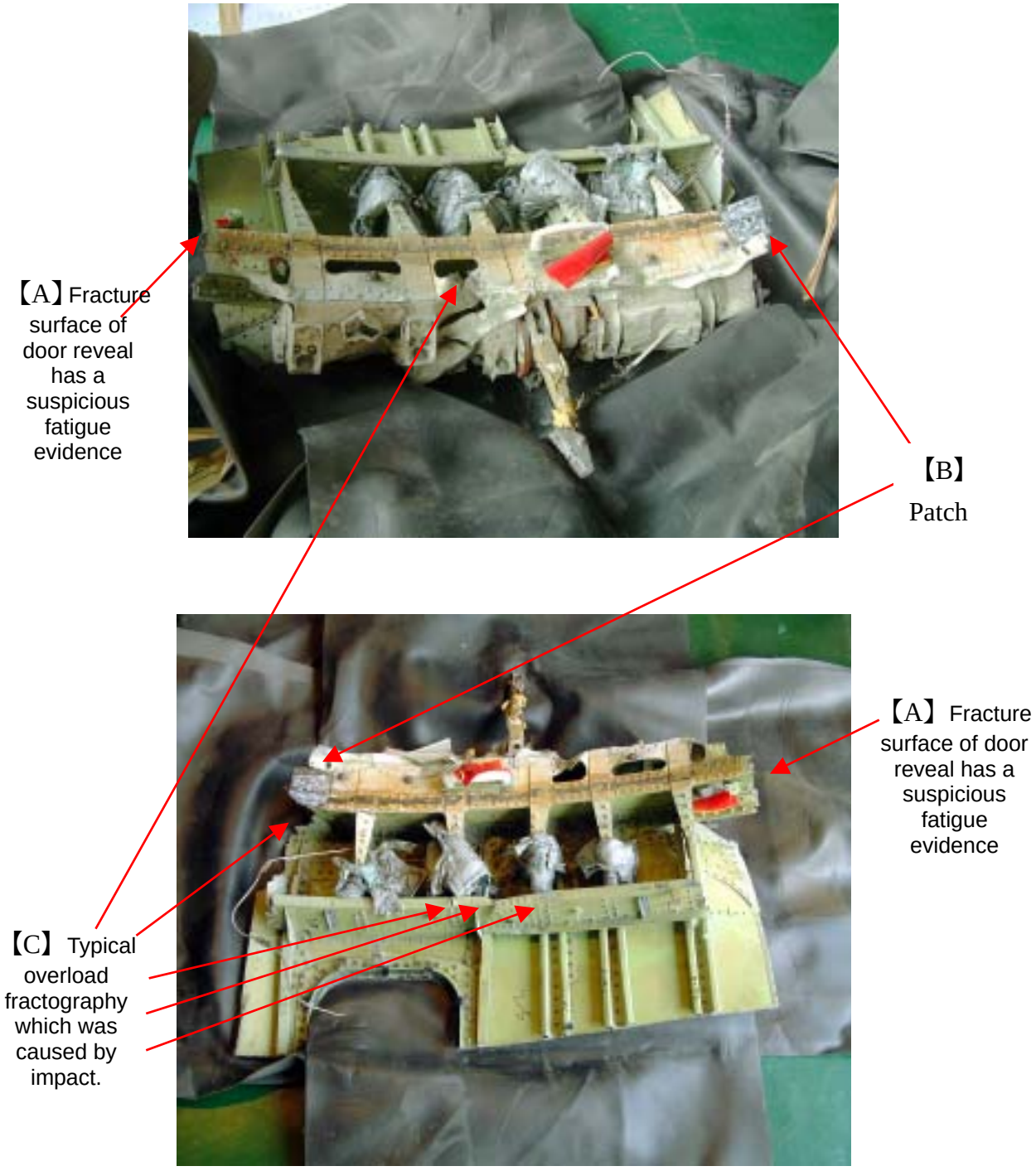

Figure 1.16-149 Overall appearance, ITEM 751,of #5 LH door reveal.

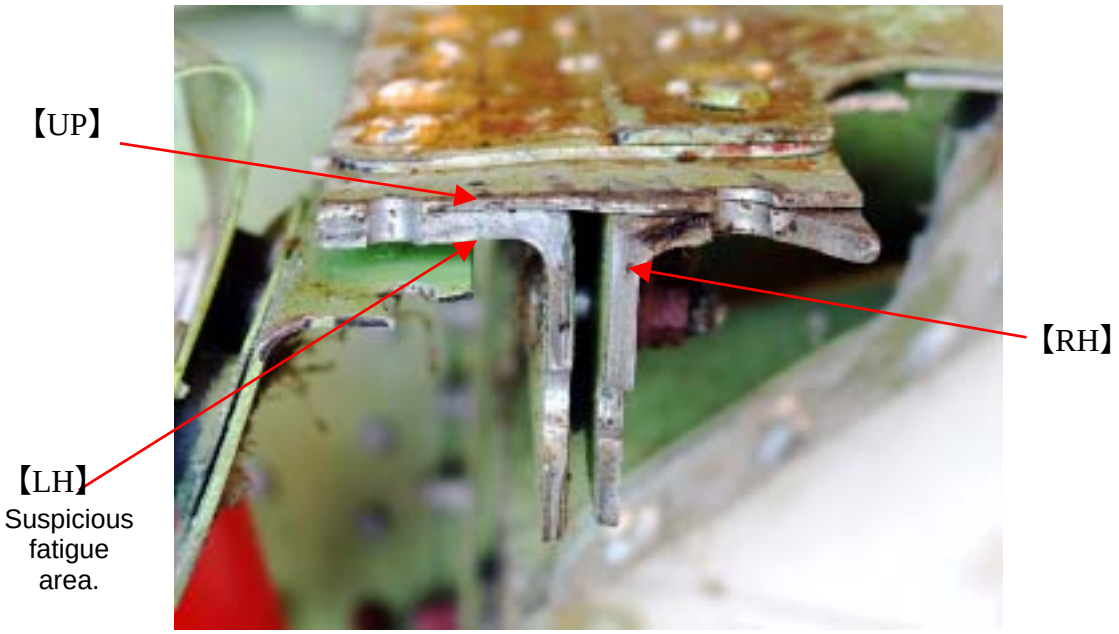

Figure 1.16-150 Macro fractographic examination of upper door reveal.(1.5X)

Figure 1.16-151 Macro fractographic examination of lower door reveal (1.53X)

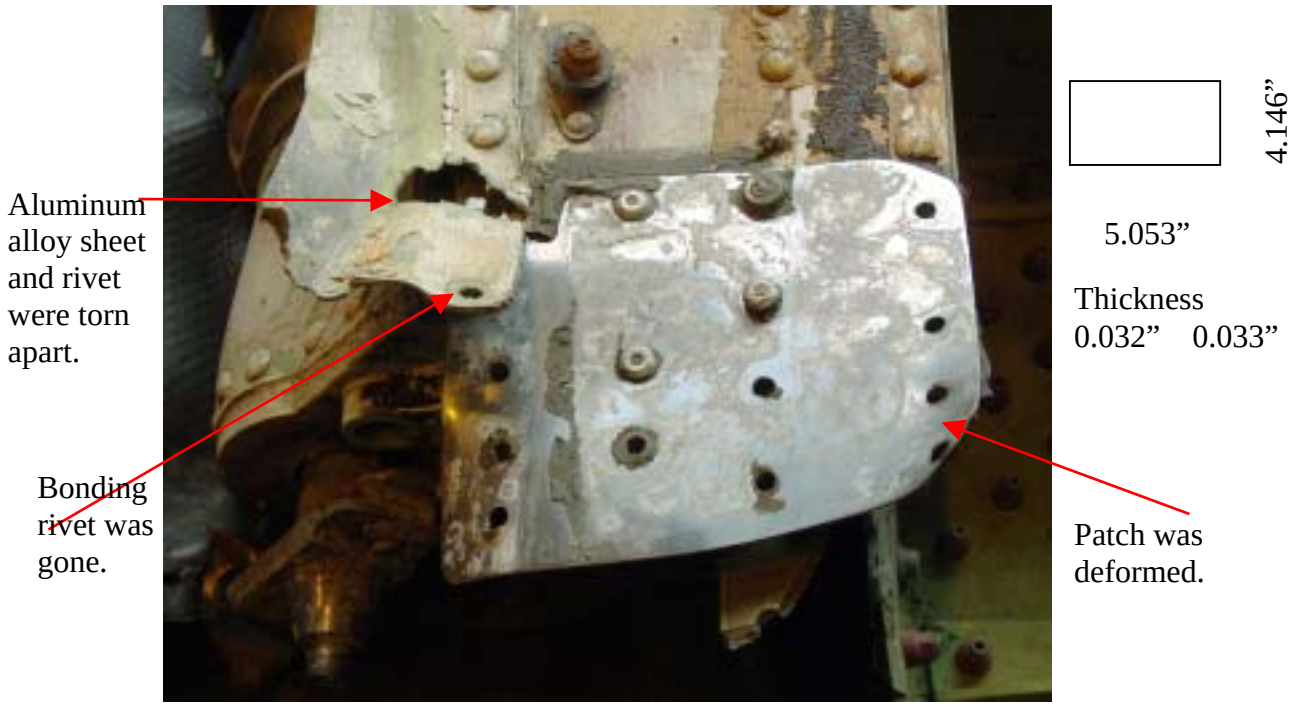

Figure 1.16-152 Higher magnification of patch which was located at the opposite side of the door reveal.(0.46X)

Figure 1.16-153 Macro examination of Left fractography as in figure 2.(2.3X)

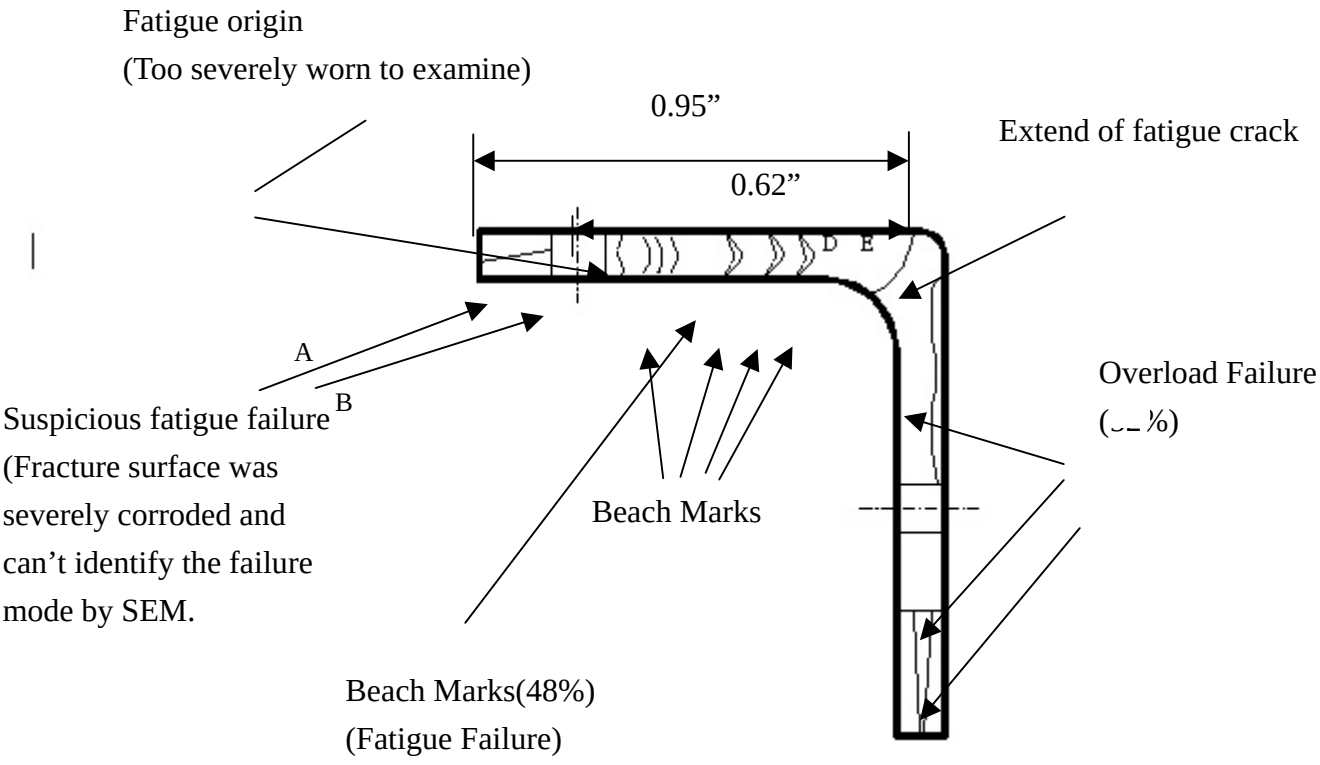

Figure 1.16-154 Sketch of Left fractography as in figure 1.16-150.

Figure 1.16-155 Macro examination of the fractography down below the patch.(0.53X)

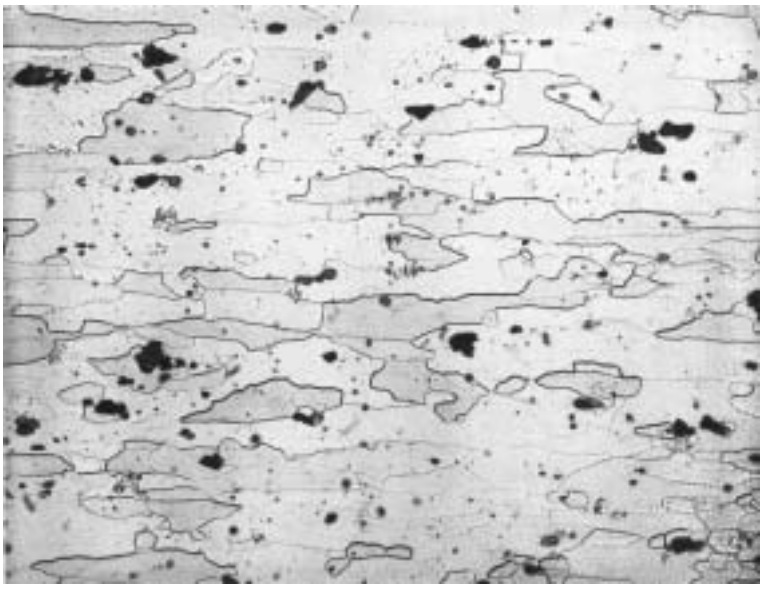

Figure 1.16-156 Metallographic examination of Left fractography as in figure 2.(400X)

Figure 1.16-157 Metallographic examination of patch.(400X)

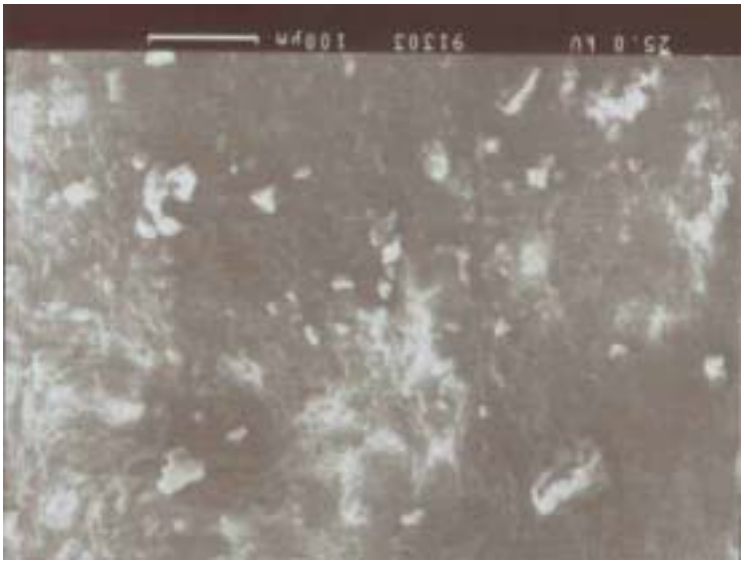

Figure 1.16-158 SEM photograph of upper door reveal (LH), which was taken from area A as in figure 6.(170X)

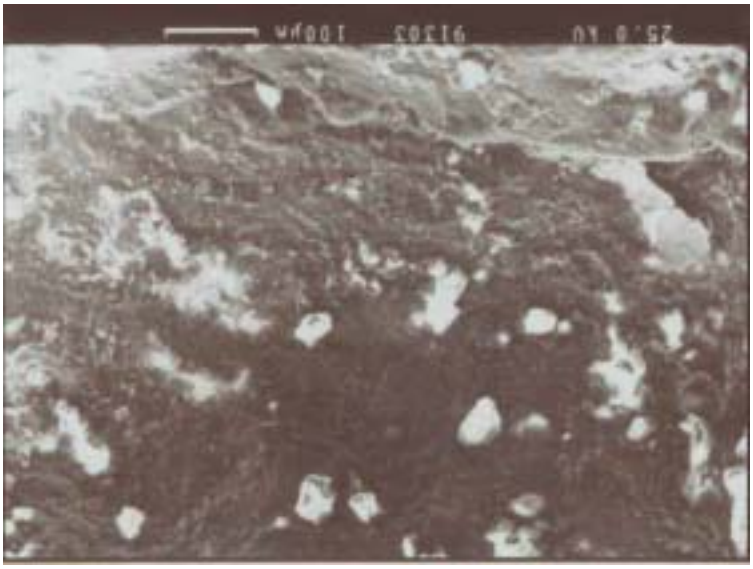

Figure 1.16-159 SEM photograph of upper door reveal(LH) , which was taken from area B as in figure 6. (140X)

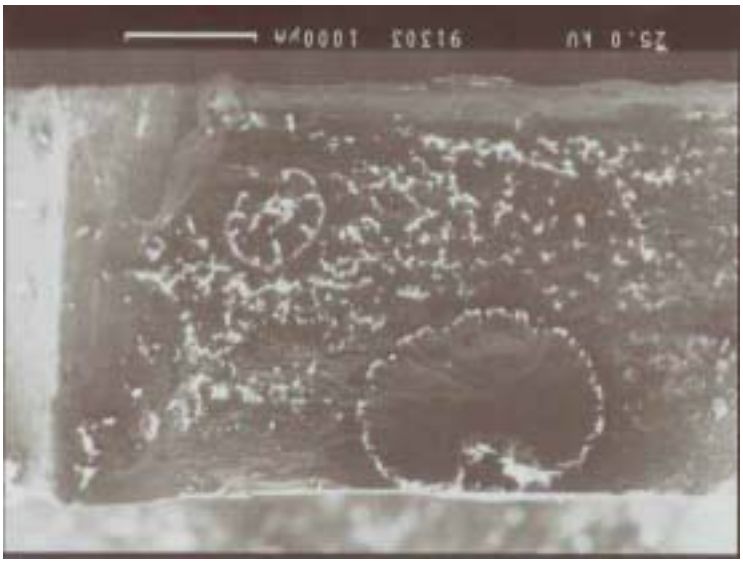

Figure 1.16-160 SEM photograph of upper door reveal (LH), which was taken from suspicious fatigue fracture area as in figure 6.(21X)

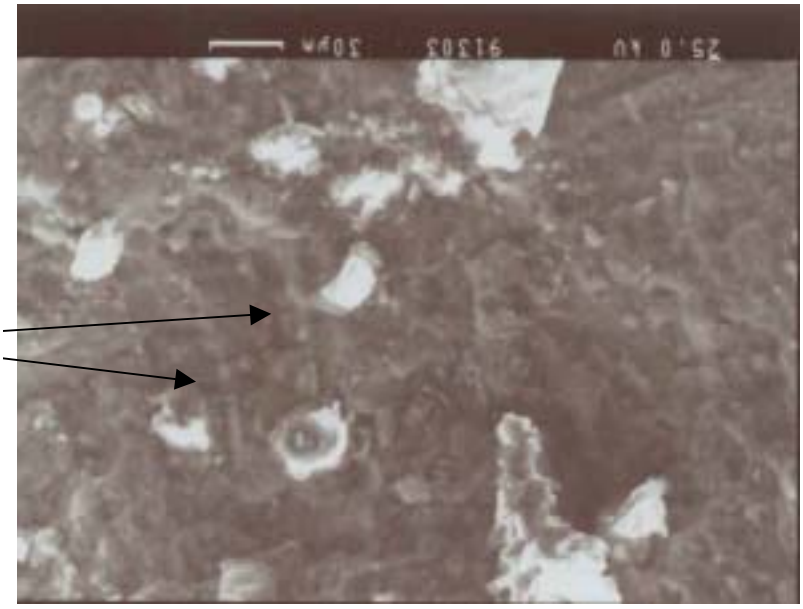

Figure 1.16-161 SEM photograph of upper door reveal (LH), which was taken from area D as in figure 6.(360X)

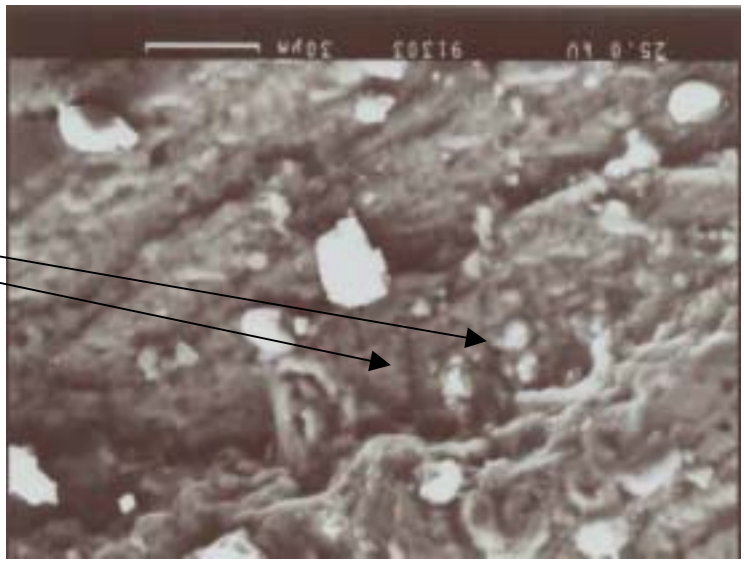

Figure 1.16-162 SEM photograph of upper door reveal(LH) , which was taken from area E as in figure 6. (610X)

Table 1.16-13 Chemical composition analytical results of door reveal, L type extrusion, by EDS analysis.

Element	Gross	Net	%Wt	%At Wt	K-Ratio	7075 Standards
Al	1970.38	1923.15	090.42	094.38	000.90	REM
Fe	010.55	002.65	000.28	000.14	000.00	0.00 ~ 0.50
Mg	093.78	033.15	001.88	002.18	000.02	2.10 ~ 2.90
Zn	038.38	029.53	005.71	002.46	000.06	5.10 ~ 6.10
Si	010.10	000.54	000.11	000.11	000.00	0.00 ~ 0.40
Cr	010.38	002.58	000.22	000.12	000.00	0.18 ~ 0.28
Cu	015.44	008.33	001.38	000.61	000.02	1.20 ~ 2.00
TOTAL :			100.00	100.00		

Table 1.16-14 Chemical composition analytical results of patch by EDS analysis.

Element	Gross	Net	%Wt	%At Wt	K-Ratio	17-7 STANDARDS
Al	018.26	001.49	000.16	000.33	000.00	0.75 ~ 1.25
Fe	906.86	871.35	075.38	074.31	000.74	REM
Ni	068.91	050.20	006.38	005.99	000.06	6.50 ~ 7.75
Mn	035.09	000.00	000.00	000.00	000.00	0.00 ~ 1.00
Si	032.94	005.87	000.62	001.21	000.00	0.00 ~ 0.50
Cr	324.47	300.41	016.80	017.79	000.20	16.00 ~17.25
Mo	027.27	004.47	000.66	000.38	000.00	
TOTAL :			100.00	100.00		

1.16.3.4 Discolorations And Transfer Marks tested by BMT

Background

China Airlines Flight CI611, a Boeing 747-200, experienced an in-flight breakup near Makung, Taiwan on 25 May 2002. During the examination of the wreckage, investigators noted discolored areas of the wing center section upper and lower surface and light and dark blue transfer marks on the leading edge of the left horizontal stabilizer. The ASC provided Boeing samples of the discolored areas of the wing center section, reference wing material, transfer marks from the horizontal stabilizer, and reference light and dark blue materials from the airplane and asked that Boeing analyze these samples.

The purposes of the analysis of the discolored area of the wing center section were

(1) To determine if the discoloration was the result of a recent fuel-fed fire, and

(2) To determine the likely source of the discoloration.

The purposes of the analysis of the transfer marks were

(1) To determine if the transfer marks matched any of the reference materials provided from the airplane, and

(2) To determine specifically if the transfer marks matched the paint from the forward fuselage.

Experimentation and Results

<u>Discolored Areas of the Wing Center Section</u>

Four samples from China Air CI611 were submitted for analysis.

- Wing center section discolored upper skin (642C3, see Figures 1.16-163 and 164 for approximate location of sample)
- Wing center section discolored lower skin (547C3, see Figures 1.16-163 and 1.16-165)
- Reference un-discolored outboard wing upper skin (628C3, see

Figures 1.16-163 and 166)

- Reference un-discolored outboard wing lower skin (628C6, see Figures 1.16-163 and 167).

Production drawings were used to determine the as-delivered wing center section finishes for China Airlines CI611. The finishes for the wing center section upper skin upper surface were chromic acid anodize, BMS 10-20 Type II fuel tank primer, BMS 10-11 Type I interior primer, and BMS 5-81 Type I secondary fuel barrier in that order. The finishes for the wing center section lower panel lower surface were chromic acid anodize, BMS 10-20 Type II fuel tank primer, BMS 10-79 Type I exterior primer, and BMS 10-100 flexible wing coating in that order.

Unburned fuel residues are expected from oxygen limited, quickly quenched fuel fed fires. Subsequent exposure to the environment would cause weathering of the fuel residues. For this reason, a test was performed to determine if weathered, unburned fuel was present in the samples provided.

In order to simulate weathered fuel, two samples of Jet A were artificially weathered. The first sample was heated uncovered in an oven at 43°C for 1 hour (referred to as dry). The second sample was diluted approximately 10 to 1 in ultra-pure (18Mohm) laboratory water and then heated at 43°C for 1 hour (referred to as wet).

Samples 642C3 (see Figures 1.16-168 and 169), 547C3 (see Figures 1.16-170 and 171) and 628C6 (see Figures 1.16-172 and 173) were analyzed for the presence of weathered fuel via Gas Chromatography – Mass Spectrometry (GC-MS) using thermal desorption with cryo-focusing. GC-MS provides chromatographic separation based on the vapor pressure of the constituents of the sample and their affinity for the stationary phase of the column. The method uses a mass spectrometer in the place of the normal GC detector. In this analysis, the total ion current was measured and the chromatogram was normalized so that the peaks ranged between 0 and 100% of the peak ion current. This is referred to as the Reconstructed total Ion Chromatogram (RIC).

Thermal desorption with cryo-focusing is a method of pre-concentrating volatile and semi-volatile components of a sample on the GC column to provide added sensitivity. In this case, the samples were heated at 225°C for 5 minutes to evolve the volatile components, while the column was maintained at

a temperature of 35°C. These temperatures were chosen as the samples had been at room temperature for extended periods of time and any highly volatile components would have already evaporated.

The wing center section of a retired 747 was examined for similar discolored areas. The retired 747 (line number 229) is located at Boeing's Everett facility and differs from CI611 in that the final surface coating on the wing center section lower skin an enamel rather than BMS 10-100. Discolored areas were found in crevices and around joints in the wing center section and the wheel wells. Samples were taken from the bottom of the keel beam below the wing center section (see Figure 1.16-174 for approximate location of sample) and from the wing-to-body fairing chord (see Figure 1.16-175) for comparison to the discolored areas found on the wing center section of CI611.

Fourier-Transform infrared spectroscopy (FT-IR) was used to analyze sample 642C3 as well as the sample from the wing-to-body fairing chord of the retired 747 (see Figure 1.16-176). As can be seen, the two spectra are very similar except for bands around 3400 cm^{-1} and 1700 cm^{-1}. The band around 3400 cm^{-1} is likely due to a combination of amine functional groups and organic acid hydroxyl functional groups. The band around 1700 cm^{-1} is likely due to organic acid carbonyl functional groups. Taken together, these are consistent with biological (protein) contamination of the retired 747 in addition to mixed organic and inorganic material similar to that found on sample 642C3.

Electron microprobe using energy dispersive x-ray spectroscopy (EDX) was used to analyze the elemental composition of the discoloration on sample 642C3 (see Figure 1.16-177). The elemental composition is consistent with environmental contamination, being rich in silicon, aluminum, calcium, magnesium, chlorine, sulfur, carbon, oxygen, iron, chromium, sodium and potassium.

The FT-IR spectra from sample 547C3 indicate the presence of hydrolyzed protein (peaks at 3270cm^{-1}, 1627cm^{-1}, 1533cm^{-1} and 1411cm^{-1} in Figure 1.16-178), mixed hydrocarbons (peaks at 2955cm^{-1}, 2924cm^{-1}, and 2855cm^{-1}, 1448cm^{-1} and 1398cm^{-1} in Figures 1.16-178 and 179) and inorganic minerals (peaks at 1015cm^{-1} and 1032cm^{-1} in Figures 1.16-178 and 179). The primary contributor to the mineral peaks is aluminum hydroxide from the filler. EDX spectroscopy of discolorations from sample 547C3 (see Figure 1.16-180) is typical of BMS 10-100 with greater than normal levels of sulfur present (compare to EDX of sample 628C3 in Figure 1.16-184). To determine if the

elevated sulfur were present only on the surface of the coatings, the sample was cross-sectioned and the layers were independently analyzed by EDX (see Figures 1.16-181 and 182 of the BMS 10-79 Type I exterior primer and the BMS 10-20 Type II fuel tank primer respectively). As can be seen, the elevated sulfur extends through the BMS 10-79 Type I exterior primer, but does not extend into the BMS 10-20 Type II fuel tank primer. Both the BMS 10-100 top coat and the BMS 10-79 Type I primer are more porous than the BMS 10-20 Type II fuel tank primer.

The FT-IR spectra from sample 628C3 (clean material from the upper wing skin) were all similar to that shown in Figure 1.16-183, which was considered a standard spectrum for the BMS 10-100 for this airplane. The EDX spectrum shows the high aluminum and chlorine levels expected from BMS 10-100, with typical environmental contamination (oxygen, sodium, magnesium, silicon, phosphorus, sulfur, potassium, calcium and iron). This spectrum differs from the 547C3 primarily in the extent of sulfur present.

FT-IR and EDX spectra of clean areas of sample 628C6 (see Figures 1.16-185 and 186) are very similar to the clean regions of sample 628C3, confirming that the surface finish is consistent between the two.

The discolored areas found on the wing center section of CI611 match the discolored areas from the retired 747 and are consistent with environmental contamination. No evidence of unburned fuel was found in the submitted samples. Sample 547C3 had an elevated level of sulfur. The origin of the sulfur was not determined.

Transfer Marks

Two colors of transfer marks were found on a coating applied to the leading edge of the horizontal stabilizer. Samples of these transfer marks were taken (see Figures 1.16-187, 188 and 189) for analysis to identify their possible origins. Reference samples were taken of exterior decorative paint from the forward fuselage (see Figure 1.16-187 for approximate locations of these samples), and from various materials used in the aircraft interior. The samples were designated 656C3 (Dark Blue Paint, see Figure 1.16-190), 650C3 (Light Blue Paint, see Figure 1.16-191), 640C5 (Very Light Blue Paint, see Figure 1.16-192), 284C3 (Light Blue Plastic Seat Surround, see Figure 1.16-193), 526C3 (Dark Blue Plastic Trim, see Figure 1.16-194) and 284C6 (Dark Blue Seat Arm Rest, see Figure 1.16-195).

A FT-IR spectrum of the dark blue transfer mark was obtained with a FT-IR microscope in transflectance mode. Spectra were also obtained of the paint samples and the interior material samples for comparison to the spectrum of the dark blue transfer mark, with no positive matches. These spectra are shown in Figures 1.16-196 through 202. Based on these spectra, the organic class of each material was identified as shown in the second column of Table 1.16-15.

Elemental data was obtained from the transfer marks, the paint samples and the interior samples. These are shown in Figures 1.16-203 through 212. The dark blue transfer mark was found to contain barium and sulfur rich particles that were on the order of 1 micron in diameter (see EDX in Figure 1.16-204). These particles were not found in any of the other samples. Due to the limited amount of material that could be separated, it is possible that these particles could have been missed in the light blue transfer sample. The elemental data is summarized in Table 1.16-15, which indicates the presence or absence of particular elements in the various samples.

Table 1.16.15 Summary of chemical and elemental properties of transfer marks and provided reference samples.

Sample ID	Organic ID (Color)	O	Na	Mg	Al	Si	P	S	Cl	K	Ca	Ti	Fe	Cu	Br	Sn	Sb	Ba
630C3 Dk Bl Xfer Mrk	Epoxy (Dark Blue)	X		X	X	X		X	X	X	X	X	X					X
630C3 Lt Bl Xfer Mrk	ISF Sample (Light Blue)	X	X	X	X	X			X	X	X	X	X					
656C3 Dk Blue Paint	Urethane (Dark Blue)	X			X	X						X		X				
650C3 Lt Blue Paint	Urethane (Light Blue)	X	X		X	X			X			X						
640C5 VLt Blue Paint	Urethane (Light Blue)	X			X	X	X					X						
284C3 Lt Bl Seat Srnd	PVC (Light Blue)	X			X	X			X		X	X				X		
526C3 Dk Blue Trim	ABS (Dark Blue)								X						X		X	
284C6 Dk Bl Arm Rest	Plasticized Vinyl (PVC?) (Dark Blue)	X	X		X	X	X		X		X	X	X					
630C3 HS LE Coat	Epoxy (Gray)	X		X	X	X			X	X	X	X	X	X				

ISF Sample = Insufficient sample obtained x = element present blank = element not present

Comparison of the properties of the two transfer mark samples to the reference

samples shows that none of the reference samples match either of the transfer marks. The closest match to the transfer marks is the horizontal stabilizer leading edge coating (630C3), which was also an epoxy but can be differentiated based on the presence of copper, the absence of barium, and the difference in color.

The transfer marks do not match the paint samples provided for comparison. They differ in both in elemental composition and in the polymer base materials from any of the reference samples.

(Detailed information refer ATTATCHMENT 5 Analysis Of Discolorations And Transfer Marks From China Airlines CI611)

Figure 1.16-163 Photo of CI611 showing general locations from which discoloration samples were taken. Samples 642C3 and 547C3 were from wing center section as indicated by A and B. Samples 628C3 and 628C6 were from the right wing corresponding to the location indicated by C and D.

Figure 1.16-164 Discoloration sample 642, showing locations of samples 642C1, 642C2 and 642C3.

Figure 1.16-165 Discoloration sample 547 before cutting, showing the location from which samples 547C1, 547C2 and 547C3 were taken.

Figure 1.16-166 Discoloration sample, showing the locations of samples 628C1, 628C2 and 628C3.

Figure 1.16-167 Discoloration sample 628, showing the locations of samples 628C4, 628C5 and 628C6.

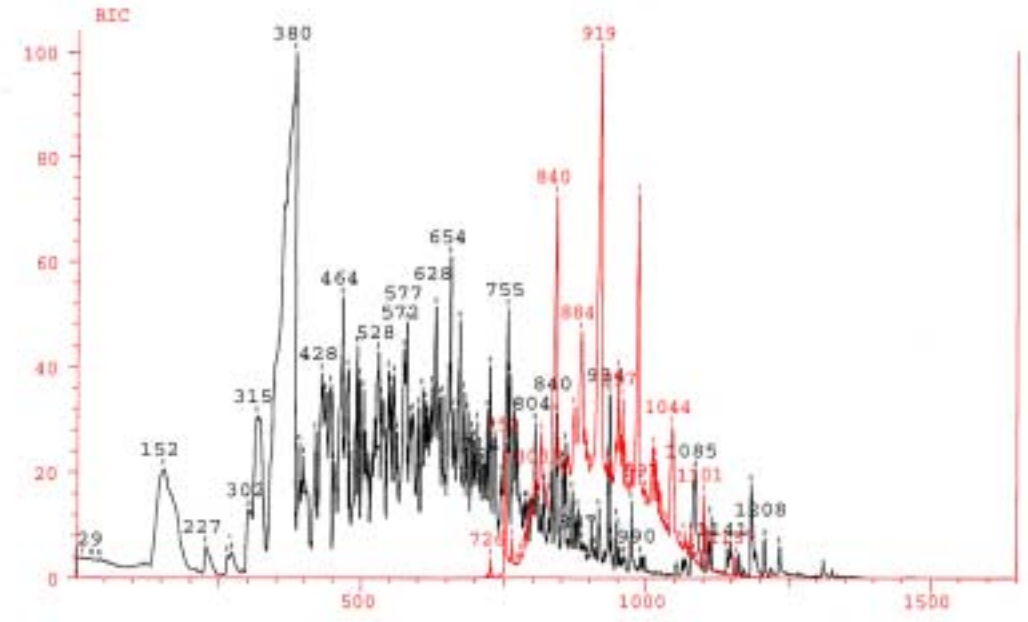

Figure 1.16-168 Comparison of the GC-MS RIC from sample 642C3 (black) to the RIC of dry weathered fuel

(red).

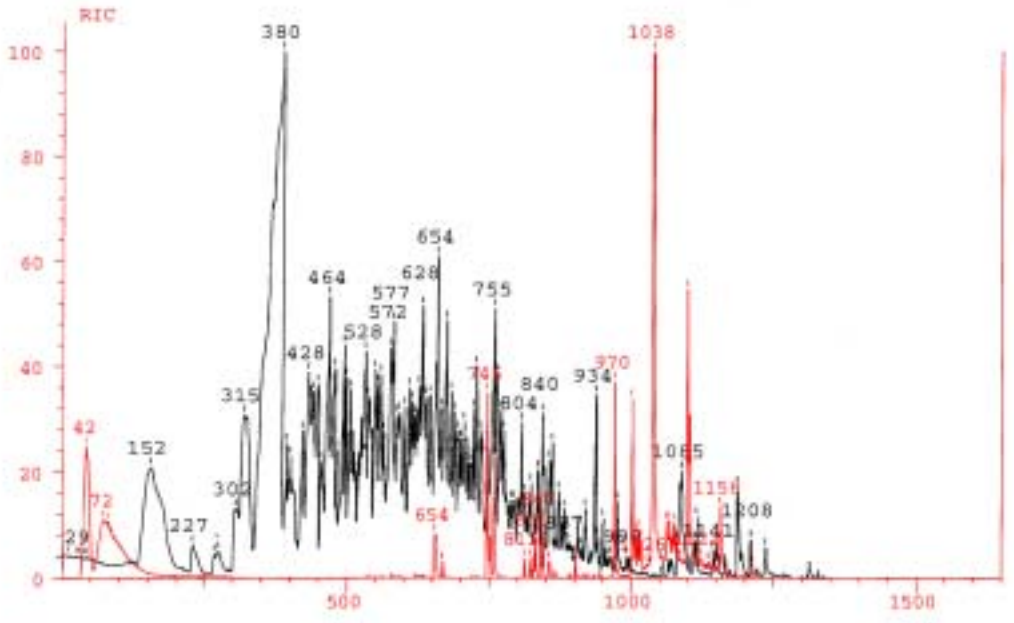

Figure 1.16-169 Comparison of the GC-MS RIC from sample 642C3 (black) to the RIC of wet weathered fuel (red).

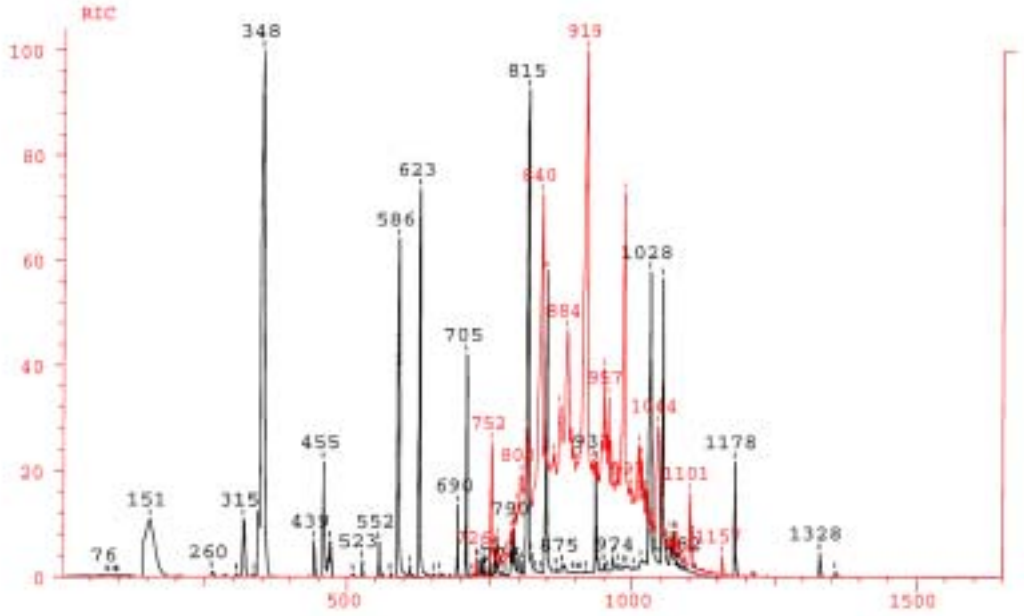

Figure 1.16-170 Comparison of the GC-MS RIC from sample 547C3 (black) to the RIC of dry weathered fuel (red).

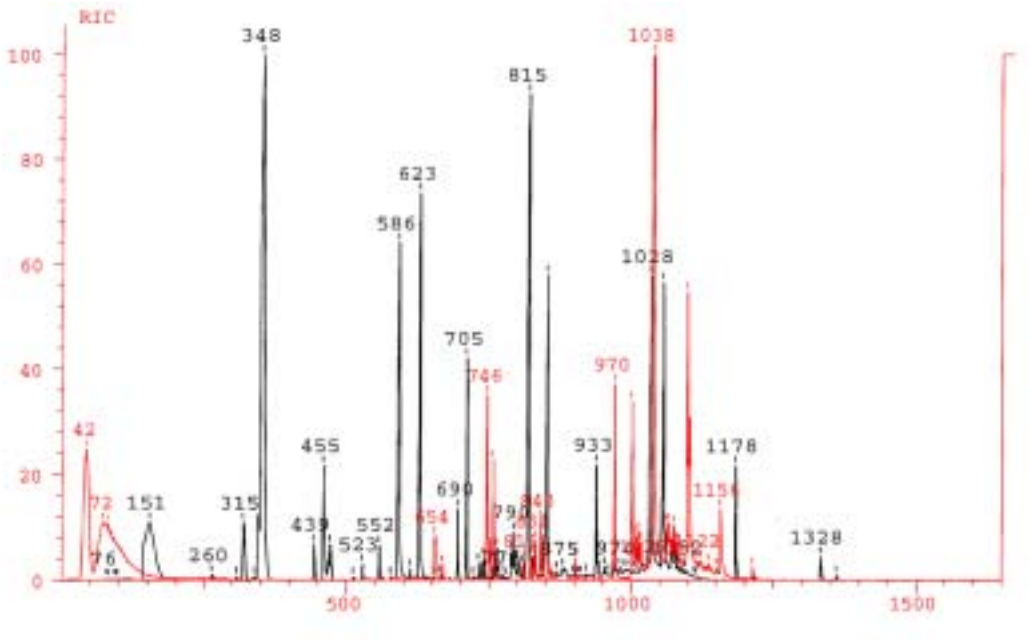

Figure 1.16-171 Comparison of the GC-MS RIC from sample 547C3 (black) to the RIC of wet weathered fuel (red).

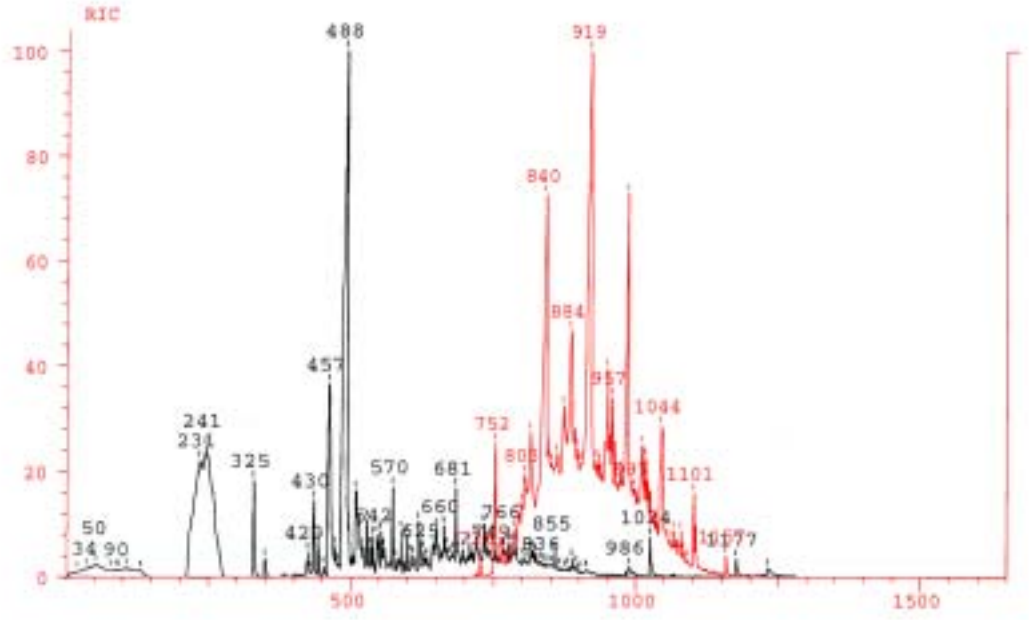

Figure 1.16-172 Comparison of the GC-MS RIC from sample 628C6 (black) to the RIC of dry weathered fuel (red).

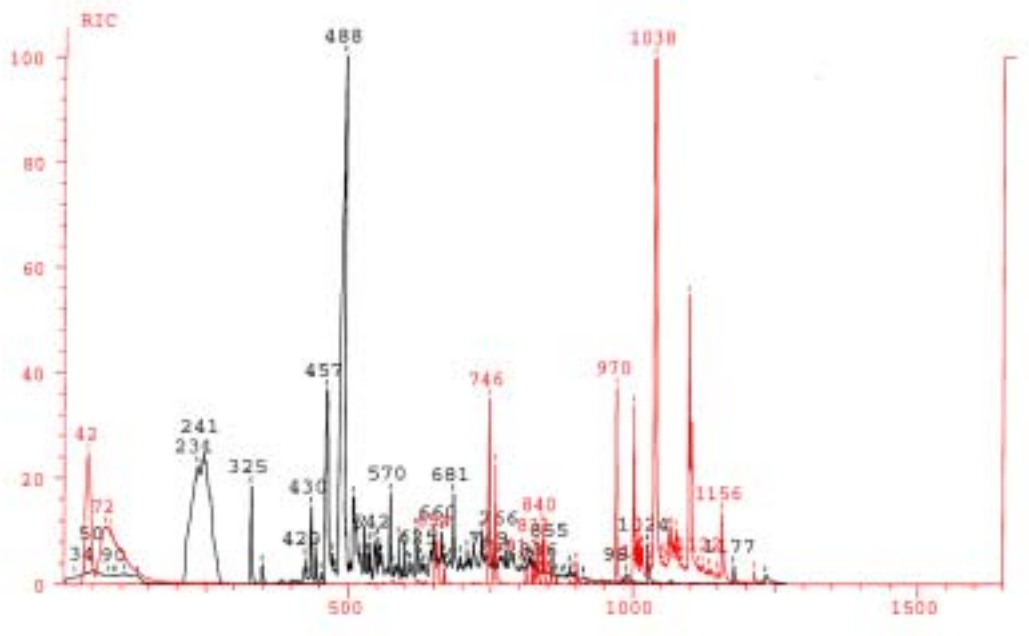

Figure 1.16-173 Comparison of the GC-MS RIC from sample 628C6 (black) to the RIC of wet weathered fuel (red).

Figure 1.16-174 Photo showing location of reference discoloration sample from keel beam of retired 747.

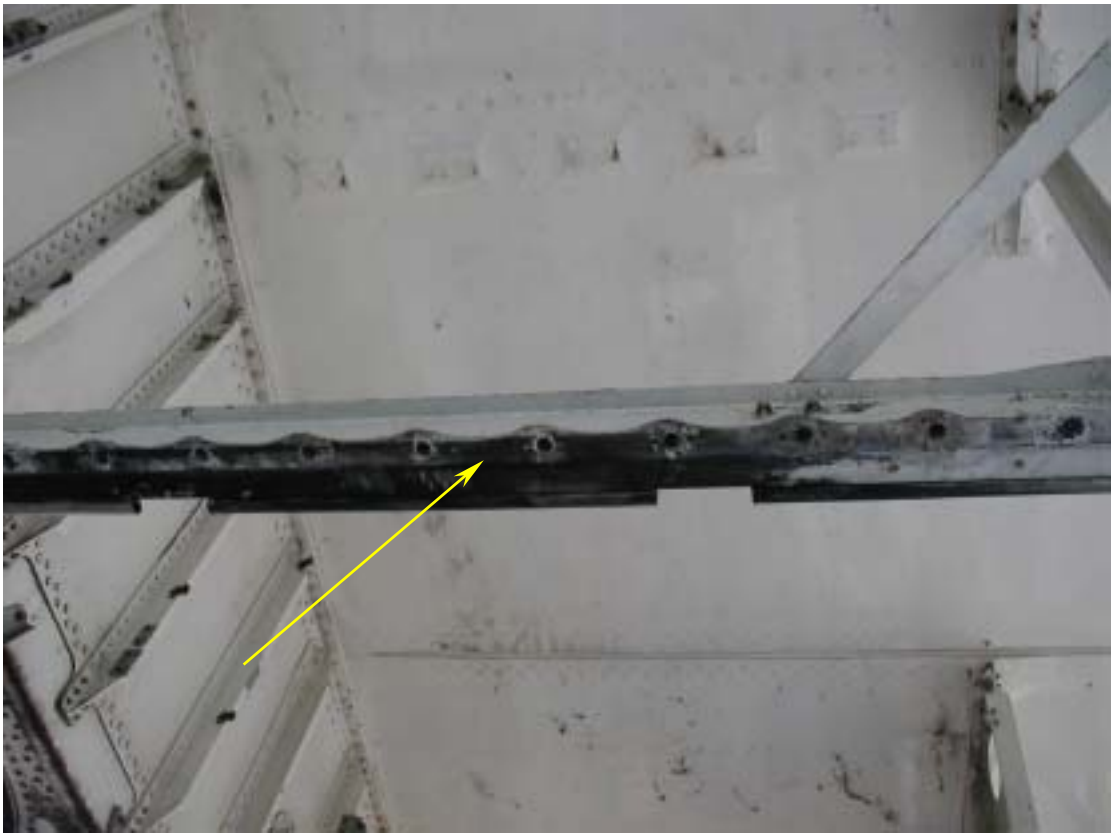

Figure 1.16-175 Photo showing location of sample taken from wing-to-body fairing chord from retired 747

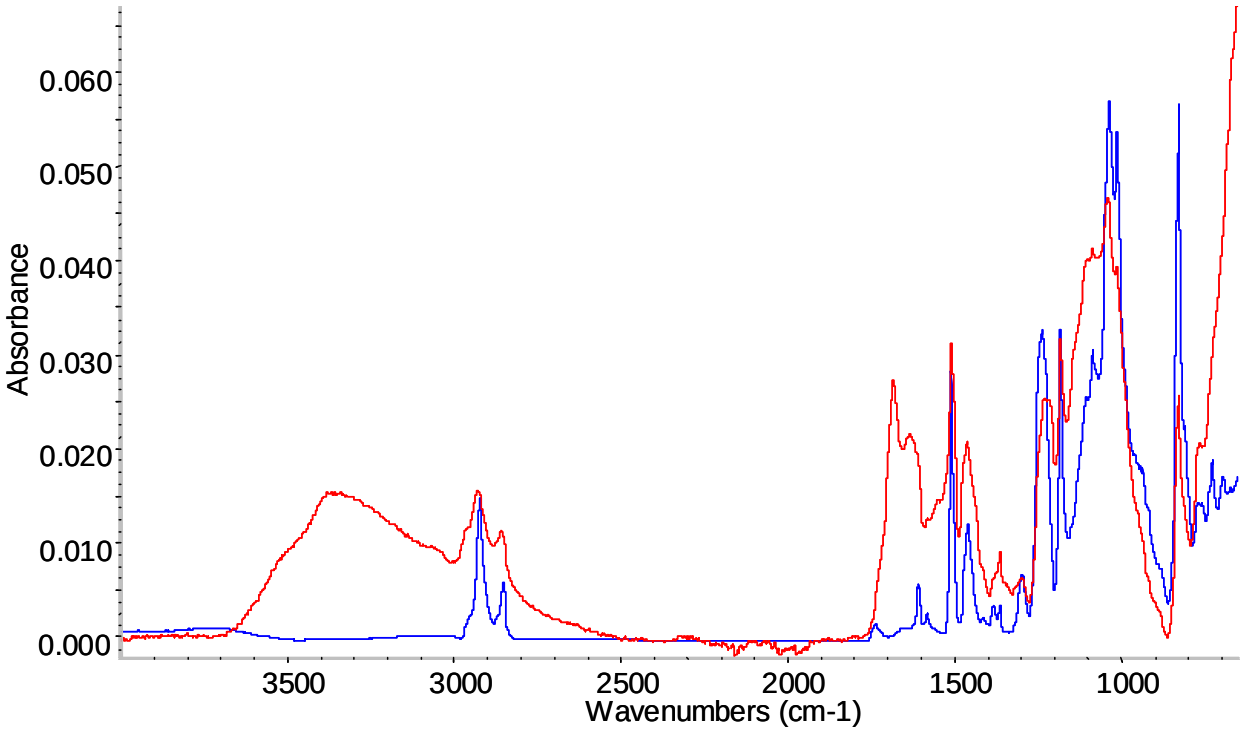

Figure 1.16-176 FT-IR spectrum of sample 642C3 (blue) and a reference spectrum of a sample from the wing-to-body fairing chord from the retired 747 (red)

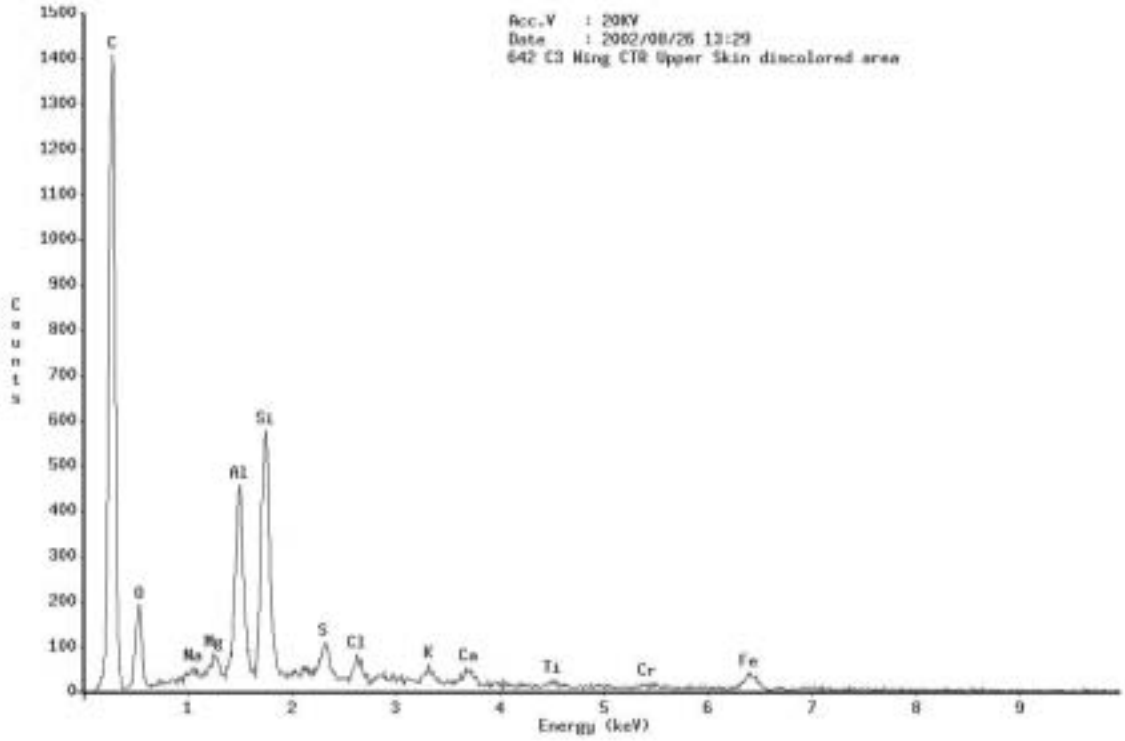

Figure 1.16-177 EDX spectrum of discolorations from sample 642C3.

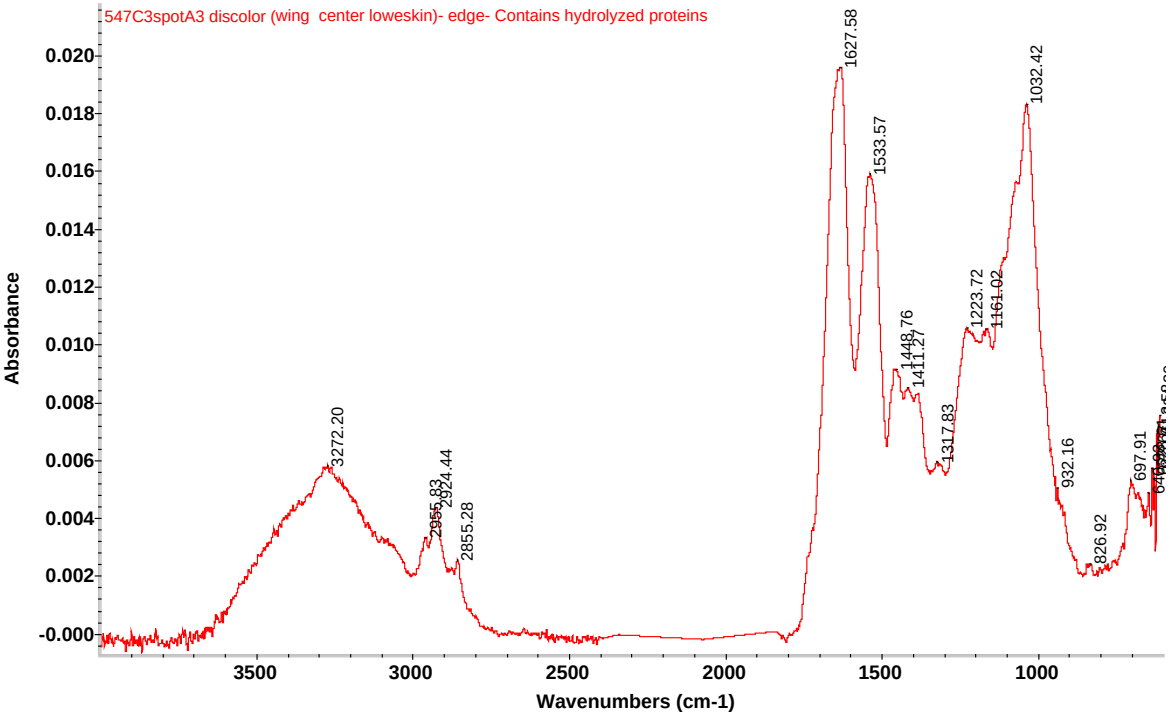

Figure 1.16-178 FT-IR spectrum of discoloration from sample 547C3.

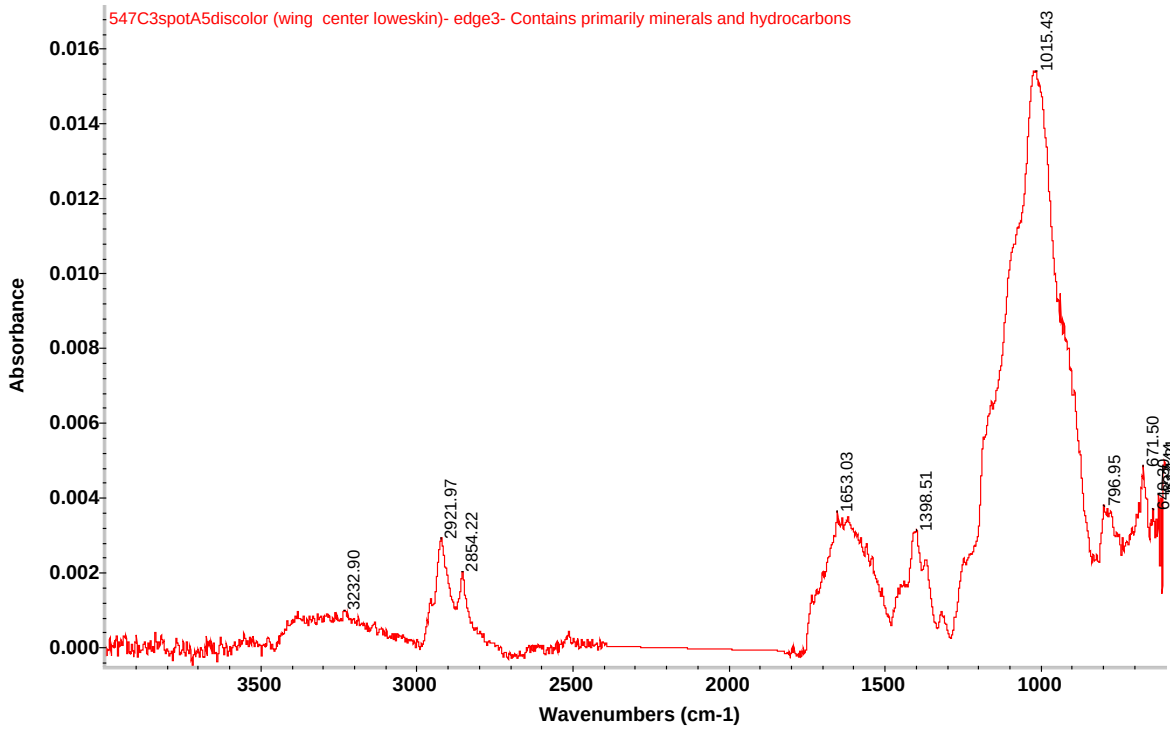

Figure 1.16-179 FT-IR spectrum of discolorations from sample 547C3.

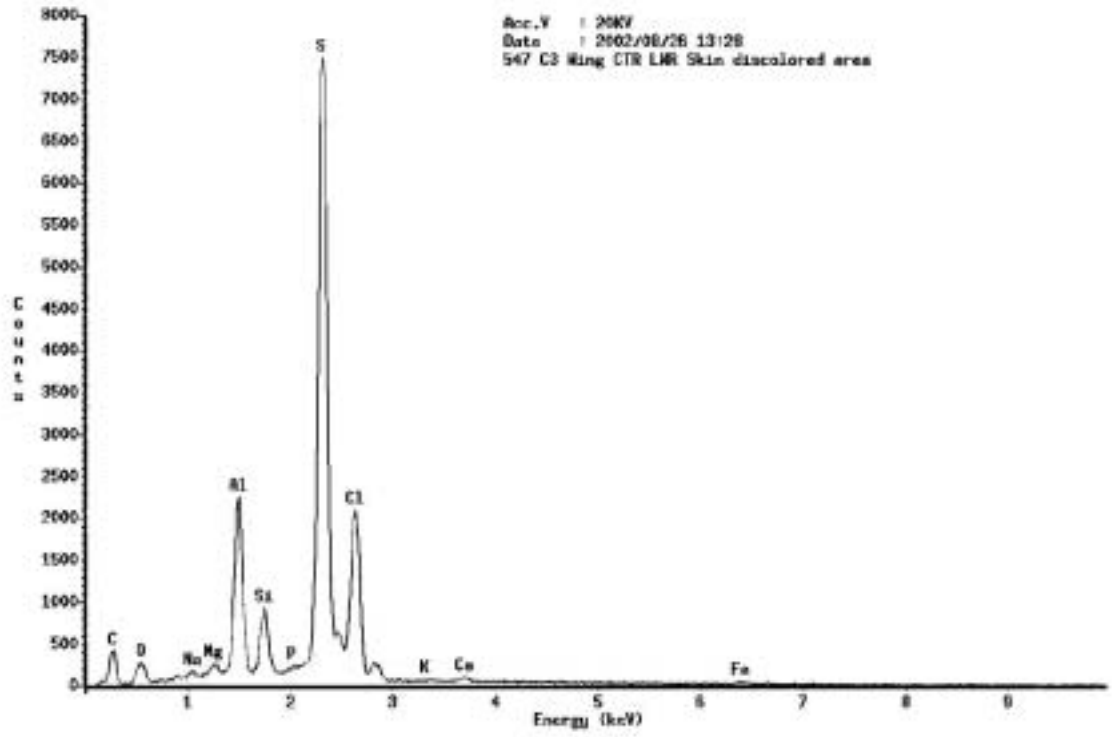

Figure 1.16-180 EDX spectrum of discolorations from sample 547C3. This sample is typical of 10-100 but has elevated sulfur.

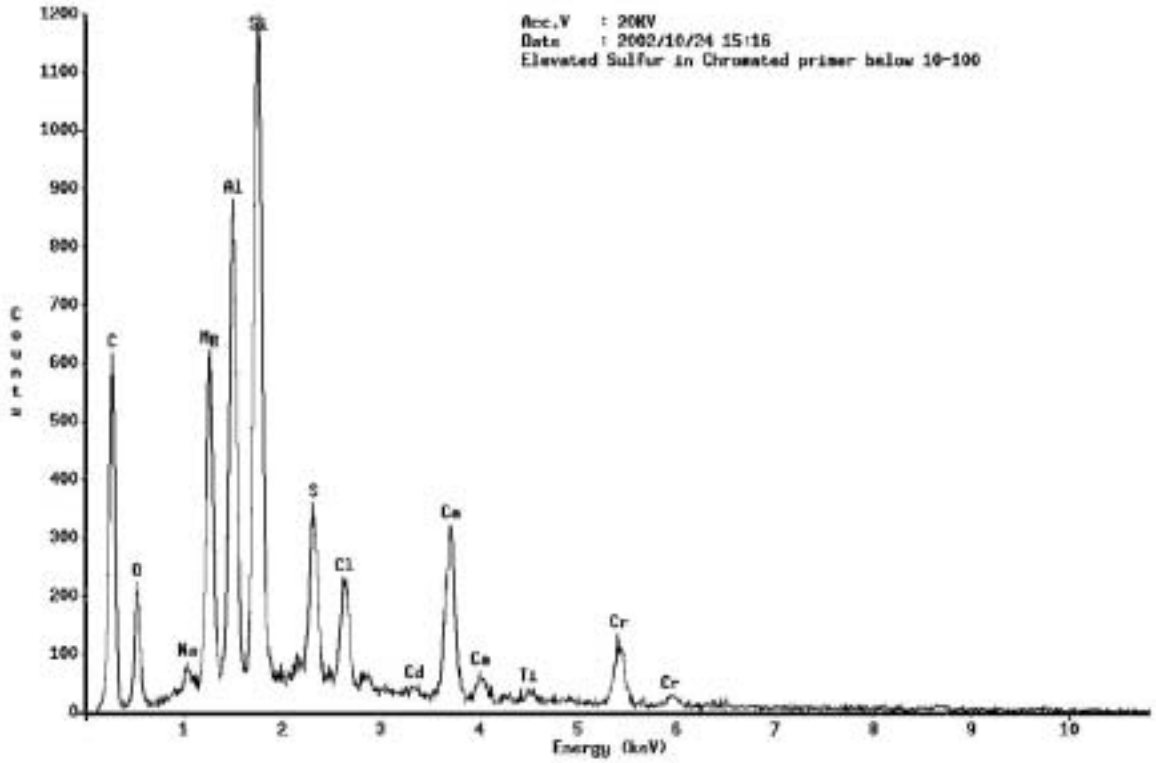

Figure 1.16-181 EDX spectrum of BMS 10-79 Type I primer showing elevated sulfur levels in first primer layer.

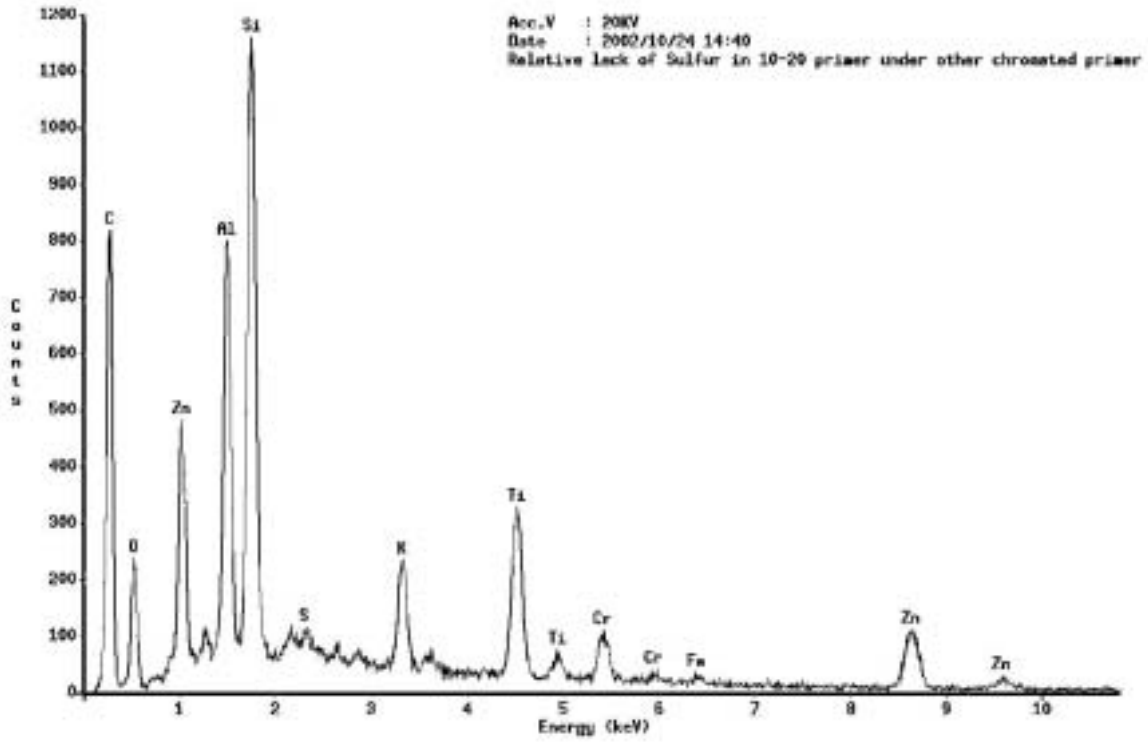

Figure 1.16-182 EDX spectrum of BMS 10-20 Type II fuel tank primer in cross-section. The elevated sulfur found in the 10-100 and 10-79 is not found in this layer.

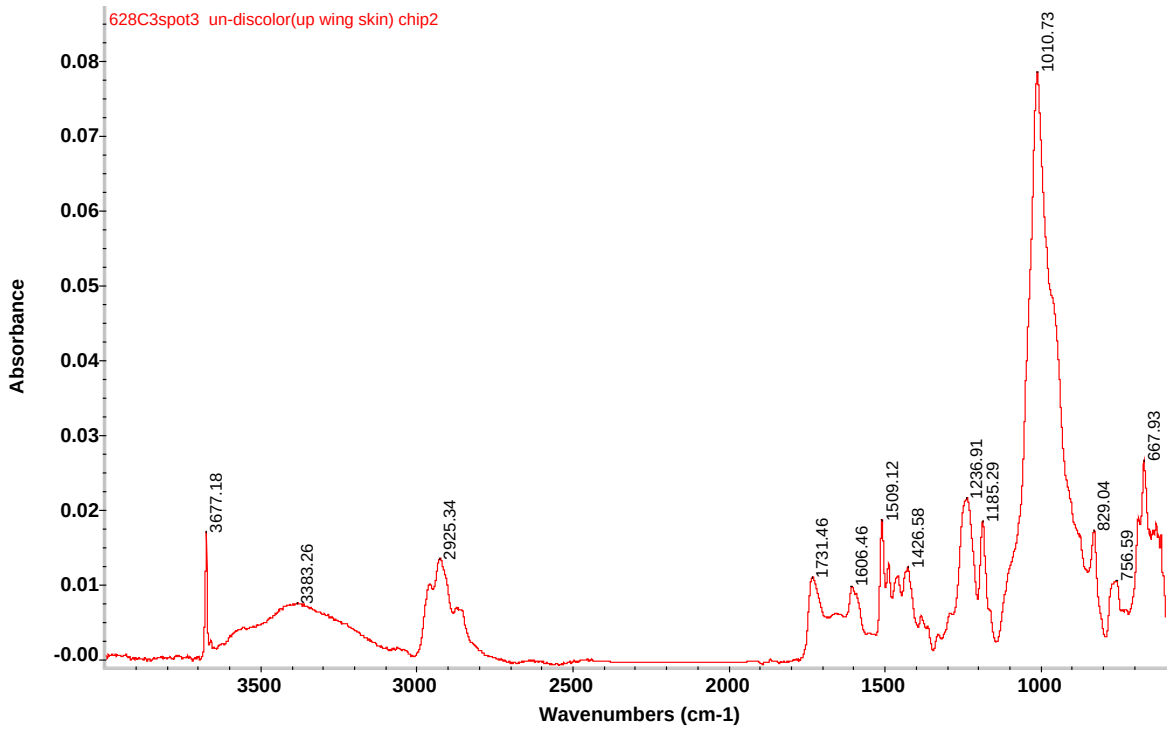

Figure 1.16-183 FT-IR spectrum of a clean area of sample 628C3.

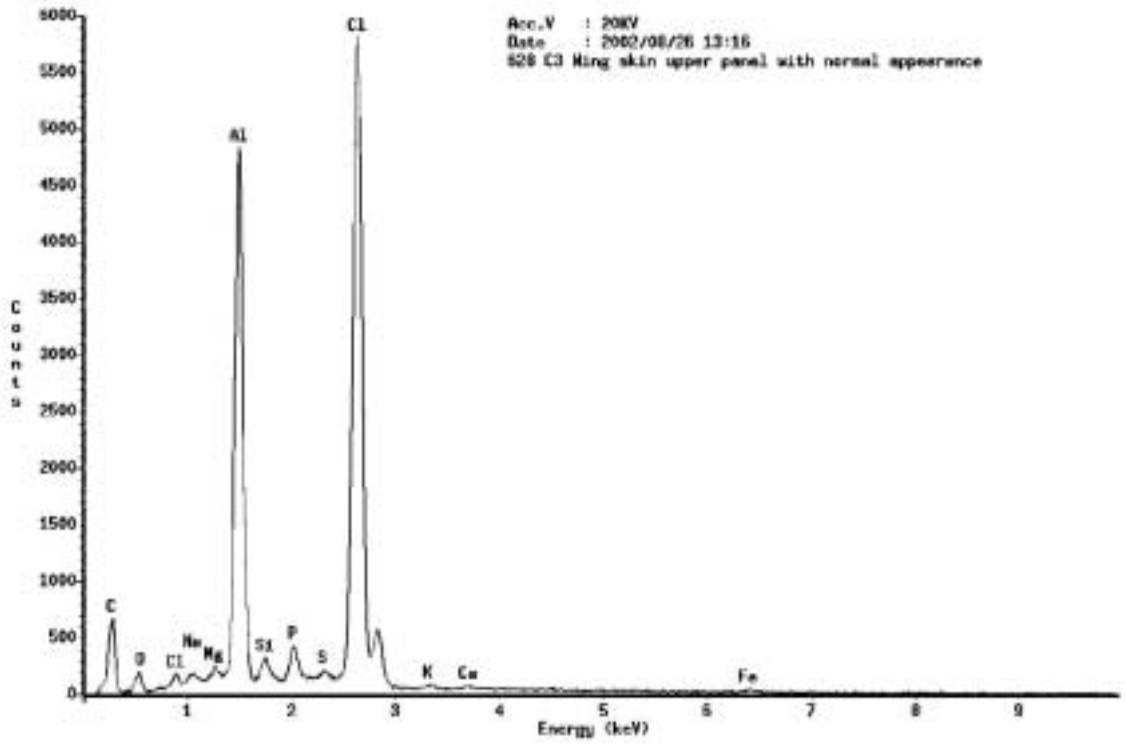

Figure 1.16-184 EDX spectrum of clean area of sample 628C3.

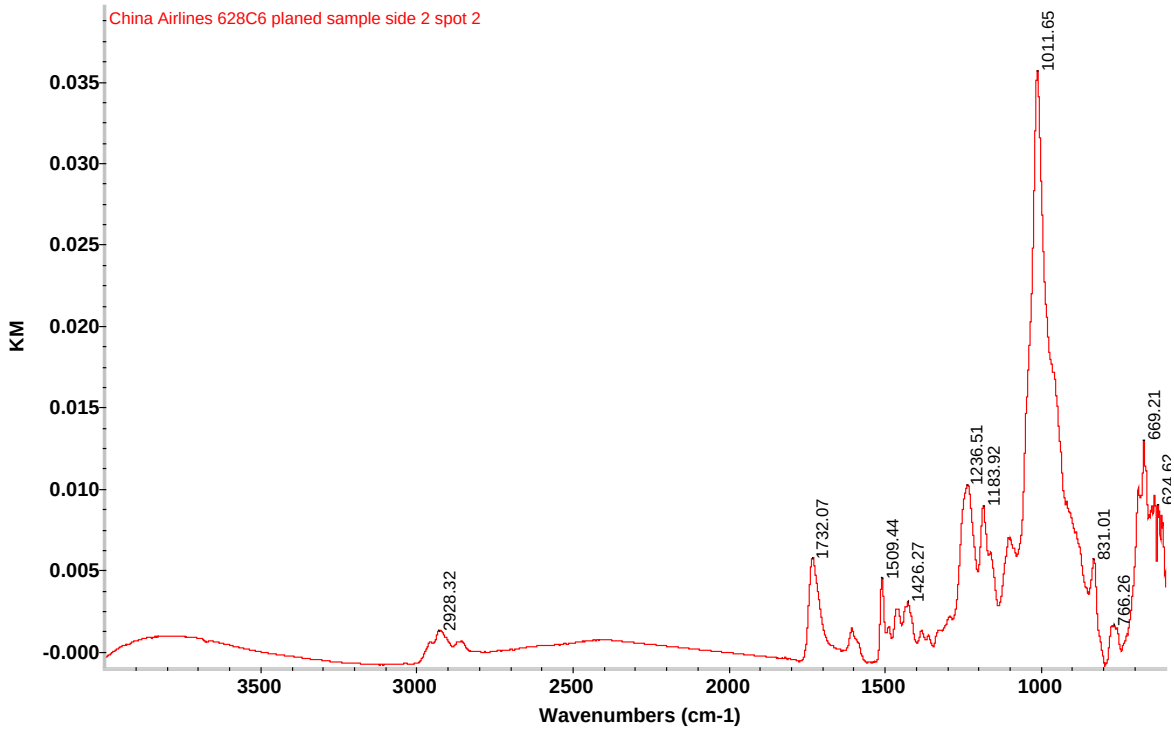

Figure 1.16-185 FT-IR spectrum from sample 628C6.

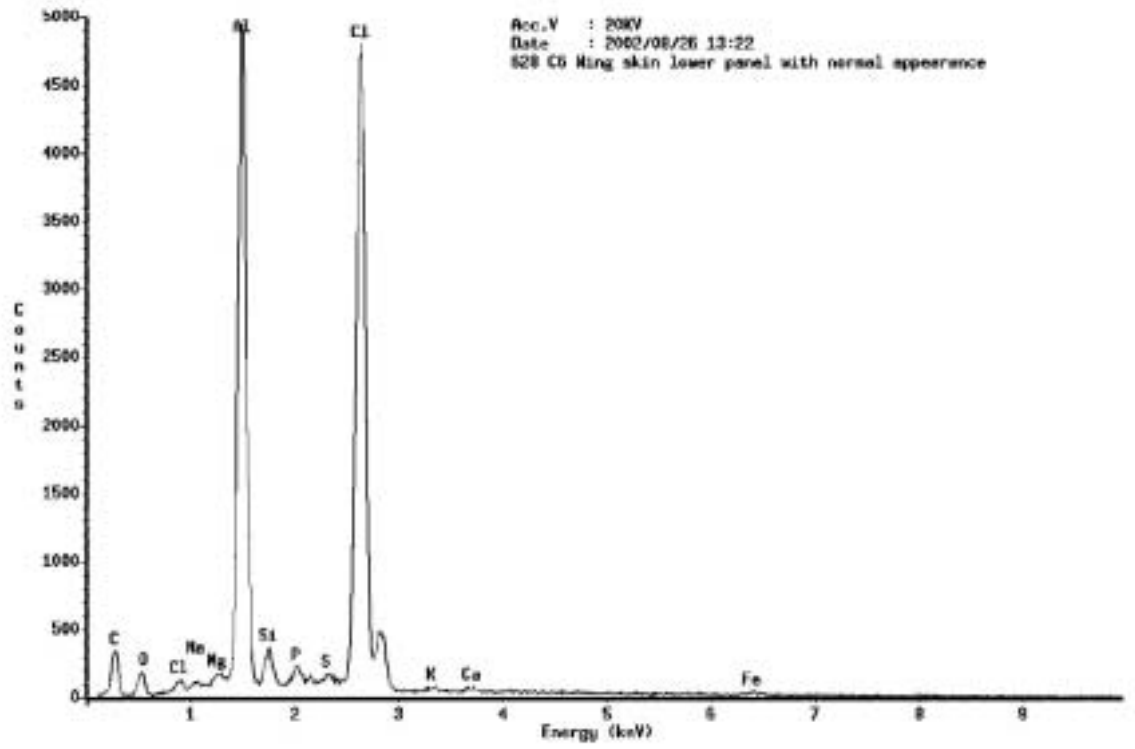

Figure 1.16-186 EDX spectrum of clean area of sample 628C6.

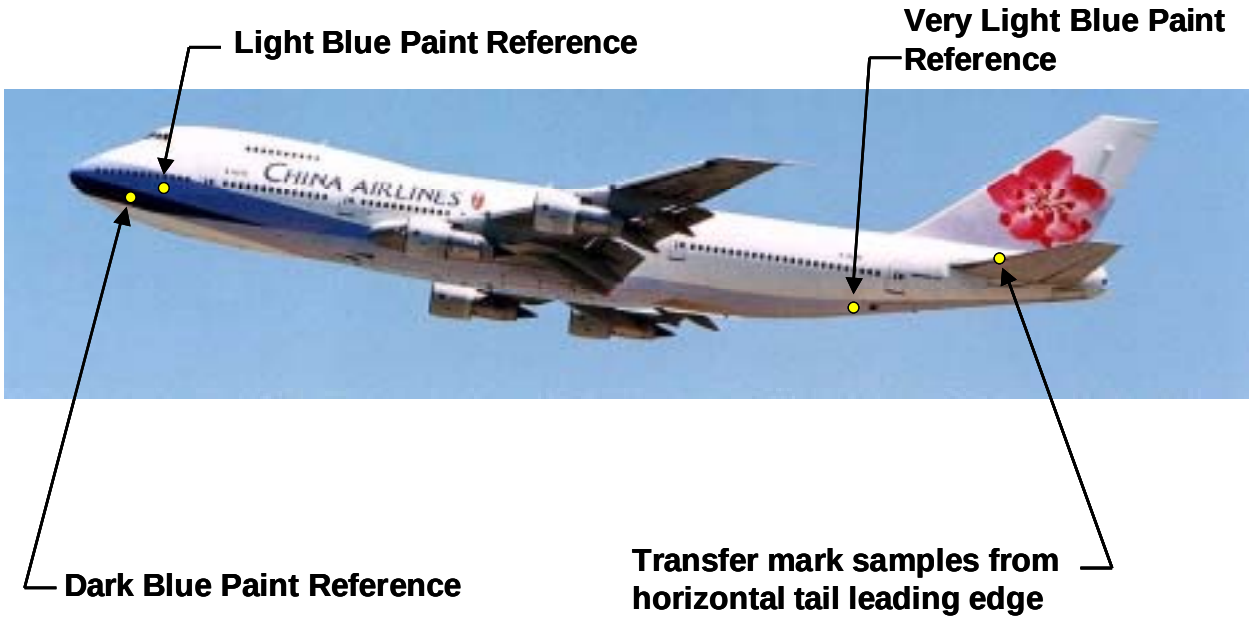

Figure 1.16-187 Locations from which the transfer mark samples and paint reference samples were taken.

Figure 1.16-188 Photograph of the left horizontal stabilizer leading edge showing transfer marks on the applied coating.

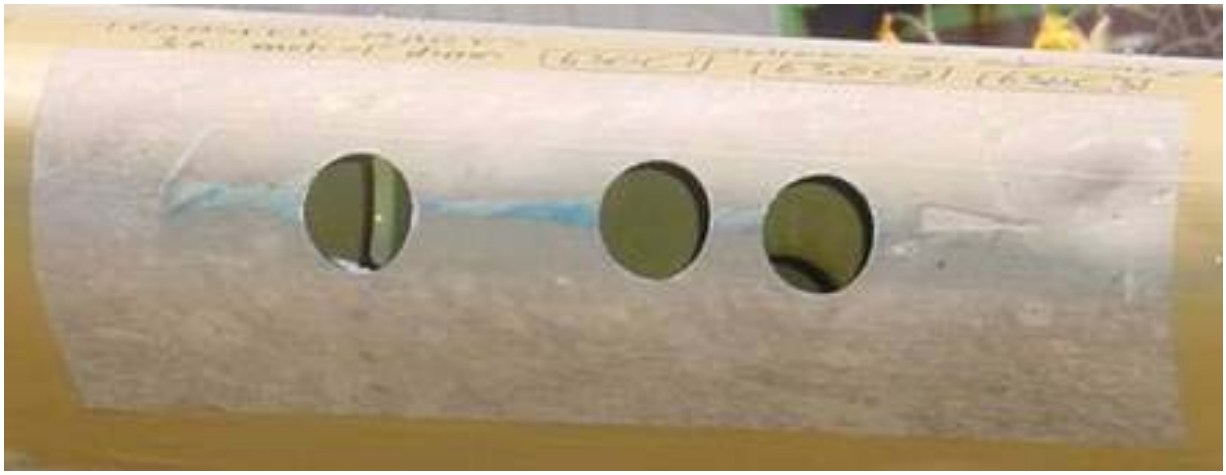

Figure 1.16-189 Enlarged image of the transfer marks showing that they end at the edge of the coating.

Figure 1.16-190 Photo of the source location of the dark blue paint sample (656C3).

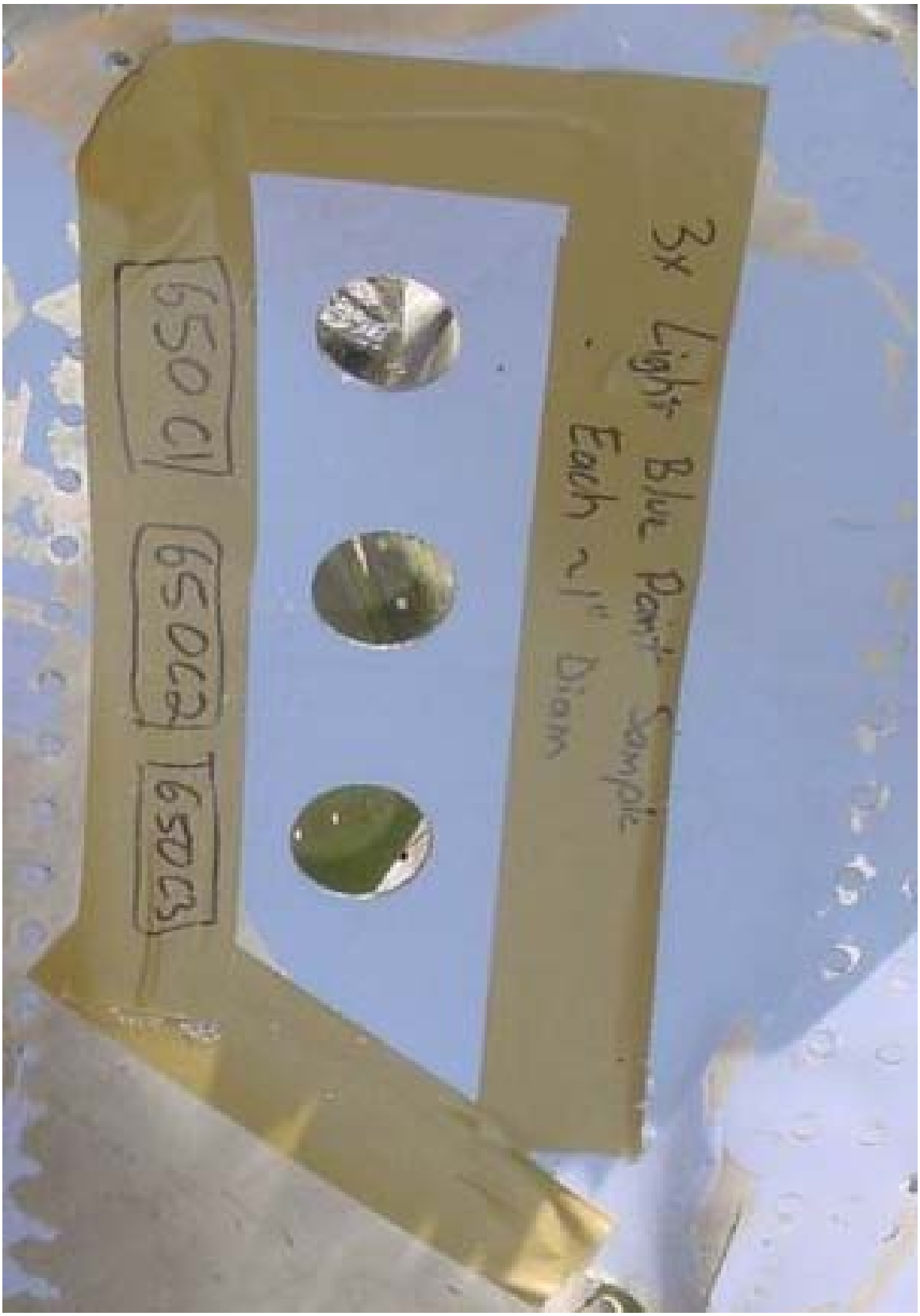

Figure 1.16-191 Photo of the source location of the light blue paint sample (650C3).

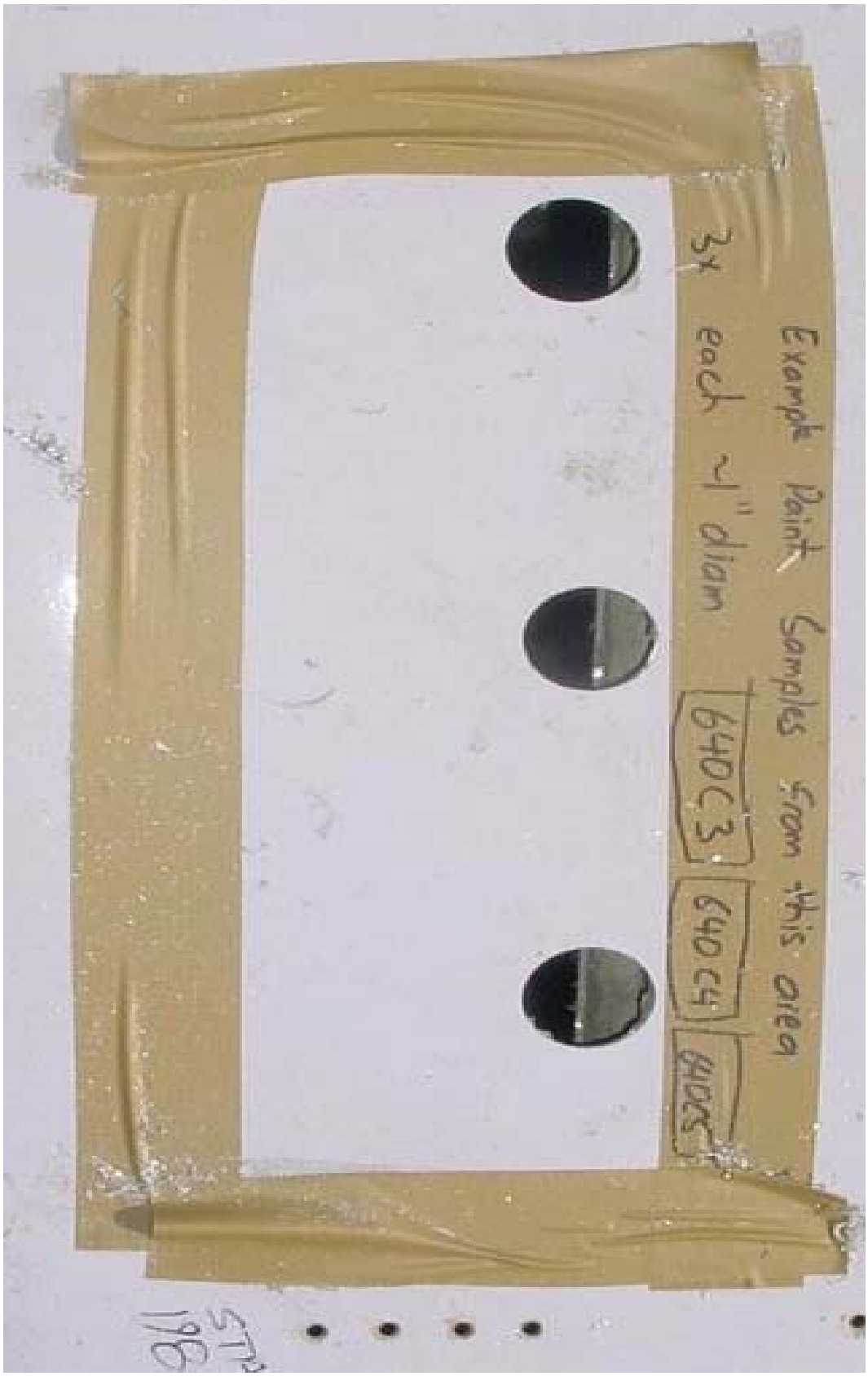

Figure 1.16-192 Photo of the source location of the very light blue paint sample (640C5).

Figure 1.16-193 Photo of the source location of the light blue plastic seat surround sample (284C3).

Figure 1.16-194 Photo of the source location of the dark blue plastic trim sample (526C3).

Figure 1.16-195 Photo of the source location of the dark blue seat arm rest sample (284C6).

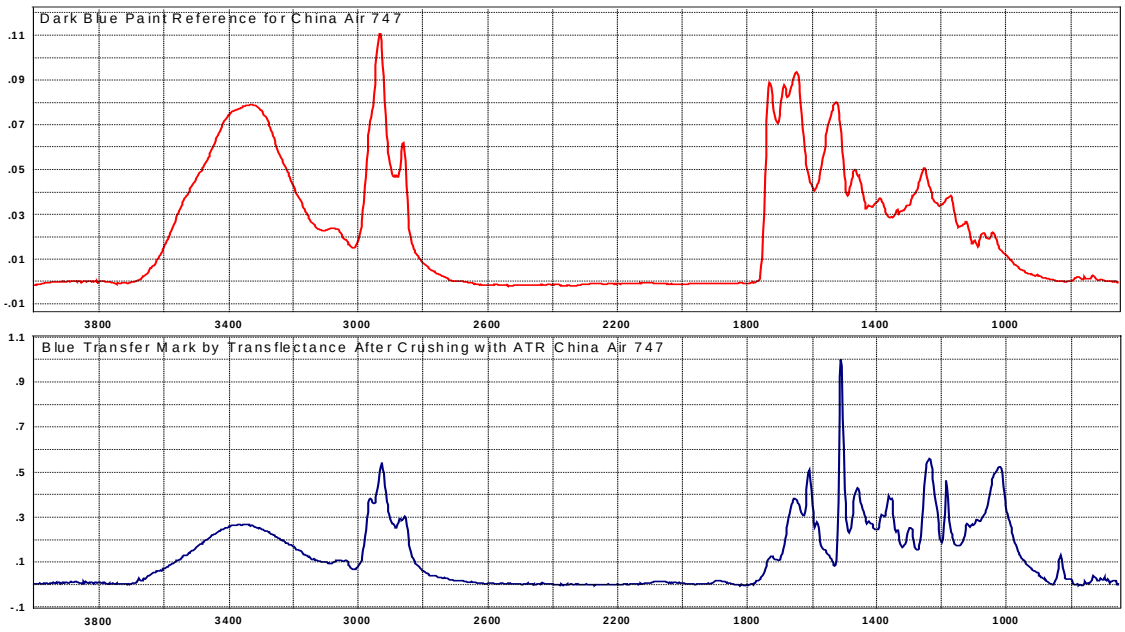

Figure 1.16-196 FT-IR spectrum of dark blue paint sample (656C3, upper spectrum) compared to the spectrum of the dark blue transfer mark (lower spectrum).

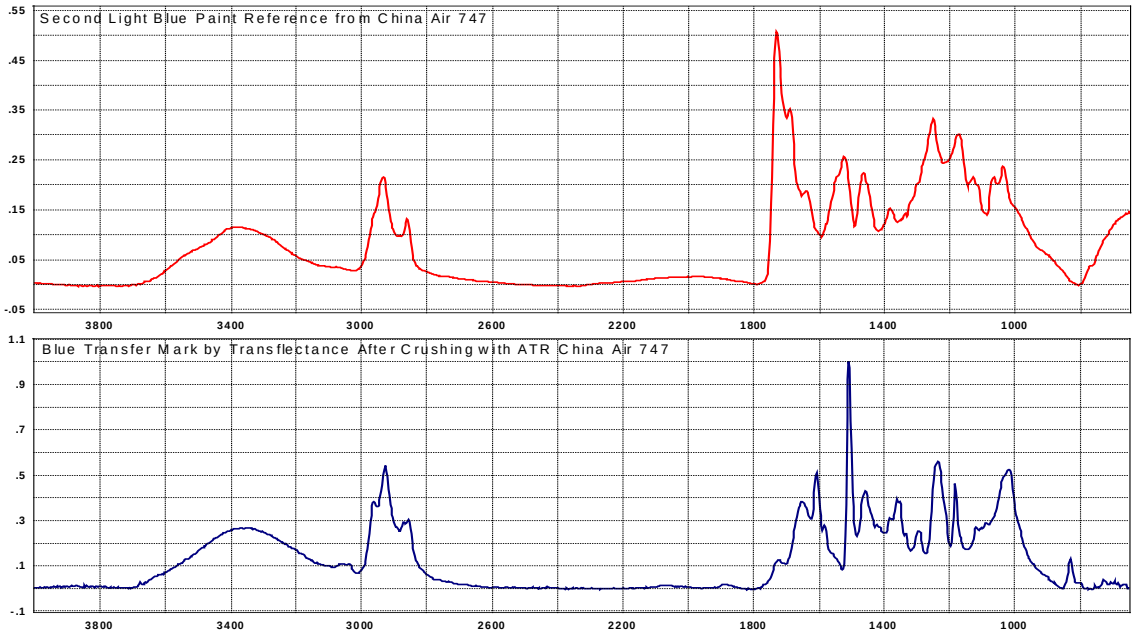

Figure 1.16-197 FT-IR spectrum of light blue paint sample (650C3, upper spectrum) compared to the spectrum of the dark blue transfer mark (lower spectrum).

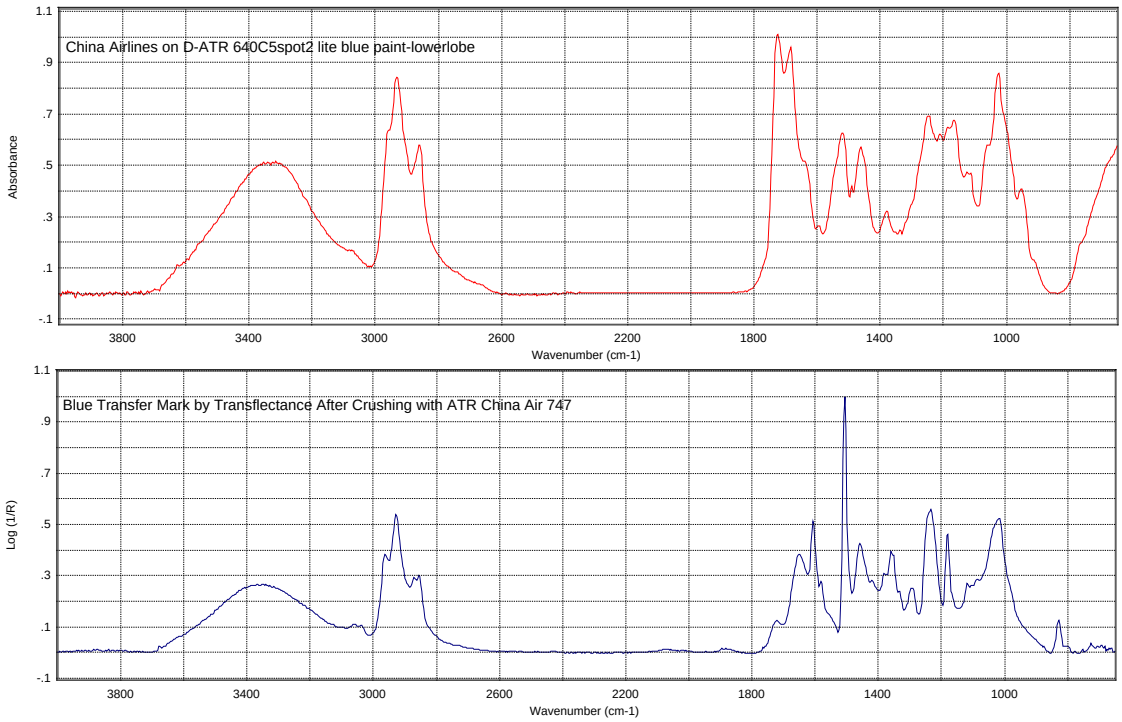

Figure 1.16-198 FT-IR spectrum of very light blue paint sample (640C5, upper spectrum) compared to the spectrum of the dark blue transfer mark (lower spectrum).

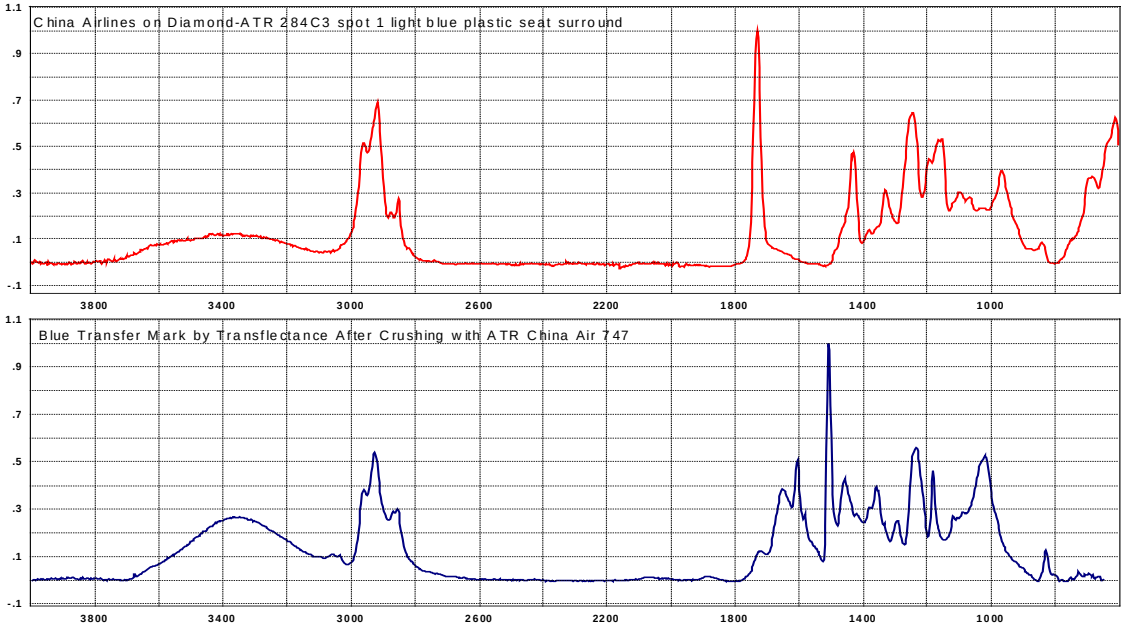

Figure 1.16-199 FT-IR spectrum of light blue plastic seat surround sample (284C3, upper spectrum) compared to the spectrum of the dark blue transfer mark (lower spectrum).

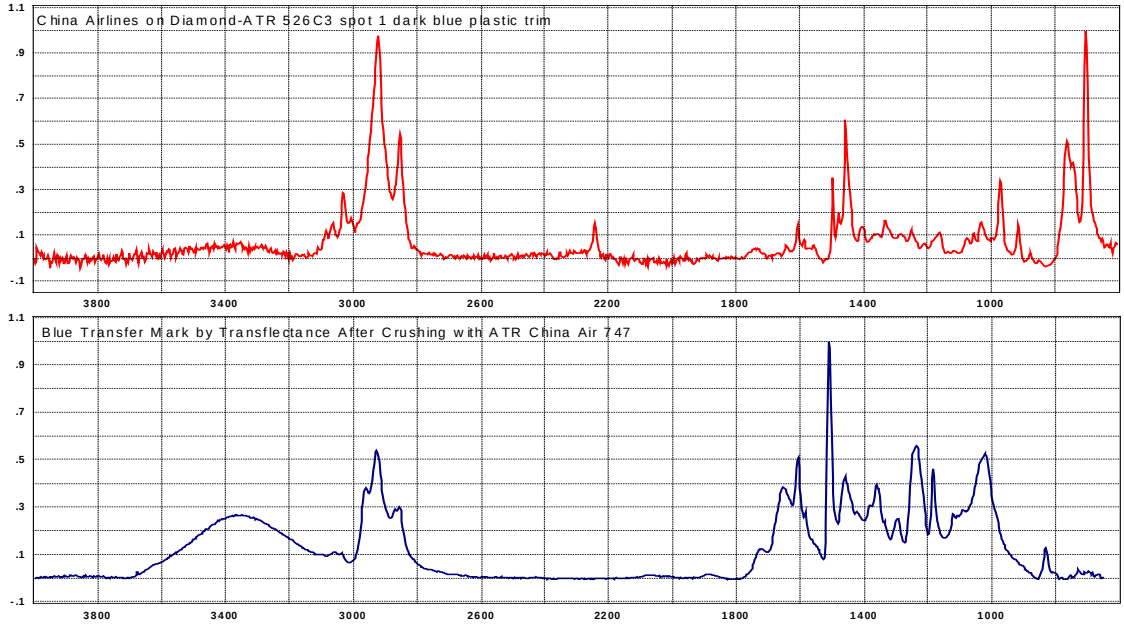

Figure 1.16-200 FT-IR spectrum of dark blue plastic trim sample (526C3, upper spectrum) compared to the spectrum of the dark blue transfer mark (lower spectrum).

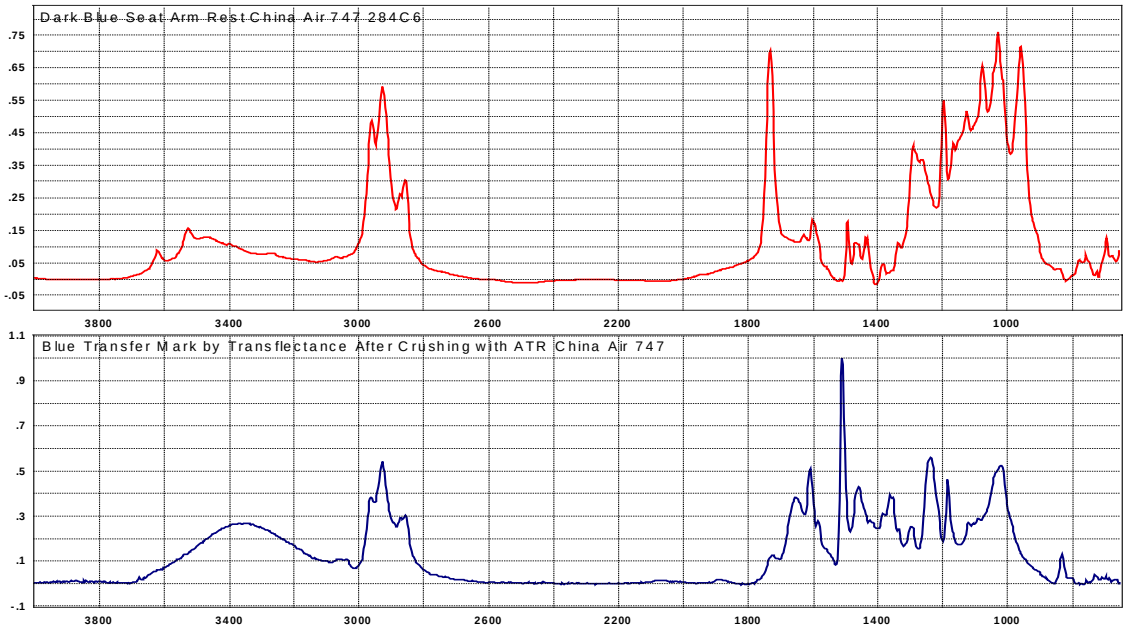

Figure 1.16-201 FT-IR spectrum of dark blue seat arm rest sample (284C6, upper spectrum) compared to the spectrum of the dark blue transfer mark (lower spectrum).

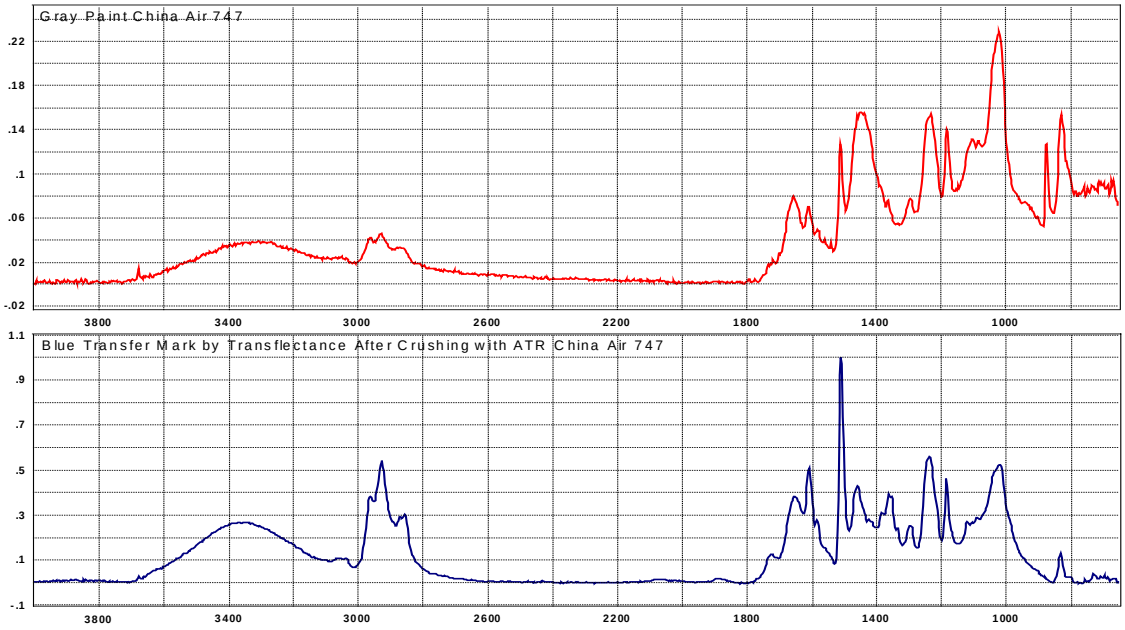

Figure 1.16-202 FT-IR spectrum of the horizontal stabilizer leading edge coating (630C3, upper spectrum) compared to the spectrum of the dark blue transfer mark (lower spectrum).

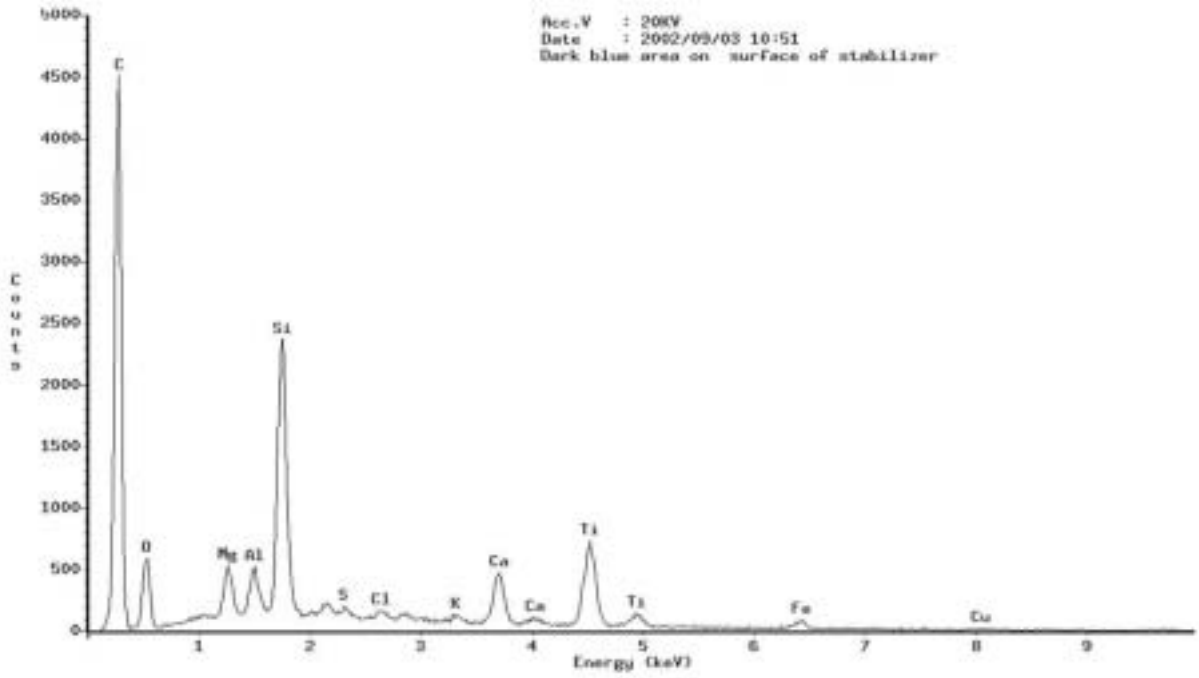

Figure 1.16-203 EDX spectrum of dark blue transfer mark.

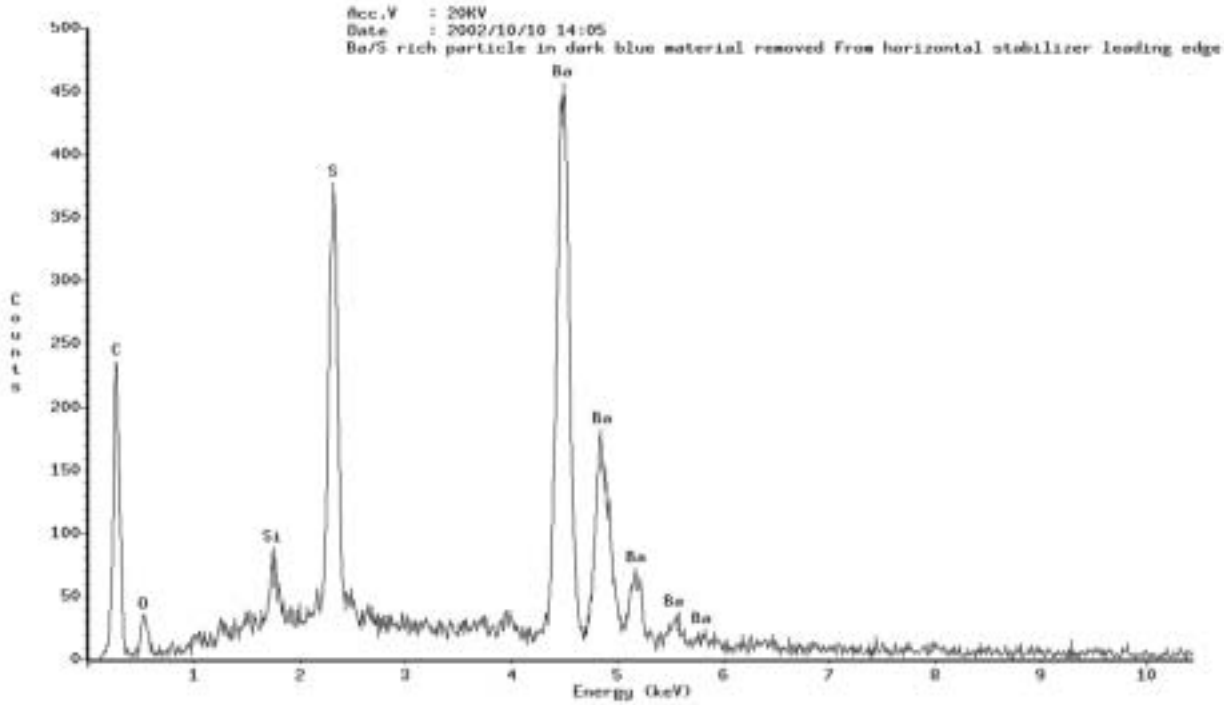

Figure 1.16-204 EDX spectrum of barium and sulfur rich particle found in dark blue transfer mark.

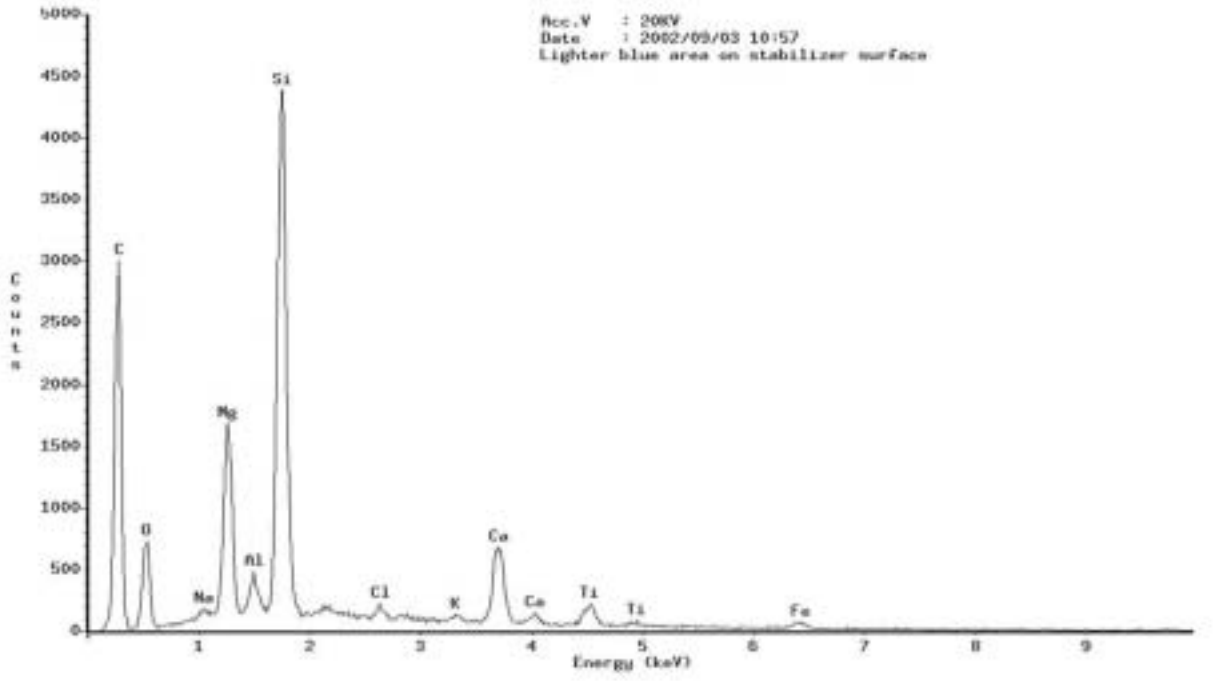

Figure 1.16-205 EDX spectrum of light blue transfer mark.

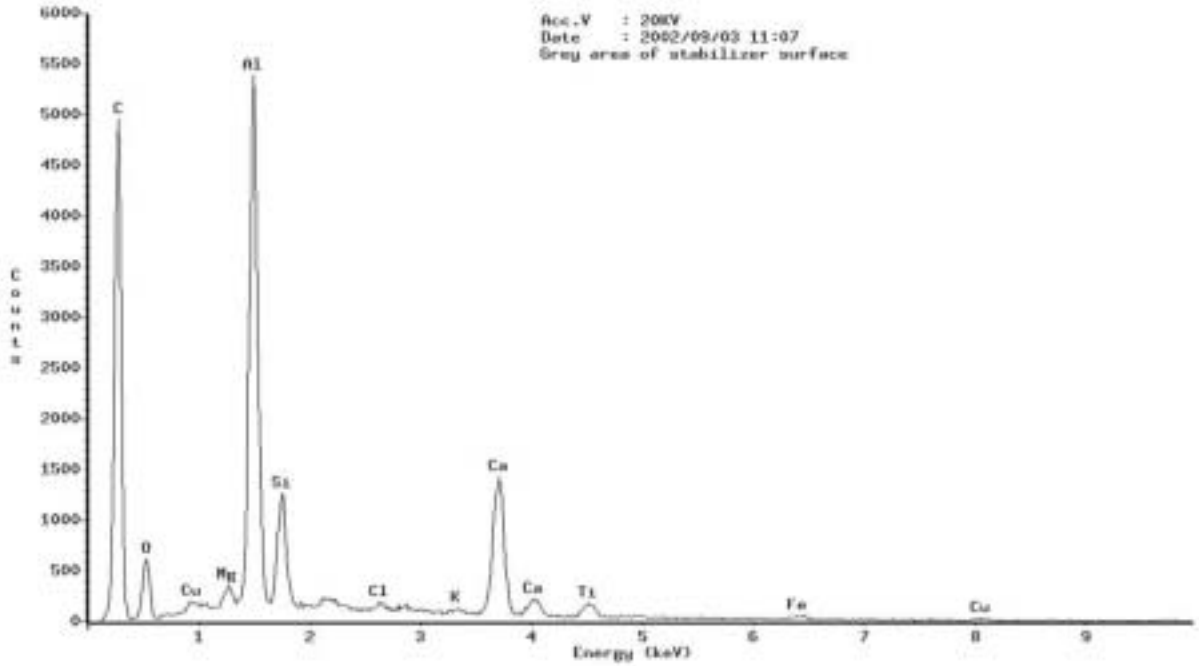

Figure 1.16-206 EDX spectrum of gray portion of transfer mark sample.

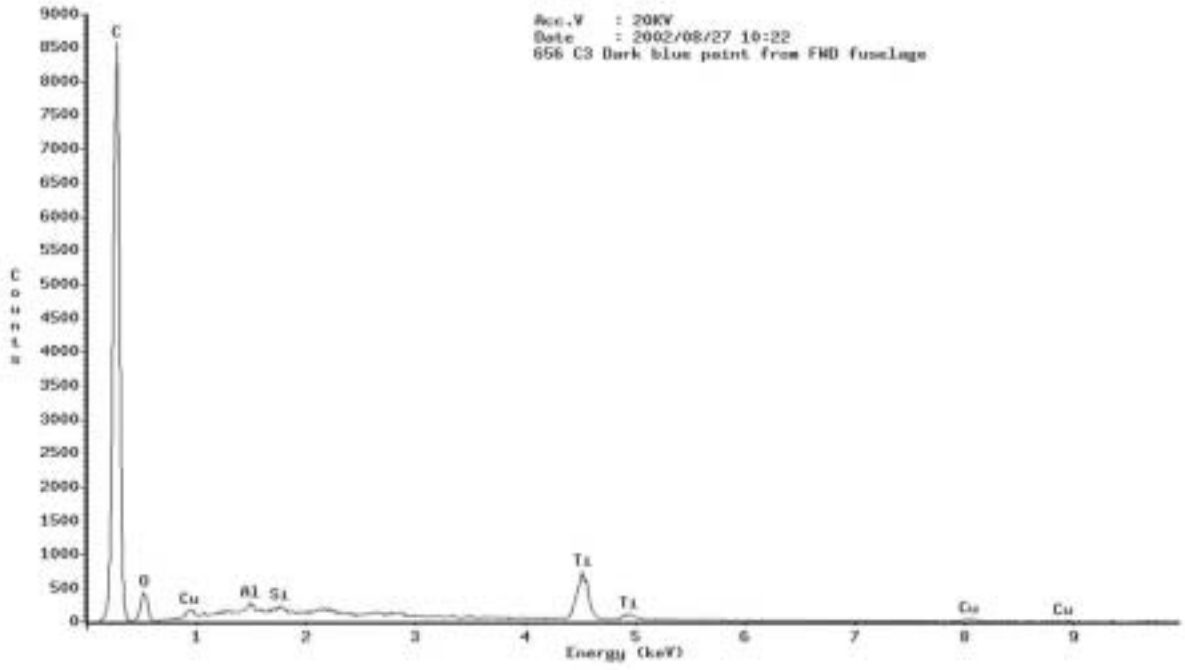

Figure 1.16-207 EDX spectrum of dark blue paint sample (656C3).

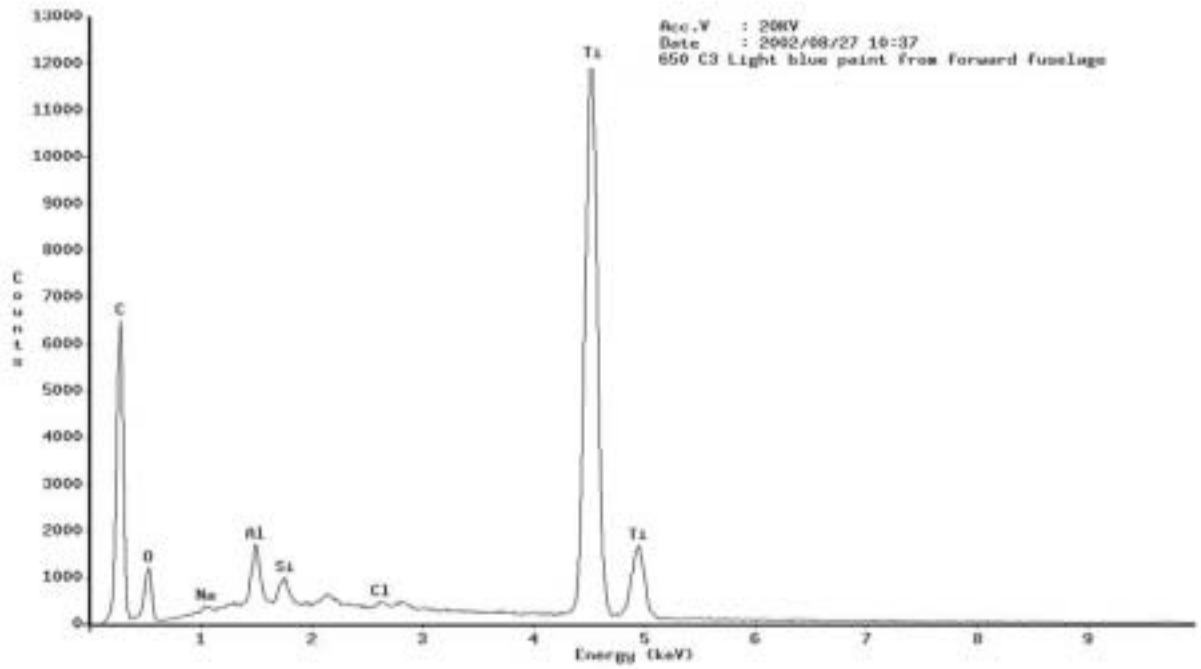

Figure 1.16-208 EDX spectrum of light blue paint sample (650C3).

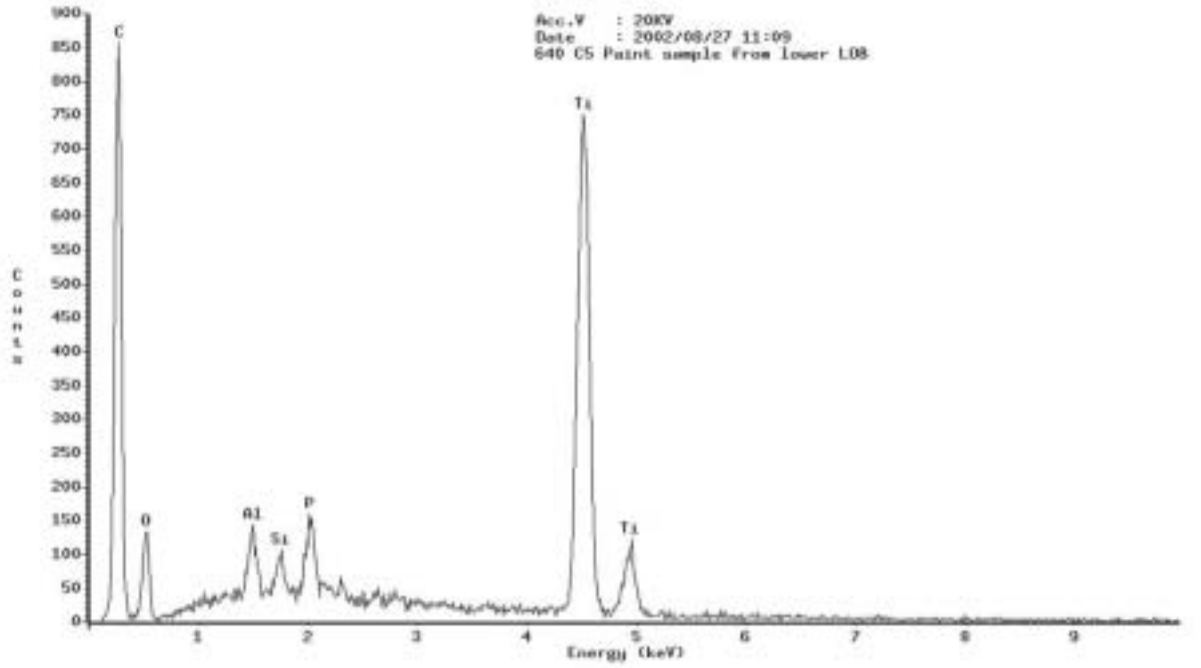

Figure 1.16-209 EDX spectrum of very light blue paint sample (640C5).

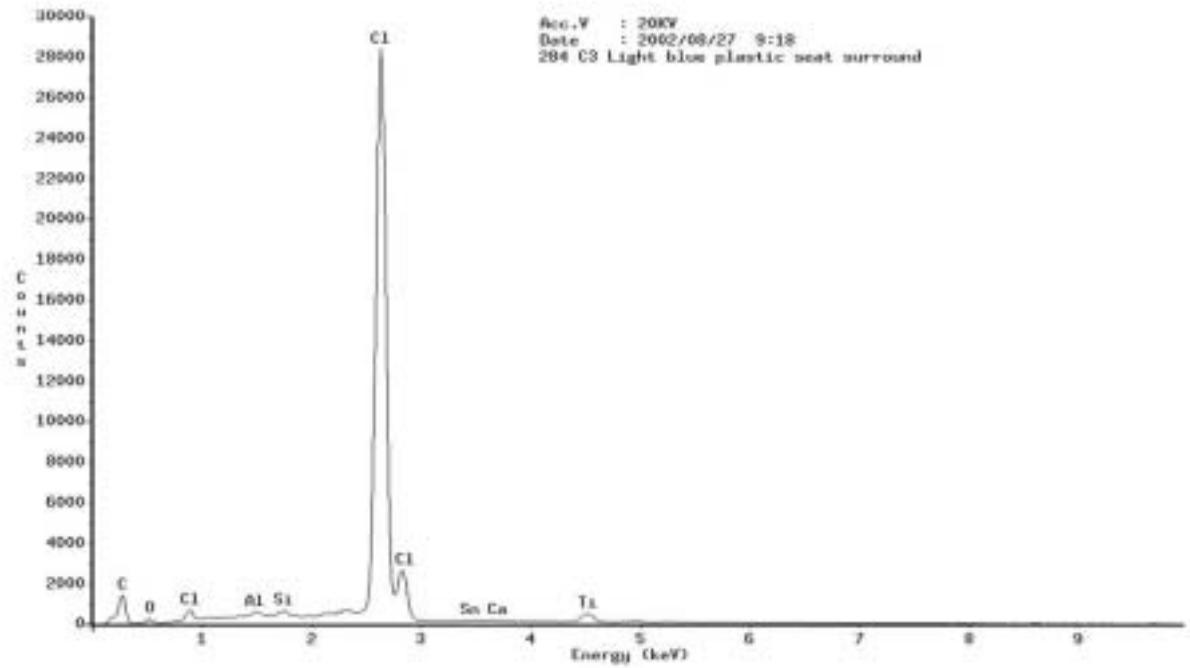

Figure 1.16-210 EDX spectrum of light blue plastic seat surround (284C3).

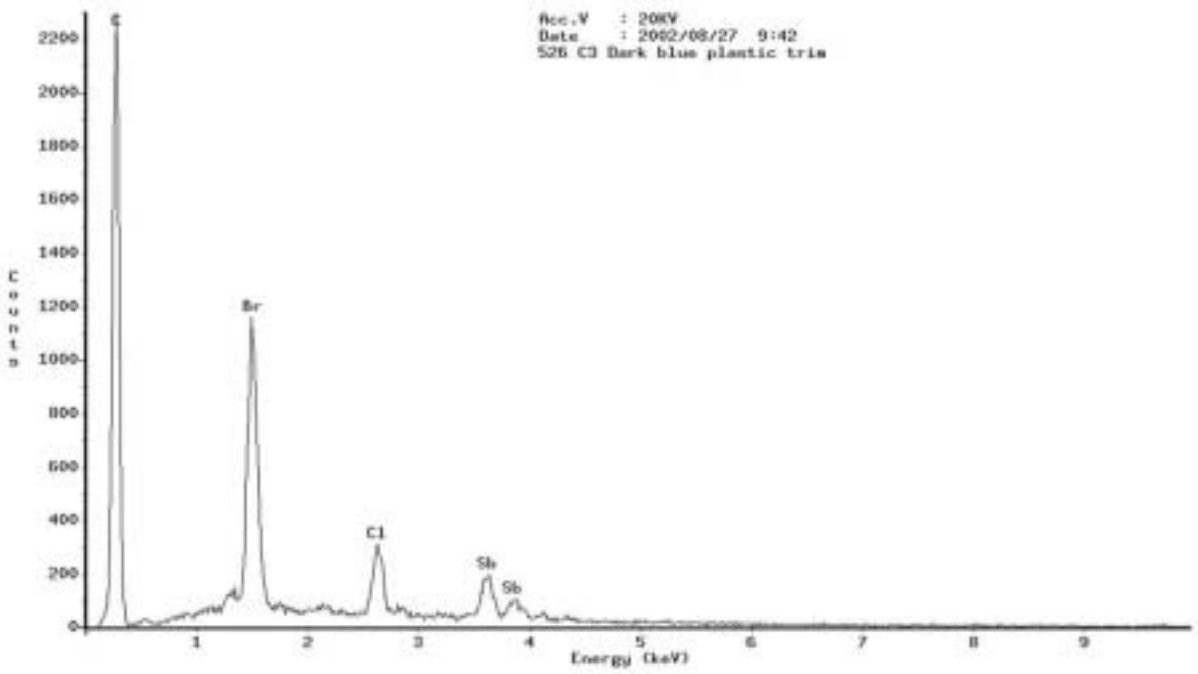

Figure 1.16-211 EDX spectrum of dark blue plastic trim (526C3).

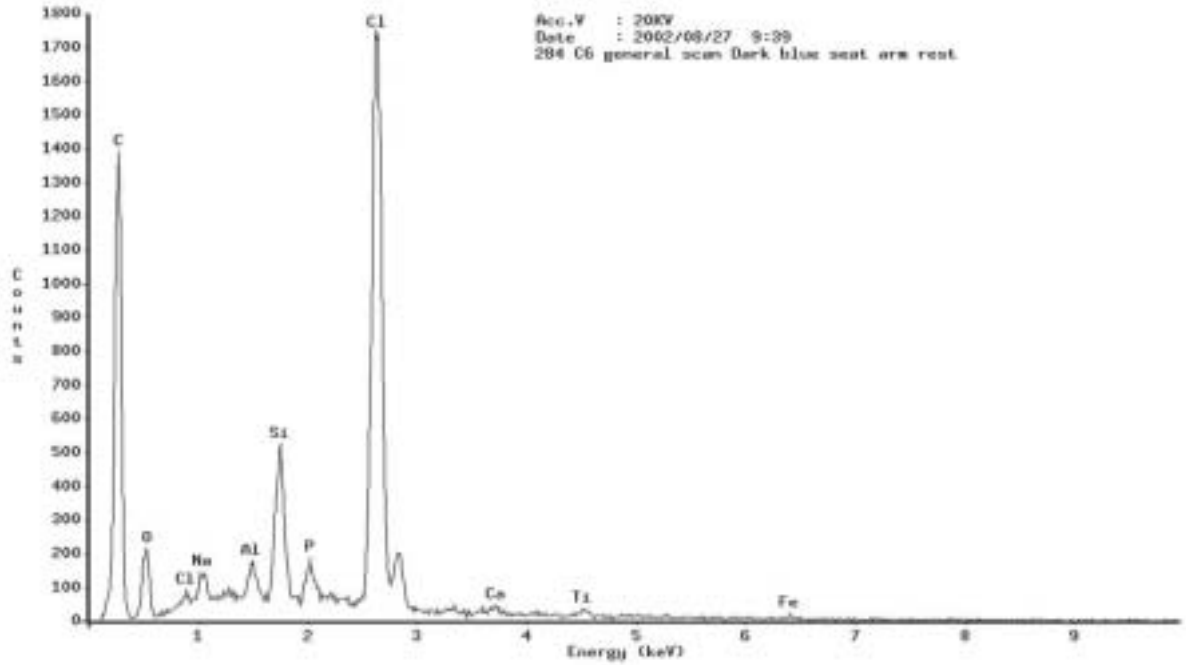

Figure 1.16-212 EDX spectrum of dark blue seat arm rest (284C6).

1.16.3.5 Upper chord of the right wing front spar & left side of body, rear spar internal splice upper tee fitting test by BMT

Background

During a supplemental examination of the wreckage of China Airlines flight CI611, a 747-200 airplane, two structural details were identified to contain areas of cracking that may have existed prior to the accident. As noted in the referenced Sequencing Document Supplement, the two areas identified were the upper chord of the right wing front spar at approximately WS 1116 (Figure 1.16-213) which was thought to possibly contain an area of stress corrosion cracking, and the left side of body, rear spar internal splice upper tee fitting, believed to contain a region of fatigue cracking (Figure 1.16-214). Portions of both details were extracted and submitted for metallurgical analysis (Figure 1.16-215).

Results

Portions of the fracture surfaces of both parts were removed for cleaning and detailed optical and scanning electron microscopic (SEM) examination. The fracture surfaces of both parts were heavily corroded and detailed surface features were difficult to resolve.

Several areas along the aft edge of the upper chord fracture surface where this local portion of the fracture initiated, as well as at locations in the interior, had a dimpled morphology, indicative of ultimate tensile or shear separation (Figures 1.16-216 and 217), not stress corrosion cracking (SCC). In addition, further evidence of plastic deformation from tensile separation (necking) along this edge was observed on metallographic cross sections (Figures 1.16-216 and 218).

The fracture surface of the tee fitting contained a flat profile “thumbnail” region that generally extended forward to approximately 0.75 inches from the aft edge of the part (Figure 1.16-219). Fatigue striations could be resolved in several areas (Figure 1.16-220). The striation spacing, which is an indicator of crack growth rate for a fatigue cracking mechanism, was observed to remain constant at the extent of the fatigue region, which transitioned abruptly to a dimpled morphology due to ultimate tensile separation (Figure 1.16-221). The initiation location was observed to be on the upper surface of the flange near

the aft edge transition radius (Figure 1.16-212). No geometrical anomalies that may have contributed to the initiation were observed.

Induction Couple Plasma (ICP) analysis, hardness, and electrical conductivity measurements on specimens of the upper chord and tee fitting, determined that both parts were fabricated from 7075 aluminum alloy, and were in the –T73XXX condition as required by the design drawing.

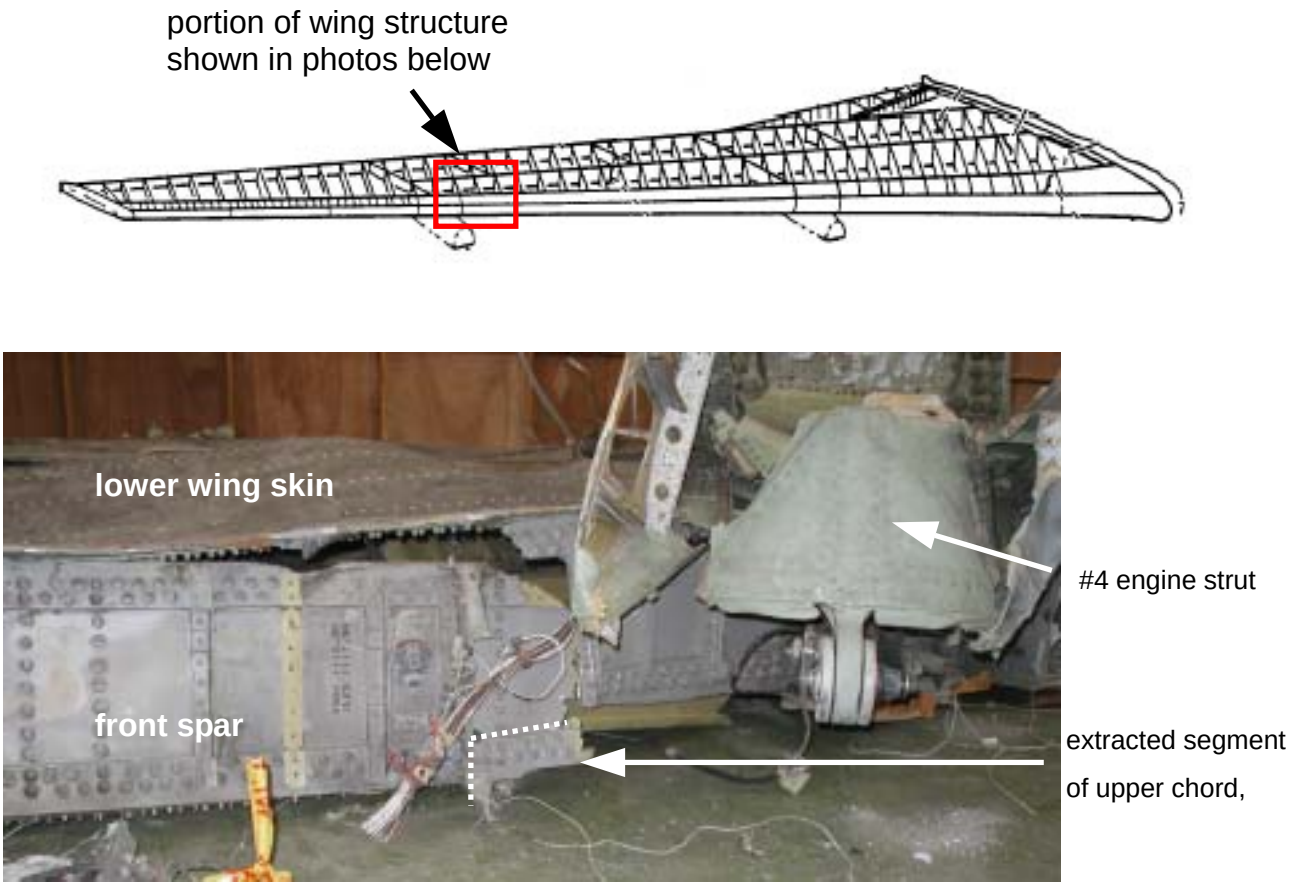

Figure 1.16-213 Diagram of the right wing and photographs showing where the specimens of the upper chord with mating fracture portions were extracted.

Figure 1.16-213(Cont) Diagram of the right wing and photographs showing where the specimens of the upper chord with mating fracture portions were extracted.

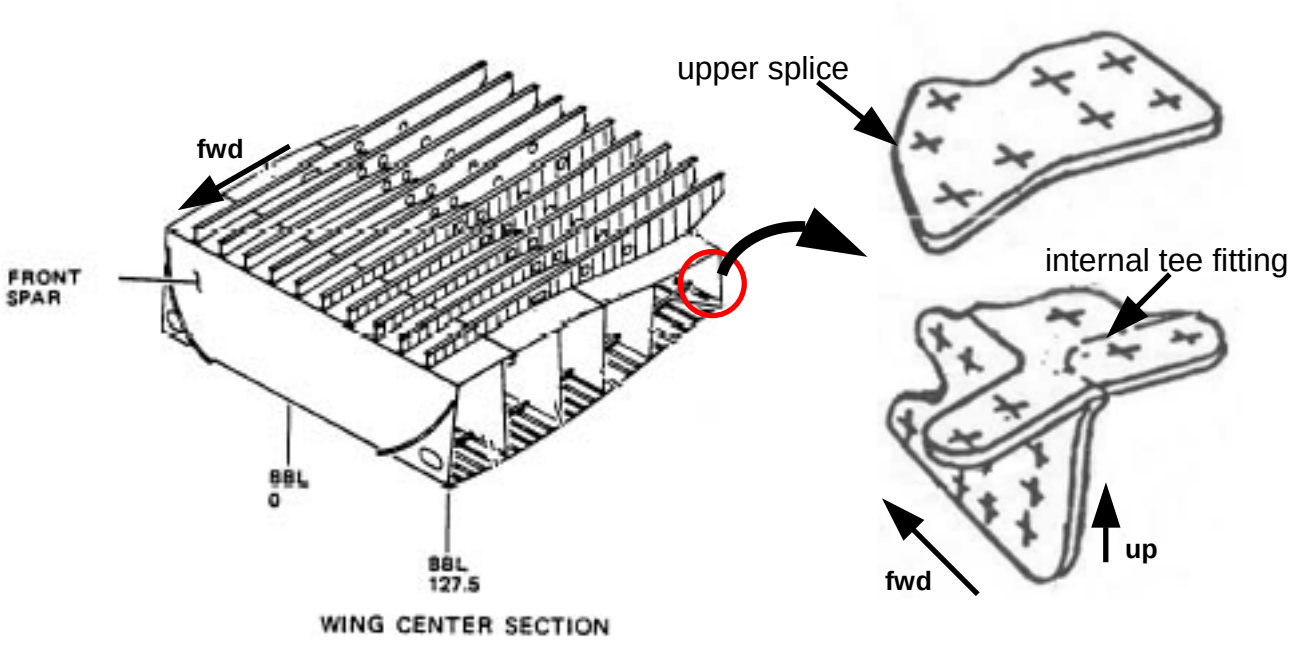

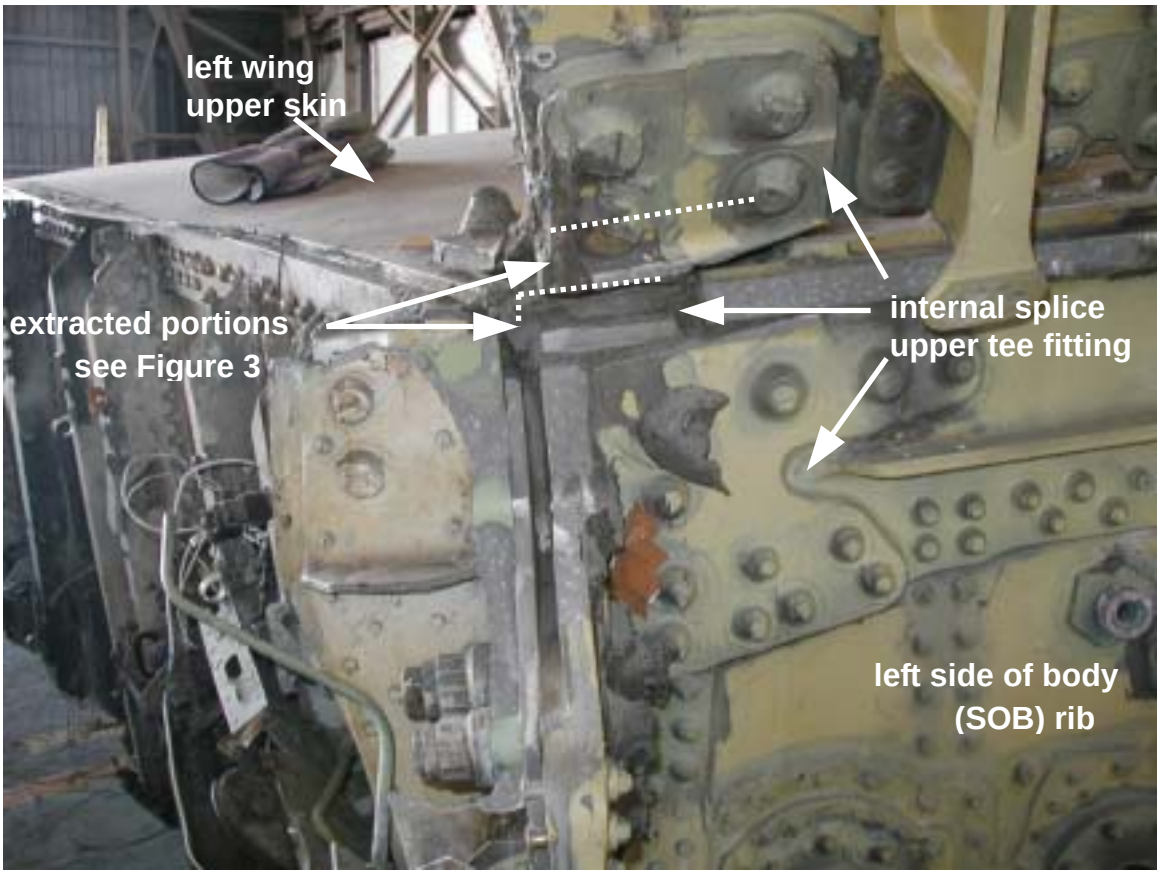

Figure 1.16-214 Diagram and photograph showing the location of the internal splice upper tee fitting and the portions extracted.

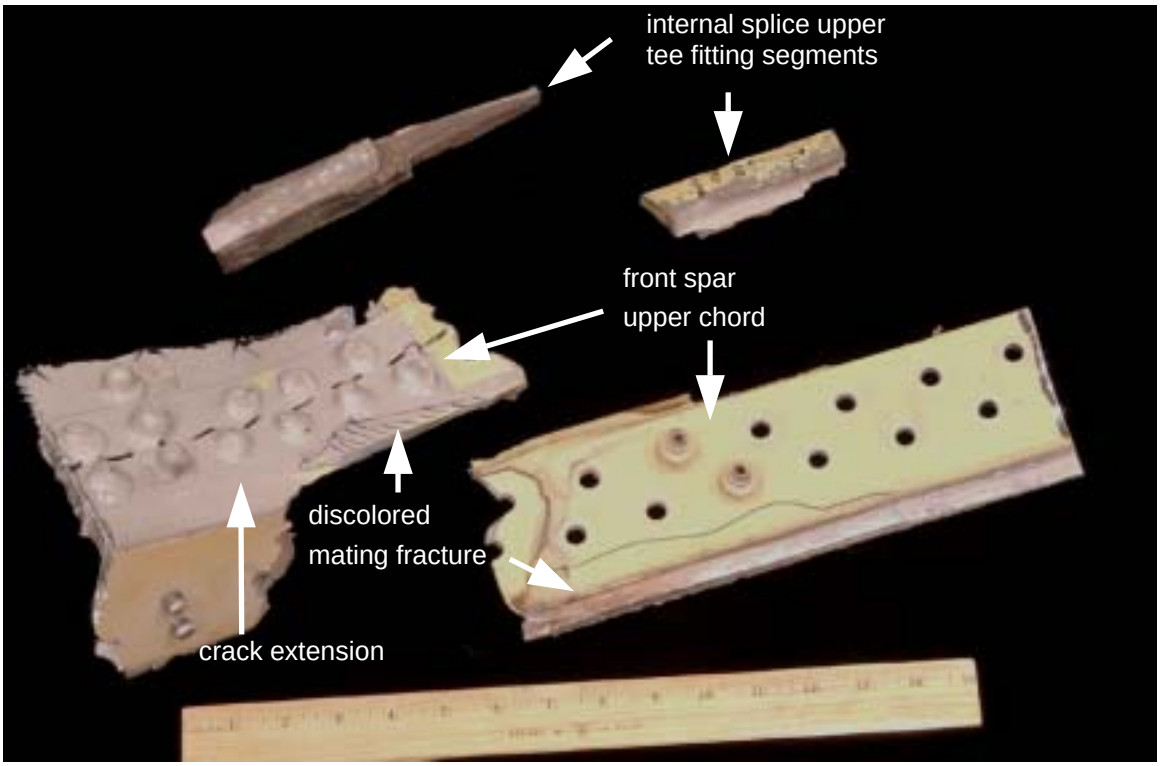

Figure 1.16-215 Photograph of the extracted specimens in the as-received condition.

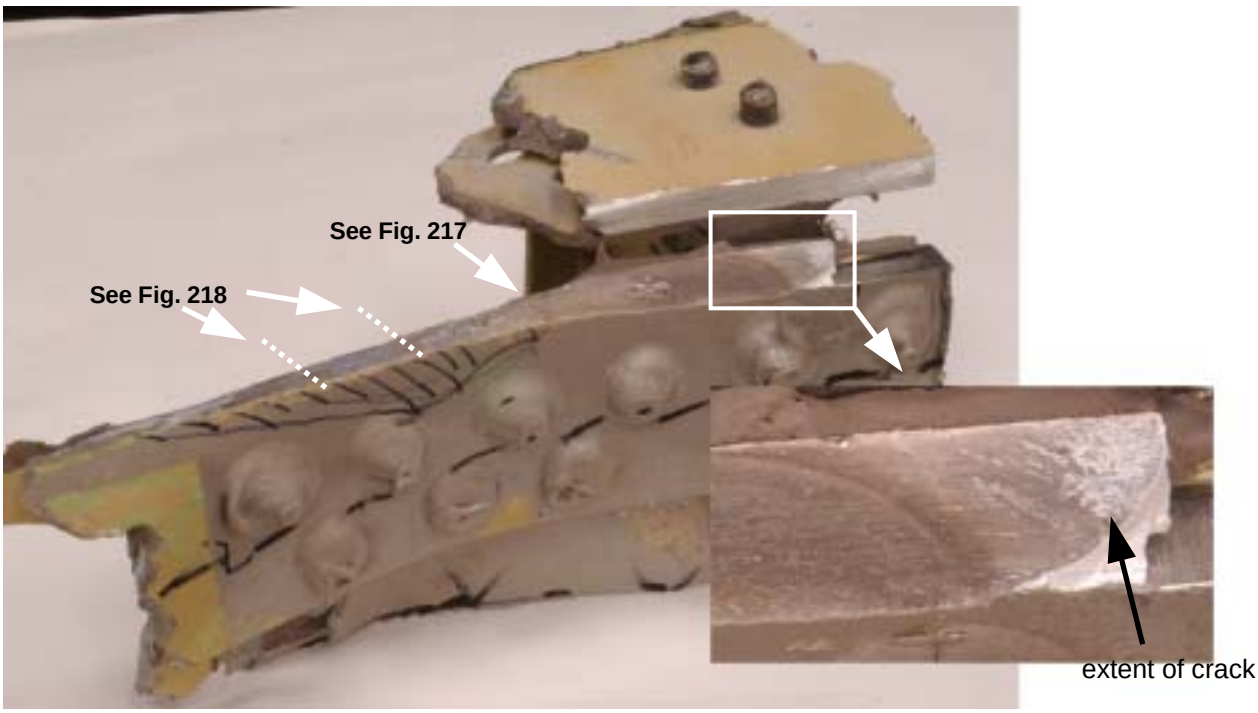

Figure 1.16-216 Photograph showing the discolored fracture of the upper chord after opening the extension of the crack and the locations shown in Figures 5 and 6, where the fracture was characterized on the mating portion by SEM and metallography.

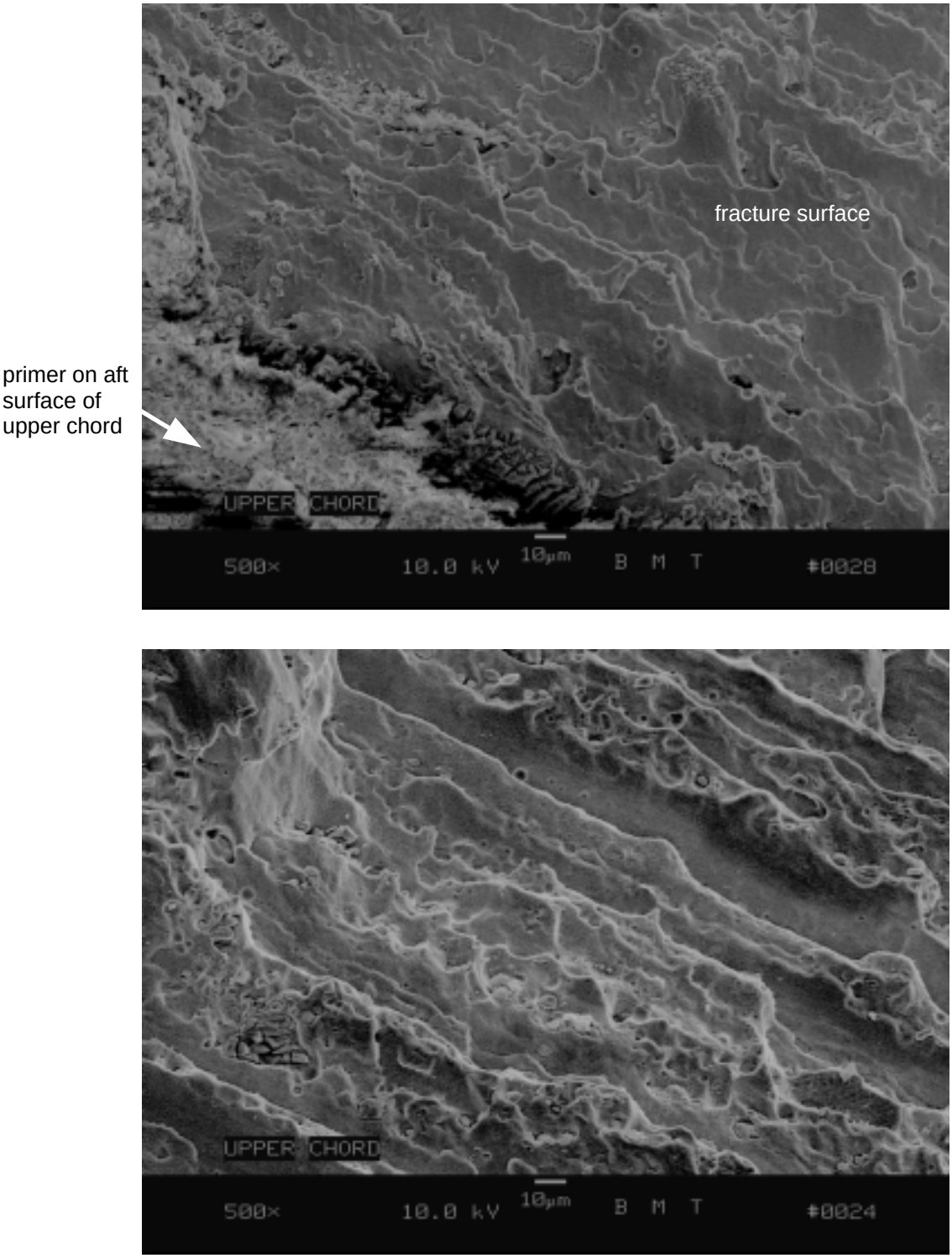

Figure 1.16-217 SEM photographs of portions of the mating fracture to that shown in Figure 4 at the corresponding location indicated. The entire fracture surface suffered from heavy corrosion. However, evidence of ductile separation represented by the remnant dimpled morphology was observed at locations along the aft edge (top photo) as well as through the interior (bottom photo).

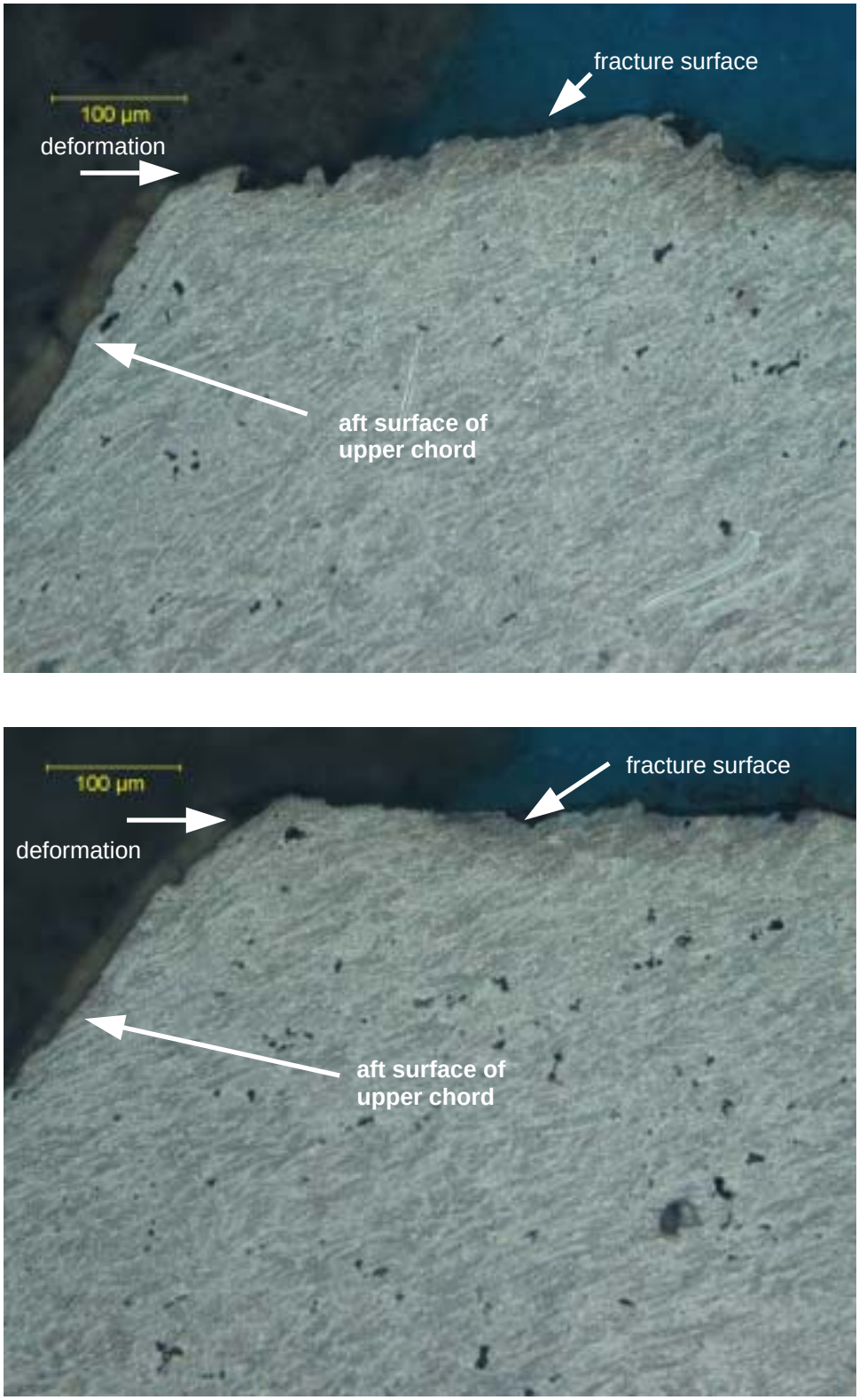

Figure 1.16-218 Metallographic cross sections showing the residual inward deformation, commonly known as “necking”, adjacent to the fracture surface consistent with an ultimate tensile/shear separation mechanism.

Figure 1.16-219 Photograph of the outboard half of the fracture of the upper tee fitting showing the distinct “thumbnail” region, associated with a flat profile.

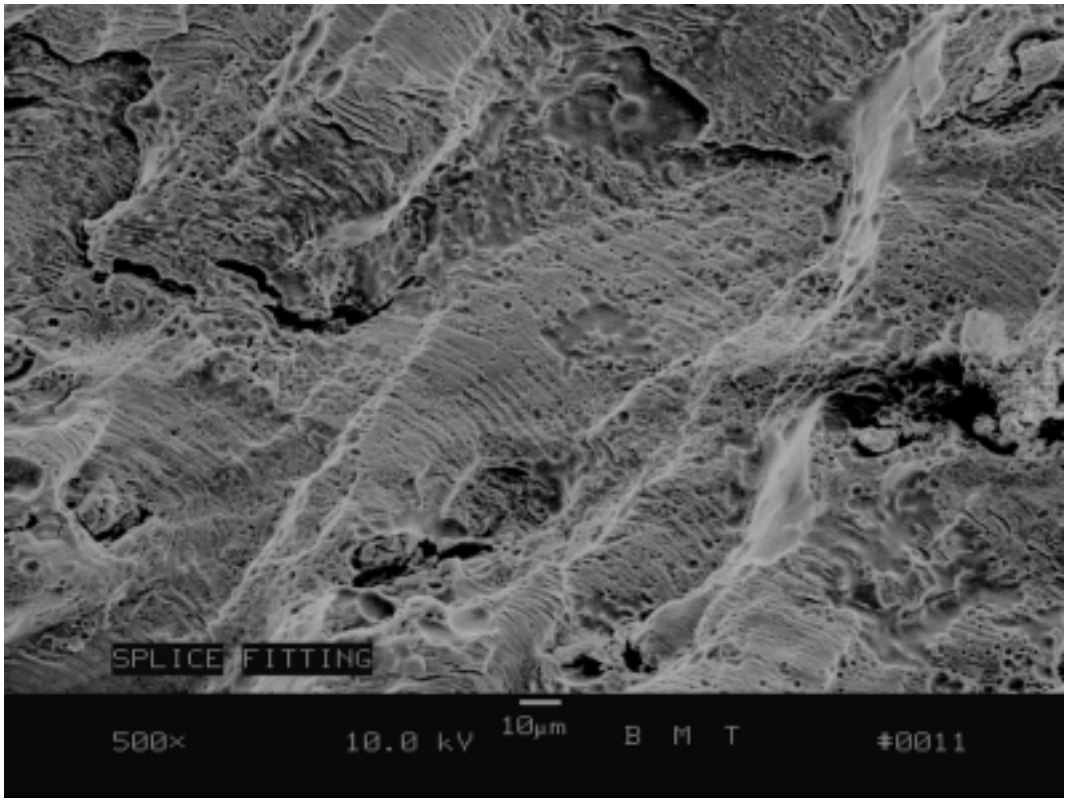

Figure 1.16-220 SEM photograph of the inboard fracture of the tee fitting within the flat profile (thumbnail) region showing fatigue striations.

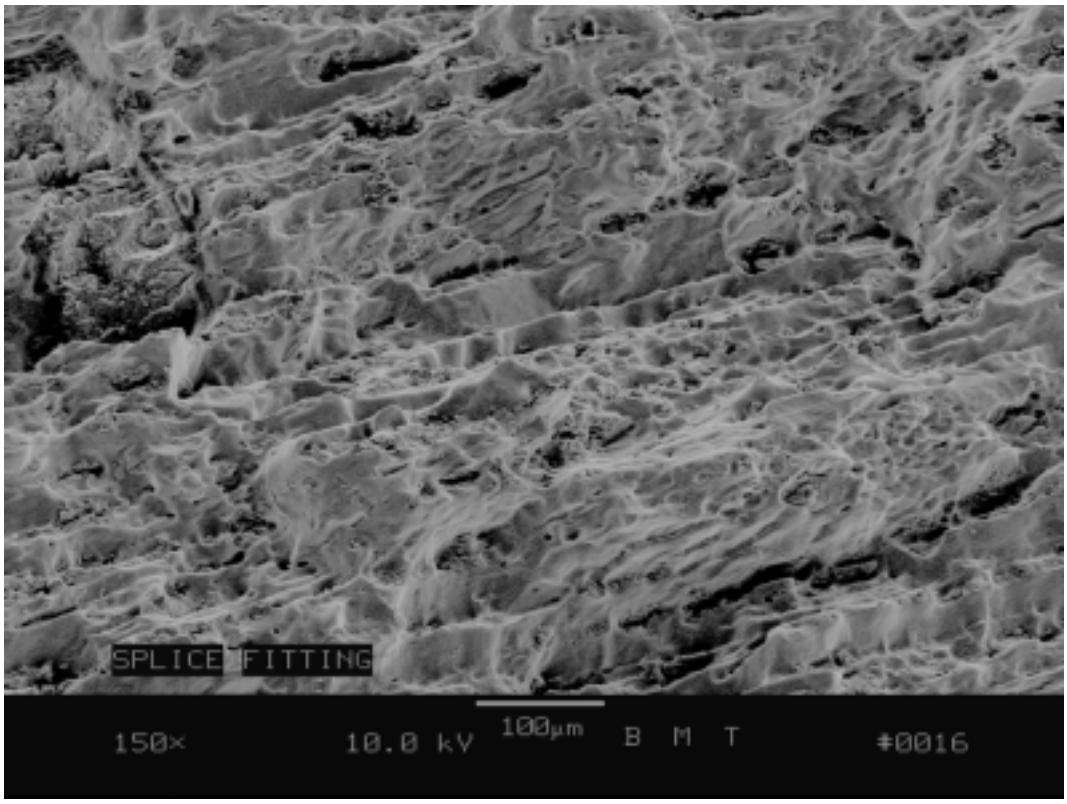

Figure 1.16-221 SEM photograph of the upper tee fitting fracture surface showing the typical dimpled morphology beyond the “thumbnail” region.

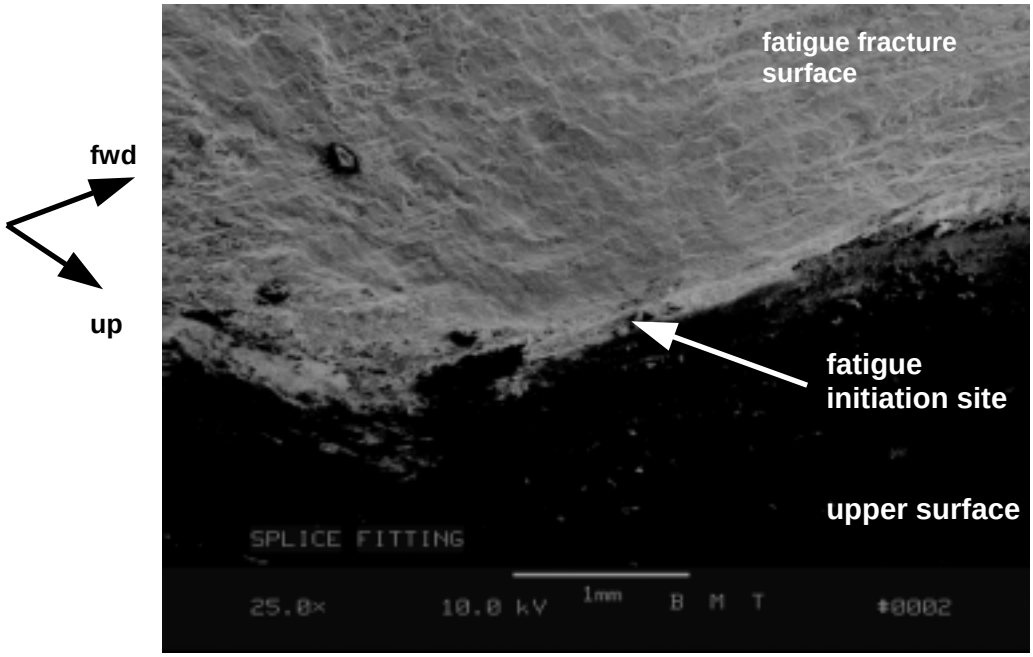

Figure 1.16-222 SEM photograph of the fatigue initiation location adjacent to the radius of the aft edge of the fitting.

IV. Appendix

7-1 Boeing Materials Technology MS 22570 Appendix I

Hole # +3

Cycles	Crack Length (mm)	da/dN (micron/cycle)	Photo #209	x0=27.100	y0=11.848	slope	theta (absolute)	deviation angle
	1.410175876		EOC *	26.84	13.234	-5.3308	1.3853613	
	0.218141585	0.07692	210	26.999	12.051	-2.0099	1.1091211	0.2762402
217	0.237307988	0.10000	211	26.991	12.069	-2.0275	1.1125933	0.2727679
703	0.304387564	0.09091	212	26.995	12.138	-2.7619	1.2234104	0.1619509
116	0.315506745	0.10000	213	26.988	12.148	-2.6786	1.2134876	0.1718736
207	0.333257722	0.07143	214	27.009	12.17	-3.5385	1.2953702	0.089991
1594	0.45660262	0.08333	215	27.049	12.303	-8.9216	1.4591743	0.0738131
2746	0.669085336	0.07143	216	27.168	12.516	9.82353	1.4693494	0.0839881
997	0.754529998	0.10000	217	27.141	12.608	18.5366	1.5169012	0.1315399
222	0.776705955	0.10000	218	27.144	12.63	17.7727	1.5145896	0.1292284
543	0.821917337	0.06667	219	27.144	12.676	18.8182	1.5177062	0.1323449
614	0.8862313	0.14286	220	27.125	12.745	35.88	1.5429329	0.1575716
34	0.908282451	1.14286	221	27.106	12.771	153.833	1.5642959	0.1789346
26	0.944648127	1.66667	224	27.106	12.808	160	1.5645464	0.1791852
47	1.043245758	2.50000	225	27.161	12.898	17.2131	1.5127663	0.1274051
25	1.111370594	2.85710	226	27.168	12.966	16.4412	1.5100483	0.124687
80911	**Total between 1st and Last**		x0, y0	27.1	11.848			

105	Last Point to EOC
2836	Initiation to First Point
11031	**Total (including extrapolation)**

* EOC(not completely through thickness)

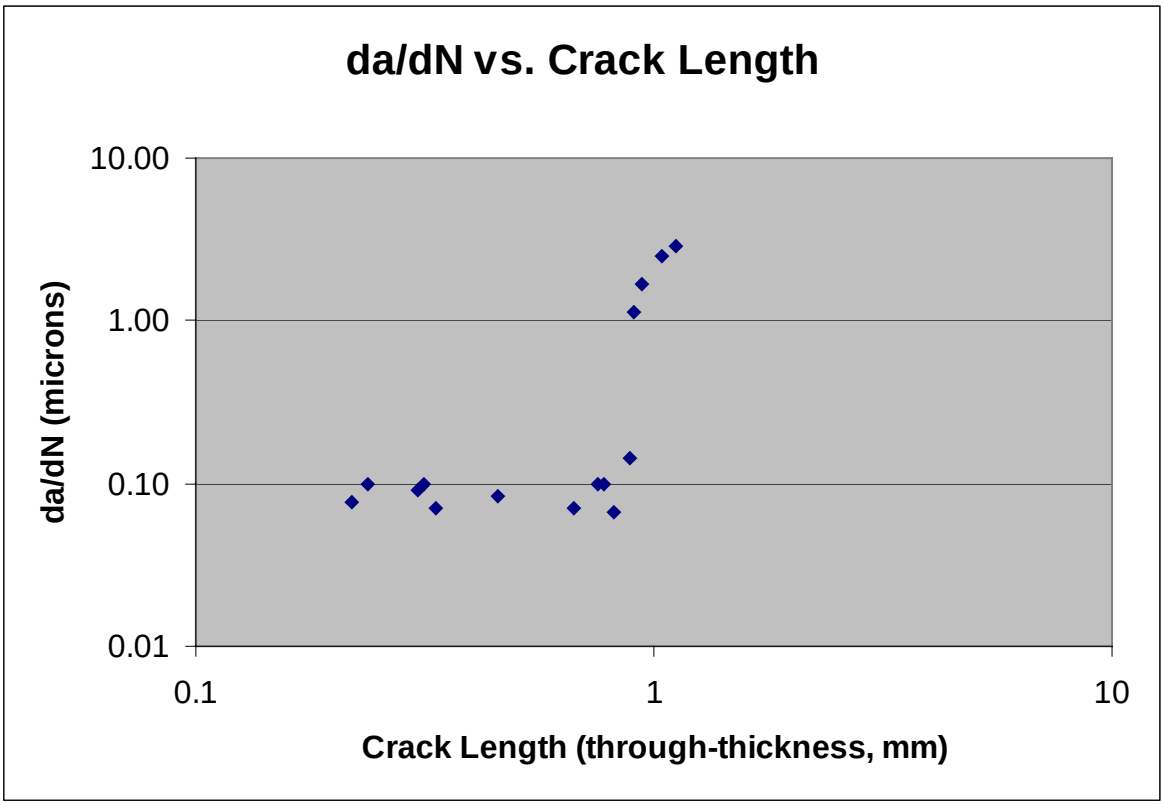
da/dN vs. Crack Length
10.00
1.00
0.10
0.01
da/dN (microns)
0.1
1
10
Crack Length (through-thickness, mm)

Hole #5

Cycles	Crack Length (mm)	da/dN (micron/cycle)	Photo #154	x0=1.671	y0=1.130	slope	theta (absolute)	deviation angle
	1.828415981		EOC	2.039	2.921	4.86685	1.368145	
	0.214554568	0.08333	170	2.226	1.235	0.18919	0.1869793	1.1811657
2713	0.497134683	0.12500	155	1.693	1.633	22.8636	1.5270866	0.1589416
43	0.502522298	0.12500	152	1.6709	1.643	-5130	1.5706014	0.2024564
591	0.5887145	0.16667	156	1.71	1.723	15.2051	1.5051236	0.1369786
122	0.604990884	0.10000	157	1.713	1.739	14.5	1.5019398	0.1337948
145	0.630324834	0.25000	158	1.654	1.77	-37.647	1.5442401	0.1760951
129	0.658275257	0.18182	159	1.676	1.801	134.2	1.5633449	0.1951999
257	0.702984995	0.16667	160	1.684	1.845	55	1.5526165	0.1844715
89	0.719247706	0.20000	161	1.721	1.854	14.48	1.501845	0.1337
511	0.84338029	0.28571	162	1.744	1.976	11.589	1.4847211	0.1165761
432	0.958965584	0.25000	163	1.744	2.094	13.2055	1.4952144	0.1270694
200	1.00894874	0.25000	164	1.749	2.144	13	1.4940244	0.1258794
645	1.161125817	0.22222	165	1.601	2.301	-16.729	1.5110894	0.1429444
288	1.265076451	0.50000	166	1.873	2.38	6.18812	1.4105814	0.0424364
266	1.384968752	0.40000	168	1.909	2.495	5.73529	1.3981727	0.0300277
249	1.683444595	2.00000	169	2.039	2.773	4.46467	1.3504524	0.0176925
66791	**Total between 1st and Last**		x0, y0	1.671	1.13			

145 Last Point to EOC

2575 Initiation to First Point

9398 Total (including extrapolation)

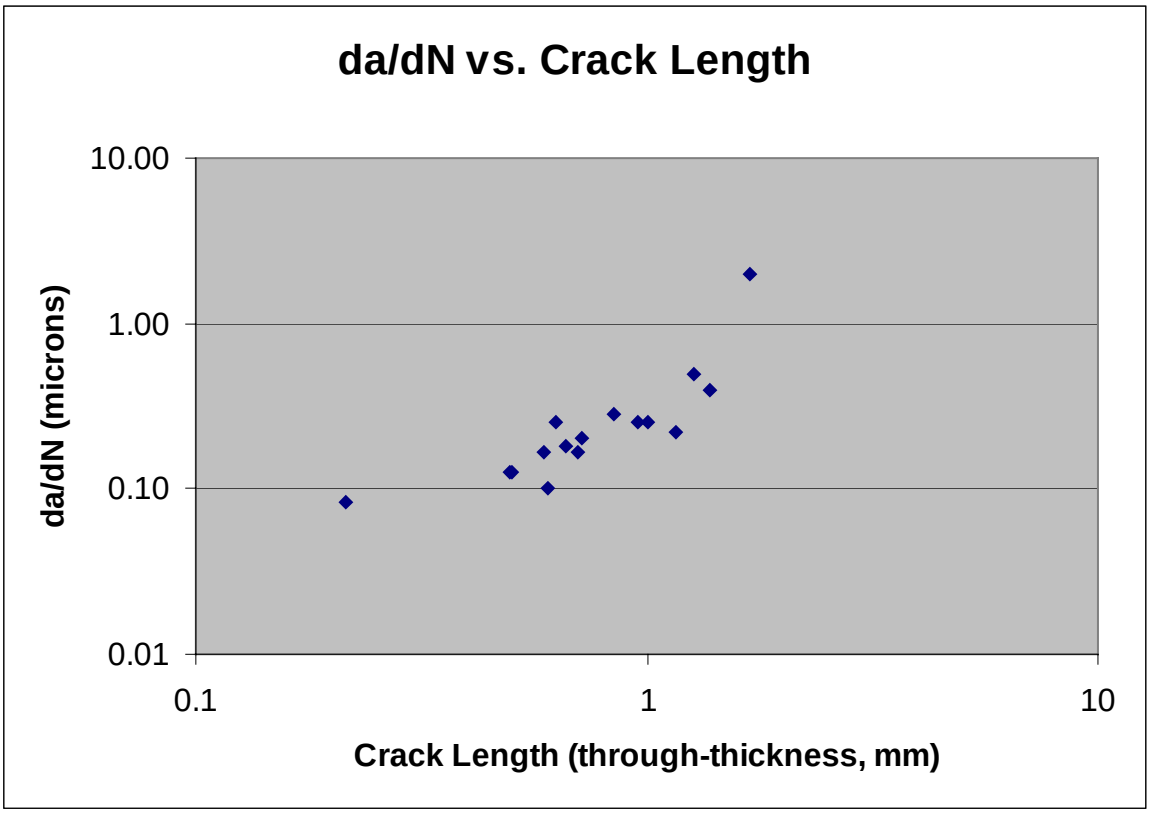
da/dN vs. Crack Length
10.00
1.00
0.10
0.01
da/dN (microns)
0.1
1
10
Crack Length (through-thickness, mm)

Hole #12

Cycles	Crack Length (mm)	da/dN (micron/cycle)	Photo #	x0=-19.036	y0=-19.500	slope	theta (absolute)	deviation angle
	1.921595691		EOC	-19.845	-17.757	-2.1545	1.1362441	
	0.234756459	0.25000	2	-19.111	-19.276	-2.9867	1.2477071	0.111463
322	0.30184081	0.16667	4	-19.154	-19.222	-2.3559	1.1693828	0.0331387
444	0.41279287	0.33333	5	-19.159	-19.102	-3.2358	1.271062	0.1348178
202	0.486907836	0.40000	6	-19.195	-19.037	-2.9119	1.2400021	0.103758
102	0.548358328	0.80000	7	-19.216	-18.979	-2.8944	1.2381455	0.1019013
117	0.642332831	0.80000	10	-19.241	-18.887	-2.9902	1.2480673	0.1118232
97	0.729314708	1.00000	11	-19.23	-18.786	-3.6804	1.3054926	0.1692485
102	0.848713914	1.33333	12	-19.296	-18.685	-3.1346	1.2619841	0.1257399
123	1.0074778	1.25000	13	-19.574	-18.639	-1.6004	1.0123014	0.1239427
34	1.063129986	2.00000	14	-19.592	-18.586	-1.6439	1.0242852	0.1119589
74	1.230416997	2.50000	15	-19.845	-18.519	-1.2126	0.8811934	0.2550507
1618	**Total between 1st and Last**		x0, y0	-19.036	-19.5			

276	Last Point to EOC
939	Initiation to First Point
2834	**Total (including extrapolation)**

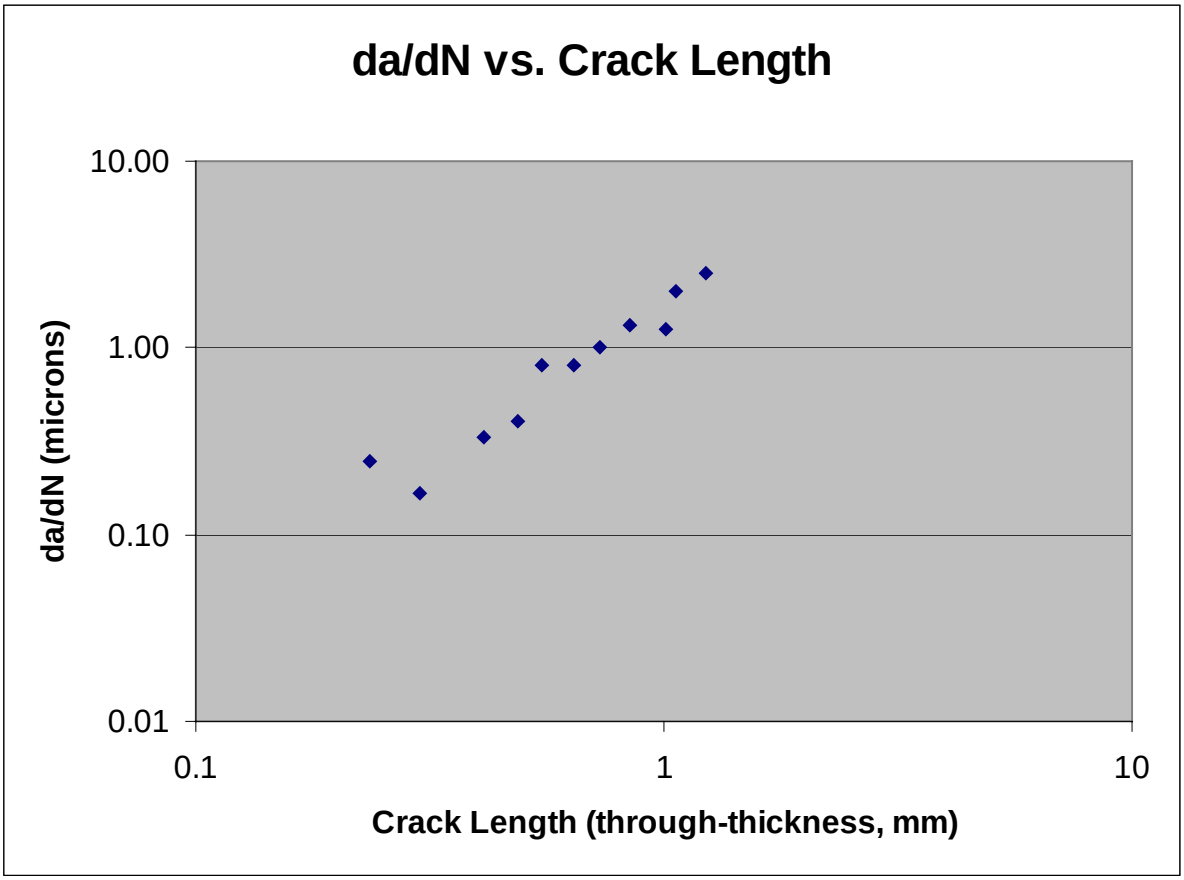
da/dN vs. Crack Length
10.00
1.00
0.10
0.01
da/dN (microns)
0.1
1
10
Crack Length (through-thickness, mm)

Hole #13

Cycles	Crack Length (mm)	da/dN (micron/cycle)	Photo #	x0=5.086	y0=-2.795	slope	theta (absolute)	deviation angle
	1.797220632		EOC	5.445	-1.034	4.90529	1.3696906	
	0.043691352	0.12500	24	4.985	-2.771	-0.2376	0.233297	1.1363937
1510	0.20094194	0.08333	23	4.963	-2.615	-1.4634	0.9713438	0.3983468
466	0.241515144	0.09091	22	4.961	-2.574	-1.768	1.0560469	0.3136438
242	0.262634421	0.08333	21	4.973	-2.55	-2.1681	1.1386474	0.2310432
1159	0.426819605	0.20000	20	4.931	-2.391	-2.6065	1.2044521	0.1652385
240	0.46797315	0.14286	19	4.931	-2.349	-2.8774	1.2363204	0.1333702
57	0.477771613	0.20000	18	4.931	-2.339	-2.9419	1.2431365	0.1265542
91	0.502145916	0.33333	25	5.015	-2.297	-7.0141	1.4291804	0.0594898
51	0.517796192	0.28571	28	5.074	-2.269	-43.833	1.5479866	0.178296
5	0.519631804	0.40000	26	5.055	-2.271	-16.903	1.5117049	0.1420143
67	0.544289879	0.33333	27	5.064	-2.244	-25.045	1.5308901	0.1611995
163	0.594823463	0.28571	29	5.101	-2.191	40.2667	1.545967	0.1762764
518	0.798194153	0.50000	30	5.083	-1.981	-271.33	1.5671108	0.1974202
496	1.087818582	0.66667	31	5.136	-1.695	22	1.525373	0.1556824
180	1.227972215	0.88889	32	5.249	-1.575	7.48466	1.4379764	0.0682857
176	1.376450368	0.80000	33	5.335	-1.441	5.43775	1.3889288	0.0192382
5422	**Total between 1st and Last**		x0, y0	5.086	-2.795			
526	Last Point to EOC							
350	Initiation to First Point							
6297	**Total (including extrapolation)**							

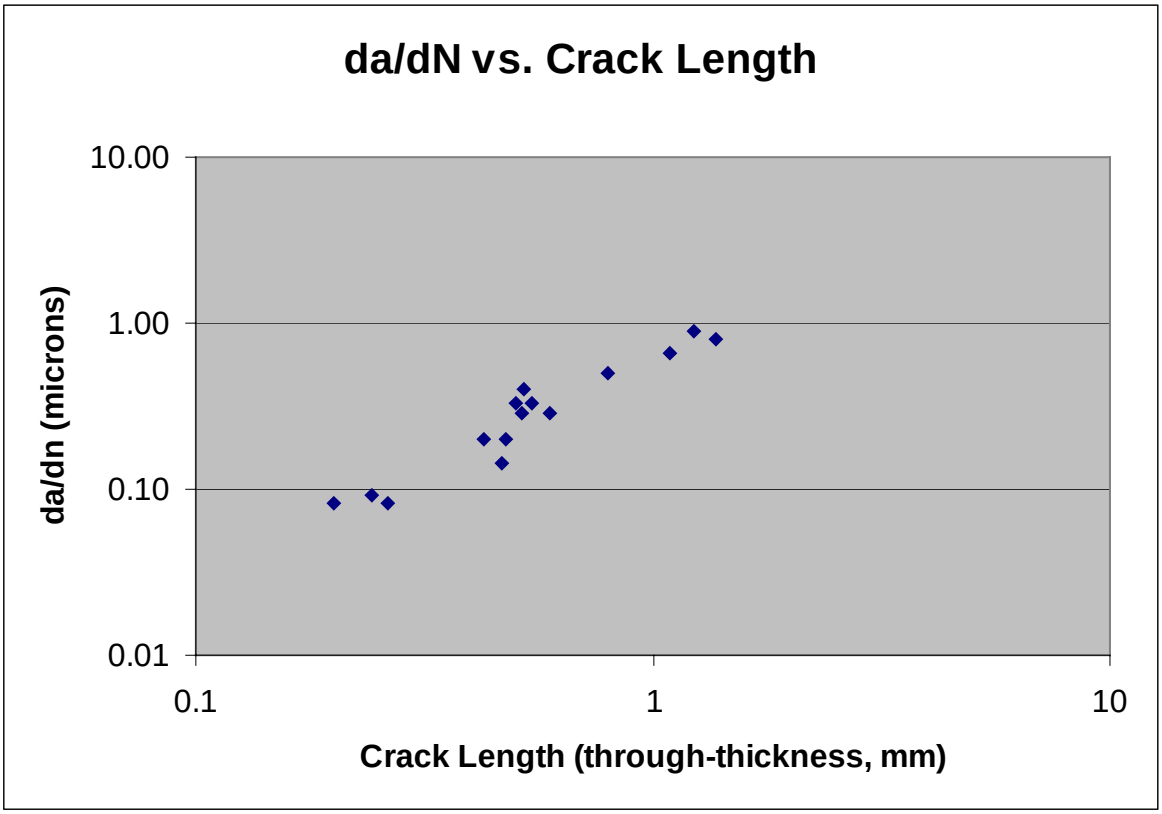
da/dN vs. Crack Length
10.00
1.00
0.10
0.01
da/dn (microns)
0.1
1
10
Crack Length (through-thickness, mm)

Hole #13-14

Cycles	Crack Length (mm)	da/dN (micron/cycle)	Photo 35	x0=15.920	y0=-6.992	slope	theta (absolute)	deviation angle
	1.797220632		EOC	*	*	4.90529	1.3696906	
	0.02727378	0.11111	41	15.911	-6.966	-2.8889	1.237552	0.1321386
159	0.044967768	0.11111	42	15.944	-6.951	1.70833	1.0412067	0.3284839
369	0.096224691	0.16667	40	15.921	-6.894	98	1.5605926	0.190902
730	0.289891508	0.36364	44	15.934	-6.699	20.9286	1.5230511	0.1533605
17	0.296332009	0.40000	43	15.913	-6.691	-43	1.5475447	0.1778541
275	0.600986312	1.81818	45	16.01	-6.397	6.61111	1.4206738	0.0509832
42	0.660767509	1.00000	46	15.961	-6.326	16.2439	1.5093124	0.1396217
239	0.950667364	1.42857	47	16.029	-6.044	8.69725	1.4563201	0.0866295
206	1.355110194	2.50000	48	16.278	-5.682	3.65922	1.3040276	0.065663
5	1.368241582	2.85714	49	16.123	-5.637	6.67488	1.4220868	0.0523962
Total between								
2042 1st and Last			x0, y0	15.92	-6.992			

150 Last Point to EOC

245 Initiation to First Point

2438 Total (including extrapolation)

* x, y coordinates for end of cracking (EOC) was not recorded for traverse between 13 and 14.
Slope and length of path at hole 13 is used as reference for this path as well

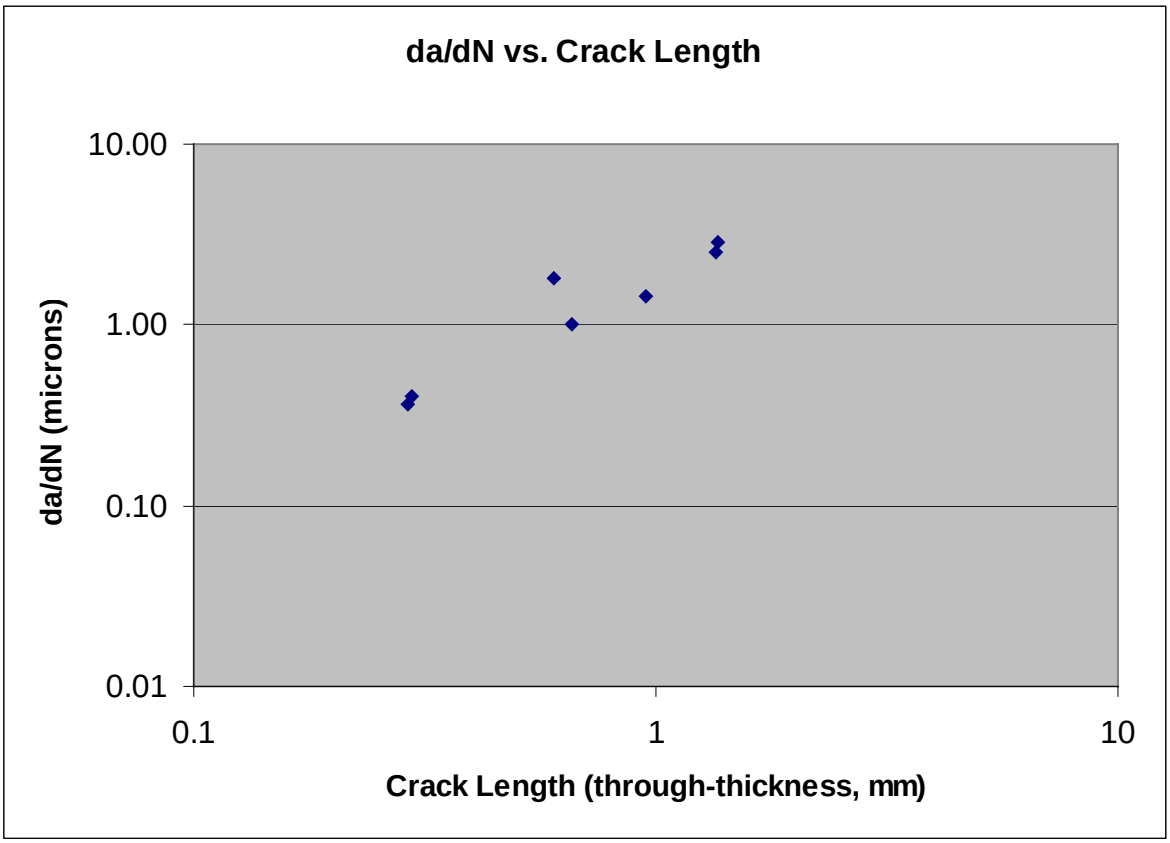
da/dN vs. Crack Length
10.00
1.00
0.10
0.01
da/dN (microns)
0.1
1
10
Crack Length (through-thickness, mm)

Hole #15

Cycles	Crack Length (mm)	da/dN (micron/cycle)	Photo #39	x0=-13.396	y0=1.229	slope	theta (absolute)	deviation angle
	1.768373264		EOC	-13.246	2.991	11.7467	1.4858706	
	0.206262449	0.09091	50	-13.3961	1.436	-2070	1.5703132	0.0844427
111	0.21590012	0.08333	53	-13.404	1.445	-27	1.5337762	0.0479057
2101	0.603610121	0.28571	54	-13.652	1.813	-2.2813	1.1576675	0.3282031
900	1.332083021	1.33333	55	-13.712	2.539	-4.1456	1.3340968	0.1517737
13	1.346959971	1.00000	57	-13.304	2.573	14.6087	1.5024506	0.01658
13	1.359847522	1.00000	56	-13.387	2.593	151.556	1.5641982	0.0783276
3137	**Total between 1st and Last**		x0, y0	-13.396	1.229			

409	Last Point to EOC
2269	Initiation to First Point
5815	**Total (including extrapolation)**

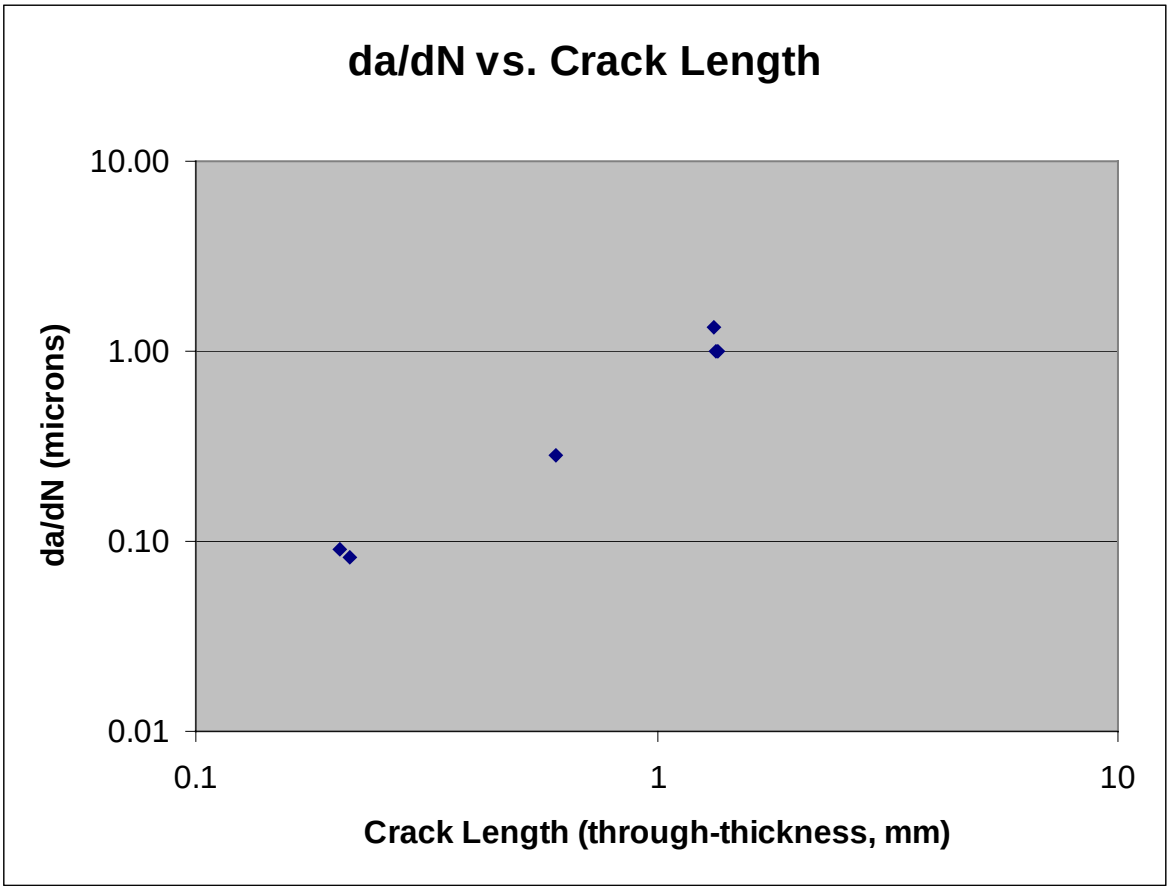
da/dN vs. Crack Length
10.00
1.00
0.10
0.01
da/dN (microns)
0.1
1
10
Crack Length (through-thickness, mm)

Hole #16-17

Cycles	Crack Length (mm)	da/dN (micron/cycle)	Photo # 71	x0=13.979	y0=-6.860	slope	theta (absolute)	deviation angle
	1.879377823		EOC	15.069	-5.329	1.40459	0.9520932	
	0.090482072	0.14286	58	13.9791	-6.749	1110	1.5698954	0.6178022
753	0.186094034	0.11111	59	14.158	-6.759	0.56425	0.5137147	0.4383785
203	0.207482495	0.10000	60	14.171	-6.742	0.61458	0.5510736	0.4010196
166	0.222712536	0.08333	61	14.179	-6.729	0.655	0.5798821	0.3722111
169	0.239102534	0.11111	62	14.189	-6.716	0.68571	0.6010738	0.3510194
738	0.548519828	0.72727	63	14.509	-6.564	0.55849	0.5093385	0.4427547
42	0.58667022	1.11111	64	14.52	-6.525	0.61922	0.5544348	0.3976584
42	0.647948478	1.81818	65	14.731	-6.6	0.34574	0.3328789	0.6192143
135	0.866433019	1.42857	66	14.89	-6.445	0.45554	0.4274542	0.524639
56	0.962263138	2.00000	67	14.801	-6.264	0.72506	0.6273481	0.3247451
74	1.159757753	3.33333	68	14.921	-6.107	0.79936	0.6743524	0.2777408
200	1.659100135	1.66667	69	14.935	-5.504	1.41841	0.9567127	0.0046195
57	1.801846313	3.33333	70	15.021	-5.39	1.41075	0.9541597	0.0020665
2633	**Total between 1st and Last**		x0, y0	13.979	-6.86			

23	Last Point to EOC
633	Initiation to First Point
3290	**Total (including extrapolation)**

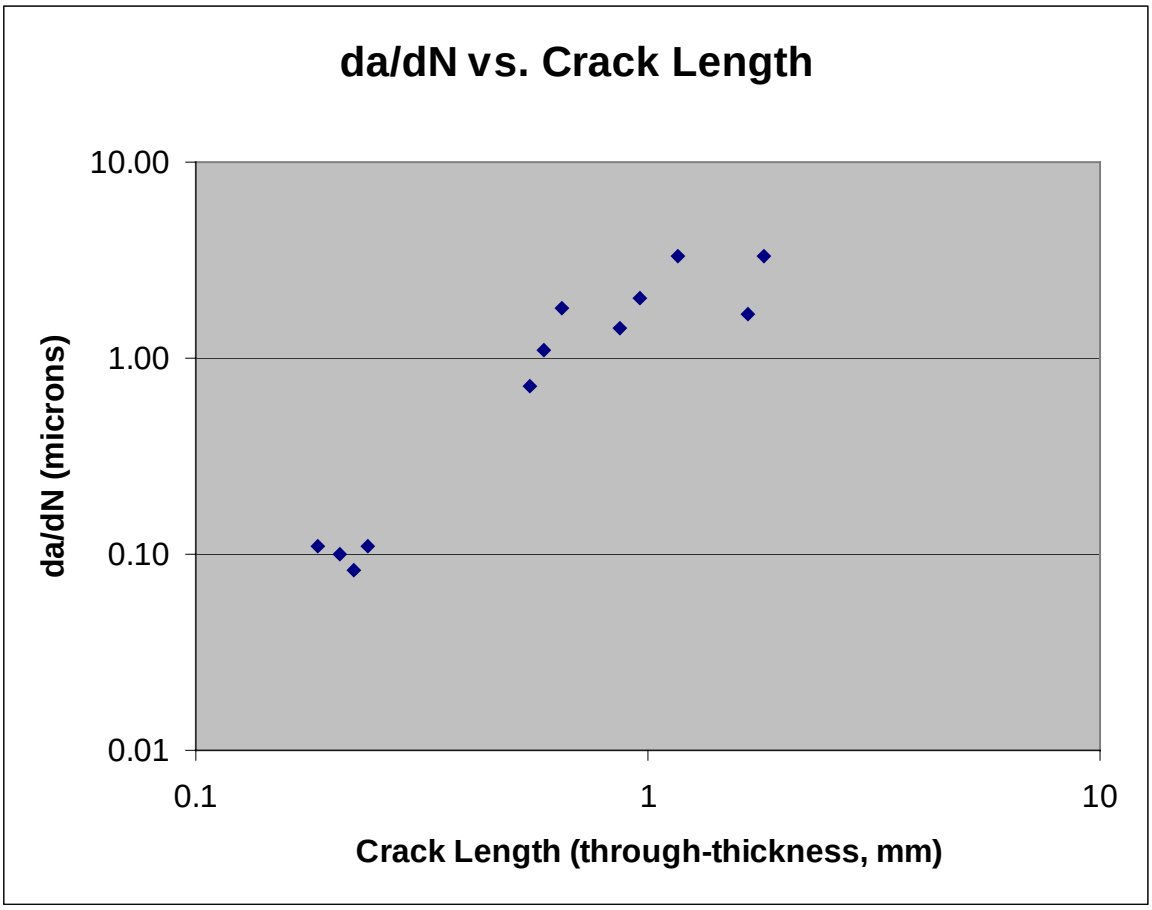
da/dN vs. Crack Length
10.00
1.00
0.10
0.01
da/dN (microns)
0.1
1
10
Crack Length (through-thickness, mm)

Hole #17-18

Cycles	Crack Length (mm)	da/dN (micron/cycle)	Photo #73	x0=35.713	y0=-13.901	slope	theta (absolute)	deviation angle
	1.884662569		EOC	37.066	-12.589	0.9697	0.7700148	
	0.085517165	0.09091	74	35.74	-13.806	3.51852	1.2938875	0.5238727
479	0.16368129	0.23529	75	35.781	-13.736	2.42647	1.1798845	0.4098697
100	0.18969974	0.28571	76	35.793	-13.711	2.375	1.1722739	0.4022591
87	0.219590502	0.40000	77	35.823	-13.699	1.83636	1.0721436	0.3021288
93	0.261228725	0.50000	78	35.849	-13.666	1.72794	1.0461683	0.2761536
143	0.360842843	0.88889	79	35.916	-13.592	1.52217	0.9895453	0.2195305
59	0.429674263	1.42857	80	35.976	-13.555	1.31559	0.9208526	0.1508378
344	1.247689129	3.33333	81	36.906	-13.339	0.47108	0.4402462	0.3297686
13051	**Total between 1st and Last**		x0, y0	35.713	-13.901			
191	Last Point to EOC							
941	Initiation to First Point							
2437	**Total (including extrapolation)**							

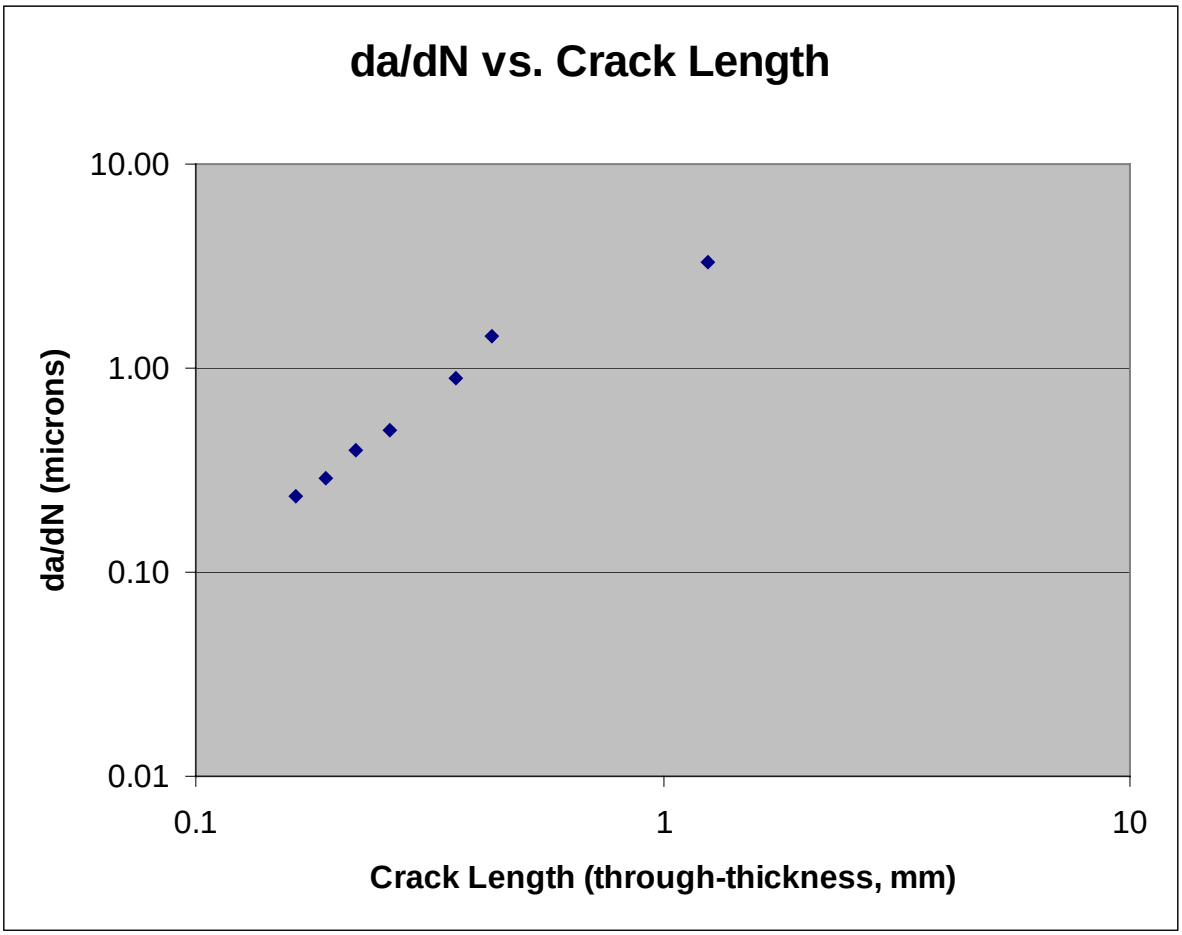
da/dN vs. Crack Length
10.00
1.00
0.10
0.01
da/dN (microns)
0.1
1
10
Crack Length (through-thickness, mm)

Hole #19

Cycles	Crack Length (mm)	da/dN (micron/cycle)	Photo #228	x0=-1.41	y0=-2.202	slope	theta (absolute)	deviation angle
	1.767900733		EOC	-2.577	-0.874	-1.138	0.8498379	
	0.319586383	0.16667	230	-1.629	-1.969	-1.0639	0.8163617	0.0334762
126	0.338002009	0.12500	229	-1.6	-1.919	-1.4895	0.9795391	0.1297012
564	0.443756816	0.25000	231	-1.676	-1.845	-1.3421	0.9304399	0.080602
166	0.48513923	0.25000	232	-1.7	-1.811	-1.3483	0.9326362	0.0827983
271	0.552881156	0.25000	233	-1.715	-1.734	-1.5344	0.9932204	0.1433825
871	0.71624836	0.12500	234	-1.81	-1.6	-1.505	0.9843286	0.1344908
540	0.803999327	0.20000	235	-1.795	-1.47	-1.9013	1.0866	0.2367621
343	0.855488644	0.10000	236	-1.807	-1.412	-1.9899	1.1051255	0.2552876
2805	1.151581626	0.11111	238	-2.152	-1.321	-1.1873	0.8708336	0.0209957
79	1.160892103	0.12500	237	-2.124	-1.284	-1.2857	0.9097532	0.0599153
652	1.388063229	0.57143	239	-2.236	-1.08	-1.3584	0.9361954	0.0863575
6418	**Total between 1st and Last**		x0, y0	-1.41	-2.202			

665	Last Point to EOC
1918	Initiation to First Point
9000	**Total (including extrapolation)**

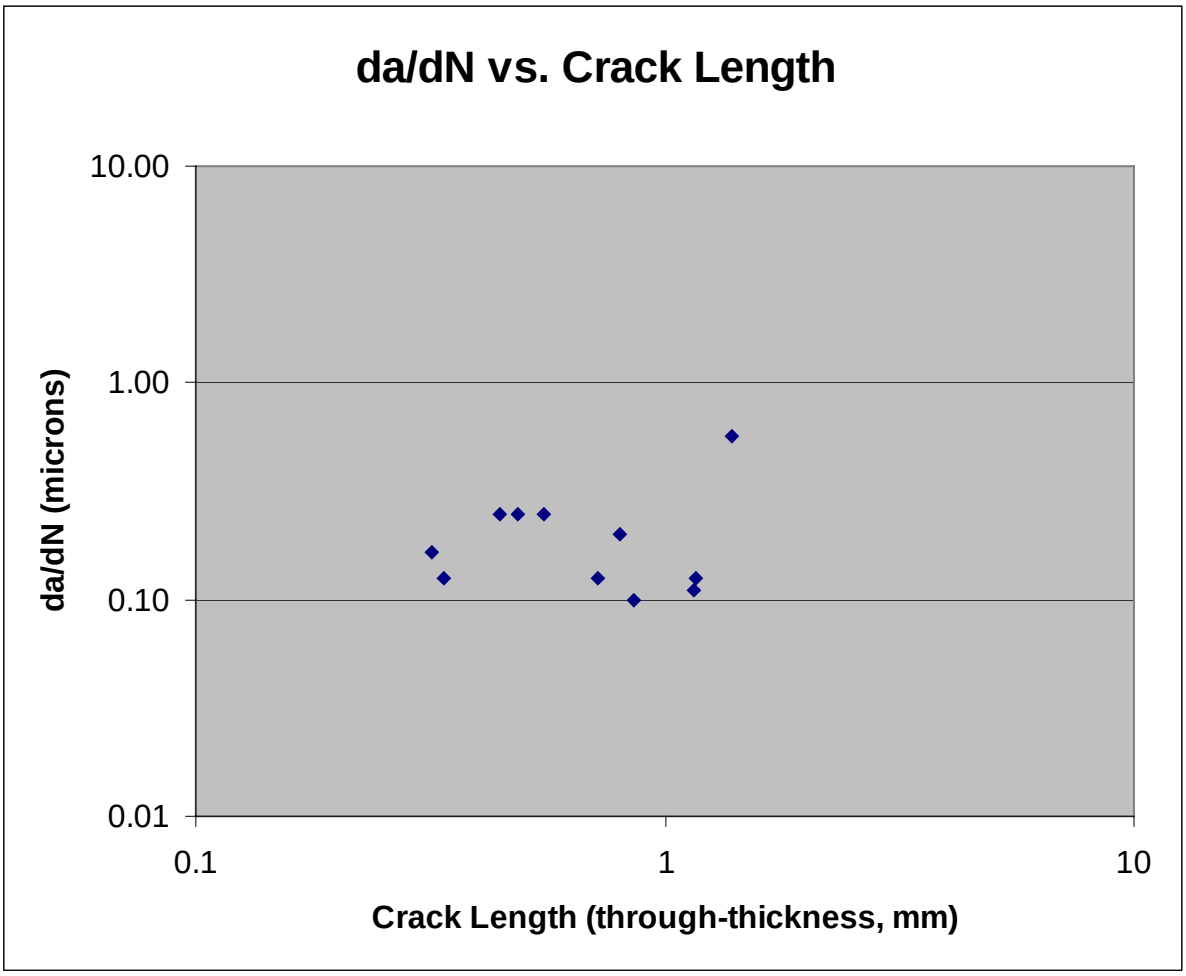
da/dN vs. Crack Length
10.00
1.00
0.10
0.01
da/dN (microns)
0.1
1
10
Crack Length (through-thickness, mm)

Hole #21

Cycles	Crack Length (mm)	da/dN (micron/cycle)	Photo #101	x0=32.938	y0=2.231	slope	theta (absolute)	deviation angle
	2.006024177		EOC	32.811	4.233	-15.764	1.5074447	
	0.155177093	0.14286	102	32.993	2.383	2.76364	1.2236109	0.2838337
60	0.161593267	0.07143	104	32.984	2.39	3.45652	1.2891772	0.2182675
16	0.162859453	0.08333	103	33.004	2.39	2.40909	1.1773457	0.330099
69	0.16764454	0.05556	105	32.985	2.396	3.51064	1.2932973	0.2141473
1082	0.246850963	0.09091	106	32.975	2.476	6.62162	1.4209086	0.0865361
105	0.256019347	0.08333	111	33.041	2.481	2.42718	1.1799881	0.3274565
440	0.296370805	0.10000	107	32.969	2.526	9.51613	1.4660958	0.0413488
641	0.374214333	0.14286	108	32.969	2.604	12.0323	1.487877	0.0195677
294	0.416256698	0.14286	109	32.971	2.646	12.5758	1.4914452	0.0159994
1070	0.559614392	0.12500	110	33.06	2.784	4.53279	1.3536597	0.153785
3024	1.050943964	0.20000	112	32.811	3.276	-8.2283	1.4498583	0.0575863
413	1.133602489	0.20000	113	32.798	3.358	-8.05	1.4472059	0.0602388
1038	1.533946617	0.57143	114	32.906	3.766	-47.969	1.5499524	0.0425078
8253	**Total between 1st and Last**		x0, y0	32.938	2.231			

826 Last Point to EOC

1086 Initiation to First Point

10165 Total (including extrapolation)

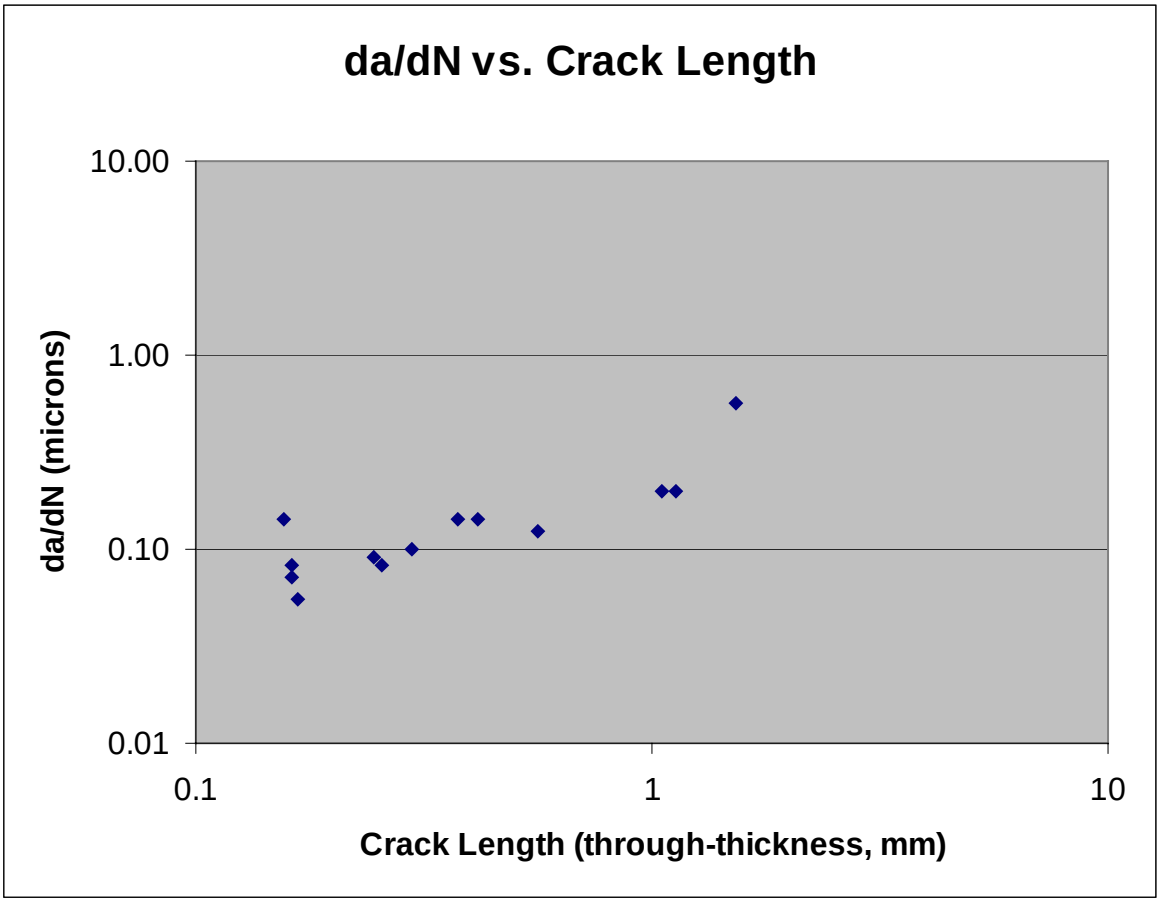
da/dN vs. Crack Length
10.00
1.00
0.10
0.01
da/dN (microns)
0.1
1
10
Crack Length (through-thickness, mm)

Hole #23

Cycles	Crack Length (mm)	da/dN (micron/cycle)	Photo #130	x0=1.903	y0=-0.774	slope	theta (absolute)	deviation angle
	1.807458437		EOC	2.244	1.001	5.20528	1.3809961	
	0.120702637	0.08333	131	2.168	-0.702	0.2717	0.2652939	1.1157022
2227	0.324889905	0.10000	132	2.178	-0.496	1.01091	0.7908231	0.590173
236	0.349756867	0.11111	128	1.909	-0.419	59.1667	1.5538965	0.1729004
582	0.408552133	0.09091	133	2.179	-0.411	1.31522	0.9207164	0.4602797
3320	0.743945738	0.11111	134	2.239	-0.081	2.0625	1.1193432	0.2616529
704	0.841777586	0.16667	135	2.211	0.024	2.59091	1.2024474	0.1785487
718	0.991342851	0.25000	136	2.249	0.169	2.72543	1.2191334	0.1618627
1227	1.417370352	0.44444	137	2.196	0.613	4.73379	1.3626098	0.0183863
52	1.454687946	1.00000	138	2.196	0.651	4.86348	1.3680085	0.0129876
90661	**Total between 1st and Last**		x0, y0	1.903	-0.774			

353	Last Point to EOC
1448	Initiation to First Point
10868	**Total (including extrapolation)**

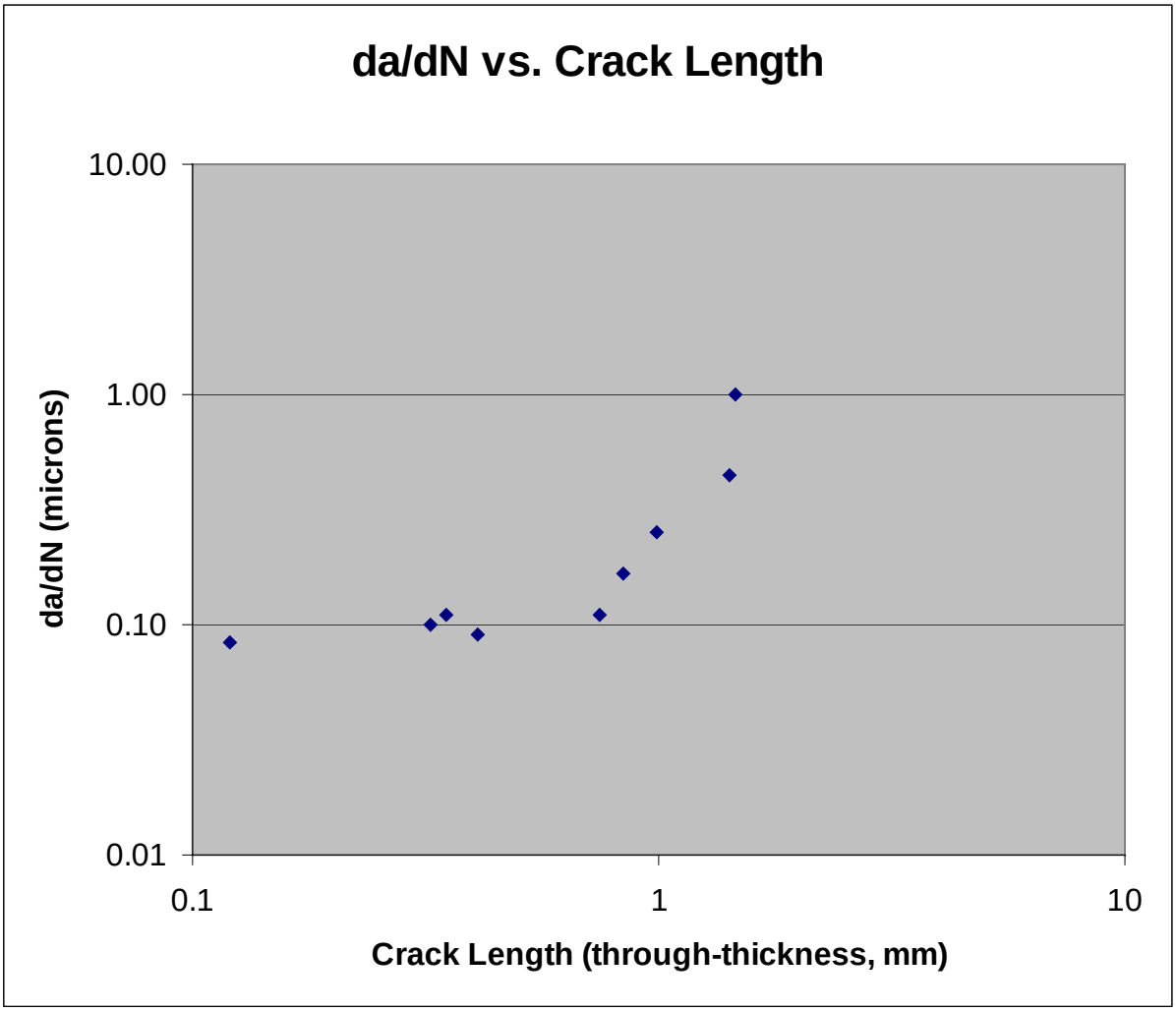
da/dN vs. Crack Length
10.00
1.00
0.10
0.01
da/dN (microns)
0.1
1
10
Crack Length (through-thickness, mm)

Hole #25

Cycles	Crack Length (mm)	da/dN (micron/cycle)	Photo #142	x0=3.578	y0=1.068	slope	theta (absolute)	deviation angle
	1.83623773		EOC	3.941	2.868	4.95868	1.3717987	
	0.236263689	0.11111	140	3.5781	1.309	2410	1.5703814	0.1985827
441	0.294697136	0.15385	139	3.596	1.365	16.5	1.5102643	0.1384656
234	0.332144902	0.16667	143	3.559	1.403	-17.632	1.5141406	0.1423419
174	0.361157485	0.16667	144	3.595	1.433	21.4706	1.5242546	0.1524559
315	0.444684251	0.36364	145	3.72	1.493	2.99296	1.2483401	0.1234587
141	0.563962924	1.33333	146	3.768	1.605	2.82632	1.2307247	0.141074
79	0.682674678	1.66667	147	3.709	1.738	5.1145	1.3777098	0.0059111
121	0.935181198	2.50000	148	3.573	2.021	-190.6	1.5655498	0.1937511
91	1.149870883	2.22222	149	3.5781	2.241	11730	1.5707111	0.1989124
42	1.238890239	2.00000	150	3.559	2.328	-66.316	1.5557181	0.1839194
106	1.496837232	2.85714	151	3.801	2.55	6.64574	1.4214445	0.0496458
17441	**Total between 1st and Last**		x0, y0	3.578	1.068			

119 Last Point to EOC

2126 Initiation to First Point

3989 Total (including extrapolation)

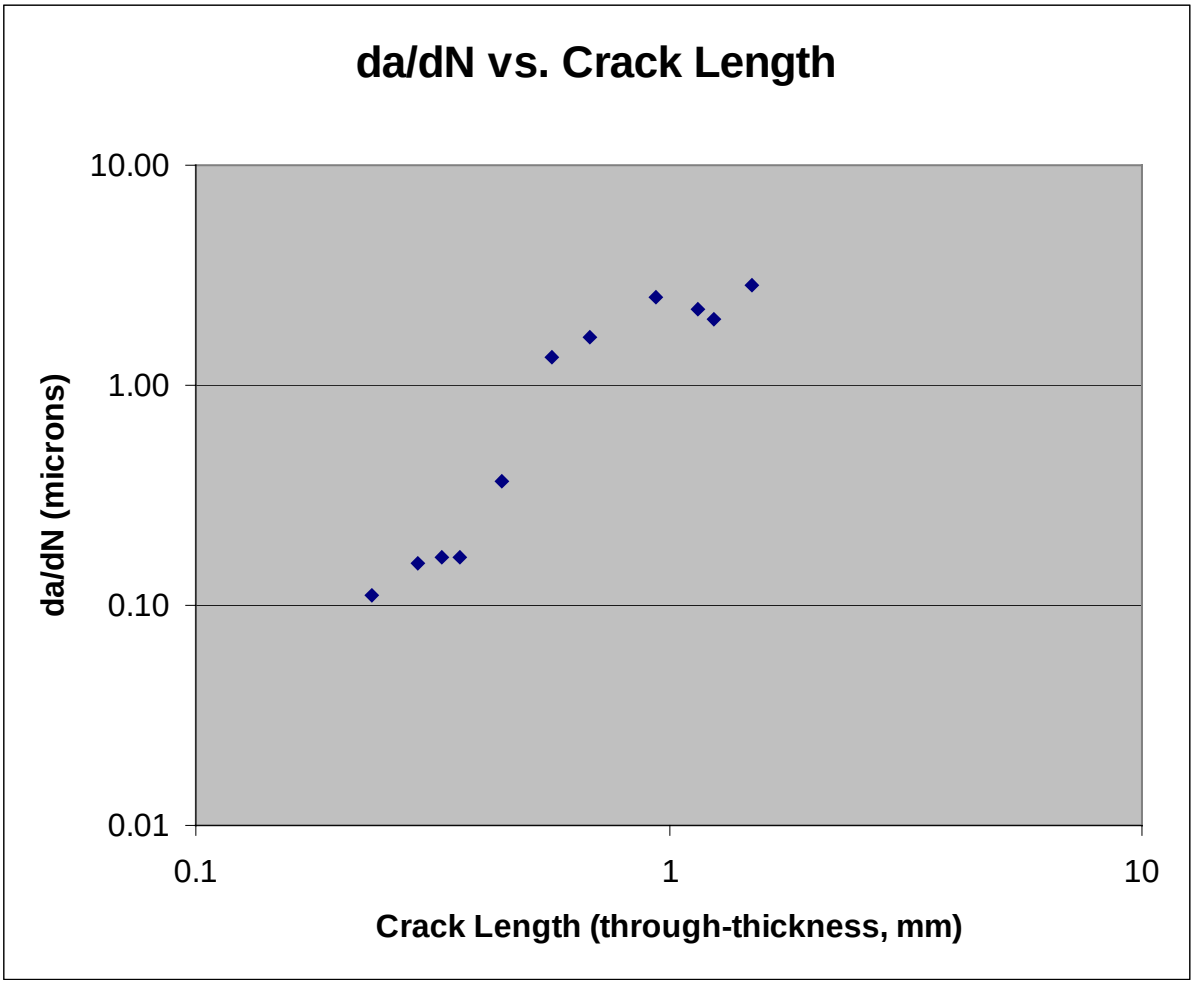
da/dN vs. Crack Length
10.00
1.00
0.10
0.01
da/dN (microns)
0.1
1
10
Crack Length (through-thickness, mm)

Hole #27

Cycles	Crack Length (mm)	da/dN (micron/cycle)	Photo	x0=-7.440	y0=-1.291	slope	theta (absolute)	deviation angle
	1.765007082		EOC	-7.705	0.454	-6.5849	1.4200854	
	0.299429393	0.14286	192	-7.742	-1.034	-0.851	0.7050705	0.7150149
1587	0.500952664	0.11111	191	-7.787	-0.837	-1.3084	0.918195	0.5018904
788	0.623521577	0.20000	190	-7.8	-0.715	-1.6	1.012197	0.4078884
16	0.626762358	0.20000	189	-7.815	-0.714	-1.5387	0.994482	0.4256034
790	0.762246233	0.14286	188	-7.835	-0.58	-1.8	1.0636978	0.3563876
66	0.77720368	0.30769	187	-7.77	-0.555	-2.2303	1.1492991	0.2707863
101	0.802784314	0.20000	186	-7.756	-0.527	-2.4177	1.1786103	0.2414751
573	0.931761134	0.25000	185	-7.759	-0.397	-2.8025	1.2280559	0.1920295
126	0.958993319	0.18182	184	-7.756	-0.369	-2.9177	1.2406099	0.1794755
272	1.017701299	0.25000	183	-7.719	-0.304	-3.5376	1.295309	0.1247764
323	1.079536745	0.13333	182	-7.716	-0.241	-3.8043	1.3137539	0.1063315
128	1.098760464	0.16667	180	-7.686	-0.217	-4.3659	1.3456301	0.0744553
42	1.108346827	0.28571	181	-7.684	-0.207	-4.4426	1.3493941	0.0706913
73	1.126882164	0.22222	179	-7.656	-0.184	-5.125	1.3780956	0.0419898
79	1.15315118	0.44444	178	-7.64	-0.155	-5.68	1.3965259	0.0235595
182	1.216275573	0.25000	177	-7.639	-0.091	-6.0302	1.4064586	0.0136268
9	1.218465366	0.25000	176	-7.647	-0.09	-5.8019	1.4001169	0.0199685
307	1.512325376	1.66667	193	-7.609	0.213	-8.8994	1.4588987	0.0388133
546	**Total between 1st and Last**		x0, y0	-7.44	-1.291			

152	Last Point to EOC
2096	Initiation to First Point
7710	**Total (including extrapolation)**

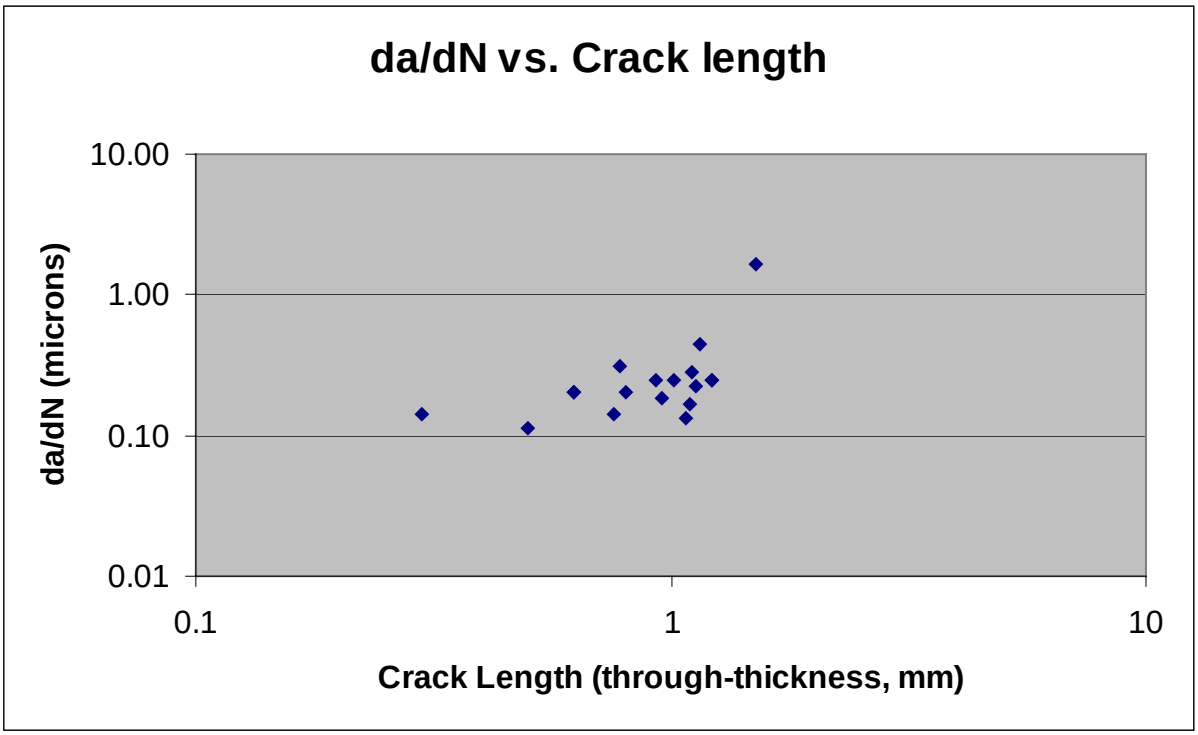
da/dN vs. Crack length
10.00
1.00
0.10
0.01
da/dN (microns)
0.1
1
10
Crack Length (through-thickness, mm)

V. Attachments

No	Item
7-01	Structures Group Field Notes Summary and Sequencing
7-02	Structures Group Field Notes Summary and Sequencing Document Supplement
7-03	Wing Center Section Documentation
7-04	CSIST Materials Test Report of ITEM 640
7-05	Boeing Document Engineering Number : MS22570
7-06	MS22570 Appendix A, B, C, D
7-07	CSIST Materials Test Report of ITEM 626
7-08	CSIST Materials Test Report of ITEM 751
7-09	Boeing analytical engineering report NO. B-KC15-WP-03-159
7-10	Boeing Document Engineering Number : MS22590